©2020

Jieyu Zhu

ALL RIGHTS RESERVED

FABRICATION, CHARACTERIZATION, AND APPLICATIONS OF ZEIN-BASED COLLOIDAL PARTICLES

by

JIEYU ZHU

A dissertation submitted to the

School of Graduate Studies

Rutgers, the State University of New Jersey

In partial fulfillment of the requirements

For the degree of

Doctor of Philosophy

Graduate Program in Food Science

Written under the direction of

Dr. Qingrong Huang

And approved by

_____

_____

_____

_____

New Brunswick, New Jersey

May, 2020

ABSTRACT OF THE DISSERTATION

Fabrication, Characterization, and Applications of Zein-based Colloidal Particles

By JIEYU ZHU

Dissertation Director:

Dr. Qingrong Huang

With an increasing trend on the development of "clean-label" food products, environmental friendly materials have attracted more and more attentions during the recent years. As a natural biodegradable protein from maize, zein has a good potential to be used to develop new carrier systems due to its Generally Recognized as Safe (GRAS) status, abundant source, commercial availability, low cost, and low digestion properties. The water-insoluble and amphiphilic characteristic of zein makes it a perfect candidate to form colloidal particles to stabilize Pickering emulsions. The successful assembly of particles at emulsion interface largely relies on their surface activities, which can be tuned through the modification of surface charges and hydrophobicities.

In this study, zein was hydrophilically modified with sodium caseinate (SC) to form zein/SC complexes and hydrophobically modified with saturated fatty acids (FA) to form zein/FA complexes. The obtained zein/SC complexes displayed good emulsification capacities, which were suitable to stabilize a wide range of oils with middle or low polarities including toluene, n-octane, hexane, and general cooking oils extracted from vegetables. The fluorescence image of fluorescein isothiocyanate (FITC)-labeled zein particles indicated that the emulsions

were stabilized mainly by zein-based colloidal particles. With the presence of polyglycerol polyricinoleate, zein/SC complexes were able to stabilize W/O/W double emulsions either through magnetic stirring method or through high speed homogenization method. The Pickering emulsions stabilized by zein/SC complexes were further utilized to encapsulate resveratrol, a plant phytoalexin extracted from grape, peanut and other few plants.

Resveratrol has been widely reported for its health beneficial potentials, such as anti-oxidation, anti-inflammation, anti-obesity, anti-tumor activities, etc. However, the applications of resveratrol in the food industries are quite limited because of its low chemical stability, low oral bioavailability, and poor water solubility. In this study, a series of delivery systems were developed to compare their delivery efficacy and bioaccessibility of resveratrol using *in vitro* models. Zein/SC complexes were utilized to fabricate Pickering emulsions through high speed homogenization, while conventional emulsions were stabilized by lecithin using high pressure homogenization. The Simulator of the Human Intestinal Microbial Ecosystem (SHIME) and TNO gastro-Intestinal Model (TIM-1) were utilized to mimic the digestion in the upper GI tract. The results from TIM-1 indicated that conventional emulsions displayed the highest bioaccessibility compared with Pickering emulsions and bulk oil solutions. In SHIME experiment, the structure of Pickering emulsions was still observable after 2-hour digestion in the stomach, which explained why Pickering emulsion showed slower release effect of RES compared with conventional emusions. After 180 min digestion in the jejunum by the TIM-1 model, the digested samples were loaded on Franz Cell Diffusion apparatus to see the permeability of various formulations through porcine small intestine membrane. It was found that Pickering emulsions had significantly lower permeability as compared with conventional emulsions and bulk oil solutions ($P < 0.05$). The permeability of resveratrol was driven by concentration gradients between donor compartment and receptor compartment. Through

anaerobic fermentation study, it was found that lecithin stabilized emulsions after SHIME digestion retarded the growth of probiotics, *Lactobacillus rhamnosus GG*, while zein/SC complexes stabilized Pickering emulsions even promoted its growth, since zein and sodium caseinate could serve as a protein source for bacteria. Conclusively, Pickering emulsions are more suitable for target delivery of RES into colon, while conventional emulsions can be used to improve the bioaccessibility in small intestine.

Besides Pickering emulsion, zein/SC complexes were further utilized to fabricate colloidosomes that are characterized by their hollow shell structures through layer-by-layer (LbL) self-assembling technique. Quartz crystal microbalance equipped with dissipation monitoring (QCM-D) was applied to simulate the deposition process of polyelectrolytes (chitosan, sodium alginate, and zein) on the zein/SC surface. The result from QCM-D analysis showed that the adlayer on zein/SC surface had a soft and viscoelastic property. This presented method successfully produced robust colloidosomes, which not only survived from multiple washing steps, but also did not show flocculation and coalescence phenomenon during the LbL coating process. And the polysaccharide coatings strengthened the structure of shells, and offered them a viscoelastic property to stand harsh dehydration conditions.

In the following section, fatty acid (FA)/zein (Z) complexes were prepared by using FAs with different chain lengths (i.e. lauric acid (LA), myristic acid (MA), palmitic acid (PA), stearic acid (SA) and oleic acid (OA)), different FA/Z ratios (i.e. 0.1:1, 0.2:1, 0.4:1, and 1:1), and different pH values (i.e. 3.5, 5.0, 8.0, 10.5) in order to precisely tune the surface activities of zein. Results showed that stable FA/Z complexes were able to be formed under alkaline condition, rather than acidic or neutral pH, which was due to the film forming property of zein in acidic conditions. According to the contact angle (CA) measurement, the CA increased gradually from 64.88 ± 4.09˚ (LA/Z, 0.5:1) to 85.25 ± 2.00˚ (SA/Z, 0.5:1) with an increase of the carbon

chain length. However, oleic acid, a monounsaturated omega-9 fatty acid, reduced the hydrophobicity, giving the lowest CA of 61.08 ± 6.14˚. Scanning electron microscopic (SEM) images indicated that FAs could lead to the partial fusion of the particles, which explained why FAs could reduce the brittleness and increase the plasticity of zein. The SA/Z complexes showed good emulsification capacity to stabilize O/W/O double emulsions through handshaking. The LA/Z complexes were further applied to improve the bioavailability of lipophilic ingredients, i.e. hesperidin in this study. Based on *in vitro* study conducted through the TIM-1 model, the bioavailability of hesperidin was successfully enhanced from 53% to around 70% as compared with bulk oil solutions. This study indicated the good potentials of using zein as an environmental friendly particle emulsifier to develop novel delivery systems for various nutraceuticals.

ACKNOWLEDGEMNET

First of all, I would like to give my sincere thanks to my advisor, Dr. Qingrong Huang, who offered me a precious opportunity to study in his group, and also provided me numerous kind supports and valuable suggestions throughout my studies at the Rutgers University. I have learnt a lot from him about developing formulations for the delivery of functional nutraceuticals, which is very important and helpful for me in my career development. He not only cares about my studies, but also cares about my life, providing me financial supports as a research assistant in the lab and offering me insightful suggestions for my future life plan. I am deeply grateful and honored to have Dr. Huang as my advisor.

I would like to express my deepest appreciation to my committee members, Dr. Chi-Tang Ho, Dr. Qing-Li Wu, and Dr. Shiming Li. I am very thankful for Dr. Chi-Tang Ho for teaching me as my course teacher, guiding me as my committee member, and writing recommendation letters for me. I am very impressed and inspired by Dr. Ho's profound knowledge on chemistry and biology, enthusiastic attitude towards scientific research, and charming personality in helping students. It was my great fortune and honor to learn from Dr. Ho. I am also very grateful for Dr. Qing-Li Wu for being my committee member, caring about my research progress, providing me opportunities to get the GC-MS training in his lab and offering me insightful suggestions for my studies. I would also like to express my sincere gratitude to Dr. Shiming Li. Dr. Li is more than an admirable teacher for me, but also like a loving parent who cares a lot about my studies and my life. No matter how busy he was, he was willing to spend time in helping me and teaching me. And it was also very kind of Dr. Li to introduce me valuable internship opportunities and build up connections with industries.

Other professors in the Rutgers University also helped me a lot during my Ph.D studies. Dr. Richard Ludescher was very supportive to me in my Franz Cell experiment. And also many

thanks to Dr. Ludescher for being my course teacher and writing recommendation letter for me. I would also like give my gratitude toward Dr. Michael Chikindas and Dr. Maria Falduto for helping me with the SHIME experiment, and Dr. David M. Ribnicky from Department of Plant Biology for the TIM-1 experiment. I highly appreciate their patient instructions on me. And I still remember how we discussed the experimental design and how we adjust the instruments together.

Very importantly, I would also like to thank my parents, my husband Chuxu, all my friends and labmates, and the visiting scholars in our lab for accompanying me and supporting me. Special thanks to Dr. Weiping Jin, Man Zhang, Yijun Pan, Xuanxuan Lu, Xudong Tang, Junjia Zhang, Chloé Garat, Ting Zheng, Dr. Xin Zhang, Dr. Yike Jiang, and Dr. Zhenyu Lin for helping me with my research work and also made my life at Rutgers University colorful, fruitful, and enjoyable.

CONTENT

LIST OF TABLES

LIST OF ILLUSTRATIONS

CHAPTER I. INTRODUCTION

Partial contents in this chapter were adapted from "Zhu J., Huang Q., Nanoencapsulation of functional food ingredients, Advances in food and nutrition research 88 (2019): 129-165." Copyright © 2019 with permission from Elsevier Inc. And partial contents in this chapter were adapted from the paper "Determination of the Oxidation Stability of Fish oil-in water Pickering Emulsion by using zein/carnosic acid complexes" and "Metabolism of Resveratrol by Gut Microbiota and its Colon-related Health Beneficial Effects" which were ready for submission.

1. Research Rationale and Hypothesis

With an increasing awareness of consumers on having a healthy diet and maintaining a healthy body shape, people have tried to add functional food ingredients into foods and beverages. However, many of them are poor in aqueous solubility, limited in oral bioavailability, unpleasant in flavor or taste, sensitive to environmental stress, easy for chemical degradation, incompatible with other food matrix, or burst released/excreted without a sustainable release. Therefore, more and more novel delivery systems have been developed for the encapsulation of various functional components to improve the flavors and colors of food products, to provide safer and "clean-label" food products, to increase the acceptability of consumers on the food products, to increase the bio-absorption and bioavailability of nutraceuticals, and to prevent microbial spoilage and prolong the shelf-life of food products (*1*). As illustrated in the Table I-1 (*1*), the

nano-encapsulation is of great necessity for various functional food ingredients, including health beneficial phytochemicals (e.g. epigallocatechin gallate, resveratrol, polymethoxylated flavones, curcumin, etc), flavors, antimicrobial agents, natural food colorants, etc. As a natural biodegradable protein from maize, zein has a good potential to be used to develop new carrier systems due to its Generally Recognized as Safe (GRAS) status, abundant source, commercial availability, low cost, and low digestion properties. The water-insoluble and amphiphilic characteristic of zein makes it a perfect candidate to form colloidal particles to stabilize Pickering emulsions. The successful assembly of particles at emulsion interface largely relies on their surface activities. However, the emulsification capacity of zein itself is very limited. And there is a lack of researches that fulfill its potential applications in controlled delivery of bioactive nutraceuticals. Therefore, based on current published papers and my preliminary data, here comes my hypothesis:

1) Since zein is an amphiphilic protein which has both hydrophobic apolar surface and hydrophilic polar surface, the surface activity of zein can be adjusted through hydrophilic modification with water-soluble proteins or hydrophobic modification with long-chain fatty acids.
2) As an alcohol-soluble prolamin, the zein-based insoluble colloidal particles can be formed through anti-solvent precipitation method with proper emulsification capacity to stabilize emulsions, Pickering emulsion in this case.
3) The obtained Pickering emulsions can be utilized as functional delivery systems of bioactive compounds for different purposes, such as improved bioavailability or sustained release.

4) The obtained Pickering emulsions can serve as a template to build superior structures. And the structure, mechanical strength, and surface morphology can be tuned through different strategies.

2. Research Objectives

In order to prove my hypothesis, four research objectives have been listed here to systematically study the structure and surface activities of zein colloidal particles on the development of Pickering emulsions and colloidosomes with tunable morphology, permeability, and release profile.

A. Synthesis of zein-based colloidal particles with tunable wettabilities

Zein colloidal particles with high surface activity, good barrier performance, and strong tensile strength can be achieved by forming complexes with proteins or fatty acids of different chain lengths, such as lauric acid, palmitic acid, oleic acid, and stearic acid. Besides hydrophobic modification with fatty acids, a hydrophilic protein, sodium caseinate (SC), will also be applied to form complexes with zein in this study. Through different detection approaches, the size, structures, shapes, hydrophobicity and emulsification capacity of zein colloidal particles are will determined.

B. Manipulation of particle self-assembly behavior through the formation of single emulsions and double emulsions

The synthesized colloidal particles should have high surface activity to produce both oil-in-water emulsions and water-in-oil emulsions. Water-in-oil-in-water or oil-in-water-in-oil double emulsions can be fabricated on the basis of the obtained primary emulsions.

C. Nano-encapsulation of bioactive compounds using emulsions stabilized by zein-based colloidal particles

Health beneficial bioactive compounds will be encapsulated in various delivery systems, including zein/SC stabilized Pickering emulsions, zein/FA stabilized Pickering emulsions, bulk oil solutions, and traditional nanoemulsions. And the digestion property of these formulations will be tested using different digestion models.

D. Fabrication of colloidosomes through layer-by-layer (LbL) self-assembling technique using zein-based colloidal particles

Colloidosomes with hollow shell structures will be fabricated through layer-by-layer (LbL) self-assembling technique on the templates of Pickering emulsions that are stabilized by zein/SC complexes. The colloidosomes structure will be strengthened by electrostatic deposition of polysaccharide coatings. The obtained colloidosomes should have good elasticity and be robust enough to maintain good integrity during the processing procedures.

Table I- 1. Reasons and Examples of nano-encapsulation of various functional food ingredients

Categories	Examples	Functional attributes	Reasons for encapsulation	Examples of delivery systems
Health beneficial phytochemicals	EGCG	Anti-oxidant, anti-inflammation, anti-obesity, anti-hypertensive effect, anti-cancer, and UV-protection, etc.	Active efflux pumps, rapid Phase II metabolism, rapid elimination from feces, and low bioavailability	Chitosan-tripolyphosphate nanoparticles (*2*), chitosan-caseinophosphopeptide nanoparticles (*3*)
	Resveratrol	Anti-oxidation, anti-inflammation, anti-obesity, anti-colitis, and anti-cancer, etc.	Poor solubility, limited stability, high metabolism rate, high absorption in small intestine, rapid elimination from urine, and low bioavailability	Oil-in-water emulsions (*4, 5*), water-in-oil emulsions (*6*), and water-in-oil-in-water double emulsions (*7-9*), solid lipid nanoparticles (*10*), liposomes (*11*), and biodegradable

				nanoparticles (*12-14*)
	Polymethoxylated flavones	Anti-inflammation, anti-cancer, anti-atherogenic, and anti-obesity and anti-diabetic effect, etc	Poor solubility and low bioavailability	Nanoemulsions (*15, 16*)
	Curcumin	Anti-cancer, anti-inflammation, antioxidant, antimicrobial, and anti-obesity and anti-diabetic effect, etc.	Poor absorption, rapid metabolism, and rapid systemic elimination	Micelles (*17*), conventional O/W emulsions (*18*), Pickering emulsions (*19*), self-emulsifying system (*20*), nanoparticles (*21*), organogels (*22*) and organogel derived emulsions (*23*)
Flavors	Citral	Lemon aroma	Susceptible to acid-catalyzed cyclization and oxygen-induced oxidation	Nanoemulsions (*24, 25*) and multilayer nanoemulsions (*26*)
Anti-microbial agents	Essential oils	Anti-bacterial, anti-fungal, antioxidant, and insecticidal effects	Improve anti-microbial efficacy, prevent un-desired evaporation during food production, and provide sustained release during shelf-life	Nanoemulsions (*27-30*), organogel-derived nanoemulsions (*31*), microemulsions (*32, 33*), and films(*34*)
	Anti-microbial peptides	Anti-bacterial and anti-fungal properties	Improve the anti-microbial efficacy and stability, provide sustained release during shelf-life	Liposomes (*35*), nanocapsules (*36*), niosomes (*37*)
Natural colorants	Anthocyanins	Colorants and antioxidant	Susceptible to chemical degradation	Polymer complexes (*38*), hydrogels (*39*), microcapsules (*40*)
	β-carotenes	Colorants, antioxidant, enhance immune system, prevent Alzheimer's disease, and precursor to vitamin A	Poor solubility, susceptible to chemical degradation, improve bio-absorption and bio-efficacy	Nanoemulsions(*41*), spray-dried powders (*42*), nanotubes (*43*), solid-lipid nanoparticles (*44*), electrospun fibers (*45*)

3. Key Concepts Involved in the Thesis

3.1. Zein Protein

Zein is the major storage protein found in corn or maize (*Zea mays* L.). It was first identified in 1897 as an alcohol soluble protein and commercially available from corn gluten meal in 1939 (*46*). Zein displays poor nutritional quality, because even though it has abundant glutamic acid (21–26%), leucine (20%), proline (10%) and alanine (10%), it has notable absence of essential amino acids, such as tryptophane and lysine (*46*). There are four classes of zein: α (22 and 19 KDa), β (15 KDa), γ (27 and 16 KDa), and δ (10 KDa), which are expressed sequentially in maize (*47*). α-Zein accounts for 75–85% of the total zein, consisting of Mr 21,000–25,000 polypeptides plus a Mr 10,000 minor polypeptide (*48*). β-Zein is a methionine-rich polypeptides containing 10% methionine and 8% tyrosine, which accounts for 10–15% of the total zein (*49*). β-Zein is soluble in 60% ethanol but insoluble in 95% ethanol (*46*). Compared with β-zein, α-zein contains less histidine, arginine, proline and methionine (*46*), but high in leucine (20%) and phenylalamine (6%) (*49*). γ-Zein accounts for 5–10% of the total zein, and is rich in proline (25%) and histidine (8%) (*49*). δ-zein is another minor polypeptide which was originally classified to the group of α-zein due to its close interaction with both 22-kD and 19-kD α-zeins. δ-zeins are rich in methionine and serve as a sulfur sink and mediator for the interaction and accumulation of the α-zeins (*47*).

The zein proteins in alcoholic solutions are either in a prolate ellipsoid shape with length of 196 Å and cross-section diameter of 7 Å or in a rod shape with length of 153 Å and diameter of 13.8 Å, based on previous small-angle X-ray scattering (SAXS) studies (*50-52*). Zein contains nine or ten tandem repeats, and each of tandem repeats units forms single a-helix and they are connected by glutamine-rich loops (*53, 54*). The rectangular

prism-like structure provides a large hydrophobic surface, while the glutamine-rich loops provide a hydrophilic surface (*52*). The surface plasmon resonance (SPR) indicated that zein had a greater affinity onto a hydrophilic surface than onto a hydrophobic one under the similar experimental conditions (*55*). Adsorption rate of zein was higher on a hydrophilic surface treated by carboxylic acid terminated thiol (11-mercaptoundecanoic acid) than on a hydrophobic one treated by a methyl terminated alkanethiol (1-octanediol) (*55*). Therefore, zein is an amphiphilic protein with both hydrophobic and hydrophilic ends, which make it possible to adsorb at the oil-water interface to form Pickering emulsion.

As a natural hydrophobic biopolymer, zein can be applied in food and pharmaceuticals applications due to its several advantageous attributes. First of all, zein has been certified as Generally Recognized As Safe (GRAS) by FDA, and has abundant source due to the high production of corn each year all over the world. Secondly, the water-insoluble characteristic of zein and its amphiphilic behavior makes it a perfect candidate for development of new carrier systems. Furthermore, morphology, particles size, and surface hydrophobicity are highly pH-dependent.

The original wettability of zein colloidal particle is quite poor, leading to unstable Pickering emulsion (creaming and coalescence) especially at pH values around the isoelectric point (*56*). As a result, different ingredients have been added to improve the emulsification capacity of zein, such as the formation of complexes with sodium caseinate (*57*, *58*), sodium stearate (*59*), gum arabic (*60*), pectin (*61*, *62*), chitosan (*63*), tannic acid (*64*), corn fiber gum (*65*), etc.

As an amphiphilic protein, zein protein could interact with hydrophilic water soluble proteins mainly through electrostatic interactions and Van de Waals interactions. And the side area of this prism-like structure of zein provides large hydrophobic area for the absorption of hydrophobic carbon chains of fatty acids (FA), and the hydrophilic ends of fatty acids may orient themselves towards polar surfaces of zein. Therefore, in this study, zein will be hydrophilically modified with sodium caseinate and hydrophobically modified with long-chain fatty acids. Different fatty acids have been added into zein to improve the plasticity, elasticity, and barrier property of zein films, such as lauric acid (LA) (*66*), palmitic acid (PA) (*67*), stearic acid (SA) (*67*), and oleic acid (OA) (*68*). However, the formation of zein and fatty acids complexes and the subsequent obtained Pickering emulsions have not been reported before. So it is of great necessity to systemically study the particle size, morphology, hydrophobicity, self-assembly behavior, and the digestion property of zein/FA stabilized emulsions.

3.2. Pickering Emulsions

Pickering emulsions refer to emulsions that are stabilized by insoluble amphiphilic materials, which can be stabilized by either spherical particles or rod-like fibers. Due to the larger size of surfactants as compared with conventional emulsions, the average droplet sizes of Pickering emulsions are commonly in the micrometer scales (*1*). There are many studies about Pickering emulsions stabilized by inexpensive food-originated materials, such as starch (*69*), cellulose (*70*), zein (*71*), karifin (*72*), etc.

3.2.1. Approaches for the Fabrication of Pickering Emulsions

In order to stabilize Pickering emulsions, there are several requirements for the particle stabilizers, including the insolubility and the partial wettability in the two

immiscible phases, as well as suitable particle sizes (at least one order of magnitude smaller than the targeted emulsion droplet size) (*73*).

There are two major strategies to fabricate colloidal particles. One is the top-down strategy, which uses either chemical methods (e.g. enzyme-catalyzed hydrolysis and acidic hydrolysis) or mechanical methods (e.g. wet-ball milling machine, cryogenic milling machine, and high-pressure homogenizer) to break down materials for the purpose of smaller sizes, better swelling properties, and better emulsification capacities. Pickering emulsions stabilized by starch granules or cellulose crystals are usually prepared in this method. The other strategy is the bottom-up assembling method, which forms colloidal particles through aggregates or complexes, such as anti-solvent precipitation method, crosslinking method, and electrostatic interaction method (*1*).

In the anti-solvent precipitation method, the polymers are firstly dissolved in a good solvent to prepare a stock solution. And then the stock solution is trickled into a poor solvent under continuous stirring, which leads to aggregation of the polymers (*1*). The sizes of the polymer aggregates can be precisely controlled by tuning the concentration of the polymer stock solution, the stirring speed, the volume ratio of dispersed stock solution to the bulk poor solvent, the addition sequence and the speed of the two solutions (adding stock solution into the bulk poor solvent or vice versa) (*74*). And this method can be applied to fabricate prolamin-based colloidal particles, such as zein protein extracted from maize (*75*), kafirin extracted from sorghum (*72*), hordein extracted from barley, gliadin extracted from wheat, and coixin extracted from coix.

In the cross-linking method, cross linkers are added into the polymer solution to form cross-linked nanoparticles either through covalent cross-linking effect or ionic

cross-linking effect (*76*). And the cross-linking density is determined by the molar ratio between the cross linkers and the polymer repeating units.

In the electrostatic interaction method, the oppositely charged polyelectrolytes can interact with each other through direct electrostatic interaction, leading to the formation of polyelectrolyte complexes (*76*). By tuning the pH and the ionic strength of the protein and polysaccharide solutions, this method can be used to form insoluble protein-polysaccharide complexed nanoparticles to stabilize Pickering emulsions. Besides the electrostatic attraction, hydrogen bonding and hydrophobic interaction were the major driving forces for formation of protein-polysaccharide complexes (*77*). The size and the surface charge of the colloidal particles can be tuned by modifying the pH values and the concentration of protein and polysaccharide solutions, and the mass ratio of protein to polysaccharide.

Pickering emulsions are generally formed by high speed homogenization. Most of the time, split cyclic homogenization (e.g. cycles of working 60 s and resting 30 s) has better effect than continuous homogenization of several minutes, since the resting time provide colloidal particles more time to move, absorb and rearrange on the interface. The cycling number of homogenization influence a lot on the self-assembling of colloidal particles. For particle stabilized emulsions, more cycles might result in the engulfment of particles/small emulsion droplets inside large emulsion droplets, resulting in core-shell structure with a spherical core of particle aggregates. Besides high speed homogenization, a glass capillary microfluidic device can also be applied to generate monodisperse droplets easily, either though single emulsions (*78*), or double emulsions (*79*).

3.2.2. Applications

Pickering emulsion has many advantages as compared with conventional emulsions. First of all, Pickering emulsions could stabilize emulsions with high oil fractions (around 50-90%), which significantly increase the the loading capacity (LC%) of drugs in the formulation. Secondly, Pickering emulsions have better stability against coalescence due to the high detachment energy of colloidal particles from the oil-water interface, as compared with small molecular weight surfactants. What's more, in many cases Pickering emulsions are stabilized by the biologically compatible and environmentally friendly materials instead of synthetic surfactants, which make it more competitive and more attractive toward consumers. Last but not the least, it was also reported that Pickering emulsions exhibited better anti-lipid oxidation effect as compared with conventional emulsions. For instance, Pickering emulsions stabilized by silica particles (at pH 2) presented lower hydroperoxide concentration and p-Anisidine value (AV) in 20% sunflower oil-in-water emulsion after 7-day's storage, as compared with emulsions stabilized by Tween 20 alone (*80*). Microcrystalline cellulose (MCC) and modified starch (MS) particles stabilized Pickering emulsion also displayed good oxidative stability for sunflower oil-in-water emulsion due to the protection effect of a thick interfacial layer and their free radical scavenging abilities (*81*).

3.3. Colloidosomes

The structure of colloidosomes were firstly reported by Velev and co-workers in 1996 (*82*). They allowed the assembly and fixation of latex colloid particles onto an octanol based emulsions through a "interaction-tailored colloid assembly" technique, and formed shell-like microstructured clusters, which they called "supraparticles" (*82*).

The term, “colloidosomes”, coming from the analogy to the name “liposomes”, was firstly proposed by Dinsmore in 2002 (*83*). Colloidosomes and liposomes both are capsules, and they are composed of colloidal particles and phospholipid bilayers, respectively. Through precise control of size, compatibility, permeability, and mechanical strength, colloidosomes are able to encapsulate fragile and sensitive components of suitable sizes, withstand various mechanical stresses, and selectively release them under controlled environmental conditions (*83*).

The assembly of colloidal particles would lead to two types of composite structures as shown in Figure I-1. For a heterocoagulation of particles with dissimilar sizes, a solid core-shell structure will be formed by coating small particles onto the surface of a large one. The core of these particle composites is not limited to one single particle. An aggregate of small particles can also serve as the core template for the formation of this ball-like aggregates (*84*). For a homocoagulation of particles with similar sizes, ordered and spherical aggregates of colloidal particles can be achieved through gathering microspheres on emulsion droplets. An empty ball, having a hollow shell structure, is obtained through the dissolution of core material. Without the assistance of core templates, colloidal particles aggregate into shapeless fractal-like clusters (*85*). Colloidosomes belongs to the second type of particle aggregates, having a solid shell that consists of closely packed colloidal particles with similar sizes (*86, 87*).

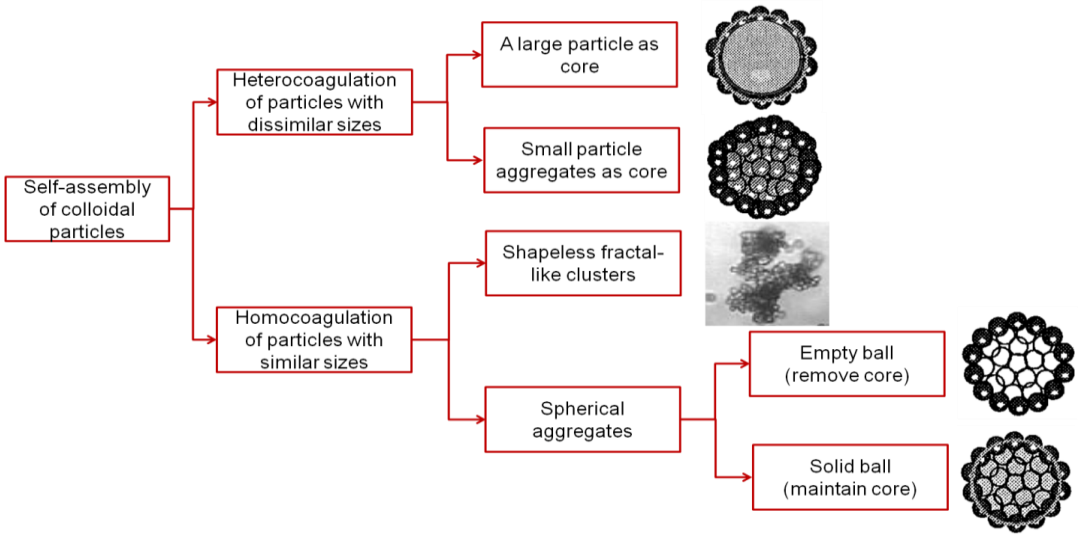

Figure I- 1. Schematic diagram of the self-assembly behavior of colloidal particles.

3.3.1. Approaches for the fabrication of colloidosomes

The colloidosomes are fabricated through precisely tailoring a series of colloid interactions between particles and droplets. Colloidosomes can be prepared both through hard solid templates and soft liquid templates. The core removal process for hard core materials, such as polystyrene lattices and melamine formaldehyde particles, are usually more severe, requiring high temperature or strong acid dissolution (*88*). Thus liquid cores have higher applicability compared with the other one. Routes of forming colloidosomes through liquid templates are commonly based on the self assembling of colloidal particles at the interface of two immiscible phases, which is typically in the same way of the formation of Pickering emulsions (*89*), either through water-in-oil emulsions (*90*) or oil-in-water emulsions (*91*).

The driving force of particle self assembly is the surface tension. If the surface energy between the two immiscible phases is larger than the difference of the surface energy between particle and dispersed phase, and the one between particles and continuous phase, the absorption of particles at interfacial areas is energetically favorable.

And particles tend to spontaneously absorb on the emulsion interface. Once particles are absorbed on the interface, the mobility of particles has been mitigated, which is less mobile than small molecular surfactants. The free energy of detachment of a microsphere is a function of its radius (R) and oil-water-particle contact angle (θ), $\Delta G_{detach} = \pi R^2 \gamma_{ow}(1 - |cos\theta|)^2$, where γ_{ow} is the oil-water interfacial tension (*89*). Generally, the desorption energy of low-molecular weight surfactants is less than 10 kT (*92*), while the particles with a size of 10 nm has a desorption energy of several thousands kT (*93*), which means the absorption of particles at the water-oil interface is almost irreversible.

After the particles have completely covered the droplet surface, the shell needs to be reinforced by locking the particles on the droplet surface. Because the last step of producing colloidosomes entail the removal of the emulsion interface. The unique point that distinguishes colloidosomes with other microcapsules is that the droplets have the same internal phase and external phase. The droplet extraction can be achieved either by transference of droplets to a fresh internal fluid or by dissolution of the internal fluid. And this no-surface tension system allows for the permeability of colloidosomes are solely influenced by interstitial holes in the shell. After the droplet extraction/collection, there will be no water-oil interface, and thus no surface tensions existing between two immiscible fluids. Even though the particle detachment energies are quite high, the fixation of particles at the emulsion interface is of great necessity when there is no surface tension to drive the self-assembling of particles.

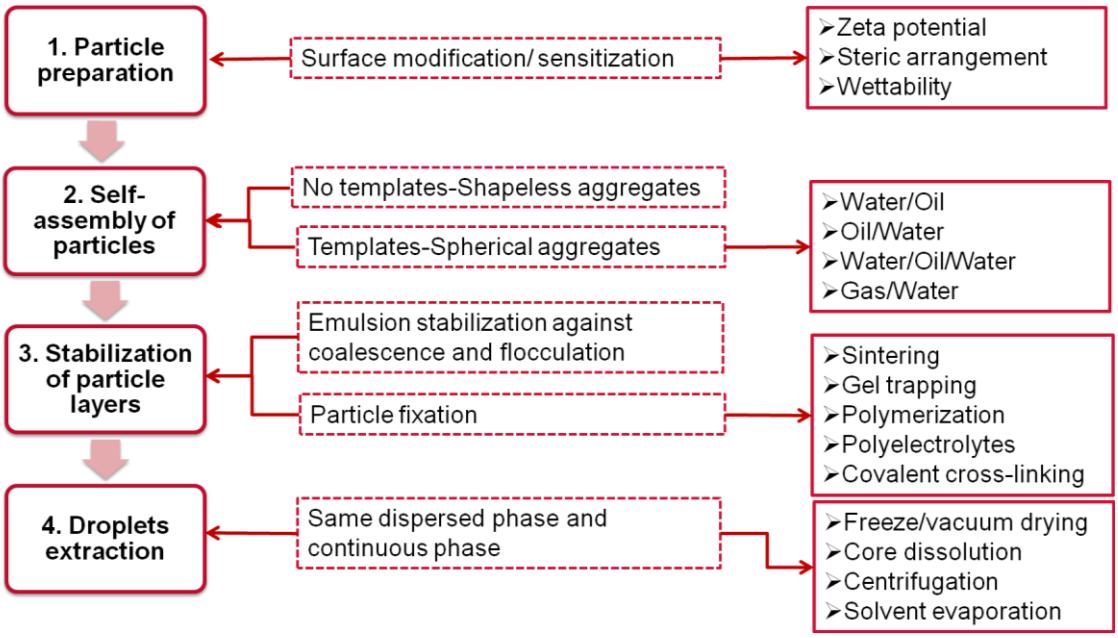

Figure I- 2. Concrete flow chart of recent methods for the fabrication of colloidosomes.

Step 1-Particle preparation: Up till now, colloidosomes have been fabricated using various colloidal particles, such as polymeric colloidal particles, e.g. poly(tert-butylaminoethyl methacrylate) latexes (*94*) and sulfate/amidine polystyrene latexes (*95*, *96*), and inorganic colloidal particles, e.g. Fe_3O_4 (*97*), TiO_2 (*98*), Laponite nanoparticles (*99*), and mostly surface modified silica particles (*87*, *100-103*). Colloidosomes are constructed based on Pickering emulsions as core templates. Materials that can be used to form Pickering emulsions are candidate materials for colloidosomes. However, there was few report about the formation of colloidosomes using biomass-based colloidal particles.

Step 2-Self-assembly of particles: The self-assembly behavior occur during the emulsification or homogenization of emulsions. The homogenization speed and time is of great significance on the stability of colloidosomes. Smaller droplets are usually more stable than larger ones, because larger droplets (diameter > 100 um), according to previous experience, can hardly survive in the droplet extraction step. Higher energy

input (revolution per mins) and longer times leads to smaller mean size of droplets. At the same time, smaller droplet size provides larger water-oil interfacial areas. Special attention should be paid on the surface coverage of particles during homogenization, checking whether there are enough particles to fully cover the interface.

Choose suitable oil phase is also very important. For oils, they do not have HLB values. But they have required HLB values for surfactants. Colloidosomes can be prepared using non-volatile vegetable oils as oil phase just like other regular emulsions (*104*, *105*), but the oil phase is not limit them. Many organic solvents that are immiscible with water have been used as the "oil" during the preparation of colloidosomes, like dichloromethane, xylene, chloroform, dodecane, toluene, etc (*105-108*). Because these organic solvents allow for a clearly defined interface between oil and water phase, and facilitate an easy droplet extraction at the same time through dissolving, washing, and evaporating (*106*). Some publications chose octanol as oil phase due to its un-dissolving and un-swelling properties towards polystyrene microspheres (*96*). However, sometimes the swelling of colloidal particles seems to be desirable. It was found that amine–latex particles would swell on the tricaprylin-water interface, and the obtained capsules remained intact during the droplet transference even without strengthening of the particle monolayer (*104*). The desired swelling of particles reduced the porosity of capsules and improved the stability of them as well.

Step 3-Stabilization of particle layers: The shell reinforcement is very important for the preparation of colloidosomes so as to survive the removal of oil/water template. There are several different strategies that lock colloidal particles together at the oil-water

interface, including heat sintering, gel trapping, polymerization, polyelectrolytes deposition, and covalent cross linking.

Heat sintering: In order to fix polystyrene latex particles on the surface of droplets, heating sintering is usually applied by heating the emulsion to above the glass transition temperature (Tg) of the particles so as to fuse them together. After particles are partially or completely melt on the droplet surface, the mobility of particles seems to be impossible. And the fusion of latex particles provides a smooth surface at the interface. The heat sintering temperature of latex particles is around 105 ˚C (*83*), which is above the boiling point of water. Thus in order to minimize the evaporation of the water phase, 50% of glycerol can be added to raise the boiling temperature (*83*). Volatile organic solvents are utilized as the oil phase. In order to reduce the loss of core template during sintering, 50% vegetable oil can be mixed with the volatile oil phase (*83*). The disadvantage of this method is that it is not suitable to encapsulate materials that are incompatible or sensitive to elevated temperatures. By choosing particles with lower glass transition temperature, the sintering temperature can be adjusted to lower level. And more importantly, Pickering emulsions stabilized by insoluble protein particles have poor heat stability under high temperature, and emulsions tend to break down when temperature is higher than 40 ˚C. So this method is not suitable to strength zein stabilized Pickering emulsions.

Gel trapping: The gel trapping technique is to use gelling agent (e.g. 1.5% agarose solution) as water phase to trap particle monolayers at the emulsion interface (*104*). During emulsification, the agarose solution was kept at 75 ˚C to permit a good fluidity of the water phase. After emulsification, the formed droplets were left to cool down to room temperature. Rigid gel cores were then formed, which firmly stick

colloidal particles on the droplets surface, and provide enough stiffness to maintain integrity in the droplet extraction step. The gelling agents usually require high temperature (over 95˚C for agarose) to fully dissolve and melt them (*104*). So this method, similarly to the heat sintering method, is not suitable to encapsulate heat sensitive materials or living cells. In addition, since encapsulated nutrients or drugs are trapped in gel matrix, the diffusion release will be largely retarded.

Polymerization: In order to traps the particles at the emulsion interface, polymerization is conducted either at the outer surfaces (*109*), or at the inner surfaces of droplets (*110*). The outer surface polymerization was achieved by grafting polymers through surface initiated-atom transfer radical polymerization (SI-ATRP) reaction (*109*). Inner surface polymerization is based on accelerated solvent evaporation (ASE) method (*111*). Polymers are firstly dissolved in a good solvent. Once the emulsion is formed, the solvent was rapidly removed by rotary evaporation. This will cause precipitation of polymers at the inner surfaces of droplets, so that colloidal particles are trapped there, forming hollow colloidosomes. For example, through evaporating dichloromethane from dichloromethane/n-hexadecane mixture, poly (methyl methacrylate) (PMMA) precipitates onto the interior surfaces of silica particles stabilized microcapsules, producing a robust shell structure (*110*). Polycaprolactone (PCL) and polystyrene (PS) are other alternative polymers that work similarly as PMMA and can form a polymer film at the interface (*112*). This strategy can be achieved only through oil-in-water emulsions. The organic oil phase should be encapsulated in the droplets, so that particle walls can provide a surface for the subsequent coating of polymers after solvent evaporation. Colloidosome cores fill up with water through interstitial holes after organic solvent is

evaporated. Therefore, one advantage of this method is that it does not require the droplet extraction step and directly producing a w/w colloidosomes. However, oil-in-water emulsion templates limit the encapsulation of water soluble ingredients. And if oil soluble components are encapsulated in the capsules, the encapsulants will precipitate or re-crystallize at the inner walls of droplets after solvent evaporation. So it seems quite hard to increase the bioavailability of oil soluble drugs/nutrients through this method.

Polyelectrolytes deposition: The deposition of polyelectrolytes with opposite charges through electrostatic attraction force is another strategy to reinforce the shells of colloidosomes. Liu and co-workers coated polyethyleneimine (PEI)–Laponite based Pickering emulsions by alternate adsorption of negatively charged sodium alginate and positively charged chitosan (*108*). Interestingly, there was another paper that used positively charged silica particles (SiO_2NH_2) and negatively charged ones (SiO_2COOH) to coat whey protein emulsions through layer-by-layer (LbL) technique (*103*) . The polyelectrolyte absorption not only improves the stability of colloidosomes, but also has great influence on their permeabilities. The larger number of polyelectrolyte layers on the microcapsules is, the slower the release profile will be. For instance, ibuprofen-loaded $(ALG–CS)_3$, $(ALG–CS)_4$, $(ALG–CS)_5$ microcapsules have a cumulative release percentage of about 80%, 60%, and 50%, respectively after 700 min diffusion at pH 7.4 (*108*). The “n” in $(ALG–CS)_n$ refers to number of polyelectrolyte double layers coated on microcapsules.

Special attention should be paid on the operation of this LbL technique. The biggest challenge of using LbL technique is to prevent emulsions from coalescence, aggregation, and flocculation in the early stage of deposition. If the polyelectrolytes

concentration is not high enough to saturate the surfaces of droplets, which means two adjacent droplets may share one polyelectrolyte, the bridging flocculation will occur. If the polyelectrolytes concentration is too high, the attractive depletion forces in the emulsions will be strong enough to overcome various repulsive forces (e.g., electrostatic repulsion and steric hindrance), resulting in a depletion flocculation of droplets (*113*). What's more, it is also possible that stabilizers would detach from the oil-water interfaces during those washing steps after the deposition of each layer.

Covalent cross-linking: For protein coated colloidosomes, glutaraldehyde is usually applied as a strong coagulant to cross bind proteins (*84*, *96*). The initial concentration of glutaraldehyde should not be too high, otherwise the coagulation would be so quick that particles have few time to form ordering structure at the interface. However, it was found that glutaraldehyde cross-linked products have poor biocompatibility and could induce apoptosis of human osteoblasts (*114*).

Step 4-Droplets extraction: In order to convert Pickering emulsion precursors into microcapsules, the core material can be removed by various approaches, including solvent evaporation(*101*), freeze-drying (*103*), and organic solvent treatment, such as ethanol (*104*) or 2-propanol (*108*). Ethanol can dramatically increase the mutual miscibility of oil phase and water phase. It was reported that 15% octanol (v/v) can be dissolved in 50% ethanol-water solution (*96*). As a result, ethanol is widely used to dissolve the oil phase in both water-in-oil emulsions (*104*) and oil-in-water emulsions (*96*). An alternative approach to remove oils from inner side of droplets is the usage of micellar solution of Tween 20 (*96*). And the oil mixed surrounding environment can be replaced by water through diluting, centrifuging, washing and re-suspending. For water-

in-oil emulsions, the oil phase is the external continuous phase. The removal of oil, in this case, does not depend on the dissolution, but the dilution of oils using alcohols, mainly ethyl alcohol. Centrifugation is the subsequent step to collect droplets at the bottom layer.

3.3.2. Controlled permeability of colloidosomes

Permeability of colloidosomes has great influence on the release of encapsulated materials. Poor permeability indicates a sustained release of drugs and nutrients. The release of encapsulated material from colloidosomes is through free diffusion process. Assuming that the shape of interstitial holes is approximately spherical, the time required for encapsulated substances to penetrate through holes is estimated as

$$t = (1 + \frac{\pi s}{4\eta R})/(4\pi DRC),$$

where D and C are the diffusion coefficient and the concentration of the encapsulated material, R is the radius of colloidosome, η(≈0.04) is the area fraction, and s is radius of interstitial holes (*115*).

Colloidosomes with thicker shell may have better mechanical strength, thus it requires larger shear-stress to trigger the release. By using novel colloidal particles, the release of the encapsulated materials from colloidosomes could be controlled by an on–off mechanism. For example, Horecha et al. prepared thermally responsive microcapsules using poly(N-isopropylacrylamide) (PNP) particles (*116*). There are various stimuli that could promote the dissolving, swelling and shrinking of the particles (*117*), such as salinity, humidity, heat (*118*), or pH (*119, 120*).

The particle fixation methods have a great influence on the permeability of colloidosomes. Through precisely tuning the structure of shell walls, the permeability of colloidosomes can be easily controlled.

Method 1-Tuning the size of colloidal particles: The interstitial holes between closely packed colloidal particles define the permeability of shells. Assume that colloidal particles are closed packed in a perfect hexagonal lattice. The size of interstitial holes is approximately estimated as 0.15 times of the diameter of colloidal particles (*83*). Therefore, the particle size sets the pore size of shells, and eventually influences the permeability of colloidosomes. For instance, colloidosomes prepared by the assembling of particles with diameter of 1.3 um and the coating of poly-L-lysine, allowed for a free penetration of 0.1um-diameter particles, while a complete impermeability of 1 um-diameter particles(*83*). From recent published papers, it was shown that the size of colloidal particles ranged widely from several micrometers (*96, 104*) to several nanometers (750-25 nm) (*106, 121*). The size of inorganic colloidal particle could be even smaller. The size of Fe3O4 nanoparticles to form colloidosomes was as small as 4-8 nm in diameter (*122*).

Method 2-Coating droplets with extra layers/films: Many shell stabilization methods mentioned in C.2.3 Section have the capacity to adjust the porosity of colloidosomes as well, including polyelectrolyte deposition, polymerization, and covalent cross-linking. So the similar content will not be discussed repeatedly here.

Method 3-Controlling the extent of sintering: For polymeric latex particles, the easiest way to reduce the interstitial holes in the shells is to heat the droplets dispersion above the glass transition temperature of the colloidal material, forming a continuous shell with smaller porosity. After sintering at 105°C for 5 min, colloidosomes prepared by 0.9 μm-diameter polystyrene particles are impermeable for 0.5 μm-diameter probe particles, while fcompletely permeable for 0.1 μm-diameter ones (*83*). With an increase

of sintering time, the pore size can be further reduced.

Method 4-Adjusting shell thickness through different emulsification methods: Besides coating droplets with extra layers or films, preparation of double emulsions is an alternative method to tune the shell thickness of colloidosomes. Thick shells allow for a relatively low permeability and a sustained release for encapsulated materials. By controlling the emulsion dimensions and the concentration of nanoparticles in the oil phase, colloidosomes with a wide range of shell thicknesses (from 100 nm to 10 mm) can be achieved through double emulsions (*123*).

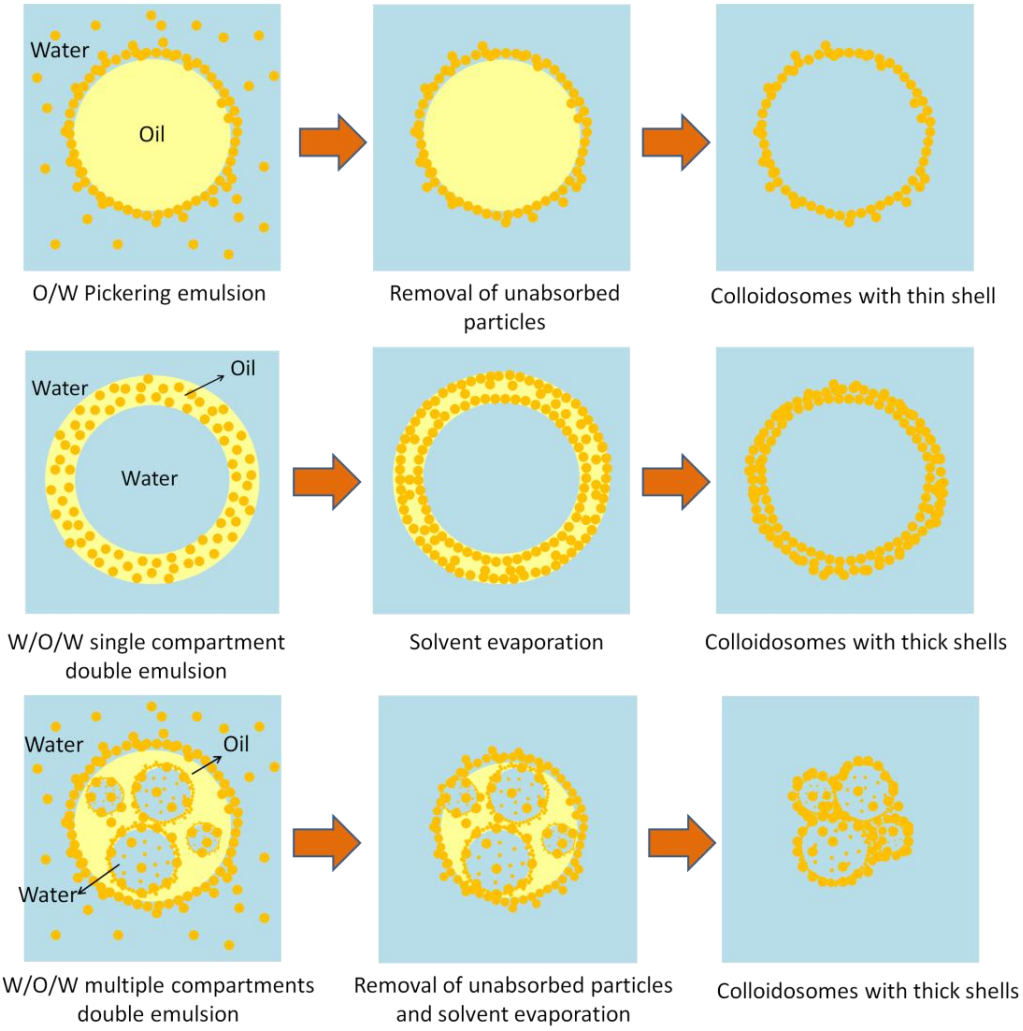

Figure I- 3. Schematic graph of colloidosomes with tunable shell thickness.

Thicker colloidosome shells are prepared either through double emulsions with single compartment, or double emulsions with multiple compartments (Figure I-3). Hydrophobic silica particles can be easily dispersed in the volatile oil phase (e.g. toluene, chloroform, dichloromethane, etc). In the case of single double emulsion, after evaporation of the middle oil phase, the hydrophobic silica particles have no place to go but gather together and form densely packed particle layers, which are inevitably thicker than the ones formed single emulsions. Increase the volume ratio of primary emulsion to the secondary emulsion will increase the volume of oils at the middle layer. Higher oil volume and colloidal particle concentration in oils lead to larger shell thickness after evaporation.

In the case of zein colloidal particles, which are more preferable to stay in water, zein particles may not disperse evenly in those volatile organic solvent. And due to the lack of glass microcapillary devices, it's very difficult to produce double emulsions with single compartment. However, through cyclic scheme of high-speed homogenization, double emulsions with multiple compartments can be prepared easily. The inner core of secondary emulsion consists of numbers of small emulsion droplets. After the evaporation of oils, the interfacial particles of secondary emulsions will assemble automatically onto the droplet surface of the primary emulsions.

The similar structure was reported by Lee and co-workers, that they used hydrophobic SiO2 nanoparticles (in the oil phase) and poly (vinyl alcohol) (in the water phase) to stabilize double emulsions (*124*). Upon the removal of the oil , nanoparticles in the oil phase eventually become the shell of colloidosomes, generating nonspherical

colloidosomes with multiple compartments (*124*), like the structure as shown in Figure I-3.

3.3.3. Applications

The biggest advantage of colloidosomes compared with other delivery system is that they can have precisely controlled size and permeability. Many literatures have mentioned that colloidosomes can serve as potent delivery devices for nutrients and drugs (*125, 126*). However, to the best of the author's knowledge, no specific example can be found for the encapsulation of certain drugs or nutrients. The superstructure of colloidosomes may provide a rigid scaffold for the growth of living cells, enhance the viability of the cells, and simultaneously offer a protection for the cells from the immune system (*127*). The high porosity allows free diffusion of gases and small macromolecular nutrients (*83*). In addition, the encapsulation of viable cells also allows for an increase of cell density, an ease of cell separation, a protection against harsh environment, and a controlled metabolism rate (*128, 129*). Through using a biologically friendly method, water-core colloidosomes, stabilized by poly (methyl methacrylate-co-butyl acrylate) latex particles, were able to an encapsulation of living microorganisms, i.e. yeast cells in this case (*129*). The encapsulation of yeast cells was able to effectively reduce the metabolizing rate of glucose from solution due to a large diffusive resistance of glucose through the colloidosome shells (*129*). Another functionality of colloidosomes is to encapsulate enzymes for biocatalytic reactions in a biphasic system (*130*). Many enzymes only have catalytic activities in water, while the reactants are only soluble in organic solvents that are immiscible with water. Biocatalysts may become denatured under a long time exposure to an organic solvent. The microencapsulation of biocatalysts increases

catalytic performance of enzymes, minimizes enzyme inactivation, and simultaneously facilitates enzyme separation and recirculation (*131*).

3.4. Resveratrol

Resveratrol is a plant phytoalexin mainly found in grape, peanut and other few plants (*132*). It was synthesized in the plant from p-coumaroyl CoA and malonyl CoA in response to fungal infection, stress, injury, or UV-irradiation (*133, 134*). A plethora of studies have shown that resveratrol exhibits good anti-oxidation (*135*), anti-inflammation (*136, 137*), anti-virus (*138-140*), neuroprotection (*141-143*), cardio-vascular protection (*144, 145*), and anti-cancer properties (*146-148*), especially for colon cancer (*149, 150*). In the lower gastro-intestinal (GI) tract, resveratrol also displayed good therapeutic effects on colitis by protecting the colonic mucosa architecture, mitigating the induced anemia, and reducing the production of systemic inflammation markers (*151*).

Even though resveratrol displays potent health beneficial effects on colon, only limited amount of resveratrol can be delivered into it. According to human clinical studies, at least 70% of resveratrol was absorbed through small intestine by a rapid passive diffusion (*152*). And then 71-98% of resveratrol was quickly excreted from urine 7-15 hrs after oral administration (*153*). The absorbed resveratrol was metabolized in enterocytes (*154*) and liver cells (*155, 156*) by sulfation and glucuronidation reactions. The amount of resveratrol excreted from feces was much smaller, varies between 3.3 and 35% (*152*). Therefore, in order to prevent resveratrol from being absorbed in the upper GI tract, colon-specific delivery systems should be developed.

3.4.1. Colon-related health beneficial effects of resveratrol

Anti-Colon cancer: The anti-colon cancer ability of resveratrol was associated

with its anti-proliferation effect and cell death promotion effect. Resveratrol inhibits the proliferation by arresting cell cycle progression (*157*) and promoting cell differentiation (*158*). After treatment with 25 μmol/L of resveratrol, a growth inhibition at the S/G2 phase transition was observed in human colonic adenocarcinoma cell line Caco-2 cells, and ornithine decarboxylase activity was reduced (*149*). At concentrations up to 50μmol/L of resveratrol, perturbation of cell cycle progression from the S to G2 phase was also observed on the Caco-2 and the colon carcinoma cell line HCT-116 (*157*). Resveratrol decreased the expression of cyclin D1 and cyclin-dependent kinase (Cdk) 4 proteins, while did not affect the levels of Cdk2, Cdk6 and proliferating cell nuclear antigen (*157*). Cyclin D/Cdk4 complexes regulate the cell cycle progression from the G1 phase to the S phase and they are responsible for the phosphorylation of a tumor suppressor, retinoblastoma protein (pRb). And the hypophosphorylated pRb could cause a blockage in G1 phase, since it sequestered the transcription factor E2F in the cytosol, and subsequently suppressed protein expression in the cell cycle (*157*). $p21^{WAF1/CIP1}$ protein, as cyclin-dependent kinase inhibitor, prevents the Cyclin E/Cdk2 induced phosphorylation of pRb, thus inhibiting cell cycle progression at G1 phase (*159*). It was reported that resveratrol reduced the $p21^{WAF1/CIP1}$ protein level in the normal surrounding mucosa, but upregulated Bax expression and inhibited growth of colorectal aberrant crypt foci in azoxymethane induced carcinogenesis of the rat colon (*160*), which indicated that resveratrol had exclusive inhibition effect on cancer cells rather than normal cells. When the concentration of resveratrol exceeding 50 μM, the phosphorylation state of the pRb changed from hyperphosphorylated to hypophosphorylated at high concentrations, which results in a reversal of the S phase arrest (*157*).

Resveratrol exhibits the anti-proliferation effects through regulating the activities of various enzymes. SIRT1 deacetylase is an important enzyme that gets involved in prolonging lifespan, reducing cell proliferation in colon cancer cell lines (DLD-1, HCT-116 and RKO cells), and suppressing of turmorigenesis in a similar way as calorie restriction in the $APC^{min/+}$ mice model of colon cancer (*161*). Resveratrol was able to increase the level of SIRT1 deacetylase by competitively inhibiting activity of cAMP-degrading phosphodiesterases and triggering a cascade of events, including elevation of cAMP, activation of Epac1, increase of intracellular Ca^{2+}, and activation of the CamKKb-AMPK pathway, which eventually ameliorated the symptoms of metabolic diseases related to aging (*162*). Therefore, it was considered that the suppression effect of trans-resveratrol against colon cancer was due to the activation of SIRT1 deacetylase (*163*). Resveratrol can also decrease the activity of ornithine decarboxylase (ODC), a key enzyme of polyamine biosynthesis, by inactivation of protein kinase C (PKC) (*149*). ODC is an essential enzyme for cell growth and the ODC level is enhanced in cancer cells, since polyamine is important for the stabilization DNA structure. An inhibition of ODC activity might one of the mechanisms that get involved in the anti-proliferative effects of resveratrol (*149*). And resveratrol mainly showed cytostatic property, rather than cytotoxic effect on the human colon cancer CaCo-2 cells in this study (*149*).

Resveratrol promotes the cell differentiation by intensifying the differentiation-inducing effect of butyrate (*158*). Butyrate is a typical metabolite from the digestion of gut microbiota on unabsorbed dietary fibers. At physiologically relevant concentrations, butyrate induces rapid cell differentiation in colon cancer cell lines, and induces apoptosis in adenoma cell lines (e.g. RG/C2 and AA/C1) and carcinoma cell lines (e.g.

PC/JW/F) (*164, 165*). And chemo-preventive benefits of butyrate are influenced by many factors, including concentrations, exposure time, and the type of fat in the diet (*166*). In the colon cancer cell lines, resveratrol can also increase the butyrate's induction of $p21^{Waf1/Cip1}$ expression (*158*).

Cell death has different pathways, including apoptosis, necrosis, mitotic catastrophe and autophagy (*167, 168*). Cell death can also be divided into unregulated cell death like necrosis, regulated cell death like apoptosis, and regulated non-apoptotic cell death like autophagic cell death, necroptosis, and PARP1-mediated cell death (*169*). Reveratrol promotes cell death through inducing caspase-independent apoptosis in the CEM-C7H2 T-ALL cell line (*170*), or inducing caspase-dependent apoptosis in human leukemia U-937 cell line (*171*), or inducing regulated autophagocytosis in ovarian cancer cells (*172*).

Apoptosis cell death is quite different from autophagocytosis. Apoptosis destructs cellular structures and organelles by explosively activating catabolic enzymes, while autophagy is a slow and circumscript phenomenon where parts of the cytoplasm are wrapped in vacuoles and gradually digested by lysosomal hydrolases (*168, 173*). The apoptotic cells undergo progressive cellular condensation and budding, and eventually form small round bodies engulfed by resident phagocytes (e.g., epithelial cells or fibroblasts) (*168*). There are two principal pathways for the apoptosis, i.e. the intrinsic pathway where the cytotoxic stress primarily influences mitochondrion to release molecules to promote the caspases activation, and the extrinsic pathway where external stimuli binds at "death receptors" on the cell surface to initiate the activation of caspases (*168, 169, 174*). The intrinsic pathway is modulated by two groups of molecules, Bcl-2

and Bax. Bcl-2 serves as an ion channel and regulates the release of cytochrome c from mitochondrial (*175*). But overexpression of Bcl-2 attenuated resveratrol-induced apoptosis and blocked the biochemical cascade of apoptosis as well, since it prevented the accumulation of cytochrome c in the cytosol and maintained caspase-3 in an inactive zymogen state (*171*). Recent evidence suggests that resveratrol-mediated apoptosis is associated with caspase-3 activation, phospholipase C-γ1 (PCL- γ1) degradation and cytochrome c release (*171*).

Present studies demonstrated that cell death activated by resveratrol can be mediated through endoplasmic reticulums (ER) (*176, 177*). The ER is a principal site for protein synthesis and protein modification before being delivered to other secretory organelles (*178*). ER stresses, also known as the abnormalities in the ER, is caused by many factors, including defective folding of ER proteins, perturbation of the Ca^{2+} gradient built up across the ER membrane (*168*), calcium store depletion, reduction of glycosylation or disulfide bonds formation, and over-expression of mutant proteins (*177*). Resveratrol leads to ER stress-induced apoptosis by inducing the expression of growth arrest-and DNA damage-inducible gene 153 (GADD153) (*176*), inducing the expression of Glucose-regulated protein 78 kDa (GRP78) and C/EBP homologous protein (CHOP), inducing splicing of XBP1 mRNA, inducing the depletion of intracellular Ca2+ stores, promoting the activity of caspase-4 (*177, 178*), and inducing the phosphorylation of eukaryotic initiation factor-2α (eIF-2α) (*178*). Typically the CHOP gene is triggered by cellular stress (*179*). Resveratrol induced the expression of CHOP in a dose-dependent manner by mediating the Sp1 transcription factor, and down-regulation of CHOP by mithramycin A and siRNA attenuated resveratrol-induced apoptosis (*176*). When the

caspase-4 activity is inhibited by z-LEVD-fmk, the resveratrol-induced apoptosis is significantly reduced (*177*).

Besides above mentioned mitochondria and endoplasmic reticulums, lysosomes, acting as death signal integrators, are the other important cytotoxic mechanism for resveratrol-induced apoptosis (*180*). In colorectal cancer cells, resveratrol cytotoxicity was related to up-regulation of lysosomal cathepsin D (CD) expression and, conversely, siRNA-mediated down-regulation of lysosomal CD expression and Pepstatin A inhibited lysosomal CD expression prevented caspase activation in resveratrol-treated cells and then abolished the cytotoxic effect of resveratrol (*180*). So there is a hierarchy of the proteolytic pathways, in which the lysosomal CD acts upstream of caspase activation, while Bax is a probable target of the lysosomal CD (*180*). And it was considered that resveratrol induces apoptosis through Bax conformational activation in colorectal cancer cell lines (*181*).

Autophagy, as a non-apoptotic cell death, is an evolutionarily conserved catabolic process, during which double membrane-bound vesicles are elongated to from autophagosomes, and then autophagosomes fuse with lysosomes to form autolysosomes, and the autolysosomes are degraded eventually by incorporated organelles (*182*). Autophagocytosis induced by resveratrol was observed on the ovarian cancer cells (*172*). In human colon cancer cells, the autophagy induced by resveratrol is mediated through intracellular reactive oxygen species (ROS), which is correlated to the induction of Casapse-8 and cleavage of Caspase-3, and the elevation of microtubule-associated protein 1 light chain 3 (LC3)-II (*182*). And the resveratrol induced autophagy was cytotoxic, since the addition of the autophagy inhibitor 3-methyladenine caused a

significant decrease in apoptosis together with a decrease in the cleavage of Casapse-8 and Caspase-3 (*182*). As for the unregulated cell death, resveratrol did not lead to necrosis even at concentrations with full inhibition of cell growth (*183*). Whether the cells will undergo necrosis or apopotosis is at least partially determined by the abundance of intracellular energy stores, and the main feature of necrosis is a dramatic increase in cell volumes (oncosis), eventually leading to a rupture of plasma membranes and the unorganized demolishment of swollen organelles (*168*).

There are four phases of carcinogenesis, including initiation (mutation of genes and transformation from normal cells to initiated cells), promotion (proliferation of preneoplastic cells), progression (transformation from preneoplastic cells to neoplastic cell), and metastasis (spread of cancer cells through the bloodstream or the lymph system) (*184*). Resveratrol was found to inhibit the initiation phase by acting as an antioxidant and antimutagen to induce the phase II drug-metabolizing enzymes (detoxifying enzymes), inhibit the promotion phase by acting as anti-inflammatory agent to reduce the activity of cyclooxygenase and hydroperoxidase, and inhibit the progression phase by inducing cell differentiation (*147*). Cyclooxygenase can catalyze the conversion of arachidonic acid to pro-inflammatory substances such as prostaglandins (*147*), so reduction of the cyclooxygenase activity effectively inhibits the inflammation and tumor cell growth. In an *in vivo* rat study on colon cancer, resveratrol was able to reduce both the initiation and the promotion phases in azoxymethane (AOM)-induced carcinogenesis and the mechanism of protective effect was involved in changes in Bax and *p21* expression (*160*). After administration of resveratrol (200 μg/kg/day

in drinking water) to male F344 rats for 100 days, the Bax expression was enhanced in the aberrant crypt foci (ACF) but not in the surrounding normal mucosa, and the *p21* expression was found in ACF of all groups and also normal mucosa of controls, but not in normal mucosa of resveratrol-treated groups, which led to the enhanced apoptosis in the ACF but not in normal mucosa of the resveratrol-treated rats (*160*). The concentration required for resveratrol to exert chemopreventive effects is relatively quite high, around 40-200 μM (*177*, *185*).

Conclusively, resveratrol was able to prevent colon cancer by interfering carcinogenesis at the initiation stage, inhibiting promotion and progression stage after the transformed cells were formed via arrest of cell cycles and promotion of cell differentiations, and eventually inducing cell death of cancer cells through apoptosis and autophagocytosis, as summarized in Figure I-4.

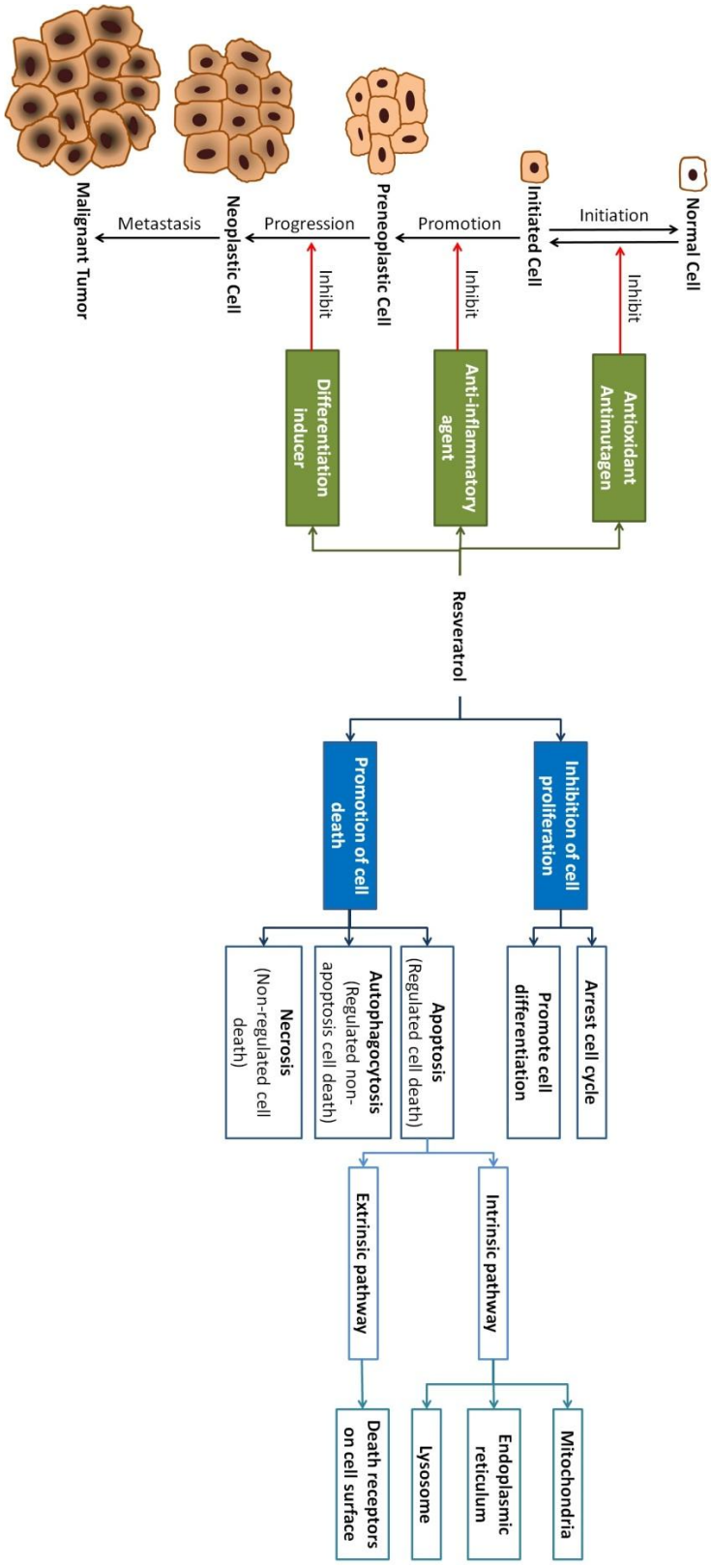

Figure I- 4. Schematic presentation of the anti-colon cancer effect of resveratrol.

Table I- 2. In vitro studies about the anti-colorectal cancer effects of resveratrol.

Cell lines/ Animal model	Concentration	Activities	References
HT-29 (colorectal adenocarcinoma)	Antiproliferation (EC50 :78.9±5.4 μM); activation of Caspase-3 (EC50: 276.1±1.7μM);	Mitochondria-mediated apoptosis: ↑production of superoxide anions in the mitochondria of cells; ↑ caspase-3 activity	(*183*)
DLD-1 (colorectal adenocarcinoma) and HT-29	1, 10, 100 μM	Caspase-dependent intrinsic pathway of apoptosis: ↑ accumulation of mature lysosomal cathepsin D (CD), ↑ lysosome leakage, ↑cytosolic immunoreactivity of CD	(*180*)
HT-29	20, 40, 60, 80, 100 μM	Endoplasmic reticulum stress-mediated apoptosis: ↑ phosphorylation of eukaryotic initiation factor-2α (eIF-2α); ↑ ER stress-specific XBP1 splicing and CCAAT / enhancer-binding proteinhomologous protein (CHOP); ↑ glucose-regulated protein (GRP)-78	(*178*)
HT-29	20, 40, 60, 80, 100 μM	Endoplasmic reticulum stress-mediated apoptosis: ↑expression of proapoptosis gene (CHOP mRNA); ↑ CCAAT/enhancer-binding protein homologous protein (CHOP)	(*176*)
HT-29	10, 20, 40, 60 μM	Endoplasmic reticulum stress-mediated apoptosis: ↑ GRP78 and CHOP expression; ↑ splicing of XBP1 mRNA; ↑ caspase-4 activity; ↑ depletion of intracellular Ca2+ stores; ⊗ Akt protein phosphorylation;	(*177*)
HTB-37 /Caco-2 (colorectal adenocarcinoma) and HCT-116 (colorectal carcinoma)	12.5, 25, 50, 100, 200 μM	Anti-proliferation: ↓ cyclin-dependent kinase (Cdk) activity; ↓ the cyclin D1/Cdk4 complex; ↓ expression of cyclin E and cyclin A; ⊗cdk2, cdk6 and proliferating cell nuclear antigen	(*157*)
HTB-37 /Caco-2	50 μM	↑ cell differentiation; ↑ butyrate's effect on the induction of $p21^{Waf1/Cip1}$ expression	(*158*)
HTB-37 /Caco-2	10, 20, 25, 30 μM	Anti-proliferation: ↓ expression of protein kinase C; ↓ ornithine decarboxylase (ODC) activity; ↓ intracellular putrescine content; ⊗ apoptosis of CaCo-2 cells.	(*149*)

HT-29/COLO 201 (colon cell line)	25, 50, 75, 100, 150 μM	ROS-triggered autophage: ↑ poly(ADP-ribose) polymerase (PARP), Caspase-8 and cleaved Caspase-3; ↑ microtubule-associated protein 1 light chain 3 (LC3-II) level; ↑intracellular reactive oxygen species (ROS).	(*182*)

Note: ↑ refers to promotion or induction; ↓ refers to down regulation; ⓧrefers to no influence.

Anti-microbes: Generally speaking, resveratrol does not have strong toxicity towards gut microbes. It has a high minimum inhibitory concentration (MIC) value (≥1000 μg/mL) for most of the human associated bacterial, and only a few bacteria, such as *Klebsiella pneumoniae* and *Yersinia pseudotuberculosis,* were quite sensitive to resveratrol, with MIC values around 250 μg/mL (*186*). But for most polyphenolic compounds, they have certain anti-microbial properties, especially for those having pyrogallol groups, while those having catechol and resorcinol rings displayed lower anti-microbial activities (*187*). And the anti-microbial potency of polyphenols provides them opportunities to serve as antibiotics for bacterial infectious diseases or preservatives for food pathogens. For instance, *Proteus mirabilis* is an important pathogen that causes the infection of the urinary tract, and resveratrol displayed inhibitory effect on swarming motility and virulence factor expression of *P. mirabilis* in a dose-dependent manner (*188*).

Anti-obesity: It was reported that the anti-obesity effect of resveratrol was due to its mediation effects on gut microbes (*189*), and gut microbes in turn influence the metabolism, energy harvest, and fat storage in the body (*189*, *190*). After feeding high-fat diet mice with resveratrol (200 mg per kg per day) for 12 weeks, resveratrol increased the *Bacteroidetes*-to-*Firmicutes* ratios, increased the growth of *Lactobacillus* and *Bifidobacterium* while reduced the growth of

Enterococcus faecalis, and at the same time, body weight, visceral adipose weight, blood glucose, serum cholesterol, and serum triglyceride levels were significantly lowered (*189*). And the Pearson's correlation coefficient indicated that the higher the ratios of *Bacteroidetes*-to-*Firmicutes* were, the lower the body weight was (*189*). Another study found similar results that resveratrol improved glucose homeostasis in obese mice and obtained a higher ratios of *Bacteroidetes*-to-*Firmicutes* as well, when compared with vehicle-treated obese mice (*191*). A decrease in the relative abundance of *Turicibacteraceae, Moryella, Lachnospiraceae*, and *Akkermansia* and an increase in relative abundance of *Bacteroides* and *Parabacteroides* were observed in resveratrol-fed obese mice (*191*). In a rat study, people compared the counteraction effect of resveratrol and quercetin against gut microbiota dysbiosis produced by high-fat sucrose diet (HFS) (*192*). Even though resveratrol improved some metabolic derangements, they found quercetin had stronger impact on gut microbiota compositions than resveratrol, which significantly increased ratio of *Bacteroidetes*-to-*Firmicutes* and inhibited the growth of diet-induced obesity related bacterial such as *Erysipelotrichaceae, Bacillus, Eubacterium cylindroides*. Resveratrol, at the species level, significantly inhibited the growth of *Gracilibacter thermotolerans, Parabacteroides distasonis* and species from *Clostridia* class (*Clostridium aldenense, Clostridium hathewayi, Clostridium* sp. MLG661), while enhanced the amount of *Clostridium* sp. XB90 (*192*). *Clostridium aldenense* and *Clostridium hathewayi* species, belong to *Clostridial* cluster XIVa, are important butyrate producer (*193*), and dietary supplementation of butyrate was able to increase insulin sensitivity and the energy expenditure in high-fat diet fed mouse

(*194*). So this paper thinks the anti-obesity effect of resveratrol may not be due to the modification of the gut microbiota composition (*192*). More studies should be conducted to further illustrate the correlations among resveratrol, anti-obesity property, and gut microbiota.

Anti-inflammation: Resveratrol was able to alleviate 5% dextran sulfate sodium (DSS) induce colon colitis, which increased the growth of *Lactobacilli* and *Bifidobacteria* in feces and diminished the increase of pathogenic enterobacteria upon DSS administration (*195*). DSS is a water-soluble chemical colitogen with anticoagulant properties, which causes damages to the epithelial monolayer and an increase of colonic permeability, allowing the dissemination of proinflammatory factors (e.g. bacteria and their products) into underlying tissue (*196*). An increased interaction between microbiota and immune system is one of the important factors that initiate ulcerative colitis (*195*). After dietary administration of 1 mg/kg/day resveratrol for 25 days, the clinical symptoms of colitis were significantly attenuated and the histological degradation of colon wall structure was obviously reduced, even remained intact in some epithelium areas (*195*). According to gene expression analysis, resveratrol was able to down regulate the expression of both endogenous nitric oxide synthases (eNOS) and inducible nitric oxide synthase (iNOS) (*195*).

The aetiology of ulcerative colitis is closely related to biodiversity of gut microbiota. Inflammatory intestinal or peripheral joint disease cannot be developed when the HLA-B27 transgenic rats were raised in a germ-free environment (*197*). When germ-free transgenic rats were colonized with facultative or strictly anaerobic bacteria, colonic proinflammatory cytokine was expressed and colitis was gradually

induced by 4 weeks after bacterial exposure (*198*). Through human probiotic infusion (HPI) of fecal suspension into the colon by retention enemas, some symptoms of ulcerative colitis were improved after 1 week, and complete reversal of symptoms was observed in all patients by 4 months post-HPI (*199*). Irritable bowel syndrome (IBS) and ulcerative colitis (UC) were usually associated with a loss of *Bacteroides* species, such as *Bacteroides vulgatus, B. ovatus, B. uniformis, and Parabacteroides* sp. as compared with healthy volunteers (*200*).Therefore, it was considered that intestinal inflammatory diseases are closely related gut microbiota. Instead of direct fermentative properties like typical prebiotics, resveratrol promotes the growth of lactic acid bacteria and bifidobacteria indirectly by inhibition of certain specific gut microbial species like *E. Coli* and other enterobacteria (*195*). Probiotics, such as *Bifidobacterium*, *Lactobacillus*, and *Bacillus*, usually showed antagonistic effect against the growth of enterobacteria via reducing the colonization and invasion of tissues by enterobacteria (*195, 201*).

Anti-cardiovascular disease: Through modifying the gut microbiota compositions, resveratrol mitigated trimethylamine-N-oxide (TMAO)-induced atherosclerosis by decreasing TMAO levels and increasing neosynthesis of hepatic bile acid (*202*). TMAO is a metabolite of dietary choline, which promotes the risk of atherosclerosis. Atherosclerosis, also known as clogging or hardening of arteries, is caused by accumulative deposition of low-density lipoprotein cholesterol on artery walls, eventually forming large plaques that narrow down arteries. Cholesterol can be synthesized into primary bile acids in the liver, and subsequently metabolized by the gut microbiota into secondary bile acids through deconjugation,

dehydrogenation, and dehydroxylation reactions in the gut (*203*). Through hepatic bile acid neosynthesis effect, the obtained secondary bile acids can be further converted into bile acids in the liver (*203*). It was reported that cocktail mixture of probiotics, such as Lactobacilli (*L. casei, L. plantarum, L. acidophilus,* and *L. delbrueckii*), Bifidobacteria (*B. longum*, *B. breve,* and *B. infantis*), and Streptococcus (*S. salivarius*), could promote hepatic bile acid neosynthesis by the down regulation of the enterohepatic FXR-fibroblast growth factor 15 (FGF15) axis (*203, 204*). Therefore, since resveratrol significantly increased levels of the genera *Lactobacillus* and *Bifidobacterium* (*202*), it has a great potential to act as therapeutics of bile acid dysmetabolism, similar to the functionality of probiotics and prebiotics. In addition, an in vivo human study showed that regular moderate consumption of red wine (272 mL/day), which is abundant in resveratrol, could reduce systolic and diastolic blood pressure, reduce the C-reactive protein, triglyceride and cholesterol level, increase the diversity of the fecal microbiota, and promote the growth of *Enterococcus, Prevotella, Bacteroides, Bifidobacterium, Bacteroides uniformis, Eggerthella lenta*, and *Blautiacoccoides–Eubacterium rectale* groups (*205*).

Table I- 3. In vivo studies about the modification effects of resveratrol on gut microbiota.

Model	**Dose of resveratrol (RES); Stress**	**Effects**	**Change on gut microbiota**	**References**
Male Kunming mice	200 mg/kg BW/day for 12 weeks; High-fat diet (50% calories in fat)	↓body weight gain; ↓liver index; ↓adiposite index. **Anti-obesity**	↑*Bacteroidete*s-to-*Firmicutes* ratios; ↓*Enterococcus faecalis;* ↑*Lactobacillus;* ↑*Bifidobacterium.*	(*189*)

Male C57BL/6N mice	Normal or high-fat/high-sugar (HFHS) diet plus 0.4% resveratrol for 8 weeks;HFHS diet (45 kcal% fat, 17 kcal% sucrose)	↑glucose tolerance; ↓fat mass. **Anti-obesity**	↑*Bacteroidete*s-to-*Firmicutes* ratios; ↓*Turicibacteraceae, Moryella, Lachnospiraceae,* and *Akkermansia*; ↑*Bacteroides* and *Parabacteroides.*	(*191*)
Wistar rats	15 mg/kg BW/day for 6 weeks; High-fat sucrose diet (45% calories in fat)	↓body weight gain; ↓serum insulin. **Anti-obesity**	↓*Gracilibacter thermotolerans, Parabacteroides distasonis* and species from *Clostridia;* ↑*Clostridium* spp.	(*192*)
Male Fischer F344 rats	1 mg/kg BW/day for 25 days (equivalent to 10 mg/day in a 70 kg person); 5% dextran sulfate sodium	↓anemia; ↓colon shortening; ↓NO, COX-2, and PTGES level. **Anti-inflammation**	↑*Lactobacillus;* ↑*Bifidobacterium;* ↓*Escherichia coli* and *Enterobacteria.*	(*195*)
C57BL/6J and ApoE$^{-/-}$ mice	A chow diet with 0.4% of RES; Diatery choline or trimethylamine	↑hepatic bile salt (BA) neosynthesis; ↑CYP7A1 expression; ↓enterohepatic FXR-FGF15 axis; ↓TMAO level; ↑BA hydrolase activity; ↑bile acid deconjugation and fecal excretion. **Anti-atherosclerosis**	↑*Lactobacillus* and *Bifidobacterium.*	(*202*)
Healthy male volunteers	De-alcoholized red wine (272 mL/d), red wine (272 mL/d), or gin (100 mL/d) for 20 days	↓systolic and diastolic blood pressures; ↓plasma triglyceride, total cholesterol, and HDL cholesterol; ↓C-reactive protein. **Anti-cardiovascular disease**	↑*Enterococcus, Prevotella, Bacteroides, Bifidobacterium, Bacteroides uniformis, Eggerthella lenta,* and *Blautiacoccoides–Eubacterium rectale* groups	(*205*)

3.4.2. Colonic bioconversion of resveratrol

After oral administration, about 70-75% of the oral-intake resveratrol can be absorbed in humans mainly through transepithelial diffusion effect (*152, 206*), and then it undergoes extensive metabolism in the small intestine and liver. Based on several human studies, the major metabolites found in plasma and in urine are glucuronides and sulfates of resveratrol, including trans-resveratrol-3-O-sulfate, trans-resveratrol-3,4'- disulfate, trans-resveratrol -3,5-disulfate, trans-resveratrol -3-glucuronide, trans-resveratrol-4'-glucuronide and trans-resveratrol-diglucuronides (*152, 206-211*). The chemical structures of main metabolites of resveratrol have been illustrated in Figure I-5. In plasma samples, the detected metabolites, resveratrol-3-sulfate and resveratrol monoglucuronides, were up to 23 times greater than resveratrol in the area under the plasma concentration-time curve (AUC) values (*208*). The rapid sulfate conjugation by the intestine/liver was considered as the rate-limiting step for the bioavailability of resveratrol (*152*). Around 46% of the total detected trans-resveratrol diglucuronides was bounded with proteins in plasma, and the mean urinary excretion of trans-resveratrol-sulfate conjugates was quantitatively higher than that of the glucuronides, (*210*).

After the digestion and absorption in the upper gastric intestinal tract, the unabsorbed portion enters into colon for further colonic bacterial metabolism. And it is worth noticing that the colon not only receives unabsorbed bioactive compounds from small intestine, but also phase I and II metabolites excreted back by the enterohepatic cycle (*212*). The colonic microbiota transformation of resveratrol is

quite different from the intestine/liver metabolism, mainly in two aspects. First of all, instead of sulfation, glucuronidation and methylation reactions (*213*), bacterial transformation reactions of polyphenolic compounds usually include ring fission, reduction, demethylation, decarboxylation, dehydroxylation, and deglycosylation by certain bacterial enzymes (*212, 214*). And these colonic bioconversions usually converted resveratrol into more hydrophobic compounds. Secondly, colonic bacterial metabolism is very variable, highly depending on the individual differences of the gut microbiota composition. For instance, in an in vitro fermentation study, trans-resveratrol was incubated with feces donated from 3 volunteers. One fecal sample dehydroxylated resveratrol and reduced it into lunularin, and one reduced the double bound and transformed resveratrol into dihydroresveratrol, and the other one produced a mixture of dihydroresveratrol and lunularin (*215*). The in vitro fermentation result was further confirmed by an in vivo human study, in which volunteers were given an oral dose of 0.5 mg trans-resveratrol/kg body weight (*215*). By using the metagenomics approach to study the bacterial diversity of the feces at the phylum, family, and genus levels, it was found that feces sample which cannot produce dihydroresveratrol had a lower relative abundance in *Firmicutes* and higher abundances in *Bacteroidetes, Actinobacteria,Verrucomicrobia,* and *Cyanobacteria* than other feces samples (*215*). Dihydroresveratrol was considered mainly produced by *Slackia equolifaciens* and *Adlercreutzia equolifaciens*, which both belong to *Coriobacteriaceae* (*215*). In another study, *Eggerthella lenta* was identified as dihydroresveratrol producer (*186*). They incubated resveratrol with animal/human-associated bacterial, finding

that 11 of the 43 bacteria have the capability to transform at least 20% of the resveratrol by 48 h (*186*). Dihydroresveratrol was found significantly promoted the proliferation of the hormone-sensitive breast cancer cell line MCF-7 at a picomolar concentration, while trans-resveratrol was inactive at this concentration, and this proliferative effect was not observed in cell lines without hormone receptors (*216*). Another type of main metabolites of resveratrol was resveratrol glucosides, such as resveratrol-3-O-glucoside (piceid) and resveratrol-4'-O-glucoside (resveratroloside). *Bacillus cereus*, *Achromobacter denitrificans*, and *Escherichia coli* were identified as the producer of resveratrol glucosides (*186*). Besides resveratrol glucosides, *Bacillus cereus* was also able to produce phosphorylated resveratrol glucosides and glycerol adducts of phosphorylated resveratrol glucosides (*186*). Similar result was found in another study, saying that *Bacillus cereus* could transform resveratrol into piceid (*217*). Resveratrol is one of the main polyphenols in red wines, and it was reported that the gut microbial-derived metabolites of the polyphenolic red wine extract were small molecular weight phenolic acids like p-coumaric acid, benzoic acid, 4-hydroxyphenylacetic acid, etc (218). Therefore, the end microbial metabolites of resveratrol may be like the phenolic acids of other dietary polyphenols, but the specific types of phenolic acids produced by resveratrol were still unknown.

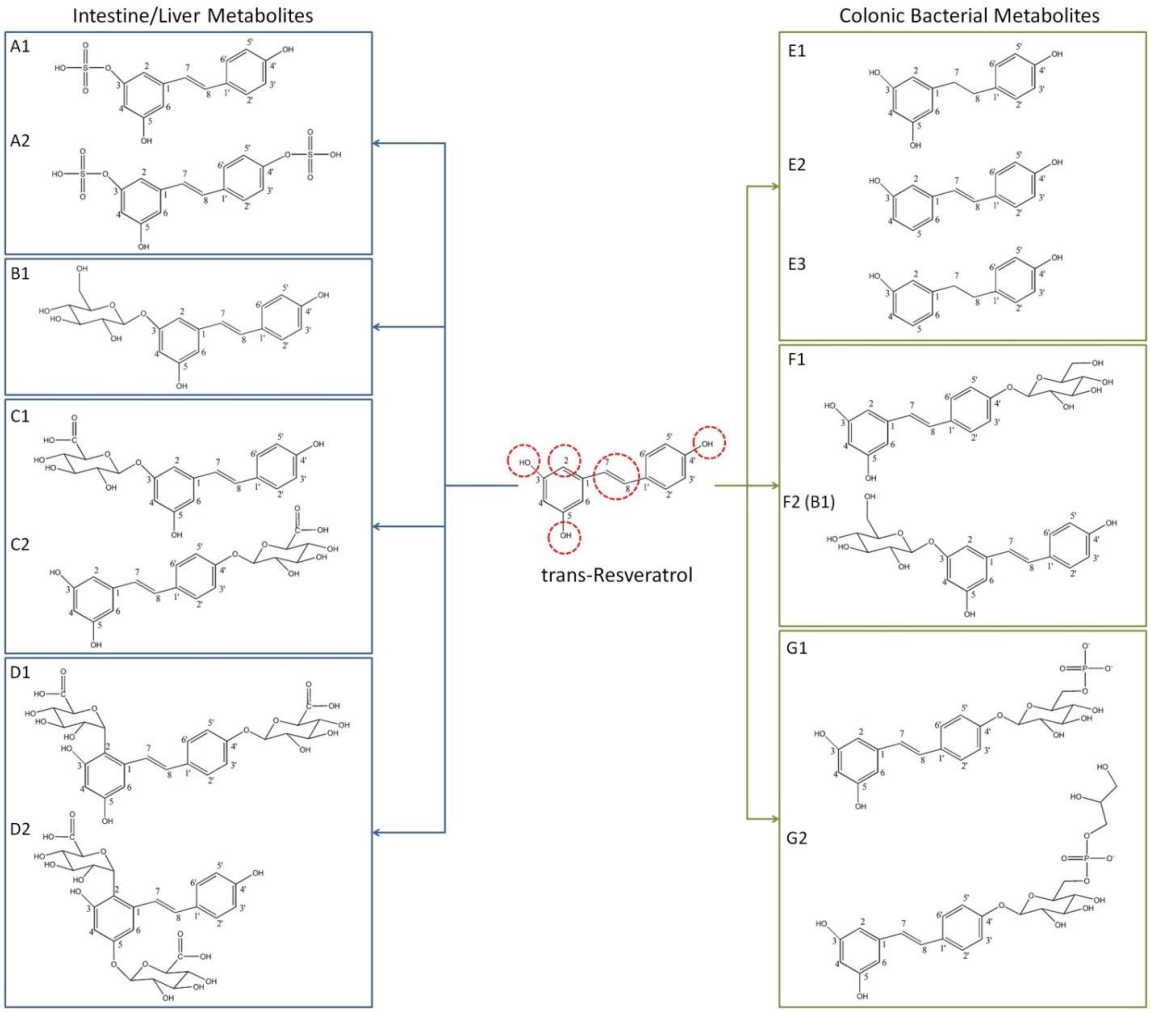

Figure I- 5. Proposed chemical structures of the metabolites of trans-resveratrol; trans-resveratrol-3-O-sulfate (A1), trans-resveratrol-3,4'-O-disulfate (A2), trans-resveratrol-3-O-glucoside (piceid) (B1, F2), trans-resveratrol-3-O-glucuronide (C1), trans-resveratrol-4'-O-glucuronide (C2), trans-resveratrol-2,4'-diglucuronide (D1), trans-resveratrol-2,5-diglucuronide (D2), dihydroresveratrol (E1), 3,4'-dihydroxy-trans-stilbene (E2), 3,4'-dihydroxybibenzyl (lunalarin) (E3), trans-resveratrol-4'-O-glucoside (resveratroloside) (F1), trans-resveratrol-4'-phosphorylated glucoside (G1), and trans-resveratrol-4'-glycerated phosphorylated glucoside (G2).

CHAPTER II. FABRICATION OF PICKERING EMULSIONS USING ZEIN AND SODIUM CASEINATE COMPLEXES, AND ITS APPLICATION ON ENCAPSULATION OF RESVERATROL

Partial contents in this chapter were adapted from the paper "Fabrication of Colloidosomes through Layer-by-layer Self-assembling using Biomass-based particles" and "Study of the bioaccessibility of formulated resveratrol using different dynamic gastric-intestinal digestion models" which were ready for submission.

1. Introduction

Successful assembly of particles at emulsion interface largely relies on their surface activities. The modification of surface properties, such as zeta-potentials and wettabilities, is always required so that particles are more preferable to absorb onto the interfacial areas. Particles with high electrostatic charges are quite stable when they are dispersed in fluid. However, surface charge should not be extremely high, because highly charged microspheres are too hydrophilic to absorb on the oil-water interface. And the assembly of these particles is energetically unfavorable due to the strong electrostatic repulsions between the adjacent particles. The pH of zein particle dispersion prepared by typical anti-solvent preparation method was around 4.0 (*57*), lower than the isoelectric point of zein. The isoelectric point of zein was initially estimated in a wide pH range of 5–9 due to its highly heterogeneous charge (*219*). Recently many papers have agreed that the isoelectric point of zein was around 6.2-6.8 (*57, 71, 220*). So zein colloidal particles were positively charged at pH 4.0, which enabled the formation of particle complexes

with negatively charged sodium caseinate (SC) through the electrostatic attraction force. What's more, due to the steric hindrance effect of casein, the Pickering emulsions stabilized by zein/SC complexes were more stable. It was found that after a coating of β-casein layer on the droplets of Pickering emulsions, the irreversible adsorption of casein protects emulsions against flocculation and coalescence and prevents further adsorption of unattached particles (*96*). In this study, the obtained zein/SC complexes will be then utilized to encapsulate resveratrol.

Resveratrol (RES), a naturally occurring polyphenol, has been widely reported for its health beneficial potentials, such as anti-oxidation, anti-inflammation, anti-obesity, anti-tumor activities, etc (*153, 221, 222*). However, the applications of RES on these health beneficial effects are quite limited because of its low chemical stability, low oral bioavailability, poor solubility (*221*) and rapid metabolism in liver and small intestine (*153*). RES is very susceptible to chemical degradation when exposed to high temperatures (*223, 224*), alkaline conditions (*224, 225*), ultraviolet light (*225*), or certain enzymes (*226*). After oral administration of RES, it was highly absorbed (46-80%) through the small intestine, and then undergoes rapid metabolism (sulfation and glucuronidation reactions) in the liver cells and enterocytes (*153*). The majority of RES (71-98%) was rapidly excreted from kidney 7-15 hrs post-administration (*153*). As a result, very few amounts of RES can be delivered into colon. However, RES displayed good therapeutic effects on colitis (*151*) and colon cancer (*149, 150*) in the lower gastro-intestinal (GI) tract. What's more, the anti-obesity effect of RES was probably also mediated by regulating gut microbes, which in turns affects the fat metabolism and changing fat storage in adipose tissues (*189*). It was found that obese microbiome,

having the lower Bacteroidetes/Firmicutes ratio, has higher capacity to absorb energy from the diet (*190*). Since it is quite difficult for RES to be delivered into colon without suitable delivery systems, the aim of this study is to use the Pickering emulsions to control the release profile of resveratrol and slow down the absorption in the small intestine during digestion.

Recently, there have been many emulsion-based systems available for the delivery of RES, including oil-in-water emulsions (*4, 5*), water-in-oil emulsions (*6*), and water-in-oil-in-water double emulsions (*7-9*). But the loading capacities of RES in these emulsions were quite low, within the range of 0.0002 wt% - 0.05 wt% (*4-9*). The loading capacity of emulsion-based systems is determined by the solubility of RES in the dispersed phase (*221*). RES has very limited solubility in triacylglycerol oils (~ 0.18 mg/ml) (*227*) and is poorly soluble in water (~ 0.03 mg/ml) (*153*). For the water-in-oil emulsions, 10 (v/v) % of ethanol solution was used (*6*) to improve the solubility of RES in the dispersed water phase, considering it is soluble in ethanol (~ 50 mg/ml) and DMSO (~ 16 mg/ml) (*228*). So it is of great necessity to find suitable carrier oils with high solubility of RES, if we want to further improve its loadings. Furthermore, many of these recent delivery systems were aimed at improving the encapsulation efficiency (*9*), increasing the bio-absorption in the small intestine (*5*), improving the oxidative stability of emulsions (*6*), or improving the chemical stability of resveratrol (*229*). To the best of my knowledge, there were few papers about emulsion-based systems that could specifically target-delivery for the colon in order to facilitate its anti-obesity, anti-colitis, and anti-colon cancer effect.

2. Materials and Methods

2.1. Materials

Zein was bought from Freeman Industries, L.L.C. (Tuckahoe, NY). Sodium caseinate and fluorescein isothiocyanate (FITC) were obtained from Sigma-Aldrich (St. Louis, MO, USA). Toluene, n-octane, octanol, hexane, triacetin, tributyrin, and tripropionin were bought from Aldrich (St. Louis, MO, USA). Sunflower oil was bought from the local market. 99% resveratrol was purchased from Quality Phytochemicals, L.L.C. (New Jersey, USA). Capmul 908P (propylene glycol caprylate) was a gift from Abitec Inc (Columbus, Ohio, USA). Polyglycerol polyricinoleate (PGPR-4150) was donated by Palsgaard Inc. (Juelsminde, Denmark).

2.2. Preparation of Zein/SC Complexes

In order to form zein/SC complexes, 0.25 g of zein was dissolved in 10 mL 70% (v/v) EtOH-H_2O solution. Then this zein stock solution was added into 25 mL deionized water containing 0.3% (w/v), 0.4% (w/v), 0.5% (w/v), 1.0% (w/v) of sodium caseinate(SC) to form zein/SC complexes, under magnetic stirring at 600 rpm (Barnstead/Thermolyne, CIMAREC, Ashville). The obtained ratios of zein/SC (w/w) were10:3, 10:4, 10:5, and 1:1, respectively.

2.3. Particle Size and Zeta-potential Measurement

To determine particle sizes (hydrodynamic diameters) of the obtained zein colloidal particles, dynamic light scattering method was applied by using a BIC 90Plus particle size analyser equipped with a Brookhaven BI-9000 AT digital correlator (Brookhaven Instruments Corp., Holtsville, NY, USA). Particle dispersions were 1:10 diluted with MilliQ water in order to avoid multiple particle effects and aggregation effects if diluted with neutral pH water. All measurements were triplicated at a fixed

scattering angle of 90° at room temperature. The results were reported in the form of mean ± standard deviation (n = 3).

The zeta potentials were measured using a Malvern Zetasizer Nano ZS (UK) and all the measurements were conducted at 25 °C in triplicate. The refractive indexes used for protein samples and for polysaccharides were 1.450 and 1.330, respectively.

2.4. Fluorescence labeling with FITC

Labeling of zein with FITC was carried out according to the method described before (*230*) with a little modification. 10 mL of 50 mg/mL zein in DMSO solution was mixed with 0.4 mL of 10 mg/mL FITC in DMSO solution. 0.1 mL carbonate–bicarbonate buffer with pH 9.5 was added into the obtained mixture. The reaction was kept in the dark for 5 h at room temperature. Unattached FITC was removed through dialysis in carbonate–bicarbonate buffer (pH 9.5) for at least 24 h in dark. Excessive amount of deionized water was then added to accelerate the precipitation of zein protein. The FITC labeled zein, collected as precipitates in the bottom, was dried at room temperature in dark.

2.5. Preparation of Pickering Emulsions

The zein particle dispersion was used as water phase for preparing emulsions. It was added into oil with different oil fractions from 25 % to 60%. Besides regular vegetable oils (e.g. soybean oil and sunflower oil), different types of organic solvents were tried as oil core for preparing emulsions, including toluene, n-octane, octanol, hexane, triacetin, tributyrin, and tripropionin. The mixture was homogenized under high speed homogenizer (Ultra-Turrax, IKA T25) at 10 000-11 000 rpm for 2 min.

2.6. Preparation of Double Pickering Emulsions

To form a primary emulsion, 2 mL zein/SC water phase were high-speed homogenized with 6 mL toluene oil phase (containing 4% PGPR-4150) at 10 000 rpm for 2 min. Then 2 mL primary emulsion was added into 6 mL zein/SC water phase. The secondary emulsion was generated either under low speed homogenization (magnetically stirred at 600 rpm) or high speed homogenization (homogenized at 4000 rpm) for 1 min.

2.7. Estimation of Saturation Loading Range of Resveratrol in Oil

Saturation loading range estimation was conducted by preparing 20 mg/mL, 30 mg/mL, 40 mg/mL, 50 mg/mL, 60 mg/mL, and 70 mg/mL resveratrol (RES) in Capmul 908P. They were then either dissolved under room temperature (25 °C) or heated up to 130 °C with magnetic stirring at 600 rpm (Barnstead/Thermolyne, CIMAREC, Ashville) covered by aluminum foil until they were completely dissolved. 70 mg/mL of RES was heated at 130 °C for 3 hours. Long time under high temperature may lead to degradation and oxidation of RES. Therefore, the longest heating time was up to 3 hours. The ranges of the saturation loading of RES were estimated after they were stored at room temperature for 24 hours.

2.8. Nanoencapsulation of Resveratrol in Pickering Emulsions

The zein/SC complexes were synthesized based on an anti-solvent precipitation method with a little modification (*57*). Based on preliminary data, the optimum mass ratio of zein to sodium caseinate (SC) was 10:3. So 0.25 g of zein was dissolved in 10mL 70% (v/v) EtOH-H_2O solution. Then this zein stock solution was drop-wise added into 25mL deionized water containing 0.3% (w/v) of SC, under magnetic stirring at 600 rpm (Barnstead/Thermolyne, CIMAREC, Asheville). 20 mg/ml of RES was dissolved into oil

phase at room temperature under magnetic stirring overnight. Since RES is light sensitive, the container was covered by aluminum foil during the process. The zein/SC complex dispersion was added into the oil phase in an oil fraction of 50% to make an emulsion. The mixture was homogenized at 11000 rpm for 2 min by using a high speed homogenizer (ULTRA-TURRAX T-25 basic, IKA Works Inc., Willmington, USA).

2.9. Optical Microscopy

Emulsion samples (about 100 μL) were placed on a clean glass slide, and diluted with a drop of water if needed before imaging. Microscopic images were taken using the Nikon TE2000 microscope (Japan). And droplet size distributions were analyzed using Image J software. Average sizes of droplets in Pickering emulsions were calculated using 50-200 droplets.

2.10. Fluorescence Microscopy

The FITC-labeled zein was used to form complexes with sodium caseinate and then the zein/SC complexes were applied to stabilize emulsions. FITC-labeled zein was visualized at an excitation wavelength of 488 nm. The adsorption of FITC-zein/SC complexes at oil-water interfaces was observed using Nikon TE2000 fluorescence microscope (Japan).

3. Results and Discussion

3.1. Determination of the Optimum Ratio of Zein to SC

Four kinds of zein/SC complexes were made through anti-solvent precipitation method with zein to SC mass ratio of 10:3, 10:4, 10:5, and 1:1, respectively. In order to compare the emulsion capacity of these four kinds of zein/SC complexes, 5 mL of complex dispersion and 5 mL of sunflower oil were homogenized together to make

emulsions. The homogenization speed is very crucial in preparing emulsions. High energy input leads to smaller droplet size, but poor particle coverage at the same time due to the larger interfacial areas. Zein based Pickering emulsion cannot be formed at extremely high speed.

In order to clearly observe the creaming layer of Pickering emulsions, the emulsions after homogenization were washed with the same amount of de-ionized water for 3 times. After washing (to remove un-attached proteins), only zein/SC complexes at mass ratio of 10:3 and 10:4 were able to produce high amount of emulsion cream layer, while the other two groups were not much stable and behaved more likely o/w nanoemulsions with homogenous milky color after washing, as shown in Figure II-1. When the concentration of SC was more than enough to saturate the surface of zein colloidal particles, the extra free SC may compete with zein/SC at the oil-water interface and contribute to the formation of nanoemulsions, instead of Pickering emulsions. As a result, 0.3% (w/v) of SC solution was finally determined to be used for preparation of the complexes. If not mentioned specially, zein/SC complexes hereafter refer to the one prepared using 0.3% (w/v) of SC solution.

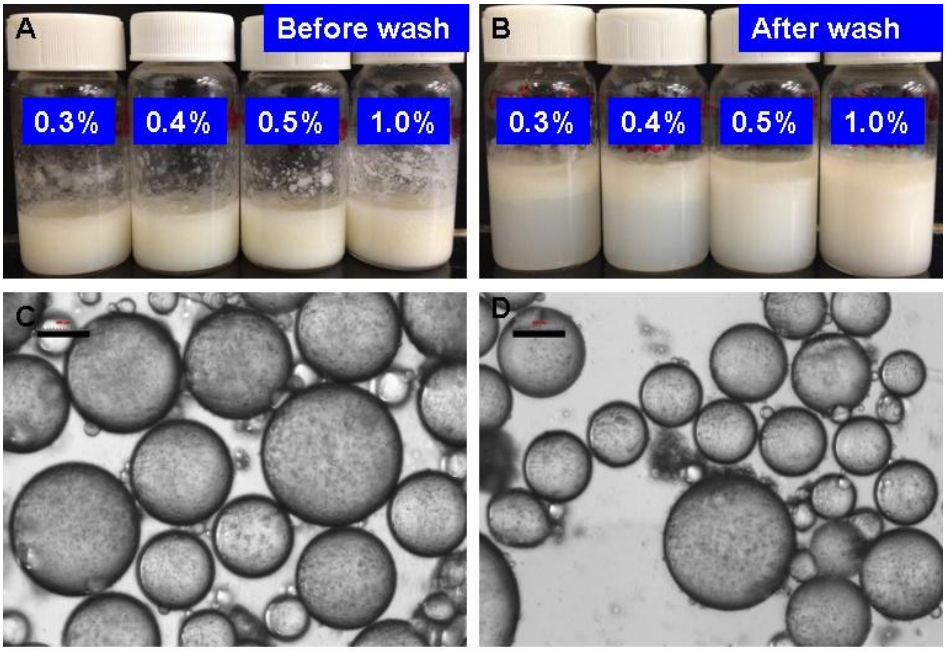

Figure II- 1. The influence of SC concentration on the formation of Pickering emulsion after washing process; A, emulsions formed before wash; B, emulsions formed after wash; C and D, optical microscopic images of washed emulsion prepared by 0.3% (w/v) of SC and 0.4% (w/v) of SC, respectively; all scale bars represent 100 μm.

3.2. Particle Size and Zeta-potential of Zein/SC Complexes

The effective diameters of zein and this zein/SC complex (10:3) were 117.5±0.7 nm and 167.9±5.2 nm, respectively, with a polydispersity of 0.227±0.012 and 0.267±0.012, respectively, as shown in Figure II-2. Positively-charged zein colloids and negatively-charged sodium caseinate are mutually electrostatic attractive to each other. With an increase of the SC ratio in the complexes, their surface charges gradually changed from positive to the negative. It was estimated that if the coverage of SC (Γ) on the surface of zein colloids was 3 mg/ m^2, the required amount of SC per weight of zein colloidal particles was 0.29 %wt, calculating through the equation $C = \frac{6\Gamma\phi_P}{d}$, where ϕ_P is the volume fraction of particles and d is the mean surface-averaged particle diameter (*231*). Therefore, 0.3 % (w/v) of SC solution could well cover zein colloids (*57*), which is

consistent with the negative zeta potential measured here, -14.00±0.56 mV (Figure II-2, A2).

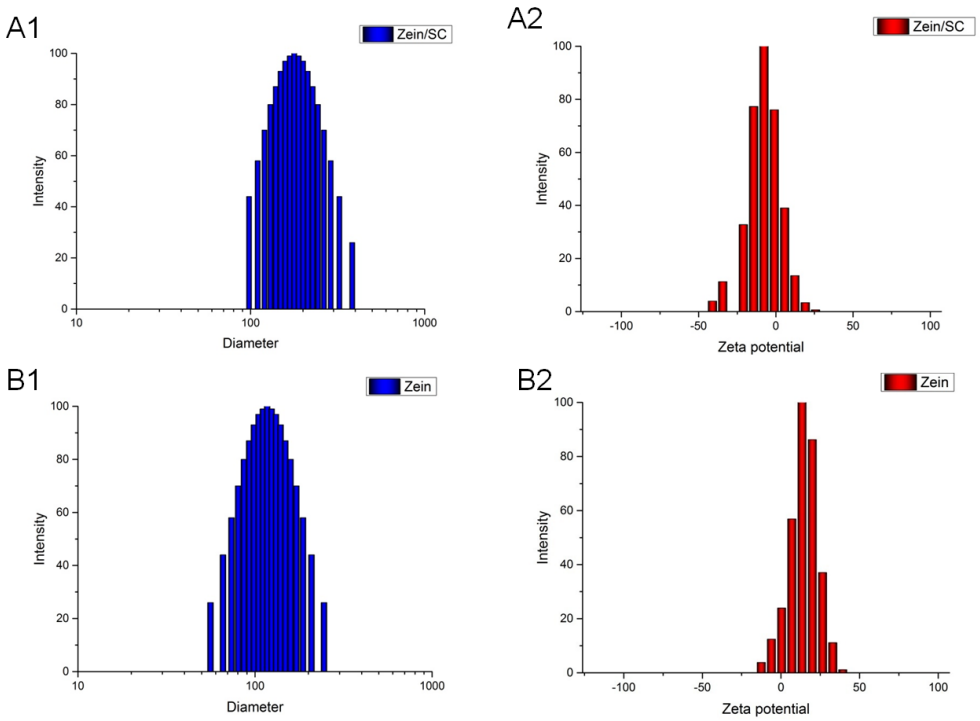

Figure II- 2. Particle diameters and zeta potentials for zein and zein/SC complexes.

3.3. Distribution of Zein/SC Complexes in Emulsions

In order to further demonstrate whether emulsions were stabilized by colloidal particles or by soluble sodium caseinate, zein was exclusively labeled with Fluorescein isothiocyanate (FITC), and free FITC was removed through excessive dialysis. The FITC-labeled zein was used to build complexes with SC. Figure II-3 depicted the fluorescence images of the toluene Pickering emulsion stabilized by FITC-zein/SC complexes. The surface of droplets was in green color, which indicated that the droplets were stabilized mainly by colloids particles either zein/SC complexes or a mixture of zein

colloids and zein/SC complexes. During the formation procedure of Pickering emulsions, some free caseinates may locate themselves at the droplet surface. However, their attachment was not as firm as the one of solid particles. The energy required to detach a single spherical particle can be estimated by the equation $\Delta G_{detach} = \pi R^2 \gamma_{ow}(1 - |\cos\theta|)^2$, where γ_{ow} is the oil-water interfacial tension, θ is the contact angle, R is the radius of spherical particles (*89*). The energy of detachment increased with an increase of particle radius. For particle with size of approximately 10 nm, the desorption energy per particle is several thousand kT, which means their adsorption at the oil-water interface is practically irreversible (*93*). The mobility of free sodium caseinate was certainly much higher than zein colloidal particles. And during washing step, SC could be easily washed away together with water. Therefore, the washed emulsions were more likely to be stabilized by colloidal particles, rather than sodium caseinate, as shown in Figure II-3.

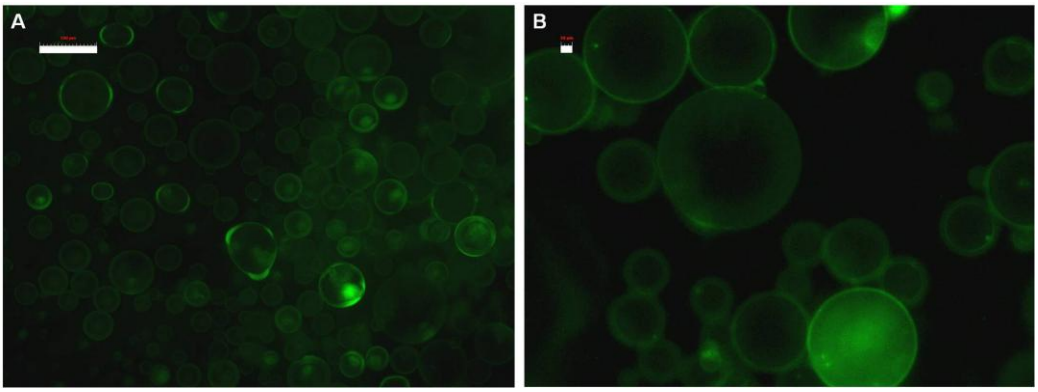

Figure II- 3. Fluorescence microscopic image of FITC-zein/SC stabilized Pickering emulsions with toluene oil core; A, scale bar is in 100 μm; B, scale bar is in 10 μm.

3.4. Emulsification Capacity of Zein/SC Complexes

Different parameters were tried in order to optimize the conditions for the preparation of colloidosomes. When the oil fraction changed from 30% to 60%, droplet sizes increased significantly (Figure II-4). At 50% of oil phase, the droplet sizes were much more even, but the surface coverage rate was obviously not as high as the one containing less amount of oil.

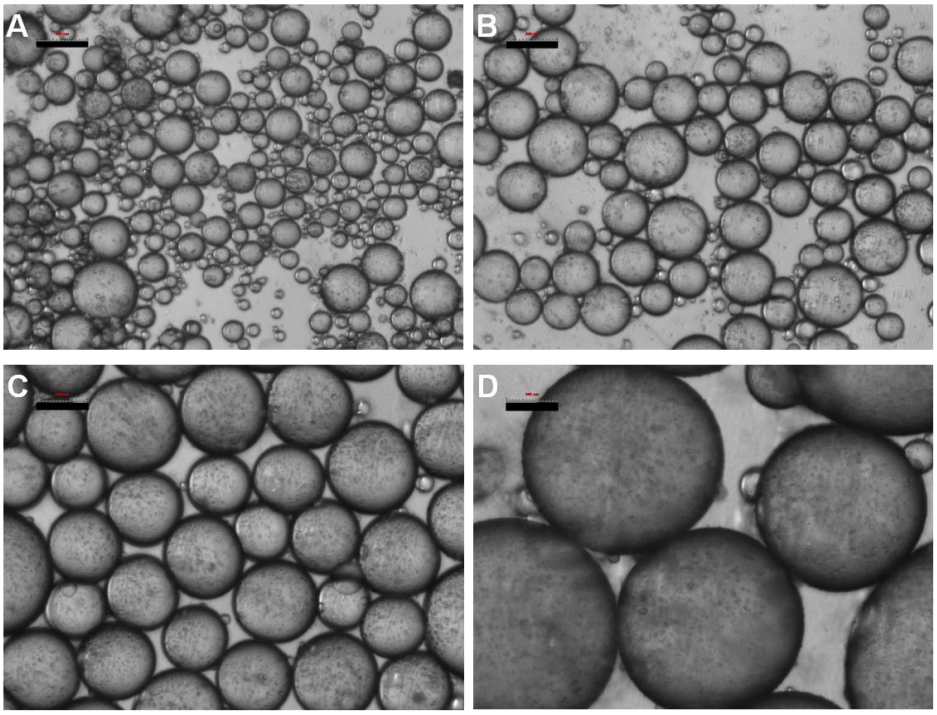

Figure II- 4. Influence of Sunflower Oil fraction on the formation of Pickering emulsions, i.e. 30% (A), 40% (B), 50% (C), and 60% (D); all scale bars represent100 μm.

The average diameter of droplets of sunflower oil was 39.3±15.6 μm. Besides sunflower oil (long-chain triglycerides), seven other oils were chosen to determine the emulsification capacity of zein/SC complexes, including volatile organic phases (toluene, n-octane, octanol, and hexane), and non-volatile short-chain triglycerides (triactin, tributyrin, and tripropionin). The droplet morphology of Pickering emulsions containing

different oil core were displayed in Figure II-5. The particle size distributions of these emulsions were analyzed via Image J software, by taking an average value of 50-200 droplets. The droplet diameters and the dielectric constant of different oils were summarized in Table II-1. Toluene-in-water emulsion has a similar droplet diameter, i.e. 46.7±7.9 μm, as compared to sunflower oil emulsion. N-octane emulsion gave the biggest droplet size, then tripropionin and hexane came the second. Dielectric Constant, ε, is a dimensionless constant that reflects how easy a material can be polarized by imposing an electric field. Therefore, the polarities of different oils can be characterized by the dielectric constant (*108*). A high dielectric constant usually implies a high polarity (*108*). From Table II-1, it is clear that oils that have high dielectric constant were not able to form Pickering emulsions, or the emulsions they produced were not quite stable, which indicated that the zein/SC complexes were not suitable to stabilize oils with high polarity.

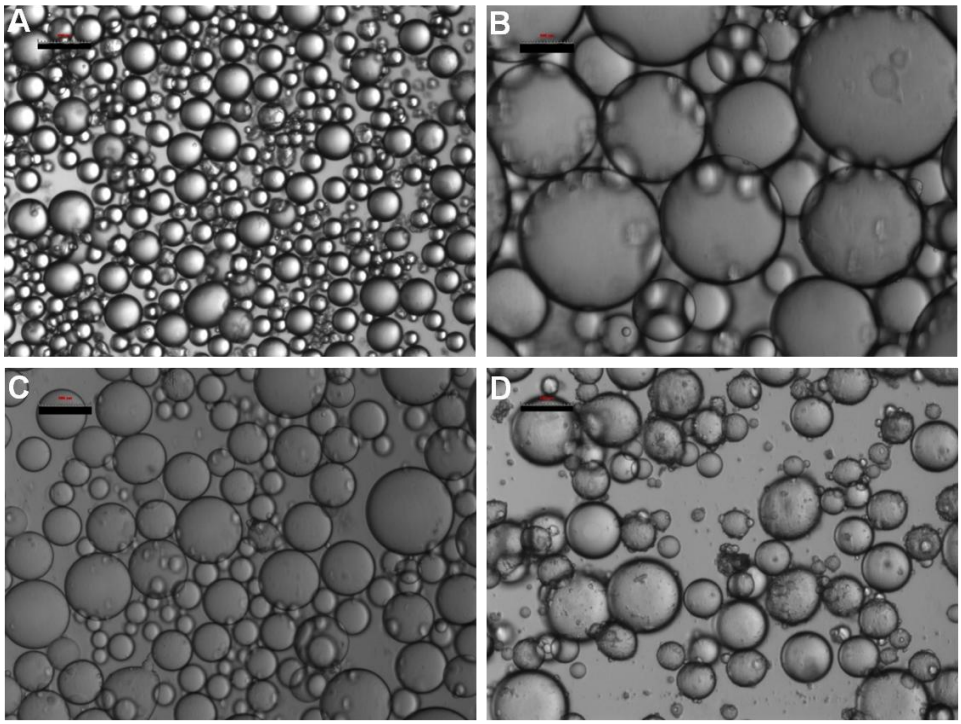

Figure II- 5. The droplet morphology of Pickering emulsions with different oil phases, i.e. toluene (A), n-octane (B), hexane (C), tripropionin (D); all scale bars represent100 μm.

Table II- 1. Dielectric constant of different organic oils and droplet diameters of Pickering emulsions they formed.

Oil	DI (μm)	ε	Reference for ε
SF Oil	39.3±15.6	~3	(*108*)
Toluene	46.7±7.9	2.38	(*232*, *233*)
n-octane	159.9±76.0	1.94	(*234*)
Hexane	71.6±30.5	1.88	(*233*)
Octanol	No	10.3	(*232*)
Triacetin	No	7.11	(*235*)
Tributyrin	No	5.72	(*236*)
Tripropionin	69.5±29.1	—	

SF, Sunflower; ε, Dielectric constant; DI, Diameter; No, no stable emulsion was formed.

3.5. Fabrication of W/O/W Double Pickering Emulsions

Multiple compartments double emulsions were prepared by homogenizing a primary emulsion in a suitable mixing power. For the preparation of primary emulsion, without the addition of PGPR-4150, the droplet sizes of zein/SC complexes stabilized Pickering emulsion were quite big due to the high oil fraction (75%) and the low particle concentration (0.7%) in aqueous phase. The obtained emulsion was an oil-in-water emulsion, which can be diluted well with water. Since zein/SC complexes alone can only form oil-in-water emulsions, PGPR-4150 was added to form desirable water-in-oil emulsions.

The overall shape of the droplets in double emulsions obtained from low-speed stirring was spherical, but not very smooth at the edges. As illustrated in the Figure II-6, no cavities were observed inside the emulsion droplets. When the double emulsions were prepared under high speed homogenization, the droplet size of secondary emulsion was slightly smaller than the size of emulsions prepared by low speed method. During the high speed homogenization, droplets of the primary emulsion were almost completely seperated with each other. They gathered loosely in the secondary emulsions. Therefore,

the emulsion droplets had better transparency than the ones prepared by magnetic stirring. Since this high-speed prepared double emulsions ecapsulated less primary emulsion droplets in the interior space, the diffusion rate of encapsulated materials from this emulsion will be faster then the one from low-speed method prepared double emulsions. The diffusion from the primary emulsions to the outside can be achieved by penetration through the droplet walls (like the trans-cellular diffusion) and/or through interval space between adjacent droplets (like the inter-cellular diffusion). When the secondary emulsions incorporate more primary emulision droplets, the diffusion distance for “inter-droplet diffusion” will be longer, so that the permeation can be retarded.

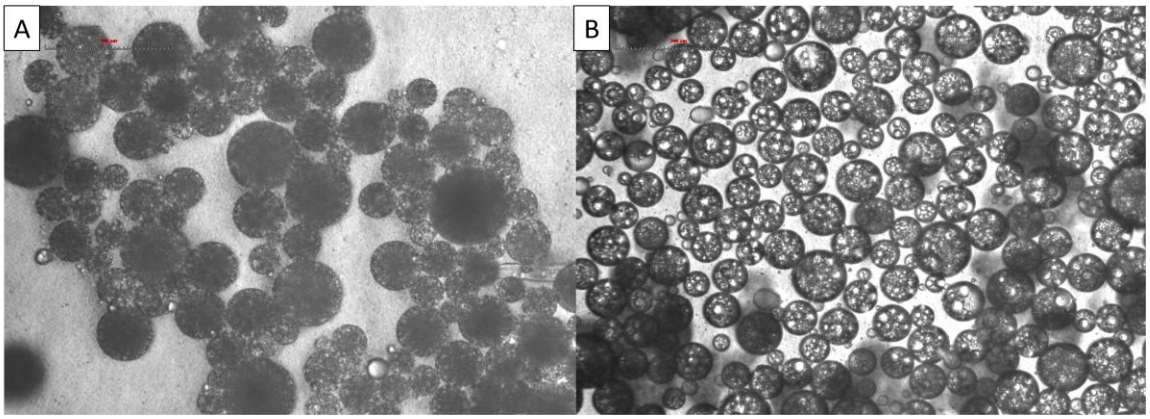

Figure II- 6. Double emulsions formed under low speed method (A) and high speed method (B); scale bars are 100 μm.

3.6. Nanoencapsulation of Resveratrol in Pickering Emulsions

RES has limited solubility both in water and in triacylglycerol oils. Even when it was heated at 37 °C for 24 h, it only dissolved 85.72±6.77 μg/g in corn oil and 47.93±7.27 μg/g in olive (*227*). Based on the chemical structure of RES, the three hydroxyl groups linked to benzyl rings increase the molecular polarity, making it less soluble in the non-polar oils. So in order to improve its solubility in the oil, the carrier oil should have higher polarity than long chain triglycerides (LCT). Propylene glycol

caprylate is an ester of propylene glycol and caprylic acid (medium chain fatty acids). Theoretically speaking, it has larger polarity as compared with LCT, since it has an extra hydroxyl group and the shorter fatty acids chain length. Consistent with the analysis, it was found in this study that 20 mg/g of RES can be completely dissolved in Capmul 908P (propylene glycol caprylate) at room temperature. And the samples were stored at room temperature over night to allow the growth of RES crystals before taking the microscopic images. As illustrated in Figure II-7, large amounts of RES crystals were observed in soybean oils, while RES crystals can be hardly found in Capmul 908P. When heated up to 130 ˚C, 20 – 60 mg/mL RES was dissolved immediately. However, after heated for 3 h, 70 mg/mL RES still cannot be fully dissolved. After storage for 24 h at room temperature, 60 mg/mL and 70 mg/mL RES have crystal precipitates, while the other concentrations still maintain good transparency (Figure II-8). In order to inhibit the possible oxidation of RES during the heating, 20 mg/mL RES was determined as the final concentration to prepare emulsions, since the concentration can be achieved without any heat treatment. So the final concentration of RES in formulations was 10 mg/mL, which was much higher than the loading capacities in the recent reported emulsion-based formulations (*4-9*).

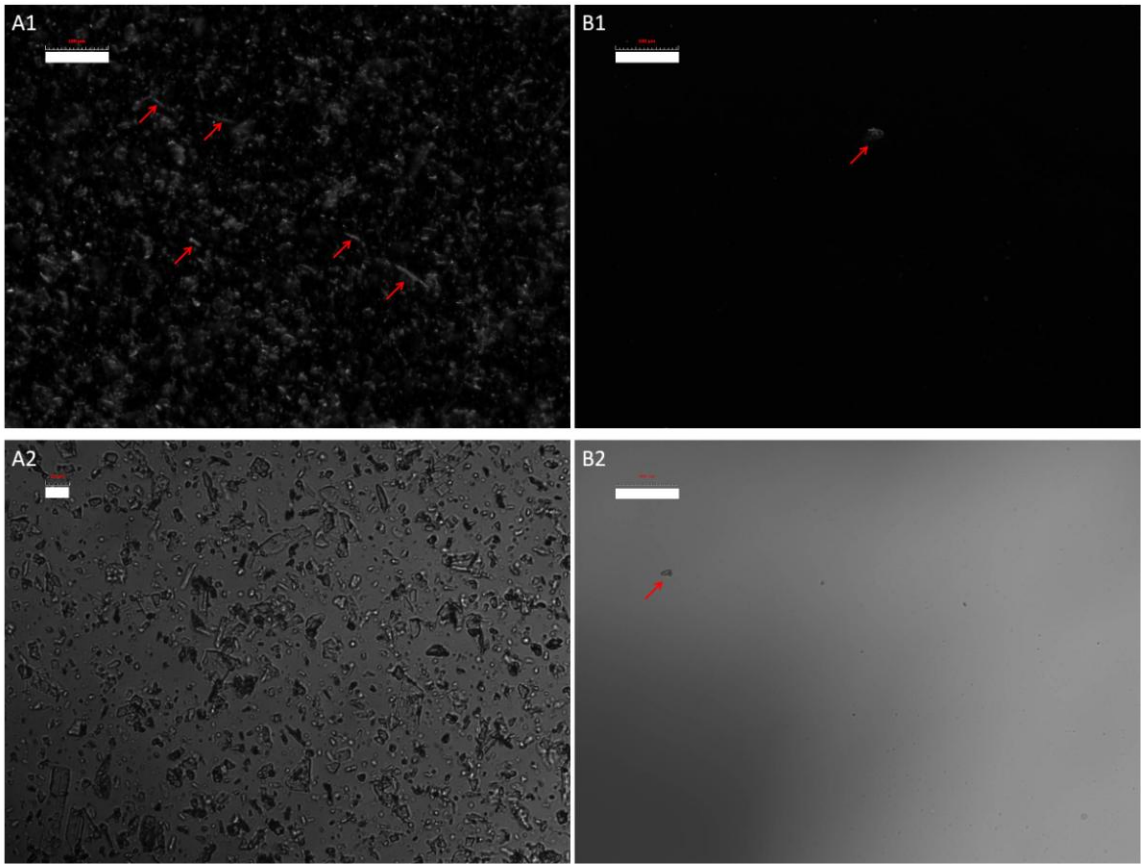

Figure II- 7. Crystal morphology of 20 mg/mL RES in soybean oil (A1 and A2) and 20 mg/mL RES in Capmul 908P (B1and B2); the red arrows indicate the locations of RES crystals; Scale bars in A1, B1, B2 represent 100 μm; Scale bar in A2 represents 20 μm.

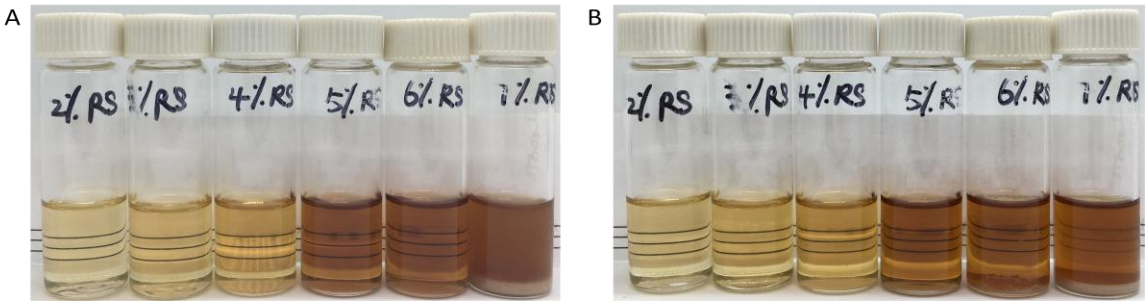

Figure II- 8. Transparency of RES in Capmul 908P immediately after heating (A) and after storage at room temperature for 24 hours (B).

Table II- 2. Solubilization concentration (mg/mL) of resveratrol at 25˚C and 130 ˚C (CS=completely soluble, PS=partially soluble).

Resveratrol	Concentration (mg/mL)	20	30	40	50	60	70
Temperature (˚C)	25	CS	PS	PS	PS	PS	PS
	130	CS	CS	CS	CS	CS	PS
	130 (after 24 h storage)	CS	CS	CS	CS	PS	PS

4. Conclusion

Zein and sodium casienate were able to form negatively charged Zein/SC complexes that have good emulsification ability to stabilize vegetable oils, toluene, tripropionin and hexane. However, they are not suitable to stabilize oils with high polarities such as octanol, triacetin and tributyrin. The fluorescence image of FITC-labeled zein particles showed that the obained Pickering emulsions were stabilized mainly by colloidal particles including zein/SC complexes and zein colloids. With an increase of the oil fraction, droplet sizes also increased significantly. Through cyclic scheme of homogenization, zein/SC complexes were able to form stable W/O/W double emulsons either through low-speed magnetic stirring or through high-speed homogenization with the existence of PGPR-4150. The droplets of primary emulsions were densely packed in low-speed prepared emulsions, while they were loosely packed in high-speed prepared emulsions. 20 mg/g of RES was completely dissolved in carrier oil (Capmul 908P) at room temperature, while up to 40 mg/mL of RES can be completely dissolved at 130 ˚C. Resveratrol was encapsulated in zein/SC complexes stabilized Pickering emulsion (50% oil fraction) in a high loading capacity of 10 mg/mL.

CHAPTER III. STUDY THE BIOACCESSIBILITY AND BIOABSORPTION OF FORMULATED RESVERATROL USING DIFFERENT IN VITRO MODELS

Partial contents in this chapter were adapted from the paper "Study of the bioaccessibility of formulated resveratrol using different dynamic gastric-intestinal digestion models" and "Metabolism of Resveratrol by Gut Microbiota and its Colon-related Health Beneficial Effects" which were ready for submission.

1. Introduction

Gut microbiota refers to microorganisms that inhabit the mammalian gastrointestinal (GI) tract, which includes mainly bacteria, as well as archaea, viruses, and unicellular eukaryotes (*237*). The amount of bacterial cells in human microbiota is 10 times greater than the amount of cells in human bodies (*238, 239*). And the colon alone is estimated to contain over 70% of all the microbes in the human body (*238, 239*). Numerous studies have shown that these commensal microbes play an important role in human health, such as the development of immune systems (*240, 241*), the development of the nervous systems (*242*), the maturation of GI tract (*241, 243, 244*), the competitive exclusion of incoming pathogens (*245, 246*), the synthesis of specific nutrients, like vitamins B12 and K (*247*), and the regulation of body weight and the prevention of related diseases like obesity and diabetes (*190, 248, 249*). These strong and symbiotic microbiota–host interactions lead to an increasing awareness of the role of gut microbiota in human health.

The initial composition of neonatal gut microbiota mainly depends on maternal–offspring exchanges of microbiota (*250*). And the composition of the gut microbiota is host specific, which evolves all the time throughout the host's lifetime (*237*), depending on their respective dietary habits and other environmental factors like smoking (*251*), air pollutions (*252*), stress (*243*), circadian disorganization (*253*), etc. Gut microbiota composition can also be modulated by various food components, including dietary fibers (*254*), proteins (*255, 256*), fats (*257*), polyphenols (*258-261*), etc. Resveratrol is one of those dietary polyphenols that have exhibited good potentials on improving the gut microbiota dysbiosis by modification of gut microbiota compositions (*189, 192, 195*). And the RES's health-beneficial effects, metabolism pathway, modulation effects on gut microbiota, and the colonic bioconversion by gut microbiota have been mentioned a lot in the previous chapters.

It was well studied that RES has high absorption rate in the small intestine and fast metabolism in the hepatocytes and enterocytes. So it is quite difficult for RES to be delivered into colon without suitable delivery systems. The aim of this study is to develop a series of delivery systems, including Pickering emulsions and nanoemulsions, to increase the loading capacity of RES in formulations and study the release profile of resveratrol during digestion in different delivery systems. Zein/SC complexes will be utilized to fabricate Pickering emulsions through high speed homogenization, while conventional nanoemulsions will be stabilized by lecithin using high pressure homogenization.

To investigate the digestion profile of the delivery systems, different dynamic in vitro digestion models have been used, including the Simulator of the Human Intestinal

Microbial Ecosystem (SHIME) and the TNO gastro-Intestinal Model (TIM-1). The SHIME system has been validated for studying the gut microbiomes in the gastrointestinal tract (*262-264*), and it normally has 3 reactors for the colon including ascending colon, transverse colon and descending colon, besides stomach and small intestine. In order to simulate the digestion and absorption in the upper GI tract, a blood dialysis method was utilized in this modified SHIME system. The TIM-1 model has been widely used to mimic the digestion in the upper GI tract, including stomach, duodenum, jejunum, and ileum (*265-268*). The digestive conditions are precisely controlled by computer programs, which involve peristaltic movements and pH controls of each individual digestion compartment, gastric emptying and physiological transit times, flow rates and composition of digestive fluids (such as gastric fluid, gastric enzyme solution, bile, and pancreatic fluid), and removal of digestion metabolites (*265*, *269*). The SHIME and TIM-1 have different arrangements of reactors and use specific standard digestion protocols in their tests. So the results obtained from these two models will be discussed and compared.

2. Materials and Methods

2.1. Materials

99% resveratrol was purchased from Quality Phytochemicals, L.L.C. (New Jersey, USA). Zein was bought from Freeman Industries, L.L.C. (Tuckahoe, NY). Rapeseed lecithin PC75 was donated by American Lecithin Company (Oxford, CT). Capmul 908P was a gift from Abitec Inc (Columbus, Ohio, USA). Pig bile was purchased from a local slaughterhouse (Farm to Pharm LLC, New Jersey, USA), stored at -20°C until usage, and aliquoted in bottles for individual TIM experiments. Rhizopus lipase

(150000 units/mg F-AP-15) was purchased from Amano Enzyme Inc. (Nagoya, Japan). The nutrition medium for the SHIME experiment was purchased from ProDigest BVBA Company (Belgium). *Lactobacillus rhamnosus* GG (ATCC 53103) was purchased from American Type Culture Collection (ATCC) (Manassas, Virginia, USA). Other chemicals were obtained from Sigma-Aldrich (Saint Louis, MO, USA) unless otherwise stated. The porcine small intestine (SI) and colon membranes were purchased freshly from local slaughter house.

2.2. Preparation of Pickering Emulsions

The zein/SC complexes were synthesized based on an anti-solvent precipitation method with a little modification (*57*). Briefly, 0.25 g of zein was dissolved in 10 mL 70% (v/v) EtOH-H_2O solution. Then this zein stock solution was drop-wise added into 25 mL deionized water containing 0.3% (w/v) of sodium caseinate (SC), under magnetic stirring at 1000 rpm (Barnstead/Thermolyne, CIMAREC, Asheville). The final mass ratio of zein to SC was 10:3. 20 mg/ml of RES was dissolved into Capmul 908P at room temperature under magnetic stirring overnight. Since RES is light sensitive, the container was covered by aluminum foil during the process. The zein/SC complex dispersion was added into the oil phase in an oil fraction of 50% to make an emulsion. The mixture was homogenized at 11000 rpm for 2 min by using a high speed homogenizer (ULTRA-TURRAX T-25 basic, IKA Works Inc., Willmington, USA).

2.3. Preparation of Nanoemulsions

Nanoemulsions were prepared under high pressure homogenization as described before with a little modification (*16*). 1 (wt/wt) % of rapeseed lecithin PC 75 was added into carrier oil and deionized water, respectively. The mixture was left stirring for several

hours at room temperature until lecithin was completely dissolved in oil. Then 20 mg/mL RES was dissolved into the oil phase containing lecithin by stirring it overnight with a cover of aluminum foil at room temperature. A coarse emulsion was obtained by 1:1 (v/v) mixing the oil and water phase together and homogenizing the mixture at 24,000 rpm for 2 min. After high-speed homogenization, the primary emulsion was immediately transferred into a high pressure homogenizer (EmulsiFlex-C3, AVESTIN Inc., Ottawa, Canada) and homogenized for 5 passes under a pressure ranging from 100 to 150 MPa. The obtained emulsions were stored at 4 °C with a cover of aluminum foil until usage.

2.4. The Simulator of the Human Intestinal Microbial Ecosystem (SHIME)

The Simulator of the Human Intestinal Microbial Ecosystem (SHIME) (Ghent University-Prodigest, Belgium) model normally consists of five double-jacketed vessels, including stomach, small intestine, and three colon regions, subdivided into ascending colon, transverse colon and descending colon. But in order to study the digestion and absorption in the upper GI tract, the colon part was simplified into one reactor. And the other reactors were modified into two vessels, i.e. sample compartment and concentrated digestion fluid compartment. The stomach and small intestine were combined into one vessel. The temperature of each vessel was maintained at 37 °C, and kept in an anaerobic condition by flushing the headspace with nitrogen. A dynamic dialysis process was implemented in the SHIME model via the approach of a “blood dialysis procedure”. The dialysis cellulose membrane (cut-off = 14 kDa) mimics the removal of metabolites from the small intestine or the absorption of metabolites by the means of a passive diffusion. In the first two hours, it mimicked the digestion in stomach by adding 50 g emulsion or 25 g

bulk oil (containing 500 mg RES), 5 mL pepsin solution (0.78 g/50 mL 10 mM HCl), and d-H_20 (61 mL for emulsion or 86 mL for bulk oil) into the sample compartment, and then tuning the pH from 4.7 to 2.0 using HCl. At the same time, 35 mL of 4X concentrated SHIME feed (pH=2.0 ±0.1) was transferred into the concentrated ST/SI compartment, which contained (g/L) Arabinogalactan (4.8), Pectin (8), xylan (2), glucose (1.6), yeast extract (12), special pepton (4), mucin (12), L-cystein-HCl (2), Starch (8). After the two hours digestion, 30 mL of specific pancreatic juice was added into sample compartment, while 15 mL of 4X pancreatic juice was transferred into the concentrated ST/SI compartment. The dialysis procedure started after 2 hours digestion in stomach plus 2.5 hours digestion in small intestine. The dialysis liquid (3.75 g/L $NaHCO_3$) entered the membrane from the bottom of the dialysis column at 8 mL/min, while the intestinal content flowed into the column in an opposite direction at 1.5 mL/min. And the dialysis membrane was pre-filled with dialysis liquid before starting the experiment. The whole SHIME experiment lasted for 370 min. Samples were taken from each reactor at different time intervals in order to see the structure change of Pickering emulsions during digestion. For the microscopic imaging, the digested emulsion samples (about 100 ul) were placed on a clean glass slide, and diluted with a drop of water. Microscopic images were taken using the Nikon TE2000 microscope (Japan).

2.5. The TNO gastro-Intestinal Model (TIM-1)

The TNO gastro-Intestinal Model (TIM-1) (TNO Zeist, Netherlands) was used to simulate the consecutive dynamic digestion in the stomach, duodenum, jejunum and ileum. Before starting the experiment, each reactor was pre-infused with individual start residues mimicking the actual gastrointestinal digestion conditions in a fed state. The

liquid formulations (50 g for emulsion or 25 g for bulk oil, with the same amount of RES like the SHIME experiment) were fed into the stomach using a funnel together with 95 g gastric electrolyte solution, 50 g water, and 5 g gastric enzyme solution. pH values of each reactors were monitored and adjusted using computer programs, which also controlled the peristaltic movements of each compartment and modulated the secretion and the transit times of various digestion fluids. The temperature was maintained at 37 °C through surrounding water jackets. In TIM-1 model, bioaccessibility is determined by the accumulative amount of compound absorbed through the simulated jejunal and ileal membranes over different time periods (*266*). Therefore, the digested samples collected from the capillary columns at jejunum and ileum at specific time intervals were considered as the bioaccessible fraction available for absorption. The collected samples were stored at -20 °C before HPLC analysis. The entire digestion in the TIM-1 model lasted for 360 min. And each formulation was tested on the TIM-1 model in duplicate.

2.6. Extraction of RES from Digested Samples and HPLC Analysis

0.5 mg/mL pterostilbine in methanol solution was prepared as the internal standard solution for RES. 200 μL internal standard and 800 μL digested samples were mixed together. 0.4 ml ethyl acetate was added into the above 1 mL mixture, vortexed for 5 min, and then centrifuged at 3000 rpm for 3 min. The upper ethyl acetate layer was transferred into 5 ml vial. Repeat the process twice. The collected ethyl acetate was filtered through 0.22 μm filter. 300 μL of the filtrates was fully evaporated under N_2 flow. Then 200 μL HPLC-grade methanol was added to re-dissolve resveratrol. Samples were stored at -20 ˚C until HPLC measurement.

The UltiMate 3000 HPLC system (Dionex, CA) combined with the Supelco's RP-

Amide C16 (15 cm × 4.6 mm id, 3 μm (Bellefonte, PA)) column was used to analyze RES in the digested samples. 0.1% phosphoric acid solution (A)/acetonitrile (B) were served as the mobile phase, with a 17 min elution gradient: 83% A at 0 min, hold it for 1 min, then linearly decrease to 50% A in 1 min, and then linearly decrease to 20% in 14 min, finally ramped to 83% at 17 min. Flow rate was 1.0 mL/min. Detection wavelength was 306 nm and the injection volume was 20 μL.

2.7. Franz Cell Diffusion

After the dynamic digestion through the TIM-1 model, Franz Cell Apparatus (PermeGear, PA, USA) was applied to test how digested samples (bulk oil, nanoemulsion and Pickering emulsion) were been absorbed through the small intestine. The porcine small intestine (SI) and colon were purchased freshly from local slaughter house. The membranes were cleaned and cut into square shape individual pieces with side-length of around 4 cm. Membranes were stored in -80 ˚C refrigerator. Before usage membranes were immersed in phosphate buffer (pH 7.4) for about 15 min. The membrane was mounted in Franz static penetration cells (9 mm of orifice diameter) consisting of an upper donor compartment and a lower receptor compartment. The internal surface (the rough side) of small intestine or colon faced the donor chamber. 1 mL sample was added in the donor compartment. 40%:60% (v:v) PEG 400: phosphate buffer (pH 7.4) was used as the receptor fluid to test the TIM-1 digested samples. In order to improve the permeability of bioactive compounds, 40% - 50% ethanol was commonly used as the receptor fluid (*270, 271*). Therefore, in order to compare the concentration influence on the permeability of RES, 50%:50% (v:v) ethanol: phosphate buffer (pH 7.4) was used as the receptor fluid to test 5 mg/mL, 10 mg/mL, and 20 mg/mL RES in bulk oil solutions.

The receptor chambers were filled with 5 ml of the receptor fluid and the cells were placed on a magnetic stirrer. 1 mL of receptor fluid was taken at various time intervals (0.5, 1.0, 1.5, 2.0, 2.5, and 3.0 h for TIM-1 180 min-digested samples from jejunum and 1.0, 2.0, 3.0, 4.0, and 5.0 h for RES in bulk oil solutions) after application of samples on the membrane. The whole instrument was maintained at 37 ˚C water bath. And each sample was tested in triplicate on 3 membranes. Samples collected from the receptor compartment were directly filtered through 0.2 μm filter (Whatman syringe filter) and analyzed via HPLC.

2.8. Porcine SI and Colon Membrane Extraction of RES

SI and colon membrane extraction of the RES was performed as follows. The membrane was cut into 6 pieces using a pair of surgical scissors and the resulting fragments introduced into a 5 mL vial containing 2 mL of HPLC-grade methanol. The resulting suspension was then homogenized by stirring at 600 rpm at room temperature for 3 h. The vials were covered by aluminum foil to avoid the light degradation of RES. Then the extraction fluid was filtered (Whatman syringe filter, 0.2 μm) and analyzed via HPLC.

2.9. Anaerobic Cultivation

Influence of RES concentration of the growth of LGG. 5% of RES in DMSO solution was added into MRS broth media to make the concentration of RES in the nutrition media to be 100 μM. Then the 100 μM RES in MRS solution was further diluted with MRS media to make the concentration of RES to be 50 μM and 25 μM, respectively. And 100 μL of the obtained RES in MRS solution was 1:1 mixed with 100 μL *Lactobacillus rhamnosus* GG solution (1% inoculation rate), to make the final

concentration of RES in the 96 well plate as 50 μM, 25 μM, and 12.5 μM, respectively. The concentration of *Lactobacillus rhamnosus* GG achieved 10^{-5} – 10^{-6} CFU/mL. The optical density was measured at 600 nm by a temperature-controlled Dynex 96-well plate reader MRX with Revelation software. The microtitre plate was incubated at 37 °C for 24 h with optical density read every 30 min. All assays were performed in triplicate and repeated twice. Experiments were conducted in Type A Coy Laboratory Vinyl Anaerobic Chamber (Coy Laboratory Products, Grass Lake, MI, USA).

Influence of formulated RES on the growth of LGG. The RES formulations were firstly digested through the SHIME system as mentioned above. And then the digested samples collected from the colon were applied in this experiment. The 5% of digested Pickering emulsion, nanoemulsion and bulk oil was added into MRS nutritional media. In order to study the influence of RES concentration in the digested samples, 5% of digested oil in MRS media solution was further diluted with MRS to make the concentration of the RES oil solution to be 2.5% and 1.25% in the MRS media. And then obtained media was 1:1 added into *LGG* inoculated MRS solution (1% inoculation rate). The optical density was measured in the same manner as mentioned before.

Influence of formulated RES on the growth of gut microbes. Feces samples were collected from four healthy volunteers (three females and one male, 25–35 years old) who did not have any gastrointestinal disorders and had not been treated with antibiotics for the previous six months. Feces sample was 1:4 diluted using sterilized 1X PBS buffer. The mixture was vortex for at least 5-10 min to make homogeneous feces slurry. Then the slurry was centrifuged at 3000 rpm for 3 min. The supernatant was used for the inoculation. The inoculation ratio of feces samples into nutrition media is 10%, i.e. 1 mL

of diluted feces solution was mixed with 9 mL of SHIME nutrition media. 0.5% of samples (blank control and different formulations, i.e. Pickering, Pickering-RES, Nanoemulsion, Nanoemulsion-RES, Bulk oil, and Bulk oil-RES) were added into the nutrition media, after the feces inoculation. The samples were then cultivated at 37 °C in 5% CO_2 and 2.5% H_2 for 24 hours using a BD BBL™ GasPak™ 100 Anaerobic System (Becton, Dickinson and Co., Sparks, MD, USA).

2.10. Short-chain Fatty Acids Analysis

2 mL sample was placed in a 12 mL tube. 500 μL H_2SO_4 work solution was added into it. The H_2SO_4 work solution was prepared by adding 100 mL of Sulfuric acid (98%) into 100 ml DI water. The preparation procedure should be conducted in the hood. Then a few amount of NaCl was added with the back of a Pasteur pipette. 400 μL internal standard solution was added into the mixture. The internal standard solution was prepared by adding 1.5 mL 2-methylhexanoic acid, 99% into 98.5 mL 0.1 M NaOH. Then 100 mL DI water added into the above 2-methylhexanoic acid solution. 2.0 mL diethylether was added with a glass pipette. The tubes were vortexed for 5 min, and then centrifuged for 3 minutes 3000 rpm. The supernatant layer (ether phase) was transferred into a GC vial and close it with a cap (+ septum) for GC measurement.

An Agilent 6850 gas chromatography was used to quantify the production of short-chain fatty acids. The GC was connected with a DB-WAX capillary column (30 m × 0.25 mm i.d.; 0.25 μm film thickness) and a flame ionization detector (FID). The detector temperature was set at 250 °C. The initial oven temperature was set at 40 °C, holding it for 2 min, and then increased to 100 °C at the rate of 15 °C /min, and finally increased to 210 °C at 5 °C/min profile and held for 2 min with a total program time of

30 min. The flow rates of hydrogen and of air were controlled at 30.0 mL/min and 300 mL/min, respectively. Nitrogen as the carrier gas flowed at 24.0 mL/min.

2.11. Statistical Analysis

All data were expressed as means ± standard deviations. All the statistic analysis was conducted by IBM SPSS Statistics 22. To compare the significance of differences among different groups, one-way analysis of variance (ANOVA) was used with the significant difference defined at $p < 0.05$.

3. Results and Discussion

3.1. SHIME experiment

As illustrated in Figure III-1 (A1 and A2), the normal SHIME model is a twin-SHIME system, which serves as two individuals (one for test sample and the other one for the control) and each one has 5 reactors mimicking stomach, small intestine, ascending colon, transverse colon and descending colon in human body. The human fecal microbiota was inoculated in different regions of the colon in order to represent the overall community of gut microbiota. However, the normal SHIME model did not take the absorption from the small intestine into consideration. Therefore, in order to investigate the bioavailability of the formulations, the original SHIME should be modified with a dialysis system as shown in Figure III-1 (B1 and B2).

Bioavailability is defined as the fraction that eventually reaches the systemic circulation after oral adiminitration, which is related to the quantity of bioactive compounds released into the small intestine, the quantity of bioactive compounds absorbed through the gut membrane, and the quantity of bioactive compound remained after the first pass metabolism (*272*). Therefore, bioaccessible compounds are not

necessarily bioavailable due the first pass metabolism, while compounds that are not bioaccessible are generally considered as not bioavailable (*266*).

In the dialysis SHIME model, the colon part was simplified into one reactor. And the other reactors were modified into two vessels, i.e. sample compartment and concentrated digestion fluid compartment. The stomach and small intestine were combined into one vessel. The food uptake and digestion was simulated by peristaltic pumps based on the fill-and-draw principle. The dialysis fluid (3.75 g/L $NaHCO_3$) went through the dialysis cellulose membrane column (cut-off = 14 kDa) from the top to the bottom, while the digested samples from small intestine went through the column from the opposite direction. The sample collected in the dialysis liquid represents the absorbed RES that can be bioaccessible for the systemic circulation.

Upon oral administration, the transition time through stomach was around 1-2 hours (pH∼1.5–3.5) and the one through small intestine was about 3–6 h (pH∼5.5–6.8) before arrival to large intestine (pH∼6.4–7) (*273*). The digestion time of large intestine ranged from 12 to 24 h (*273*), depending on their defecation status. So in the dialysis SHIME model, the digestion time in stomach was set as 2 hours. The addition and transfer of formulation, SHIME feed, pancreatic juice, concentrated pancreatic solution, and bile liquid from different reactors were precisely controlled at specified intervals. After 2 hours, pancreatic juice was added into sample compartment and the pH value in the reactor was increased from 2.0 to 7.0. After 2.5 h digestion in small intestine, digested samples flowed through dialysis column and the total dialysis time was 100 min. The overall residence time in the SHIME model was 370 min.

During the digestion in stomach and small intestine, 1 mL of Pickering emulsion

sample was collected in the 2.0 ml centrifugation tube every one hour for optical microscopic imaging. As shown in Figure III-2, the droplet structure of Pickering emulsion was still observed after 2 hours digestion in the stomach. However, when the emulsion was further digested in the small intestine, the emulsion droplets were broken down gradually, forming numerous tiny droplets that may be due to the existence of surface active compounds in the digestion fluid. The observed large droplets in the small intestine were probably due to the mixing procedure during the syringe sampling.

The flow rate of sample in the tubes during dialysis was 3.5 ml/min. The absorption rate of RE was defined as the amount of absorbed RES divided by time. By collecting sample from dialysis tube (out), we can get the absorption rate of RE; while by taking samples from the tube linked to the colon, the rate of RES delivered into colon can also be calculated. At the 40^{th} min during the dialysis, Pickering emulsions have the fastest absorption rate and fastest release rate compared with nanoemulsions and bulk oils (Figure III-3, A and B). However, at the end of dialysis, the total amount of RES absorbed through the small intestinal and the one delivered into the colon were almost the same among the three kinds of formulations (Figure III-3, C and D). The possible reasons for this phenomenon may be the short bio-absorption time. Because the dialysis time for SHIME was 100 min, which was much shorter than the real absorption status. The dialysis did occur until the samples finished the digestion in stomach and small intestine. However, it is quite different compared with the real case, where the absorption from the small intestines happened simultaneously during the digestion.

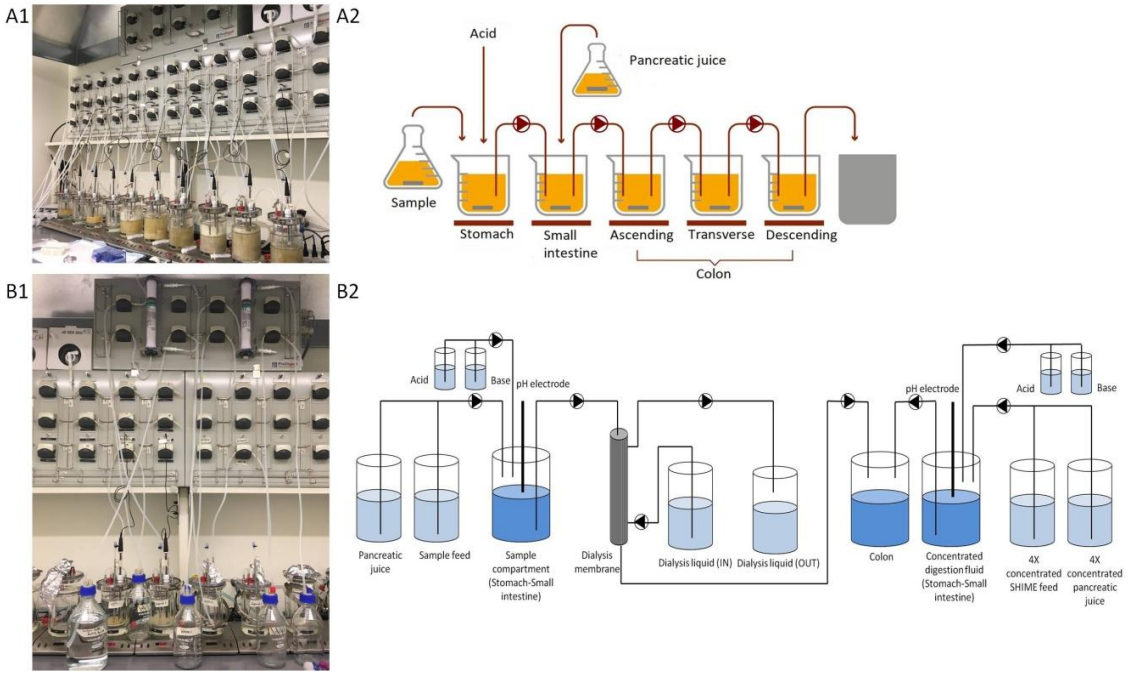

Figure III- 1. Schematic representation of the SHIME model (A1 and A2) and the dialysis SHIME model (B1 and B2).

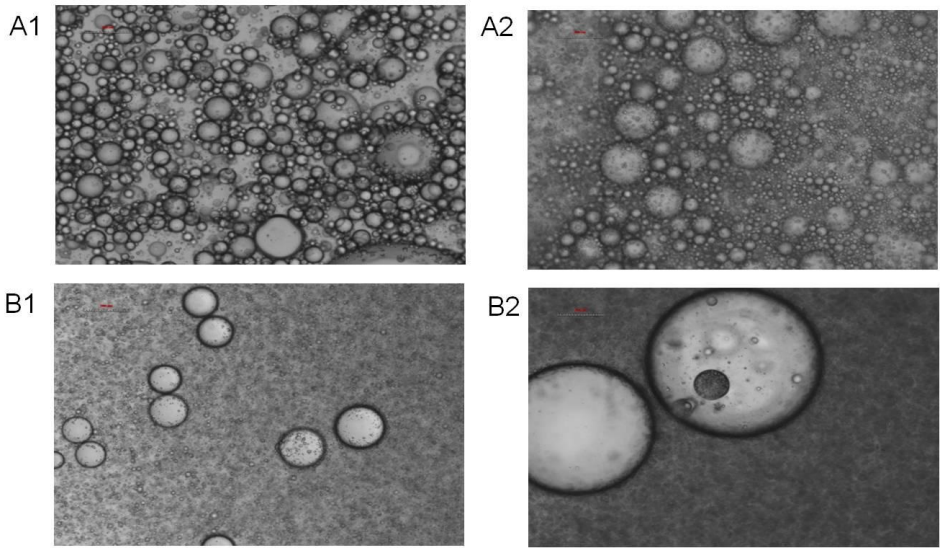

Figure III- 2. Optical microscopic images of Pickering emulsions after digestion in stomach for 1 h (A1) and for 2 h (A2), and then in small intestine for 1h (B1) and for 2 h (B2).

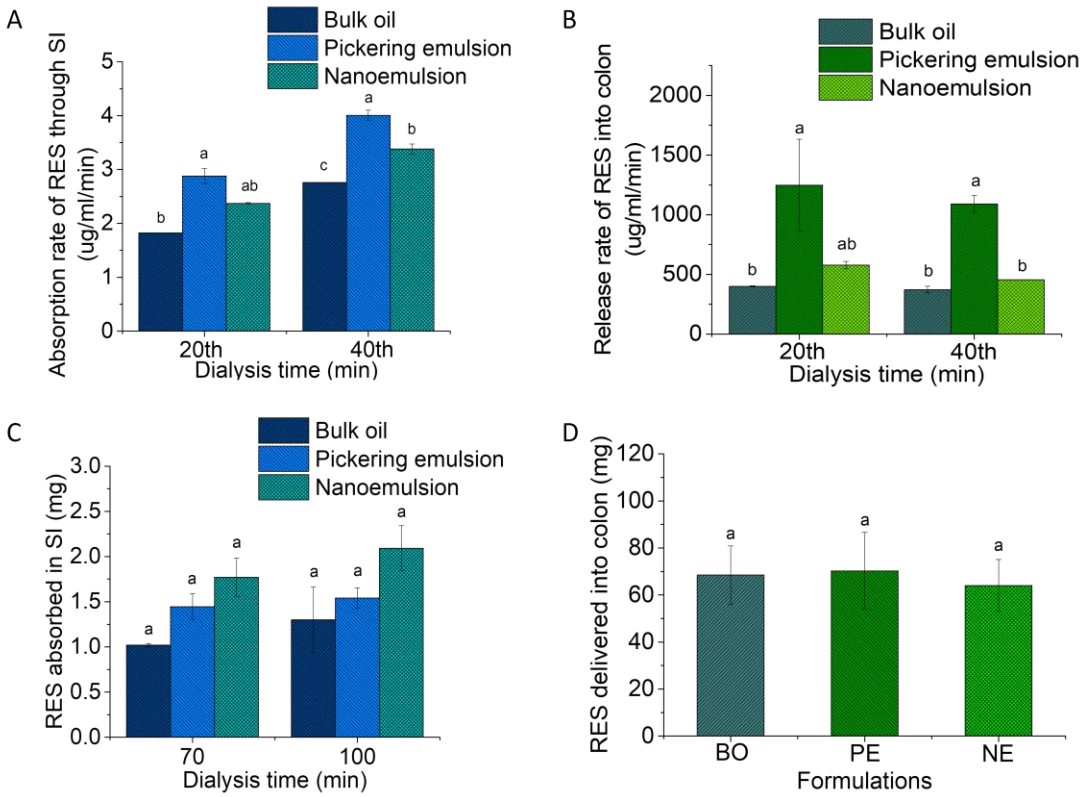

Figure III- 3. Absorbed and un-absorbed RES during the digestion; A, Absorption rate of RES through small intestine; B, Release rate of RES into colon; C, the amount of RES absorbed in small intestine; D, the amount of un-absorbed RES delivered into colon.

3.2. TIM-1 experiment

In order to better simulate the absorption process and further increase the dialysis time, the TNO gastro-Intestinal Model (TIM-1) (TNO Zeist, Netherlands) was utilized to simulate the digestion and absorption in the gastrointestinal tract. The SHIME system has single one reactor to represent small intestine. But the TIM-1 system divided the small intestine into 3 parts, including duodenum (pH 6.4), jejunum (pH 6.9) and ileum (pH 7.2). And there are two hollow fiber membranes (Spectrum Milikros modules M80S-300-01P, with 0.05 μm pore size) to mimic the absorption from jejunum and ileum. Since the experiment was conducted in a fed-state, each compartment was pre-infused with start

residues before the feeding of samples. The liquid formulations used in this study are 50 g of 10 mg/mL RES in Pickering emulsions (50% oil fraction), 50 g of 10 mg/mL RES in nanoemulsions and 25 g of 20 mg/mL RES in bulk oil solutions. The loading capacity of RES in Pickering emulsions can be further improved due to its characteristic high internal phase property, i.e. high oil phase in the emulsion. But in order to make sure lecithin-stabilized nanoemulsion deliver the same amount of RES as Pickering emulsions without compromising its stability, the oil fractions in these emulsions were set as 50%. The control group was 20 mg/mL RES in oil solutions, which is the same as the oil phase used to fabricate emulsions. The total amounts of RES in different formulations were the same, kept at 500 mg/day. The liquid samples were fed into the stomach using a funnel together with 95 g gastric electrolyte solution, 50 g water, and 5 g gastric enzyme solution.

Previously, some people have used over-saturated oil suspensions of nutraceuticals as the control group in the TIM-1 experiment, such as tangeretin in medium chain triglyceride (MCT) oil suspension VS tangeretin in lecithin stabilized nanoemulsions (*15*), curcumin in corn oil suspension VS curcumin in milled starch stabilized Pickering emulsions (*274*), and curcumin in MCT oil suspension VS ovotransferrin fibril–stabilized Pickering emulsions (*275*). However, in this study resveratrol was completely dissolved in carrier oil, and the control group should have the same oil type as the emulsions. It is unreasonable to use RES in vegetable oil or MCT oil suspension as the control in this study, because we need to avoid the variance caused the different digestion behaviors of different types of oils.

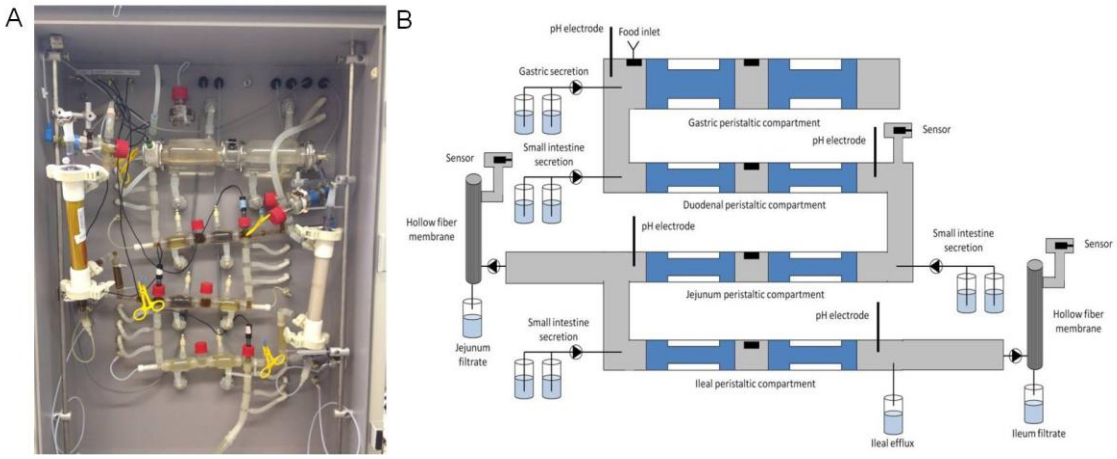

Figure III- 4. Illustration of the TIM-1 model; A, the digital image of TIM-1; B, the schematic representation of TIM-1.

The bioaccessibility of RES was calculated using the formula below, by using the mass of absorbed RES through capillary membrane column divided by the mass of RES added into the TIM-1 system.

$$Bioaccessibility\ (\%) = \frac{M_{absorb}}{M_{input}}$$

As illustrated in the Figure III-5, nanoemulsions have a burst release effect due to their smallest droplet size. The maximum release rate of RES arrived at 240 min, while bulk oil and Pickering emulsion showed shower release rate. The slow digestion rate of Pickering emulsions was probably due to the protection effect of zein/SC wall around the oil water interface, which was consistent with the result in the SHIME experiment that the droplet structure of Pickering emulsion was still observable in 2 hours digestion in stomach (Figure III-2). At the end of 6 hour-absorption, the accumulative bioaccessibility of Pickering emulsions was around half of the value of nanoemulsions (Figure III-5), which indicated that less amount of RES was absorbed into small intestine from Pickering emulsions. Therefore, Pickering emulsions were suitable for slowing down the

absorption of resveratrol in the small intestine, while nanoemulsions can be used to improve the absorption of RES.

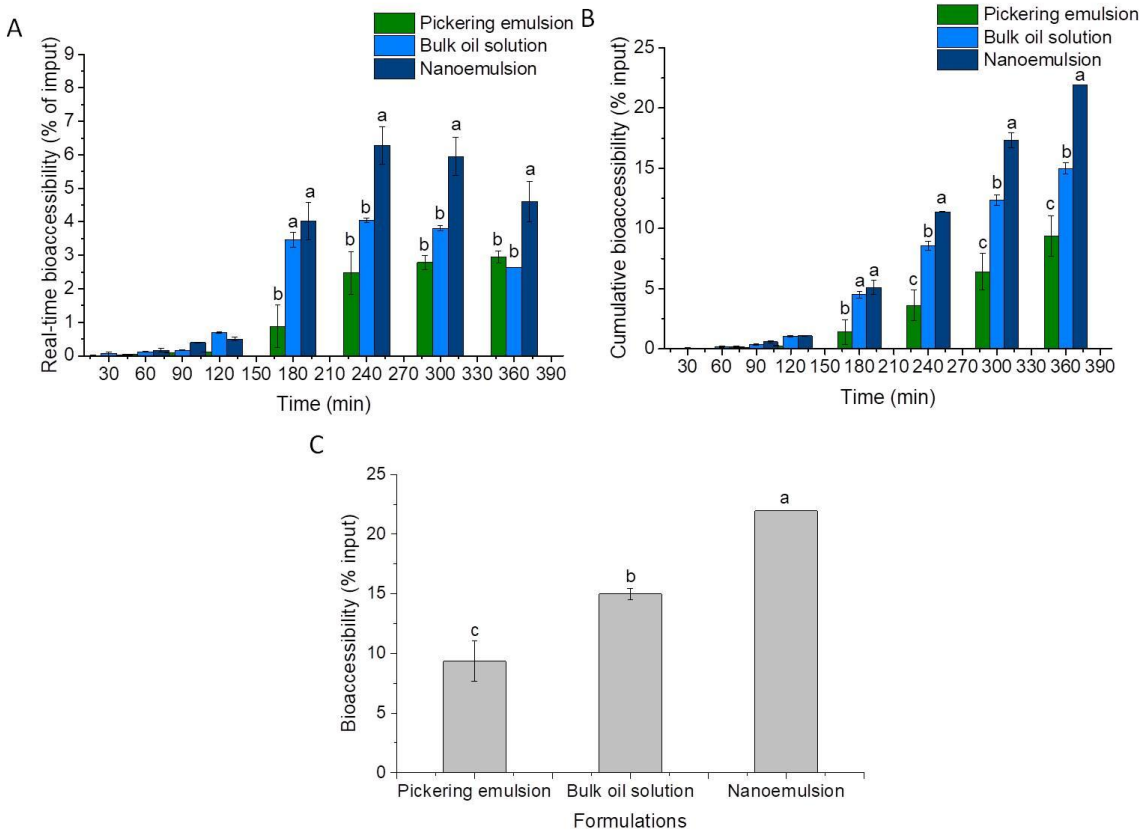

Figure III- 5. Real-time bioaccessibility (A) and cumulative bioaccessibility (B) of RES during the digestion in TIM-1 model; the cumulative bioaccessibility of RES after 360 min digestion (C).

In Table III-1 and Table III-2, they have compared different parameters and the digestion fluids used in the experiment. The total running times for both SHIME and TIM-1 were around 360 min. Both of them can be utilized to study the dynamic digestions of food matrix. The unique character of these *in vitro* models compared with *in vivo* models is that samples can be easily taken at different intervals from gastric intestinal organs. However, it is quite difficult to take samples out from jejunum or ileum when the animals are still alive. The biggest different between SHIME and TIM-1 is that

the SHIME system did not start the small intestine absorption until the stomach/small intestine digestion has finished. But the absorption in the TIM-1 model happened simultaneously within the whole digestion process, and we can clearly observe an increasing tread of the cumulative absorbed RES. Besides longer absorption time, TIM-1 model could mimic the absorption in jejunum and ileum separately by using two capillary membrane columns. However, SHIME model only has one dialysis cellulose membrane column. Generally speaking, TIM-1 model with 3 small intestinal reactors (duodenum, jejunum, and ileum) is more suitable to study the dynamic digestion and absorption in the upper gastric intestinal tract, while SHIME mode with 3 colon reactors (ascending, transverse and descending colon) is more suitable to study the interactions between gut microbiota and food matrix.

Table III- 1. Comparison of the parameters in the SHIME and TIM-1 model.

Dynamic digestion model	SHIME	TIM-1
Running time	370 min	360 min
Dialysis time	100 min	360 min
Absorption column	Dialysis cellulose membrane column X1 (cut-off = 14 kDa)	Capillary membrane column X2 (Spectrum Milikros modules M80S-300-01P, with 0.05 μm pore size)
Dosage of RES	500 mg/day	500 mg/day
Mixing	Stirring	Peristaltic movement
Reactors	Stomach, Jejunum, Duodenum, and Ileum	Sample compartment (ST/SI), Concentrated digestion fluid compartment (ST/SI), and colon

Table III- 2. Digestion fluids for the fed-state SHIME and fed-state TIM-1 experiments.

SHIME model			TIM-1 model		
Digestion fluids	**Recipe**	**Preparation amount/ Flow rate**	**Digestion fluids**	**Recipe**	**Preparation amount/ Flow rate**
Pepsin solution	15.6 g/L Pepsin in 10 mM HCl	30 mL	Gatric electrolyte solution (GES)	6.2 g/L NaCl, 2.2 g/L KCl, 0.3 g/L $CaCl_3$	500 g
Pancreatin solution for sample	13.5 g/L pancreatin, 0.76 g/L trypsin (Carl Roth, Cat.2193.1), 0.95 g/L chymotrypsin (Carl roth, CAT.0238.3), 20g/L oxgall, 18.75 g/L $NaHCO_3$	200 mL	Gastric enzyme solution (GEZS)	0.25 g/L Lipase, 0.20 g/L Pepsin, 2 g 1M CH_3COONa buffer (pH 5), 200 g GES	202 g
Concentrated pancreatin solution	3.6 g/L pancreatin, 24 g/L oxgall (dehydrated bile extract), 50 g/L $NaHCO_3$	100 mL	Pancreatin solution	70 g/L Pancreatin suspension, mix for 10 min under stirring, centrifuge for 20 min at 9000 rpm at 4 °C, collect the supernatant	267.5 g, 0.25 mL/min
Dialysis liquid	3.75 g/L $NaHCO_3$	2000 mL, 8 mL/min	Bile	Use 50 °C water bath to melt the frozen bile, filter through 2 250 um cloth filter	500 g
Concentrated SHIME feed PDNM001B	62.4g/L, autoclave and adjust the pH to 2.0 ± 0.1 with 37% HCl	200 mL	Small intestinal electrolyte solution (SIES)	5 g/L NaCl, 0.6 g/L KCl, 0.3 g/L $CaCl_3$ (pH 7.0)	2000g, 3.2 mL/min
Sample feed	50 g emulsion (500 mg RES), 61 mL d-H_2O, 5 mL Pepsin solution; or 25 g bulk oil (500 mg RES), 86 mL d-H_2O, 5 mL Pepsin solution;	116 mL	Sample feed	50 g emulsion (500 mg RES), 50 g d-H_2O, 95 g GES, 5 g GEZS; or 25 g bulk oil (500 mg RES), 75 g d-H_2O, 95 g GES, 5 g GEZS	200 g
			Duodenum	same as SIES	450 g, 0.5

	electrolyte solution		mL/min
	Jejunum secretion	4.17 g/L NaCl, 0.5 g/L KCl, 0.25 g/L $CaCl_3$, 100 g/L Bile	1800 g, 3.2 mL/min
	Ileum secretion	same as SIES	1500 g, 3.9 mL/min
	Duodenum start residue	15 g SIES, 15 g Pancreatin solution, 30 g Bile, 1 cup Trpsin solution (2 mg/cup)	60 g
	Jejunum start residue	50 g SIES, 50 g Pancreatin solution, 100 g Bile	200 g
	Ileum start residue	same as SIES	180 g

3.3. Franz Cell Diffusion

Due to the unique characteristics of low cost, good reproducibility, and easy operation, Franz Cell has been widely used to study the transdermal permeability of topical pharmaceutical products or cosmetic products through human skin (*276-278*) from cadavers or surgically removed skin, pig skin (*279*), rat skin (*280*), or artificial membrane, such as silicon rubber membrane (*281*), cellulose membrane (*271, 282*), polyacrylamide membrane (*282*), polydimethylsiloxane (PDMS) membranes (*282*), etc. In order to investigate how digested RES was absorbed through small intestine membrane, porcine small intestine purchased from local slaughter house was used in this study. The usage of animal small intestine membrane on the bio-absorption was not completely new. For instance, rat small intestine has been used like a dialysis bag to see how gold nanoparticles permeated through it (*280*). However, this is a pioneer work to mount the animal small intestine membrane on Franz Cell apparatus.

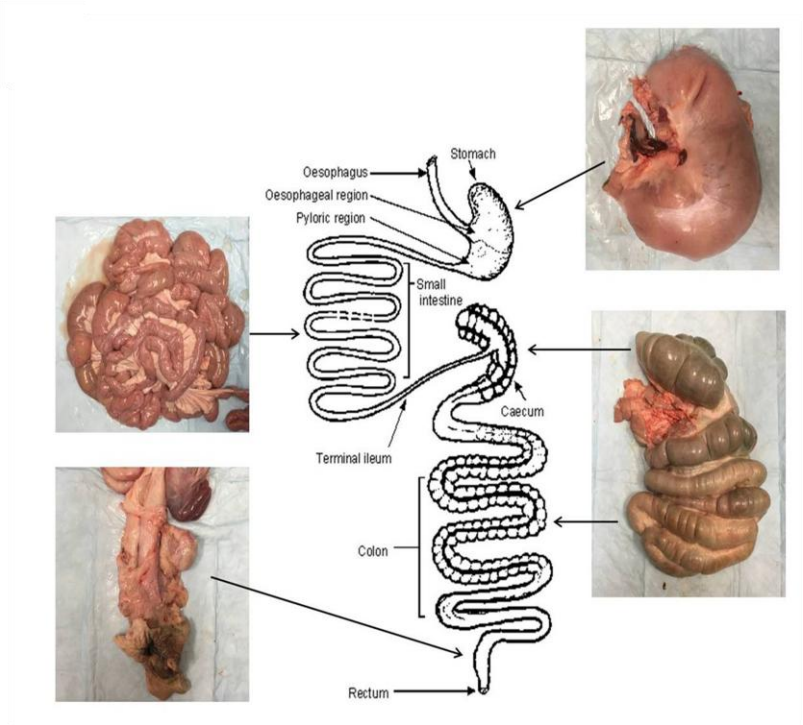

Figure III- 6. Anatomy of porcine digestion system

The slaughter house provided the whole digestion system of a pig, as illustrated in the Figure III-6. Even though the length of gut digestive tract may vary among different individuals, the total mucosal surfaces of human small intestine and of large intestine are averagely around 30 m^2 and 2 m^2, respectively (*283*). And the large surface area of the small intestine mucosa is mainly due to the existence of the plicae circulars (increased by around 1.6 times), and villi and microvilli (increased by 60–120 times) (*283*). Therefore, during the Franz Cell experiment, the rough surface of membrane containing plicae circulars, villi and mirovilli structures faced up to the sample donor chamber, while the smooth surface faced down to the diffusion receptor chamber. The fat tissues and the food residues were removed from small intestine, and the membranes were cut in to an informed size, wrapped in aluminum foil, as shown in Figure III-7. Franz Cell Diffusion is a standard system for the *in vitro* release test model. The cell has a sample donor

chamber and a cylindrical diffusion receptor chamber that is wrapped by a water jacket, keeping the whole system in 37 °C under continuous magnetic stirring (Figure III-7, A and B).

The formulations used in the Franz Cell experiment were the 180 min TIM-1 digested samples. There are several reasons for why the samples at this time point were chosen. Firstly of all, the samples being absorbed through gut mucosa should be the one that has already been digested. The time for the stomach empty is usually around 2 hours, which indicates that at 180 min the whole food matrix has been transferred into small intestine and it has already been digested for around 1 hour in small intestine. Secondly, based on the HPLC analysis of TIM-1 samples, the concentration of RES in the initial 2 hours digestion was quite low. If the concentration of RES in the donor chamber is too low, the permeated RES will be very difficult to be detected in the receptor chamber. Thirdly, the total digestion time in the small intestine is around 4-5 hours. So it is quite reasonable for the samples to be absorbed on Franz Cell apparatus for 3 hours after 3 hours digestion in TIM-1.

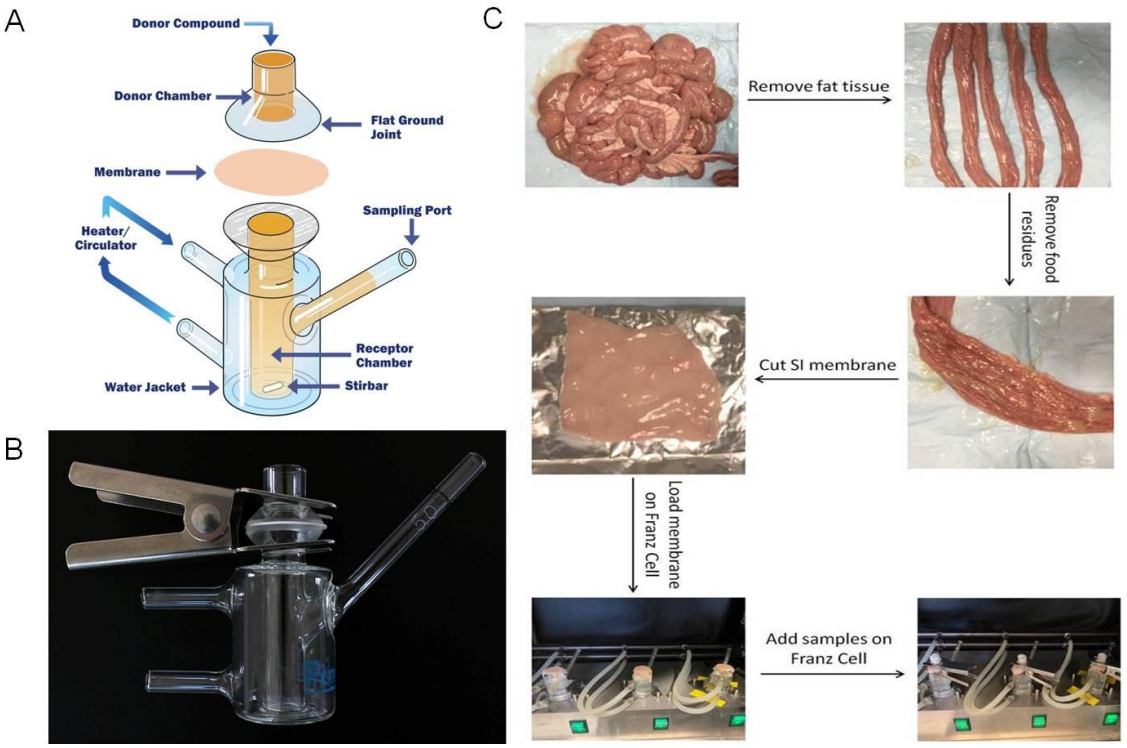

Figure III- 7. Schematic illustration of Franz Cell Diffusion apparatus (A and B); Preparation of small intestine membrane for Franz Cell experiment (C).

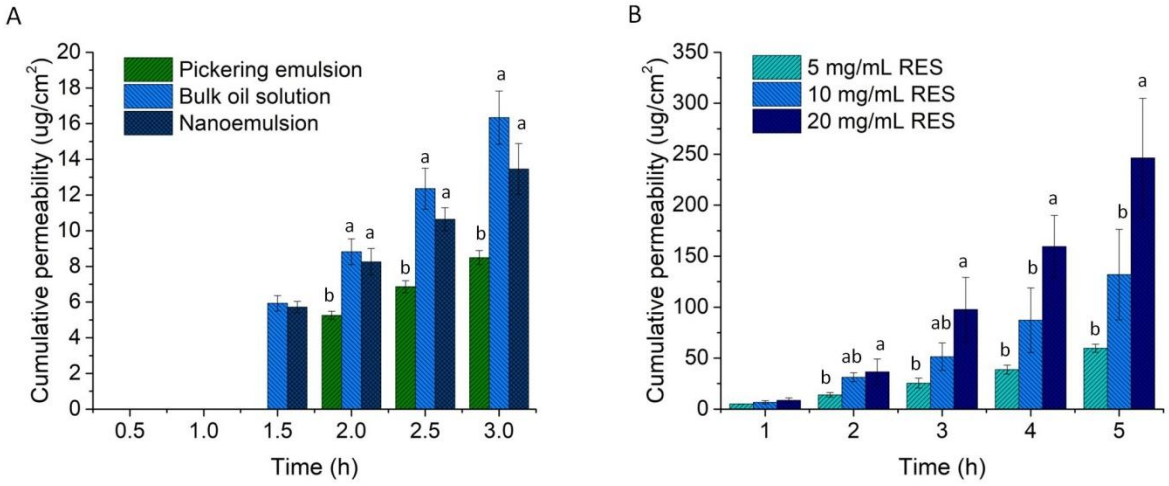

Figure III- 8. Cumulative permeability through small intestine; A, 180 min TIM-1 digested formulations; B, 5 mg/mL, 10 mg/mL, 20 mg/mL RES in bulk oil solutions.

As illustrated in Figure III-8, RES in Pickering emulsion did not permeate

through the membrane until 2 hours, while permeated RES was observed earlier at 1.5 hours for nanoemulsions and bulk oil solutions. After 3 hours absorption, nanoemulsions and bulk oil solutions had significantly higher cumulative permeability as compared with Pickering emulsions, which indicated that Pickering emulsions had slower absorption rate in the small intestine. The permeation of penetrant is usually driven by the concentration gradient through the passive diffusion approach. In order to investigate the influence of RES concentration on the permeability, different concentrations of RES in bulk oil solutions were used (Figure III-8, B). The dose dependant trend on the permeability was very obvious. And it was also interesting to find that the standard deviations at high concentrations (10 mg/mL and 20 mg/mL) were larger than the ones at low concentrations, which meant different pieces of small intestine membranes may behave different at high RES concentrations.

Even though the absorption of nutrients is mainly through small intestine, we still would like to compare the permeation property between small intestine and colon. As we can see from Figure III-9, the cumulative permeability through small intestine was slightly higher than colon, but the difference was not significant. Besides the amount of RES permeated through the membrane, the RES trapped in membrane cells was also detected. The ratio of permeated RES to trapped RES by small intestine was slightly higher than that of colon. Small intestine had around 70% of RES permeated through the membrane, while colon had 60% of RES permeated. Specifically for small intestine, it was interesting to find that even though Pickering emulsions had lower total RES absorption (~ 20 $\mu g/cm^2$) as compared with nanoemulsions (~ 35 $\mu g/cm^2$) and bulk oil solutions (~ 45 $\mu g/cm^2$), the percentages of permeated RES were almost the same for the

three groups (35-40%), as shown in Figure III-10 (A). As the concentration of RES increased, the total absorbed RES also increased gradually, but the percentages of permeated RES (70-75%) were almost the same for different RES concentrations (Figure III-10, B). Since the initial RES concentrations in formulations, around 100-200 μg/mL, were much lower than 5 mg/mL, it was considered that at high RES concentration the permeation percentage would be around 70-75%, while at low RES concentrations it would be around 35-40%.

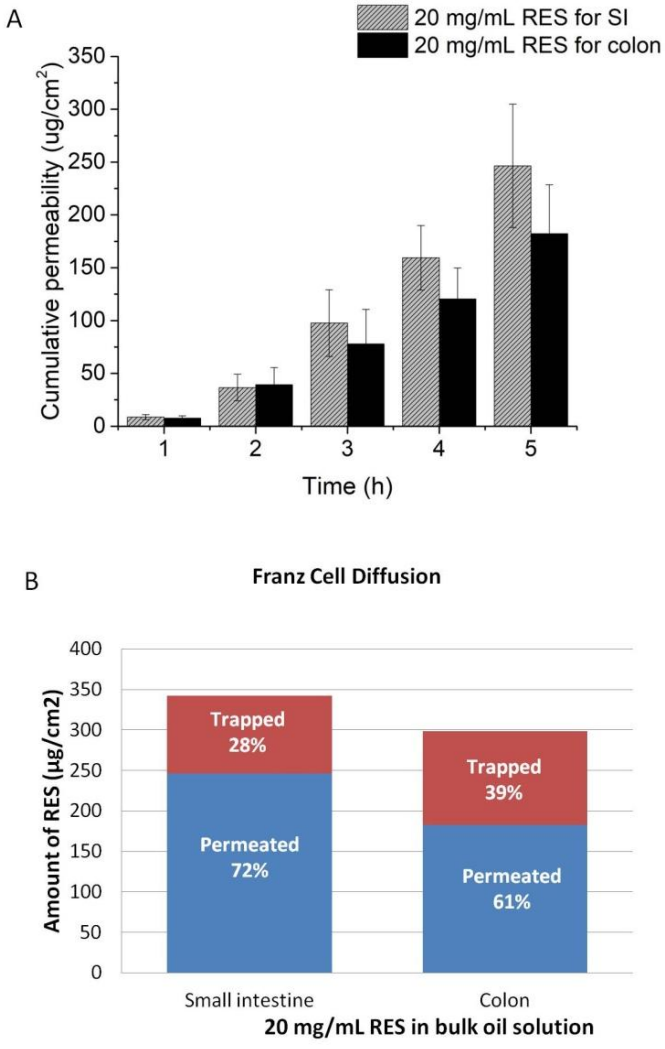

Figure III- 9. The cumulative permeability of RES (A) and the total absorption of RES (B) through small intestine and colon.

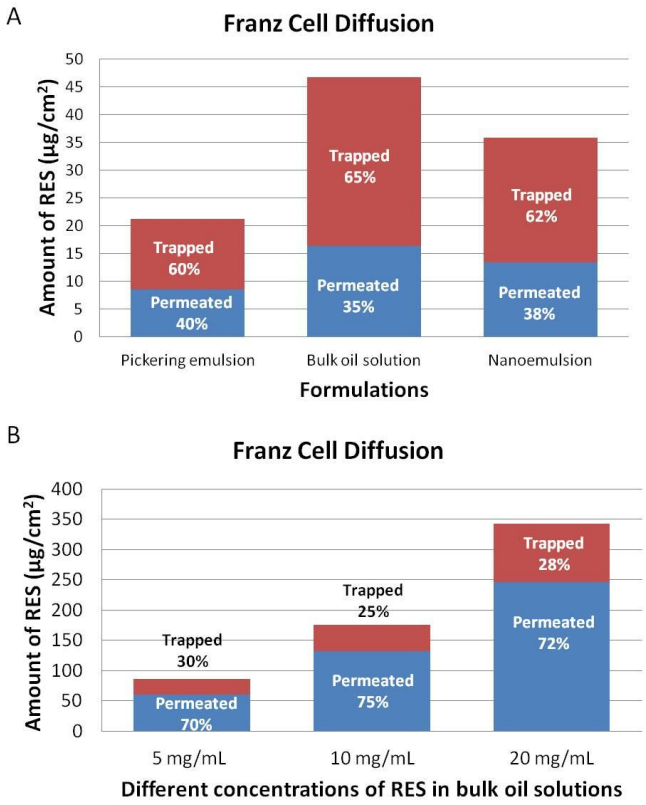

Figure III- 10. The total absorption of RES through small intestine; A, 180 min TIM-1 digested formulations; B, 5 mg/mL, 10 mg/mL, 20 mg/mL RES in bulk oil solutions.

3.4. Anaerobic cultivation

In order to see if there is any dose-dependent effect of RES on the growth of probiotics, the experiment was firstly conducted using RES ranging from 200 μM to 12.5 μM. The OD value was used to indicate the growth of bacteria. The higher the OD value is, the larger the amount of bacteria is. As illustrated in Figure III-11, 200 μM was too high to promote the growth of *Lactobacillus* GG (LGG), that the OD values were significantly lower than the other groups. When the concentration of RES was lower than 100 μM, it was very interesting to notice that with a decrease of the RES concentration, the OD values after 24 h incubation increased gradually. But it was still quite difficult to

claim that low concentration of RES promotes the growth of LGG, while high concentration of RES inhibits its growth. Because their final OD values were quite close with each other without the amplification of the image. Since the RES would not inhibit the growth of LGG, we would like to figure out if the carrier oil influences the growth of bacteria. We firstly dissolved RES in the carrier oil, and then digested it using the SHIME system. The LGG was treated with digested RES in oil samples in a concentration from 1.25% to 5.00%. As we can see from Figure III-11, higher concentrations of digested RES oils provided better effect, which also indicated the carrier oil was not toxic to the LGG.

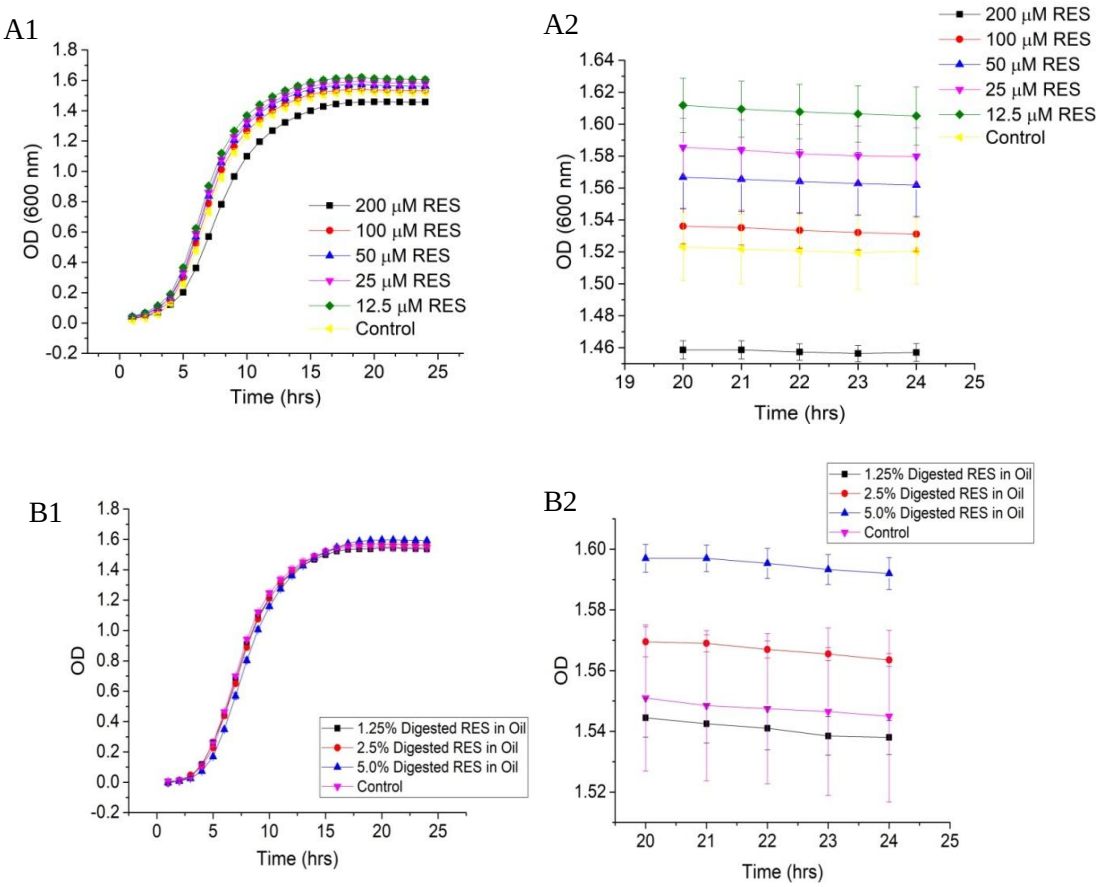

Figure III- 11. Growth curve of *Lactobacillus* GG under different concentration of RES; A, treated with RES in 2.5% DMSO solution; B. treated with SHIME digested RES in bulk oil formulation.

After we confirm the low toxicity of carrier oil, we want to know if the emulsifiers in delivery systems will influence the growth of bacteria. The 5% of digested Pickering emulsion, nanoemulsion and bulk oil was added into MRS nutritional media. And the obtained media was 1:1 added into LGG inoculated MRS solution (1% inoculation rate). As shown in Figure III-12, Pickering emulsions with or without the loading of RES gave the similar results, and they were much better than the other groups. And nano-emulsions gave the worst result. With the encapsulation of RES, the result was slightly better than blank nanoemulsion, which means lecithin as the emulsifier may have the toxic effect towards the growth of LGG. And the result of RES loaded bulk oil was better than nanoemulsions, but worse than Pickering emulsions. The mechanism may be due to the possibility that the surfactant, zein, used in the Pickering emulsions may serve as the nutrition source for microbes.

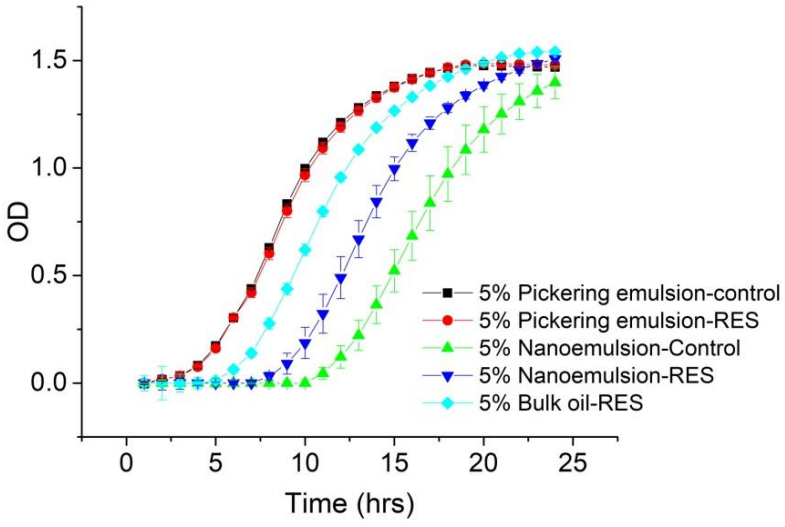

Figure III- 12. The growth curve of *Lactobacillus GG* after treated with SHIME digested RES-loaded formulations, i.e. Pickering emulsion, nanoemulsion and bulk oil solution.

The production of short-chain fatty acids was monitored during the 24 hours

anaerobic incubation (Figure III-13). There was no significant difference in the production of propionic acid and butyric acid among different formulations. Nanoemulsions produced higher amount of acetic acid at the end of incubation. There were possible several reasons for that. Firstly, the incubation time, 24 hours, may be too short to show the difference caused by encapsulated RES. Because many studies focusing on the gut microbiota used long-term in vitro fermentation models (e.g. TIM-2, SHIME), or in vivo animal models (cultivate at least several weeks). Secondly, RES may influence other bacteria that did not influence much on the production of short-chain fatty acids.

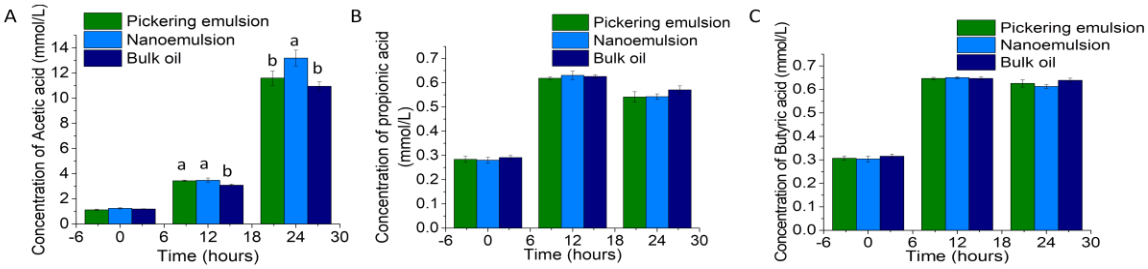

Figure III- 13. Production of acetic acid (A), propionic acid (B), and butyric acid (C) after in vitro fermentation for 0 h, 12 h, and 24 h.

4. Conclusion

This study used the SHIME and TIM-1 model to compare the digestion profile of Pickering emulsions, nanoemulsions, and bulk oil solutions. Resveratrol was encapsulated in these delivery systems with a high loading capacity of 10 mg/mL. Both TIM-1 and Franz Cell experiments indicated that Pickering emulsion effectively slowed down the bio-absorption in small intestine with the bioaccessibility and bioabsorption of RES significantly lower than the one of nanoemulsion and bulk oil solutions. Lecithin stabilized nanomemusions retarded the growth of *Latobacillus* GG, while Pickering emulsions even promoted its growth. Nanoemulsion promoted the production of acetic

acid on human feces samples. Pickering emulsions and bulk oils gave similar results on the fatty acid production by gut microbiome. Conclusively, Pickering emulsions are more suitable for delivery of resveratrol into colon, while nanoemulsions are more suitable for improvement of bioavailability of RES.

CHAPTER IV. FABRICATION OF COLLOIDOSOMES USING BIOMASS-BASED MATERIALS

Partial contents in this chapter were adapted from the paper "Fabrication of Colloidosomes through Layer-by-layer Self-assembling using Biomass-based particles" which was ready for submission.

1. Introduction

Colloidosomes belong to a class of microcapsules with a typical hollow shell structure formed by colloidal particles (*86*, *87*). The pioneering work about the production of colloidosomes is firstly reported by Velev and co-workers in 1996 (*82*). They allowed the assembly of latex colloidal particles onto an octanol based emulsion templates, and formed hollow spherical clusters, which they called "supraparticles" (*82*). The term "colloidosomes" was firstly proposed by Dinsmore, who used latex particles as the coating materials to form microcapsules through heat sintering process (*83*).

Colloidosomes can be prepared through both hard solid templates and soft liquid templates. The core removal process for hard core materials, such as polystyrene latexes and melamine formaldehyde particles, are usually more severe, requiring high temperature calcination or strong acid dissolution (*88*). Routes of forming colloidosomes through liquid templates are commonly based on the self assembly of colloidal particles at the interface of two immiscible phases, which is typically similar to the formation of Pickering emulsions (*89*), through either water-in-oil emulsions (*90*) or oil-in-water emulsions (*91*). In order to convert the oil-in-water Pickering emulsion precursors into

microcapsules, the core materials can be removed by various approaches, including solvent evaporation(*101*), freeze-drying (*103*), and organic solvent treatment, such as ethanol (*104*) or 2-propanol (*108*). For water-in-oil emulsions, the colloidosome microcapsules can simply be achieved by centrifugation (*104*). As a result, the shell reinforcement is very important for the preparation of colloidosomes in order to survive the removal of oil/water template.

The easiest way to lock polymeric particles in the shells is to heat the dispersion and form a continuous shell. But this method is not suitable for the encapsulation of heat-unstable nutraceuticals or drugs. Besides thermal annealing, other alternative shell locking methods include the use of coagulant (such as casein, HCl and $CaCl_2$ to lock in the latex particle) (*84*), polyelectrolyte deposition, polymerization of droplets, and covalent cross-link (*121*).

In this study, layer-by-layer (LbL) deposition technique was applied to build a strong shell structure on the templates of oil-in-water Pickering emulsions. The biggest challenge of using LbL technique is to prevent emulsions from coalescence, aggregation, and flocculation in the early stage of deposition. If the polyelectrolytes concentration is not high enough to saturate the surfaces of droplets, which means two adjacent droplets may share one polyelectrolyte, the bridging flocculation may occur. If the polyelectrolytes concentration is too high, the attractive depletion forces in the emulsions will be strong enough to overcome various repulsive forces (e.g., electrostatic repulsion and steric hindrance), resulting in a depletion flocculation of droplets (*113*). What's more, it is also possible that stabilizers would detach from the oil-water interfaces during those washing steps after the deposition of each layer. Therefore, it is very important to

develop a stable primary emulsions and then successfully LbL coat polyelectrolytes on the droplet surface.

Up till now, colloidosomes have been fabricated using various colloidal particles, such as synthetic colloidal particles, such as poly (tert-butylaminoethyl methacrylate) latexes (*94*) and polystyrene latexes (*95*), and inorganic colloidal particles, such as Fe_3O_4 (*97*), TiO_2 (*284*), Laponite nanoparticles (*99*), and surface modified silica particles (*87, 100, 101, 103, 285*). There are also many studies about Pickering emulsions stabilized by inexpensive food-originated materials, such as starch (*69*), cellulose (*70*), zein (*71*), karifin (*286*), etc. However, the formation of colloidosomes using biomass-based colloidal particles was scarcely reported. In this paper, zein/sodium caseinate (zein/SC) colloidal particles were utilized to fabricate colloidosomes through layer-by-layer deposition technique. The emulsification capacities of zein/SC complexes were systematically investigated using oils of different polarities, ranging from long-chain triacylglycerols to short-chain triacylglycerols, and from volatile to non-volatile. The thickness and viscoelastic properties of the polyelectrolytes adlayers (i.e., chitosan, sodium alginate, and zein) were also determined by QCM-D analyses.

Besides the layer-by-layer (LbL) deposition technique, in order to further simplify the preparation methods of colloidosomes, genipin will be used as a cross-linker to stabilize the shell structure of Pickering emulsions. Genipin is isolated from the fruits of gardenia (Gardenia jasminoides Ellis) (*287*). In traditional Chinese medicine, this plant has been used for the treatment of various inflammations, jaundice, headache, edema, fever, hepatic diseases and hypertension for years (*288-290*). It was found that genipin had a dose dependent anti-inflammation effect, which inhibited synthesis of nitric

oxide (NO) and the expression of inducible nitric oxide synthase (iNOS) (*289*) . Both the MTT assay and the colony forming assay implied that genipin was about 5000-10000 times less cytotoxic than glutaraldehyde (*290*). Compared with glutaraldehyde fixed bioprostheses, the genipin fixed ones have superior cellular compatibility, mechanical strength, and resistance against in vitro enzymatic degradation (*291*), which indicated that genipin could form stable and biocompatible cross-linked products (*290*).

Many papers have reported about the cross-linking effect between genipin and chitosan (*292-295*). However, only a few people discussed the cross-linking of proteins using genipin. The mechanism for the genipin cross-linking reaction is based on the formation of a secondary amide bond and a heterocyclic amino linkage, which results from a nucleophilic attack on the olefinic carbon atom at C-3 of genipin by primary amino groups (*296-299*). The existence of Lysine, Arginine, Glutamine, and Asparagine in proteins provides free primary amino groups for this covalent linking reaction. It was found that genipin was able to cross link gelatin film, resulting in an improved mechanical, thermal and swelling properties (*300*). Therefore, genipin will be used to cross-link zein/SC complexes.

2. Materials and Methods

2.1. Materials

Zein was purchased from Freeman Industries, L.L.C. (Tuckahoe, NY, USA). Chitosan was purchased from Golden-Shell Pharmaceutical Co.,Ltd. (Yuhuan, Zhejiang, China) with purity higher than 95%. The molecular weight of chitosan is 1000kDa. Sodium alginate (1% solution has a viscosity of 80 ~ 200mPa·s at 20°C) was purchased from Kimica Corporation (Tokyo, Japan). Genipin was purchased from Wako Pure

Chemical Industries, Ltd. (Tokyo, Japan). Dimethyl sulfoxide (DMSO), 11-Mercaptoundecanoic acid (11-MUA), N-hydroxysuccinimide (NHS), N-Ethyl-N′-(3-dimethylaminopropyl) carbodiimide hydrochloride (EDC), fluorescein isothiocyanate (FITC), casein sodium salt, triacetin, tributyrin, tripropionin were purchased from Simga-Aldrich (St Louis, MO, USA). Sunflower oil was purchased from a local market.

2.2. Preparation of colloidal particles

To prepare 1 mg/mL zein colloidal particles, 10 mg/mL zein in 70% (v/v) EtOH-H_2O solution was 1:9 diluted with deinoized water under magnetic stirring at 1000 rpm (Barnstead/Thermolyne, CIMAREC, Ashville). The formation of zein/SC complexes was based on the antisolvent precipitation method with some modifications (*57*). Briefly, 0.25g of zein was dissolved in 10 mL 70% (v/v) EtOH-H_2O solution. Then this zein stock solution was added into 25 mL deionized water containing 0.3% (w/v) of sodium caseinate (SC) to form zein/SC complexes, under magnetic stirring at the same speed as mentioned above. 1 mg/mL chitosan solution was prepared using 1% acetic acid solution as the solvent. 1 mg/mL sodium alginate solution was prepared by dissolving sodium alginate in 0.5 M sodium chloride solution. The obtained dispersions were stored at 4°C until usage.

2.3. Preparation of Pickering emulsions

The zein/SC complex dispersions were added into sunflower oil with oil fractions from 30% to 60%. The mixture was homogenized under high speed homogenizer (Ultra-Turrax, IKA T25) at 11000 rpm for 2 min. The obtained emulsions were washed three times with equal amount of deionized water and oscillated at 100 rpm for 3min in each

wash cycle to remove unattached surfactants.

2.4. Preparation of colloidosomes

In order to build layer-by-layer deposition structure on the surface of Pickering emulsions, the positively charged polysaccharide, chitosan, and negatively charged polysaccharide, sodium alginate were used. Since the Pickering emulsion was stabilized by negatively charged zein/SC complexes, the first layer of polysaccharide is chitosan. Different ratios (v/v) of chitosan (CS) solution to Pickering emulsion, i.e., 1.2:1, 1:1, 1:1.2, and 1:2, were tried to determine the optimum ratio, so as to prevent undesired flocculation and precipitation. The mixture was then oscillated at 100 rpm for 20 min to ensure CS adsorption. Ice bath was required at this step if the organic oil phase is volatile, toluene in this study. The unattached CS was removed through 3 washing cycles with excessive amount of 0.5 M NaCl solution. In each washing cycle, it formed a creaming layer in the secondary emulsion after a few minutes of quiescent storage. The excess liquid at the bottom was removed using a syringe. At the third washing cycle, 0.5 M NaCl solution was replenished to the creaming layer to keep the whole mixture in a constant volume. The coating of alginate (ALG) and zein onto the Pickering emulsion droplets was carried out in the exact same way as for the CS coating. This coating process was repeated until 3 bi-layers of CS-ALG coatings and 1 layer of zein coating were deposited on droplet surface, successively. Once the coating of polyelectrolytes was completed, the volatile oil template was evaporated by rotary vacuum evaporation at room temperature.

2.5. Particle Size and Zeta Potential

To determine particle sizes (hydrodynamic diameters) of the obtained zein and

zein/SC complexes, dynamic light scattering approach was applied by using a BIC 90Plus particle size analyzer equipped with a Brookhaven BI-9000 AT digital correlator (Brookhaven Instruments Corp., Holtsville, NY, USA). Zein dispersion and zein/SC complex dispersion were 1:3 diluted with deionized water before measurement. The zeta potentials were measured using a Zetasizer Nano ZS (Malvern, UK) and all the measurements were conducted at 25 °C in triplicate. The refractive indexes used for protein samples and for polysaccharides were 1.450 and 1.330, respectively.

2.6. Optical Microscopy

Samples (100 μL) were placed on a clean glass slide, and diluted with a drop of deionized water if needed before imaging. Microscopic images were taken using the Nikon TE2000 microscope (Japan). And particle size distributions were analyzed using Image J software. Average sizes of droplets in Pickering emulsions and colloidosomes were calculated using 50-200 droplets.

2.7. Scanning Electron Microscopy (SEM)

SEM studies were performed by using a Zeiss Sigma Field Emission SEM (Carl Zeiss Microscopy, Thornwood, NY, USA) with an accelerating voltage of 5 kV. Before measuring, colloidosomes were washed with excessive amount of water for 3 times to remove sodium chloride residues. Samples were mounted onto aluminum stubs with double sided adhesive carbon discs and dried in 40°C oven. Prior to examinations, samples were sputtered with a thin layer of gold.

2.8. Preparation of Zein/SC Surface on Au Sensor Crystal

The immobilization of zein/SC colloidal particles on the Au quartz crystal (Q-Sense AB, Sweden) surface was carried out using the method published previously with

some modifications (*301*). The fundamental frequency of crystals is 5 MHz. In order to activate the Au surface, freshly-cleaned Au quartz crystals were treated with 10 mM 11-MUA in absolute ethanol solution at 60 °C for at least 24 h, and subsequently immersed in a mixed solution containing 100 mg/ml EDC and 100 mg/ml NHS(1:1 (v/v) mixing) in deionized water for 1 h. The zein/SC complex (zein/SC (w/w), 10:3) dispersion was used to incubate the activated surfaces at 4 °C for at least 24 h. The quartz crystals were finally rinsed thoroughly with deionized water, and dried under N_2 flow.

2.9. QCM-D Measurement

The layer-by-layer coatings of CS and ALG onto the Pickering emulsion surfaces were studied by monitoring changes in frequency (Δf) and energy dissipation (ΔD) on an Au quartz crystal using a quartz crystal microbalance with dissipation monitoring (QCM-D) (Q-Sense AB, Sweden). Before the adsorption of CS and ALG, zein/SC complex particles were firstly deposited onto the Au surface as mentioned above. Prior to the coating of each layer, buffer solutions for CS and ALG, i.e. 1% acetic acid solution and 0.5M sodium chloride solution, respectively, were firstly filled into the entire loop to rinse the whole system for at least 5min at speed of 10 mL/h. After a stable baseline was established, three bi-layers of CS-ALG and one last layer of zein were coated alternately onto the quartz crystal and kept there for 20 min. The incubation time was in consistence with the time used in colloidosomes preparation (section 2.5). For all measurements, the temperature was controlled at 25.00 ± 0.02 °C. The data were analyzed using QTools software.

2.10. Cross-linking of Colloidal Particles using Genipin

In order to prevent the evaporation of oil before droplet walls are well cross-

linked, sunflower oil was used as the oil phase, rather than toluene. Cross-linking of particle layers was conducted by mixing zein/SC stabilized sunflower emulsion into an aqueous genipin solution in 1:1 (v/v) ratio to make the final concentration of genipin in the mixture solution to be 2.5 mg/mL. The container for emulsion and genipin mixture was wrapped with aluminum foil. Samples were stored in a 37 ˚C oil bath. Fluorescence images were taken at 5h, 10h, 24h, 48h, and 72h. Detailed experimental design was shown in Table IV-1.

Table IV- 1. Experimental design for genipin cross-linking reaction.

	Level				
Factor	1	2	3	4	5
A. Concentration (mg/ml)	2.5				
B. Reaction temperature (˚C)	20	37			
C. Reaction time (h)	5	10	24	48	72

3. Results and Discussion

3.1. Formation andCharacterization of Colloidal Particles

Zein/SC complexes were prepared through anti-solvent precipitation method with zein to SC mass ratio of 10:3. The effective diameters of zein and this zein/SC complex (10:3) were 117.5±0.7 and 167.9±5.2 nm, respectively, with a polydispersity of 0.227±0.012 and 0.267±0.012, respectively, as shown in Figure IV-1. Zein/SC complexes and alginate were negatively charged, while chitosan and zein particles were positively charged with zeta potentials around 15 mV.

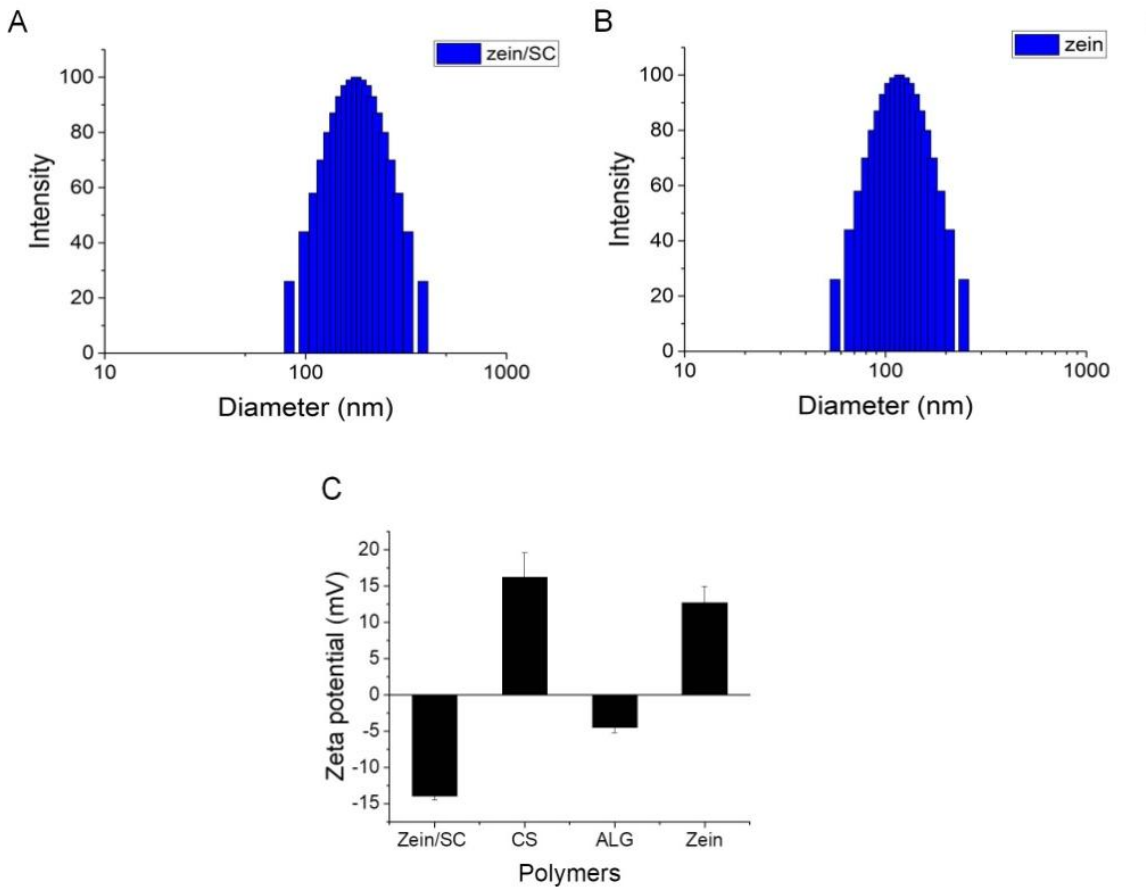

Figure IV- 1. Particle size distribution of zein/SC complexes (A) and of zein colloids (B); zeta potentials of polyelectrolytes (C), i.e. 1mg/mL zein dispersion, 7mg/mL zein/SC complex, 1mg/mL chitosan in 1% v/v acetic acid solution, and 1mg/mL sodium alginate in 0.5M NaCl solution.

3.2. Formation of Colloidosomes through LbL Deposition

When the oil fraction changed from 30% to 60%, droplet sizes increased significantly (Figure IV-2). At 50% of oil phase, the droplet sizes were much more even, but the surface coverage rate was obviously not as high as the one containing less amount of oil when the zein/SC concentration maintained the same. Stable colloidosomes should be built on the basis of Pickering emulsions which have a high surface coverage by colloidal particles. As a consequence, 30% of oil phase were applied for the following study.

The Pickering emulsions obtained were further strengthened by layer-by-layer (LbL) coating of chitosan solution and sodium alginate solution by turns. The influence of the addition ratio of polysaccharides (PS) solution to Pickering emulsions was studied. As illustrated in Figure IV-2, the morphology and stability of droplets did not change much with the changing of PS/emulsion ratio from 1.2:1 to 1:2. Therefore, from convenience perspective, the ratio of 1:1 was utilized for the coating on Pickering emulsion droplets.

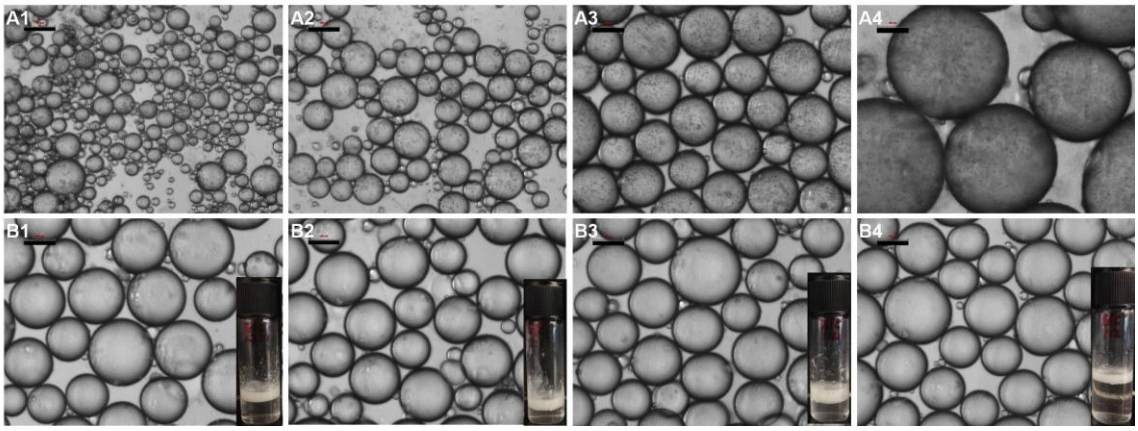

Figure IV- 2. Influence of sunflower oil fraction, i.e. 30% (A1), 40% (A2), 50% (A3), and 60% (A4), on the formation of Pickering emulsions; Influence of the ratio (v/v) of polysaccharide solution to Pickering emulsions, i.e. 1.2:1 (B1), 1:1 (B2), 1:1.2 (B3), and 1:2 (B4), on the morphology of droplets.

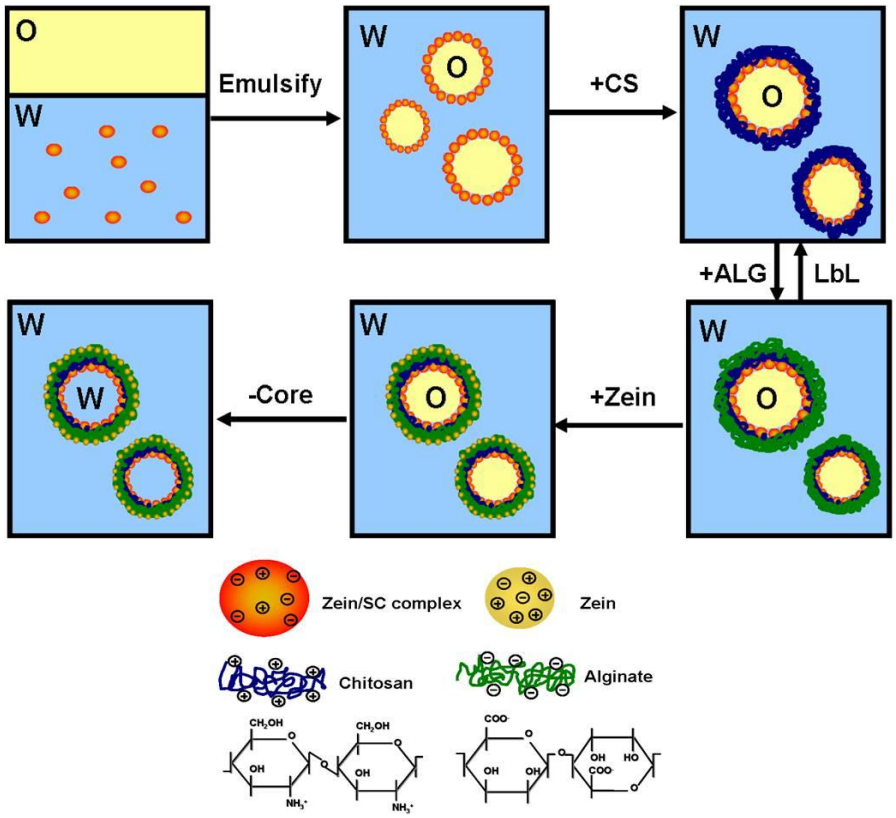

Figure IV- 3. Preparation procedure for making Layer-by-layer colloidosomes.

3.3. Characterization of Colloidosomes

The schematic graph for the preparation of colloidosomes was illustrated in Figure IV-3. Toluene Pickering emulsion stabilized by zein/SC complexes was used as templates, which was strengthened by LbL coatings of PS solutions. Zein is well known for its muco-adhesive properties, which significantly enhanced residence time of curcumin with more than 60% retention at the end of the detection (*302*). Therefore, the outside zein coating on colloidosomes was aimed at improving mucoadhesive properties of colloidosomes. In addition, it was also reported that zein coating successfully improved the release profile of chitosan/ tripolyphosphate nanoparticles against gastric fluid (*303*). Consequently, zein was chosen as the last coating layer for colloidosomes. The droplet morphologies and surface topography were shown in Figure IV-4. During the

solvent evaporation, colloidosomes with 3 layers of polyelectrolytes coating produced less stable droplets than 7 layers, as shown in Figure IV-4 (B and C). And more flocculent structures were observed in 3-layer coated droplets than the one in 7-layer coated droplets. It was because the oil phase was evaporated too fast or too vigorous; the shell wall may not stand a sudden increase of inner pressure, and would be destroyed, resulting in a flocculent structure. The droplet morphology did not change much with an addition of the last zein layer (Figure IV-4, E and F). Since the adsorption of each layer took 20 min for incubation and approximately 15-20 min for 3 washing cycles, it required at least 4-5 hours to finish the whole preparation process. Thus, when the emulsion was not prepared under ice bath and/or the whole procedures did not finish in one day, toluene, acting as the core material, would gradually evaporate and form partially collapsed microcapsules with small dents and wrinkles on the surface (Figure IV-4, A). From amplified image of 7-layer colloidosomes (Fig IV-4, D), small particles were found evenly distributed on the surface of droplets, while there were no particles in the background image, indicating that those small particles were exclusively oriented at the surface of droplets.

When a drop of colloidosomes solution were added on a glass slide and left for slow drying, their round microcapsule structures was not destroyed at all even in a completely dried state (Figure IV-4, E and F). The colloidosomes remained in their complete form without coalescence or rupture. However, if the wall material is not soft enough or too brittle to stand the deformation caused by dehydration, colloidosomes may rupture into fragments, on whose surface small cracks could be clearly seen, such as colloidosomes made by LbL deposition of poly (diallyldimethylammonium chloride)

(PDADMAC) and poly (sodium styrene sulfonate) (PSS) on CL silica particle stabilized Pickering emulsions (*101*). In the SEM image (Figure IV-5), spherical zein/SC complexes were found to distribute on the surface of colloidosomes. The surface structures of colloidosomes with or without zein remained the same, since zein particles have a similar size distribution with zein/SC complexes.

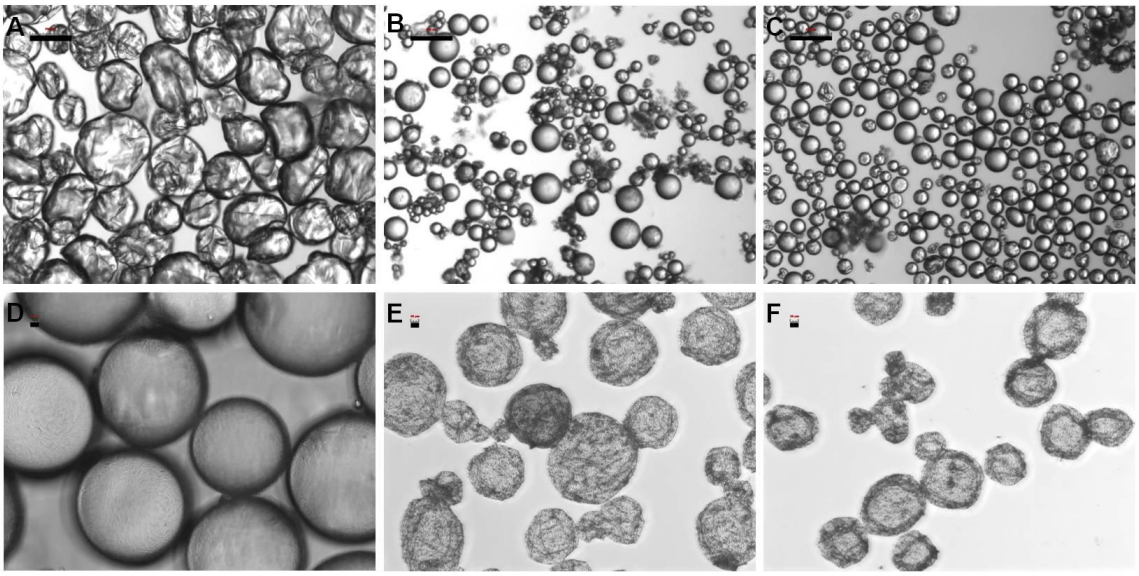

Figure IV- 4. Optical microscopic images of droplets; A, wet state of droplets with 7 layers of coating ($[CS\text{-}ALG]_3$-CS), which were prepared without ice bath; B, wet state of droplets with 3 layers of coating (CS-ALG-zein) after solvent evaporation; C, wet state of droplets with 7 layers of coating ($[CS\text{-}ALG]_3$-zein) after solvent evaporation; D, amplified image of droplets with 7 layers of coating ($[CS\text{-}ALG]_3$-CS); E and F, completely dried state of droplets with 6 layers ($[CS\text{-}ALG]_3$) and 7 layers ($[CS\text{-}ALG]_3$-zein) of coating, respectively; In A, B, and C, scale bars are in 100 μm; In D, E, F, scale bars are in 10 μm.

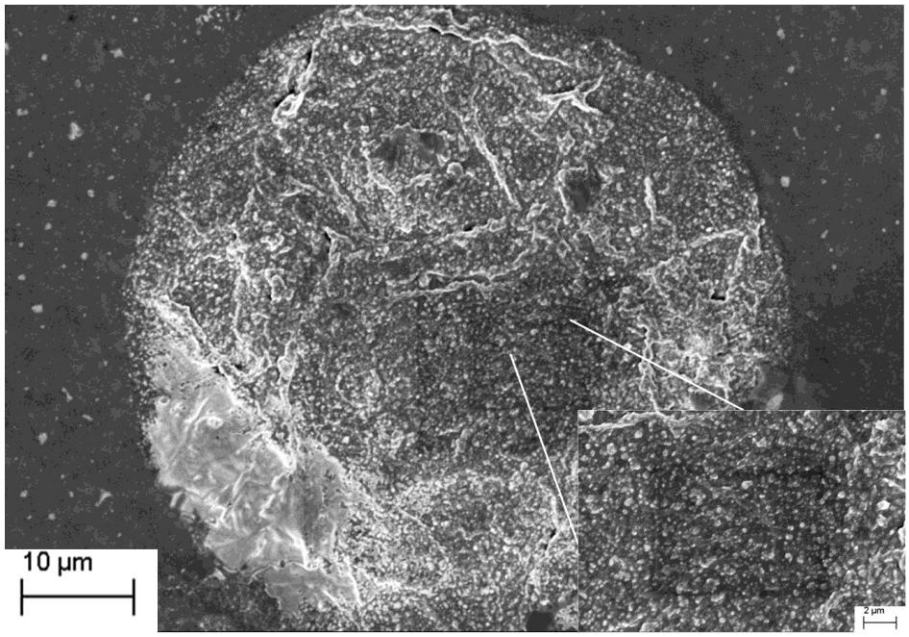

Figure IV- 5. Surface topography of colloidosomes with 6 layers of coating ([CS-ALG]$_3$) by using SEM.

3.4. QCM-D Analysis

The deposition process of CS, ALG, and zein on a flat surface was monitored by a QCM-D technique through simultaneously measuring resonance frequency change (ΔF) and energy dissipation change (ΔD), so as to monitor the assembly behavior of each layer on the surface of emulsion droplets. The ΔF and ΔD values obtained at three different overtones were normalized by their overtone number (n =3, 5, 7), as shown in Figure IV-6. Right after the injection of polyelectrolytes, a sudden decrease of Δf/n occurred simultaneously with a rapid increase of ΔD, which indicated a mass increase, i.e., an adsorption of polyelectrolytes on each layer. Then ΔF and ΔD gradually reached an equilibrium state before the deposition of another layer. For the adsorption of polysaccharides, the resonance frequency decreased around 40-50Hz for each layer, while for the last zein layer, the decrease in frequency was about 100Hz.

The adsorbed mass per unit area (Δm) and the thickness of the adlayer (h) can be

estimated by the Sauerbrey equations (*304*):

$$\Delta m = -C\Delta F/n \quad (1)$$

$$h = \Delta m/\rho \quad (2)$$

where n is the vibrational overtone number (1, 3, 5, 7), and C is a mass sensitivity constant (C =17.7 ng/cm^2/s in our device), ρ is the density (kg/m^3).

However, the Sauerbrey relationship is not suitable to analyze a viscoelastic film (ΔD >> 0), since it would underestimate the absorbed mass. In a case of a "thick" viscoelastic layer (hα>>1, hk>>1; α is a decay constant, $\alpha = \frac{1}{\delta}\sqrt{\frac{\sqrt{1+\chi^2}-\chi}{1+\chi^2}}$ where viscous penetration depth $\delta = \sqrt{\frac{2\eta}{\rho\omega}}$, viscoelastic ratio $\chi = \frac{\mu}{\eta\omega}$, ω is the angular frequency of the oscillation, and k is a wave number, $k = \frac{1}{\delta}\sqrt{\frac{\sqrt{1+\chi^2}+\chi}{1+\chi^2}}$), Voigot model was applied to fit ΔF and ΔD, which are related to the density (ρ, kg/m^3), viscosity (η, kg/ms), elasticity (μ, Pa) and thickness (h, m) of the adlayer, as shown in the following equations (*305*):

$$\Delta F \approx -\frac{1}{2\pi\rho_0 h_0}\sqrt{\frac{\rho}{2}}\left\{\eta\omega\sqrt{\frac{\sqrt{\mu^2+\eta^2\omega^2}+\mu}{\mu^2+\eta^2\omega^2}} - \mu\sqrt{\frac{\sqrt{\mu^2+\eta^2\omega^2}-\mu}{\mu^2+\eta^2\omega^2}}\right\} \quad (3)$$

$$\Delta D \approx \frac{1}{\pi F\rho_0 h_0}\sqrt{\frac{\rho}{2}}\left\{\eta\omega\sqrt{\frac{\sqrt{\mu^2+\eta^2\omega^2}-\mu}{\mu^2+\eta^2\omega^2}} + \mu\sqrt{\frac{\sqrt{\mu^2+\eta^2\omega^2}+\mu}{\mu^2+\eta^2\omega^2}}\right\}. \quad (4)$$

Where F is the resonant frequency; h_0, ρ_0, μ_0 are the thickness, density and elastic shear modulus of quartz plate, respectively.

The change of ΔD, in our case, was almost 170 (ΔD >> 0), indicating that the adlayer we formed was soft and viscoelastic, which further explained why the shell of colloidosomes would not rupture during dehydration. The changes of normalized frequency at different overtones (ΔF3/3, ΔF5/5, and ΔF7/7) almost overlapped with each other at the first two layers ([CS-ALG]), but then started from the third layer their

frequency changes tended to differentiate significantly, which indicated that it firstly formed a compact and rigid film, and then the film became softer and more viscoelastic with a further increase of the coating layers. Because of the viscoelastic property of the film, the thickness of the film was estimated to be around 145 nm, using the Voigot model (*305*) through QTools software.

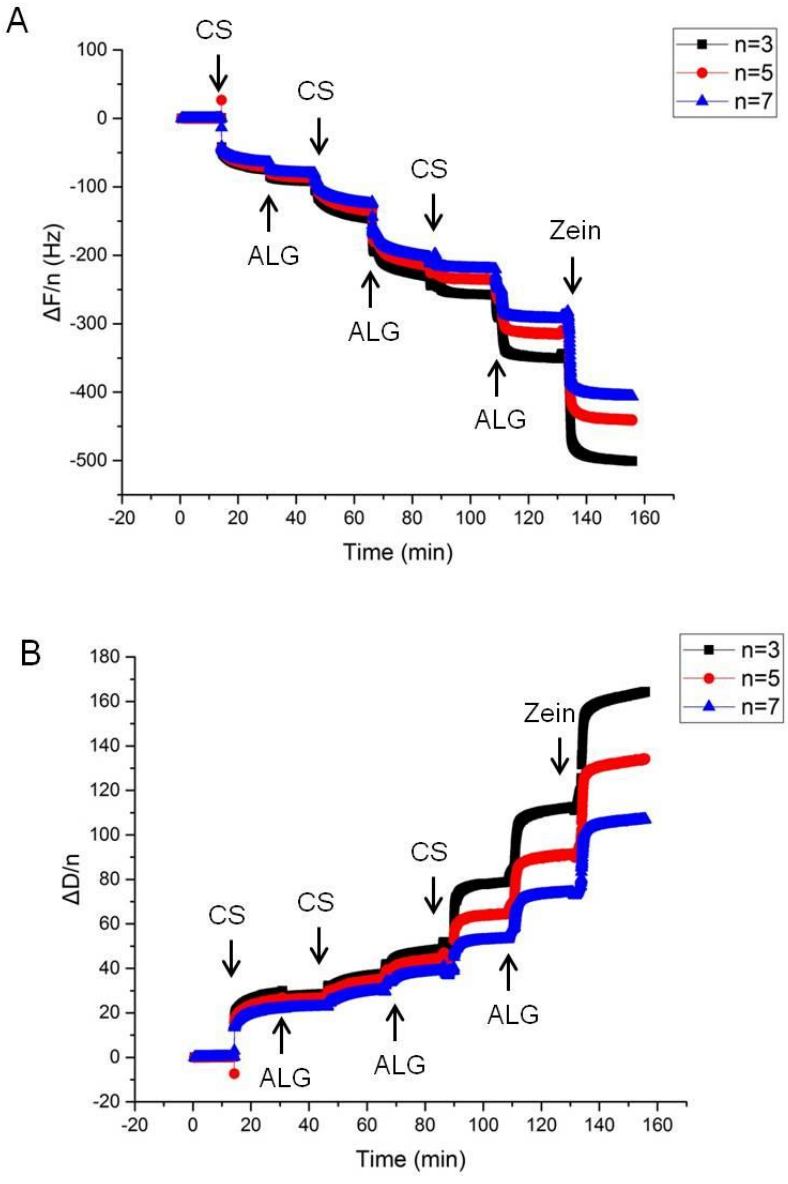

Figure IV- 6. QCM-D monitoring of the growth of polyelectrolyte multilayers on the zein/SC-coated quartz crystals.

3.5. Cross-linking of Colloidal Particles with Genipin

Through visual observation, it was very clear that emulsion droplets were cross-linked by genipin, because the droplet walls become stickier and droplets would like to stick with each other and form a large chunk. Both stirring and no stirring treatment were applied to the mixture of emulsion and genipin solution. The stirring would help droplets to fully and evenly contact with genipin and prevent the sticking together of droplets. However, long time stirring could also lead to the broken-down of emulsions. What's worse, zein based Pickering emulsions were not stable under high temperature (e.g. 40 ˚C). The long time exposure to 37 ˚C oil bath also contributed to the un-stability of emulsions. Similar phenomenon was also found in other Pickering emulsions. For instance, kafirin nanoparticle stabilized Pickering emulsions were not able to withstand high temperature neither, even though it exhibited long-term stability towards coalescence during storage (*306*).

It was reported that the amino groups on chitosan would react with ester groups of genipin, leading to the formation of secondary amide, and amino groups of chitosan would also announce a nucleophilic attack on the olefinic carbon atom at C-3 of deoxyloganin aglycone, followed by opening of the dihydropyran ring (*296*). It transformed the primary amino group in glucosamine unit into a cross-linked bridge and eventually formed a heterocyclic amine(*296*). Therefore, the formation of a secondary amide and of heterocyclic amino linkage results in the cross-linking between genipin and chitosan (*296-299*). And proteins containing Lysine, Arginine, Glutamine, and Asparagine also provide free primary amino groups for this covalent linking reaction. In accordance to the proposed mechanism, the schematic molecular structure of the genipin

cross-linked colloidosomes was shown in Figure IV-7. A neutral and alkaline condition (pH 7.0 and 9.0) is more favorable for the cross-linking reaction (*297*). Based on previous research, when the reaction temperature increased from 4 to 37 °C, the extent of cross-linking between chitosan and genipin drastically increased (*307*). And they also claimed that the extent of cross-linking could be reflected by an increase of the fluoresce intensity, and longer reaction times allowed for a higher extent of cross-linking (*307*). However, through the comparison of Figure IV-8 and Figure IV-9, the difference caused by reaction time and temperature was not obvious. A more quantitative determination of the extent of cross-linking is needed to evaluate the number of free primary amino groups before and after cross-linking (*300*).

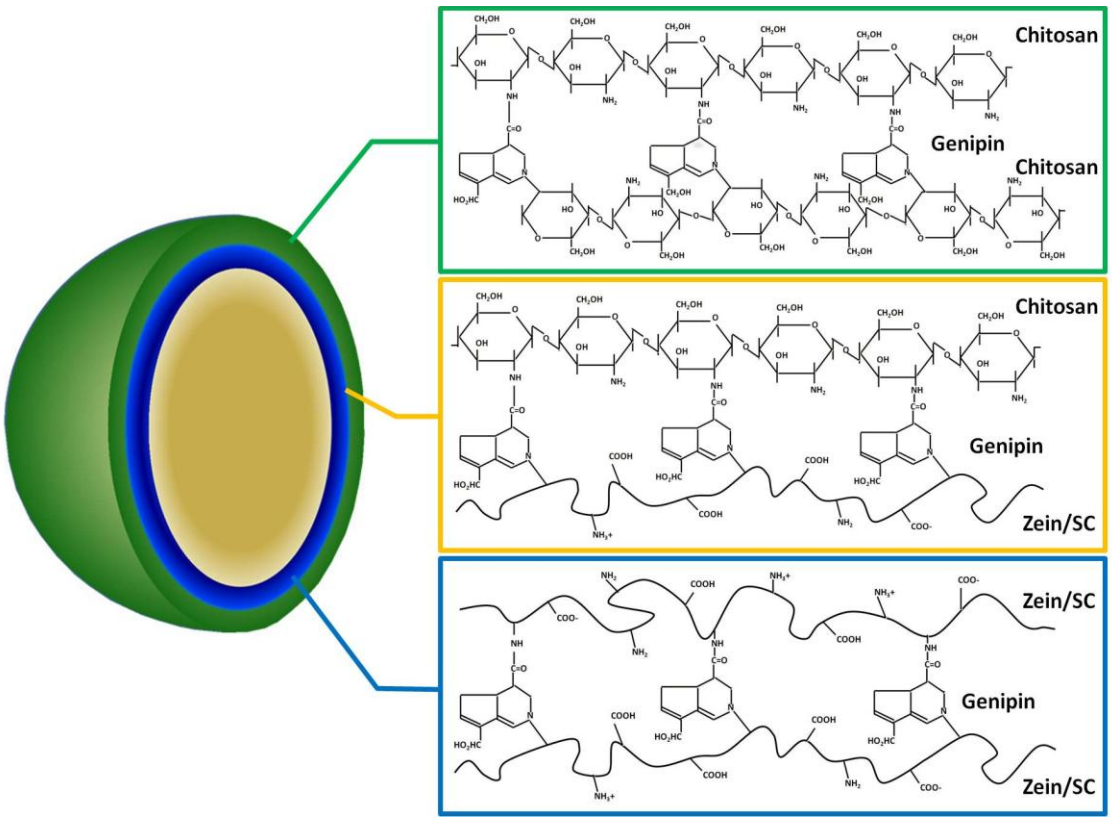

Figure IV- 7. Schematic molecular structure of the genipin cross-linked colloidosomes stabilized by zein/SC complex and chitosan.

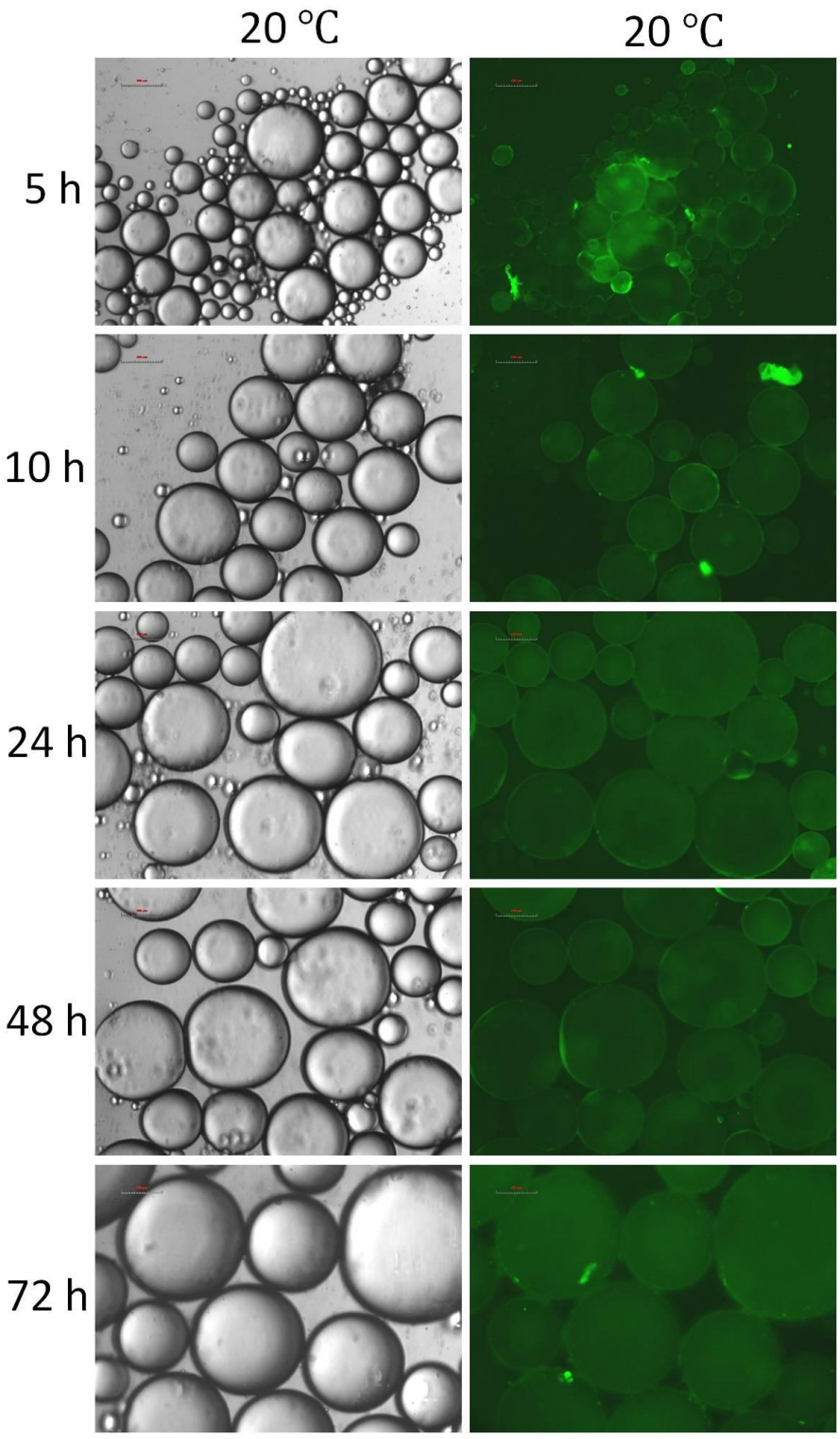

Figure IV- 8. Microscopic images of zein/SC complexes stabilized emulsions after cross-linking by 2.5 mg/mL genipin at 20 ˚C for different reaction times; all scale bars are 100 μm.

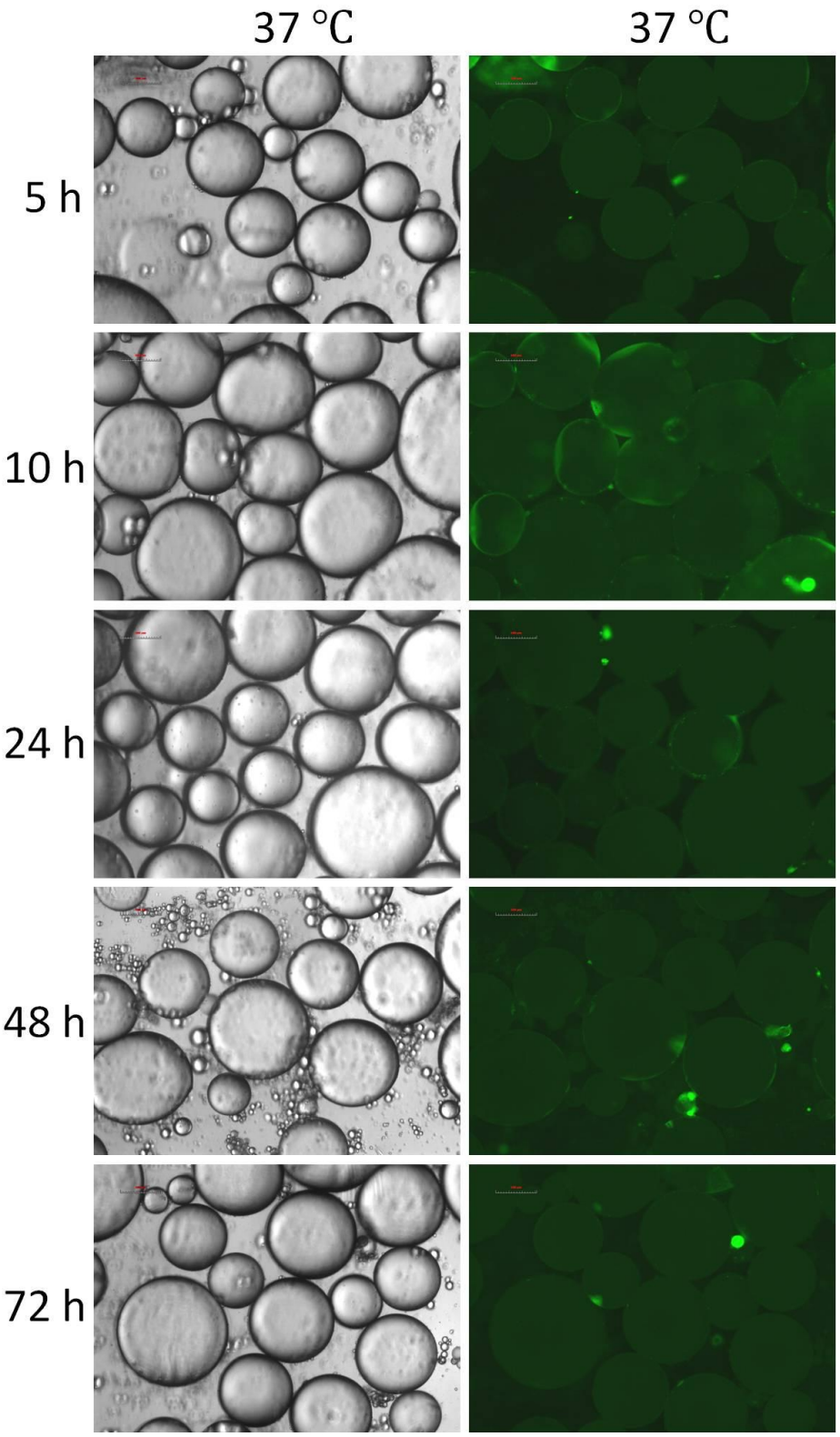

Figure IV- 9. Microscopic images of zein/SC complexes stabilized emulsions after cross-linking by 2.5 mg/mL genipin at 37 ˚C for different reaction times; all scale bars are 100 μm.

4. Conclusion

In summary, robust colloidosomes stabilized by zein/SC complexes with hollow shell structures have been successfully produced through LbL deposition process using inexpensive biopolymers of food origin. The self-assembled structure could survive from multiple washing steps without flocculation or coalescence. Polysaccharide coatings strengthened the structure of shells, and offered viscoelastic adlayers which could stand harsh dehydration conditions. The assembly of biopolymeric colloidosomes provides a promising vehicle to encapsulate and controlled release nutraceuticals, an interesting area which is worthy of further investigation. Genipin was able to cross-link zein/SC complexes on the surface of emulsion droplets, resulting in stickier droplet walls. Magnetic stirring could mitigate the sticking together of droplets. However, it would also lead to the breaking of emulsions. The Pickering emulsions were not quite stable under a long time exposure at 37 ˚C in an oil bath. And the difference caused by reaction time and temperature was not obvious.

CHAPTER V. INVESTIGATION OF THE INTERACTION BETWEEN ZEIN AND FATTY ACIDS AND ITS APPLICATION ON THE FABRICATION OF DOUBLE EMULSIONS

Partial contents in this chapter were adapted from the paper "Fabrication and characterization of zein-fatty acid complexes" which were ready for submission.

1. Introduction

Zein, a prolamin extracted from maize, has nearly equal amounts of hydrophilic and lipophilic residues (*308*). The sequence of amino acids determines the amphipathic properties and the spatial arrangement of zein. According to previous small-angle X-ray scattering (SAXS) studies on the dimension and shape of zein in alcoholic solutions (*50-52*), the zein particles are either prolate ellipsoids with length of 196 Å and cross-section diameter of 7 Å or rods with length of 153 Å and diameter of 13.8 Å (*51*). Zein contains tandem repeats, and each of tandem repeats units forms single α-helix and are connected by glutamine-rich loops (*53, 54*). The rectangular prism-like structure provides a large hydrophobic surface, while the glutamine-rich loops provide a hydrophilic surface (*52*).

Similarly, with zein, fatty acids are also amphipathic, which contain both polar carboxylic acid end and non-polar alkyl end. Through SAXS measurement, it was also observed that the adsoprtion of zein and fatty acids will lead to the development of periodic structures (*309*). A proposed mechanism for the interaction between zein and oleic acid was that the side area of the above mentioned prism-like structure provides

large hydrophobic area for the absorption of hydrophobic carbon chains of fatty acids, and the hydrophilic ends of fatty acids may orient themselves towards polar surfaces of zein (*55*). The interaction forces between protein and lipid mainly include covalent bindings and non-covalent bindings, such as van der Waals forces, hydrogen bindings and electrostatic bindings (*310*).

Due to its good stretching and kneading properties, zein has been widely used to produce edible and biodegradable films. However, the application of zein films into food packaging is limited by the brittleness and poor barrier performance. Therefore, various fatty acids have been added into zein films to improve their plasticity and elasticity. A high level of lauric acid (LA) addition (8%) significantly lowered the zein film water permeability which decreased from 0.867 to 0.674 $ng \cdot s^{-1} \cdot m^{-2} \cdot Pa^{-1}$ (*66*). When zein was plasticized with oleic acid (OA), an intermediate moldable and flexible resin was formed, which was further stretched into thin and ductile films with enhanced toughness (*68*). The addition of palmitic acid (PA) or stearic acid (SA) into zein sheets improved their tensile strength, water resistance, and viscoelastic behavior (*67*). Compared with SA, PA showed a better plasticization effect possibly because of its better distribution throughout the resin (*67*).

Most of recent studies focused on the addition of fatty acids into zein films, but little research was done to figure out how fatty acids interact with zein, how fatty acids change the structure, hydrophobicity, and surface morphology of zein, and how fatty acids/zein (FA/Z) complexes can be applied toward food matrixes. Even though zein and sodium stearate complexes were formed to fabricate Pickering emulsions (*59*), there was few paper systematically compared the differences caused by different chain lengths of

fatty acids on the formation of FA/Z colloidal complexes. And most of the recent studies about the zein modification, such as zein/chitosan (*311*), zein/tannic acid (*312*), zein/PDMS substrate (*313*), have focused on hydrophilic modification of zein colloidal particles. Since there is a lack of study on the hydrophobic modification of zein colloidal particles, the aim of this study is to figure out the interaction between zein and fatty acids with different chain lengths (i.e. lauric acid (LA), myristic acid (MA), palmitic acid (PA), stearic acid (SA) and oleic acid (OA)) and then use the hydrophobic modified zein to stabilize water-in-oil emulsions.

2. Materials and Methods

2.1. Materials

Zein was bought from Wako Pure Chemical Industries, Ltd. (Tokyo, Japan). Lauric acid, myristic acid, palmitic acid, stearic acid was bought from ACROS (New Jersey, USA). Oleic acid was bought from Fisher Scientific (Fair Lawn, NJ, USA). Corn oil was purchased from the local supermarket. Unless otherwise stated, other chemicals were purchased from Sigma-Aldrich (St. Louis, MO, USA).

2.2. Preparation of FA/Z Complexes

The synthesis of zein colloidal particles was also based on an antisolvent precipitation method with modification (*57*). 80 mg of zein was dissolved in 2 mL of 75% Ethanol-buffer solutions which were prepared by using buffer solutions of different pH values, i.e., 3.5, 5.0, 8.0, 10.5. Five fatty acids were used to form complex with zein, including lauric acid (LA), myristic acid (MA), palmitic acid (PA), stearic acid (SA) and oleic acid (OA). 8 mg, 16 mg, 32 mg, and 80 mg of fatty acids were also dissolved in 75% Ethanol-buffer solutions to make the ratio of FA to zein to be 0.1:1, 0.2:1, 0.4:1, and 1:1.

Then the dissolved zein and fatty acids mixture was trickled into 6 mL buffer solution which has the same respective pH value. For palmitic acid and stearic acid, since they have a higher melting point, a 50-60 ˚C water bath was required to fully dissolve them.

2.3. Preparation of Deposition Film of FA/Z Complexes

Forty mg of zein was dissolved in 2 mL of 75% Ethanol-buffer solutions (pH 10.5) to make the concentration of zein stock solution to be 20 mg/mL. Different amount of fatty acids (i.e. LA, MA, PA, SA, or OA) was added into the zein stock solution to make sure the fatty acid to zein ratio to be 0.1:1, 0.2:1, 0.4:1, and 1:1.Then the zein and fatty acid stock solution was trickled into 6 mL buffer solution (pH 10.5). The final concentration of the zein colloidal dispersions was 5 mg/mL. And it was stored in a 15 mL vial for at least 2 days to let the colloid particles precipitate down and form a deposition film at the bottom of the vial. After a thin film was formed, the upper supernatant was poured off and the film was removed from the bottom and dried under air.

2.4. Particle Size and Zeta Potential

To determine the particle sizes (hydrodynamic diameters) and the Zeta-potential of the fabricated zein and fatty acid colloidal particles, dynamic light scattering, and PALS Zeta-potential measurement were conducted using the Brookhaven Nanobrook 90Plus PALS particle size analyzer (Brookhaven Instruments Corp. Holtsville, NY, USA). Particle dispersions were diluted 10 times with same ratio of buffer-alcohol solution in order to avoid multiple particle effects and aggregation when diluted with neutral pH water. All measurements were triplicated at a fixed scattering angle of 90° at

room temperature. The results were reported in the form of mean ± standard deviation (n=3).

2.5. Contact Angle

The surface hydrophobicity of zein (Z) and fatty acids (FAs) complexes was studied by determining the contact angle of FA/Z films. The films were prepared through a spin-casting method (*314*) using a Laurell model WS-400A-6NPP/LITE spin coater (Laurell Technologies Corp., North Wales, PA). 10 mg/ml zein solution was prepared by dissolving zein in glacial acetic acid. Various fatty acids, i.e. lauric acid (C12), myristic acid (C14), palmitic acid (C16), and stearic acid (C18) were added into the zein solution in a FA/Z ratio of 0.5. Stearic acid is the most hydrophobic one among these fatty acids due to its higher chain length. The upper limit of hydrophobicity of FA/Z film was studied by adding stearic acid in different ratios to zein, from 0.1-1.0. The spin coater spun at 2000 rpm for 60s. The clear FA/zein films were then dried overnight in a 40 ˚C oven. The static contact angle was measured using a VCA optima setup (AST Products, INC.). Water-in-air three-phase contact angles were measured by depositing water droplet onto particle films, then the contact angle was determined automatically. All measurements were conducted at room temperature. The contact angles were shown in an average and standard deviation of at least 7 measurements.

2.6. Scanning Electron Microscopy (SEM)

SEM studies were performed by using a Zeiss Sigma Field Emission SEM (Carl Zeiss Microscopy, Thornwood, NY, USA) with an accelerating voltage of 5 kV. Samples were mounted onto aluminum stubs with double sided adhesive carbon discs and dried in

40°C oven over night to make sure samples were completely dried. Prior to examinations, samples were sputtered with gold in 5 nm thickness.

2.7. Small Angle X-ray Scattering

Zein was dissolved in 75% EtOH-solutions at different protein concentrations ranging from 5.0 to 20.0 mg/mL. The SAXS measurement was conducted at the BioCAT 18-ID beamline of Advanced Photon Sources, Argonne National Laboratory. To obtain the scattering data, the wavelength of X-ray radiation was set as 1.033 Å, and the exposure time was 1 s. After a pre-rinse treatment of the sample cell, samples were loaded to the cylindrical quartz capillary cell at a constant rate of 10 uL/s during X-ray scanning to minimize damage of radiation. The q range was from 4.3×10^{-3} to 0.38 $Å^{-1}$. The final SAXS results were displayed as the subtracted profile of solvent background after taking an average of 15 measurements.

2.8. Preparation of Double Emulsions

Influence of Stearic Acid to Zein Ratio

160 mg of zein was dissolved in 8 mL of 75% Ethanol-DI water solution. 0 mg, 16mg, 32 mg, 40 mg, 48 mg, 64 mg or 80 mg stearic acid were dissolved in 24 mL corn oil to make the SA/Zein ratio as 0:1, 0.1:1, 0.2:1, 0.25:1, 0.3:1, 0.4:1 and 0.5:1. Since stearic acid has a higher melting point, a 50-60 ˚C water bath was required to fully dissolve it in the oil phase. Then the dissolved zein solution was trickled into stearic acid oil solutions. 8 mL of blank 75% Ethanol-DI water solution was trickled into 24 mL 1.33 mg/mL stearic acid oil solutions to prepare the fatty acid control group. The particle suspensions were left stirring overnight at 100 rpm. On the other day, the mixture was shaken by hand for 1 min to form self-emulsifying emulsions. The emulsions were stored

at room temperature for 6 weeks to see the stability of emulsions. In order to determine the emulsion type, 1 mL of obtained emulsions was added into excessive amount of either deionized water or corn oil to see the dispersing properties. If the emulsion can be dispersed well in water, rather than oil, it is an oil-in-water emulsion. If the emulsion can be dispersed well in oil, rather than water, it is a water-in-oil emulsion.

Fluorescence Labeling with FITC

Labeling of zein with FITC was carried out according to the method described before (230) with a little modification. 10 mL of 50 mg/mL zein in DMSO solution was mixed with 0.4 mL of 10 mg/mL FITC in DMSO solution. 0.1 mL carbonate–bicarbonate buffer with pH 9.5 was added into the obtained mixture. The reaction was kept in the dark for 5 h at room temperature. Unattached FITC was removed through dialysis in carbonate–bicarbonate buffer (pH 9.5) for at least 24 h in dark. Excessive amount of deionized water was then added to accelerate the precipitation of zein protein. The FITC labeled zein, collected as precipitates in the bottom, was dried at room temperature in dark. 20 mg/mL of FITC-labeled zein solution was prepared using 75% Ethanol-DI water solution. Specific amount of stearic acid were dissolved in corn oil to make the SA/Zein ratio 0.2:1. The volume mixing ratio of zein stock solution to SA corn oil solution was 1:3. The particle suspensions were left stirring overnight at 100 rpm, and then observed by fluorescence microcopy.

Optical and Fluorescence microscopy

Samples (100 μL) were placed on a clean glass slide, and diluted with a drop of deionized water if needed before imaging. FITC-labeled zein was visualized at an excitation wavelength of 488 nm. Microscopic images were taken using the Nikon TE2000 microscope (Japan).

3. Results and Discussion

3.1. The Influence of pH on the Formation of FA/Z Complexes

Under different pH value, fatty acid and zein protein will have different charges as shown in the Table V-1. It was reported that zein had a highly heterogeneous charge, so previously its pI was estimated in a wide pH range of 5–9 (*219*). Recently many papers claimed that isoelectric point of zein was around 6.2-6.8 (*57, 71, 220*). Therefore, four different pH values, i.e. 3.5, 5.0, 8.0, 10.5 were chosen to study the interactions between zein and fatty acids. As listed in Table V-1, the pKa value reflects the tendency of the dissociation of carboxylic acid proton of a FA to an aqueous solution. An increase in FA chain length results in greater van der Waals interactions between FAs and zein, which attracts more FAs onto surface of zein. Besides the van der Waals interactions between the hydrophobic groups of zein and fatty acids, when they were in opposite charges, they also have electrostatic attraction force between them.

As shown in Figure V-1, with an increase of the pH value, the yellowish color of zein solution increased gradually. After the zein solution was trickled into different pH buffer solutions, zein formed large aggregate under pH 3.5, 5.0, and 8.0. Since the formation of large amount of protein aggregates, the protein concentration in the aqueous phase under these pH values was lower than that under pH 10.5. Therefore, the dispersion looked less opaque than the one under pH 10.5. The large aggregates formed under pH 5.0 and 8.0 may be because these pH values are too close the pI of zein. Even though pH 3.5 is far from pI of zein, the high surface charge of zein still cannot allow the formation of stable colloidal particles. It is probably due to the low pH increase the plasticity of zein. The aggregates at pH 3.5 were quite sticky, which further proved this possibility. Under alkaline conditions, zein was more prone to form stable negatively charged

colloidal particles.

Table V- 1. pKa value of different fatty acids, and their charges at different pH values

Fatty acid	Carbon	pKa	Melting point (°C)	Charge of FA/zein (pH 3.5)	Charge of FA/zein (pH 5.0)	Charge of FA/zein (pH 8.0)	Charge of FA/zein (pH 10.5)
Formic acid	C1:0	3.75(*315*, *316*)	8.2-8.4	Unionized/+	-/+	-/-	-/-
Acetic acid	C2:0	4.75(*315*, *316*)	16.2	Unionized/+	-/+	-/-	-/-
Lauric acid	C12:0	4.9(*315*),5.3(*317*),7.5(*318*)	44-46	Unionized/+	———	-/-	-/-
Myristic acid	C14:0	4.9(*315*)	52-54	Unionized/+	-/+	-/-	-/-
Palmitic acid	C16:0	8.6-8.8(*319*), 9.7(*320*)	61-62.5	Unionized/+	Unionized/+	-/-	-/-
Stearic acid	C18:0	9.0(*321*), 10.15(*322*)	69-71	Unionized/+	Unionized/+	Unionized/+	-/-
Oleic acid	C18:1	9.85(*322*)	13–14	Unionized/+	Unionized/+	Unionized/+	-/-
Linoleic acid	C18:2	9.24(*322*)	−5 – −1	Unionized/+	Unionized/+	Unionized/+	-/-
Linolenic acid	C18:3	8.28(*322*)	−11 – −10	Unionized/+	Unionized/+	Unionized/+	-/-

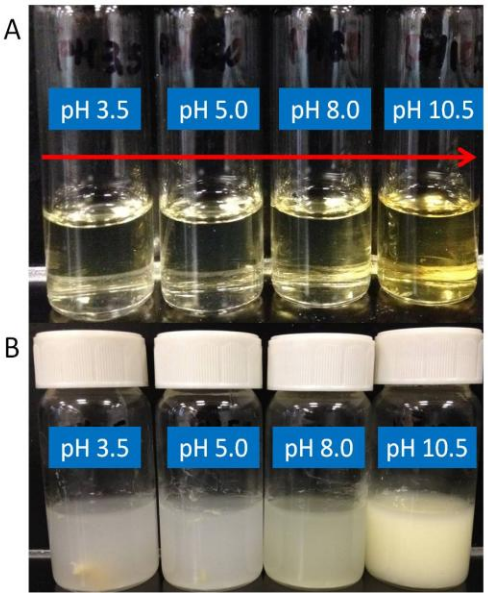

Figure V- 1. The influence of pH value on the formation of zein colloidal particles; A, zein dissolved in 75% EtOH – buffer solutions with different pH values; B, zein colloidal particles dispersed in buffer solution.

3.2. The Influence of FA Chain Lengths and FA/Z Ratios on the Formation of Complexes

As illustrated in Figure V-2, with an increase of fatty acid concentration, the yellowish color of the FA/zein solution decreased gradually. But the reason for this phenomenon is still unknown. And the decreasing trend can be seen for all the four different fatty acids, including lauric acid, myristic acid, palmitic acid and stearic acid, except for oleic acid, which does not exhibit a trend in change of colors. For lauric acid, myristic acid, and oleic acid, with an increase of the fatty acid concentration, the particle dispersions they formed become more and more clear. For palmitic acid, when the ratio increased to 1:1, the formed particles were solidified immediately after the FA/Z solution was trickled into buffer solutions. And for stearic acid, it met the same situation. Therefore, particle dispersions produced from SA/Z were pre-heated in water bath to melt the wax like structure of the formed particle dispersions.

As shown in Table V-2, myristic acid/ zein, palmitic acid/ zein, and oleic acid/ zein exhibited similar changing trend in particle size, as their hydrodynamic diameter started off from around 300 nm, decreased to the range of 200 nm, then gradually increased to above 300 nm, from fatty acid ratio of 0.1:1 to 1.0:1. The solidification of PA/Z (1:1) and SA/Z (0.2:1, 0.4:1, and 1:1) particles was so quick that their particle size could not be measured. However, for lauric acid, the hydrodynamic diameter started off at 735nm and decreased gradually to 188nm from LA/Z ratio of 0.1:1 to 1:1. But when LA/Z ratio was increased to 1.25:1, the hydrodynamic diameter of the particles increased to 600nm.

From the Table V-1, it is very clear that under pH 10.5, both FA and zein are

negatively charged, therefore the zeta-potential of FA/Z complexes should be in a negative value, which is in consistent with the measured values. The pKa values of FAs are all below 10.5, so FAs are negatively charged under this alkaline condition. FAs interact with zein protein mainly through van de Waals hydrophobic attractions. As shown in Table V-2, the zeta potential of LA/Z decreased from -26.08 mV to -38.38 mV as LA/Z ratio changed from 0.1:1 to 1:1, while the zeta potential increased to -18.00 mV for LA/Z ratio of 1.25:1. The decreasing trend in zeta potential from LA/Z ratio of 0.1:1 to 1:1 indicated more lauric acids were bonded to zein, and the steric hindrance effect and the electrostatic repulsion effect prevented the formation of large particle aggregates during the anti-solvent precipitate method. This was the reason why the particle size decreased gradually at the beginning. When the FA/Z ratios further increased, there was a sudden increase in particle size, which was probably due to excessive amount of fatty acids, leading to the growth of fatty acid crystals on the surface of colloidal particles. And the decrease of the absolute value of zeta potential at high FA/Z ratios could also be due to saturation in binding between lauric acid and zein. Therefore, the zeta potential of free fatty acids has been measured by the instrument. What's more, the particle size distributions of LA/Z (1:1) and MA/Z (1:1) were quite wide, which meant both small particles and large particles exist in the fluid.

MA/Z (1:1) and OA/Z (0.4:1 and 1:1) particle dispersions were almost transparent. And those transparent particle dispersions were more stable than the others. After long time storage, no colloidal particles would precipitate. It seems that under high FA environment, the particle distance between adjacent particles would be larger due to the steric hindrance effect and electrostatic repulsion effect caused by the negatively

charged and long side chain of FAs. Oleic acid has longer carbon chains than lauric acid and myristic acid. So, the repulsion effect of OA is more effective than that of LA and MA. This also explained why it was easier for oleic acid to form transparent particle dispersions at lower FA/Z ratio as compared with LA and MA. Tthe proposed mechanism for the self assembling of zein and fatty acids was illustrated in Figure V-3.

Table V- 2. Particle size and zeta-potential distribution of FA/Z complexes under pH 10.5.

Fatty Acids		Particle Size (nm)	ζ-potential (mV)
LA/Z (w/w)	0.1:1	735.70±115.70	-26.08±9.87
	0.2:1	658.07±53.12	-28.42±4.68
	0.4:1	371.80±92.97	-33.45±11.39
	1.0:1	187.97±14.41	-38.38±5.93
	1.25:1	600.44±72.87	-18.00±0.80
MA/Z (w/w)	0.1:1	321.56±45.70	-26.19±7.94
	0.2:1	289.44±6.97	-31.60±6.97
	0.4:1	297.51±3.00	-28.33±7.52
	1.0:1	486.96±9.83	-12.90±0.93
PA/Z (w/w)	0.1:1	310.58±2.22	-33.05±0.71
	0.2:1	252.42±4.35	-37.31±0.99
	0.4:1	298.52±53.96	N/A
	1.0:1	N/A	N/A
SA/Z (w/w)	0.1:1	314.00±11.01	-31.18±5.48
	0.2:1	N/A	N/A
	0.4:1	N/A	N/A
	1.0:1	N/A	N/A
OA/Z (w/w)	0.1:1	318.90±36.64	-24.38±1.38
	0.2:1	213.94±8.46	-49.38±1.59
	0.4:1	383.34±3.79	-13.04±1.89
	1.0:1	352.76±56.78	-13.75±0.59

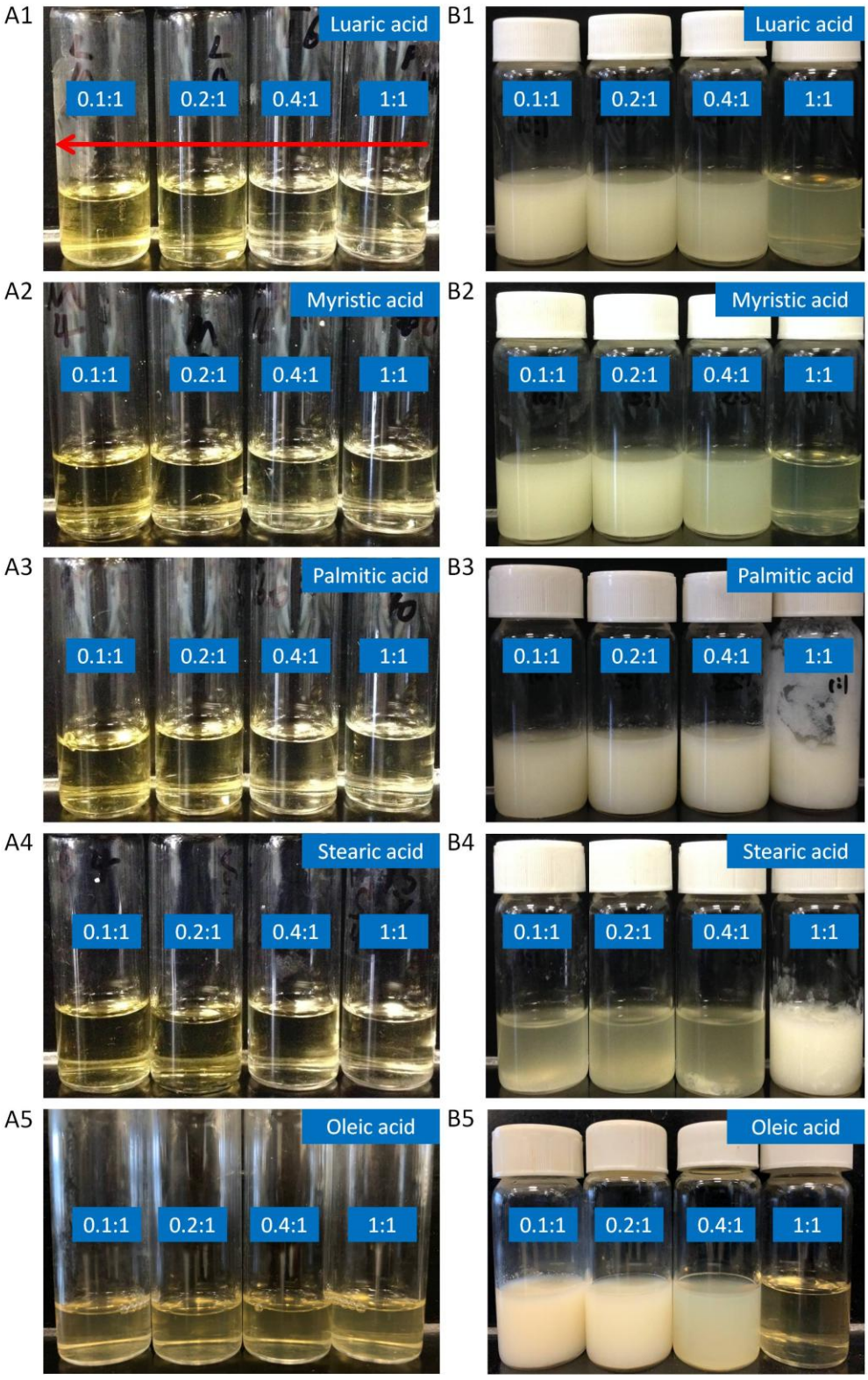

Figure V- 2. The appearance of FA/Z solutions (A1-A5) and FA/Z particle suspensions (B1-B5) with different mass ratios and chain length of fatty acids at pH 10.5.

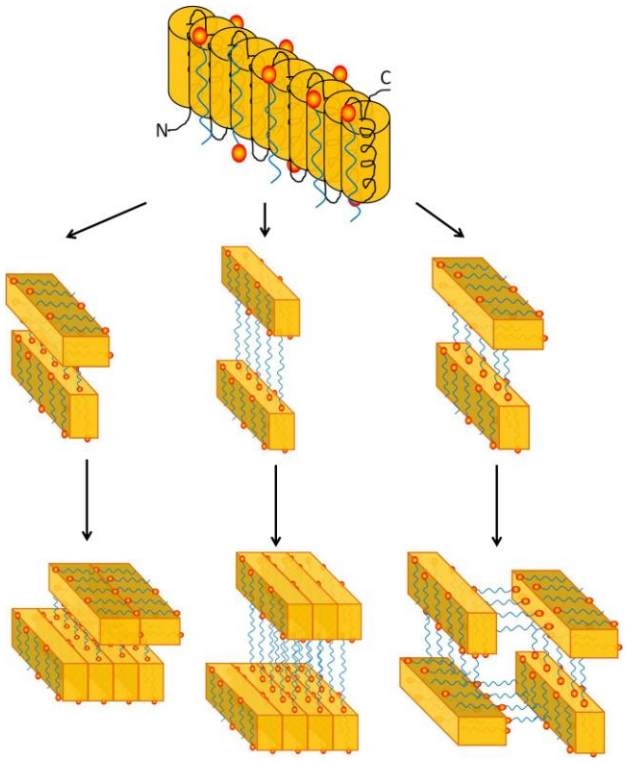

Figure V- 3. Proposed mechanism for the self assembling of zein and fatty acids.

3.3. The Influence of FA Chain Lengths and FA/Z ratios on the Formation of Films

It was found that after storage, a thin white film was formed at the bottom of the container. LA, MA, PA and OA were able to form deposition films, while SA could not, as shown in Figure V-4. When colloid particles were stored at ambient temperature for about 1-2 days, they would precipitate and form a deposition film composed of colloidal particles. After a thin film was formed, the upper supernatant was poured off and the film was removed from the bottom and dried under air. At high FA/Z ratio, the colloid dispersions may be too stable to precipitate and form deposition films. For palmitic acid and stearic acid, before the colloidal particles could form films at the bottom of container,

the colloid dispersions solidified, resulting in an opaque solid block. When the side chain of FAs increases to 16 - 18 carbons, the recrystallization is the dominant driving force for the formation of needle shaped particles (Figure V-5).

As shown in the SEM images (Figure V-6), LA/Z complexes had larger particle size than OA/Z complexes. There were two main finding from the SEM images. Firstly, with an increase of the fatty acid ratio, the pore sizes (distances) between adjacent particles become larger, which further proved the hypothesis that high FA/Z ratio results in longer inter-particle distance. But this phenomenon was not obvious to OA/Z film. Secondly, at higher FA/Z ratio the edge of particles melted a little bit, which let adjacent particles to fuse or connect together. And this linking effect was helpful to reduce the brittleness and increase the plasticity of zein films. Even though zein colloidal particles were partially melted, the granule-like structure of the deposition films was more obvious than the one of zein casting film.

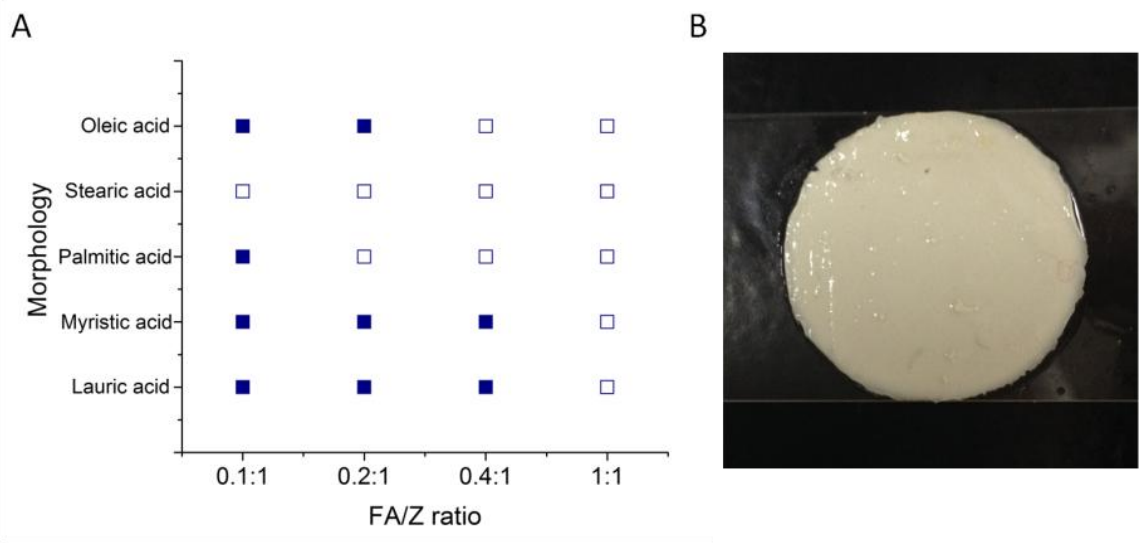

Figure V- 4. A, Phase diagram for the formation of deposition film (■ represents film; □ represent particle dispersions); B, wet state of deposition film.

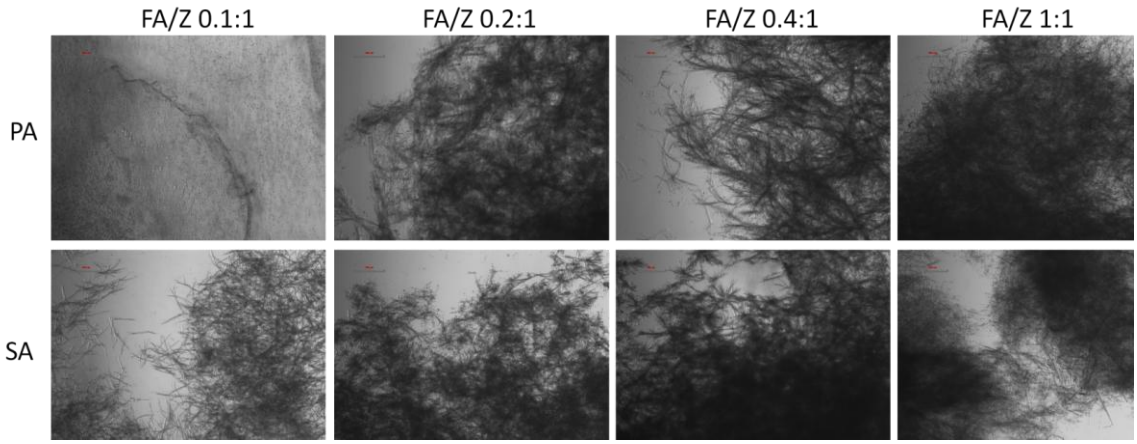

Figure V- 5. Optical microscopic images of palmitic acid/zein and stearic acid/zein complexes in different FA/Z ratios; scale bars are 100 μm.

Some other reports also gave similar result that when zein interact with fatty acids, zein spheres tended to fuse with each other (*323*). They added oleic acid (0.75 μL/mg of zein) into 1 mg/mL zein-70% ethanol solutions. And the mixed solutions were then left drying at room temperature. In the presence of oleic acid, zein spheres melted and transformed into rough sponge-like structures with empty cells. Those cells interconnected with each other through channels and tunnels (*323*). Interestingly, the empty cell structure was also observed in LA/Z (0.4:1) film (Figure V-6, B). Similarly, the fusion phenomenon of zein spheres was also observed by Lai and coworkers (*324*). They prepared cast films by dissolving 16% (w/v) of zein and 8% of oleic acid in warm (75°C) 75% EtOH solutions. Films were obtained by casting and drying the solution on a nonstick surface at room temperature for 24 h (*324*).

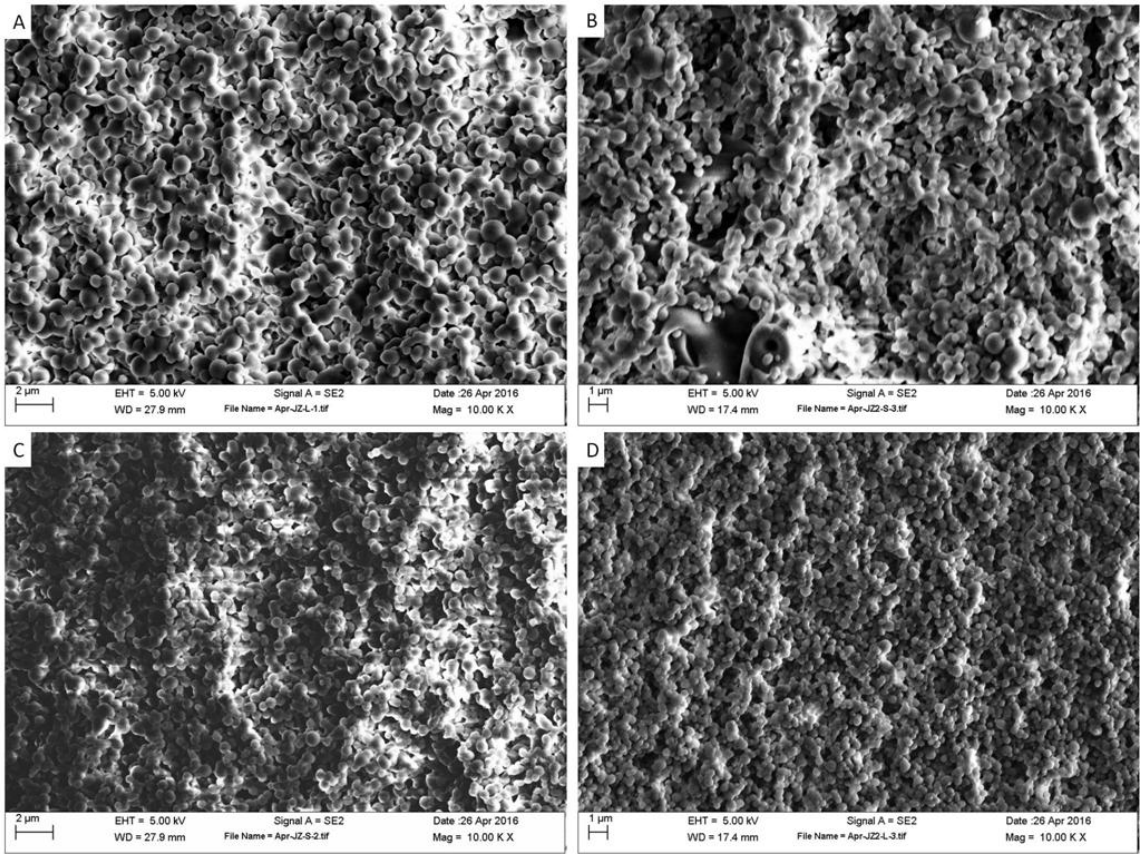

Figure V- 6. SEM images of films made by FA/Z complexes in dried state; A, LA/Z (0.1:1) film; B, LA/Z (0.4:1); C, OA/Z (0.1:1) film; D, OA/Z (0.2:1) film.

3.4. Contact angle of FA/Z complexes

Higher contact angle indicated higher surface hydrophobicity of the material. For a round particle with an infinite diameter, the surface hydrophobicity of this particle equals to the hydrophobicity of a flat surface. Since the hydrophobicity is the intrinsic property of a material, the hydrophobicity of spherical FA/zein complexes can be reflected by determining the hydrophobicity of FA/zein spinning film.

For saturated fatty acids, with an increase of chain length the contact angle increased from 64.88 ± 4.09˚ (Z) to 85.25 ± 2.00˚ (SA/Z), while oleic acid decreased the contact angle to lower value of 61.08±6.14˚ (Figure V-8). The standard deviation of

OA/Z films was quite high as compared with other groups which may be due to the uneven thickness of film formed during spinning. The center part of glass slide had lower contact angle around 49˚-55˚, while the sides had higher ones around 66˚-68˚. When SA/Z ration increased from 0.1 to 1.0, the contact angle increased from 79.86 ± 0.95˚ to 91.02 ± 1.19˚. There is a linear relationship between contact angle and FA/Z ratio (Figure V-7), which facilitates the prediction of film hydrophobicity with a known SA/Z ratio.

Shi and co-workers used the same spin coating method to detect the contact angle of zein and modified zein film (*325*). Through chemically modification of zein with lauryl chloride, the contact angles of zein based films increased from 75.6 ± 1.1˚ (zein) to 86.0 ± 1.0˚ (initial molar ratio of lauryl chloride /zein was 100:1) (*325*). The contact angle of zein was about 10 degrees higher than the one obtained here. The contact angle of LA/Z (0.5:1), 70.0± 3.1˚, was lower than the highest contact angle published in that paper. However, through forming complexes with stearic acid, the contact angle could be as high as 91.02 ± 1.19˚. With a 90-degree contact angle, the material can be used to form either oil-in-water emulsions or water-in-oil emulsions.

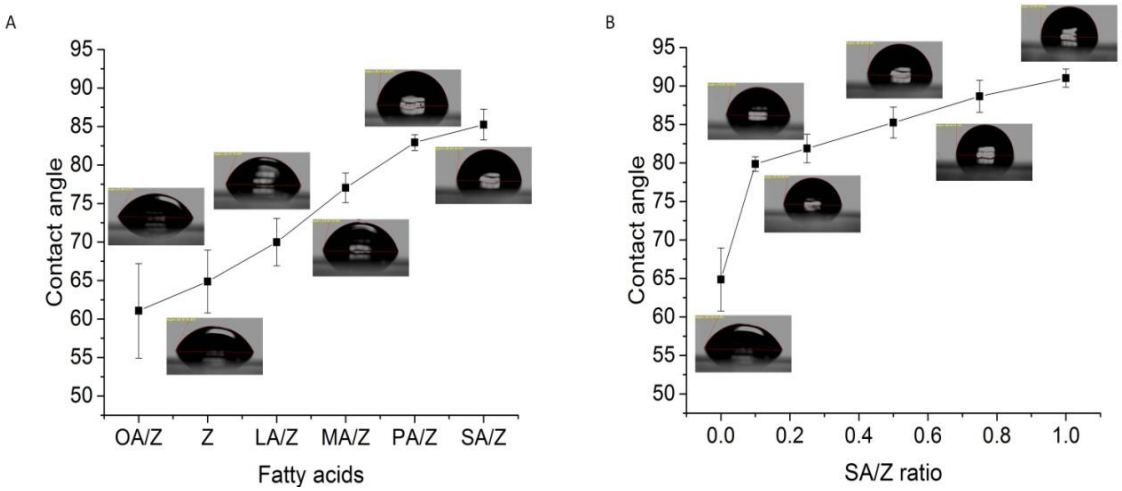

Figure V- 7. Contact angle of FA/Z films influenced by types of fatty acids (A) and contact angle of SA/Z films with different fatty acid to zein ratios (B).

3.5. SAXS Analysis

The scattering intensity profiles from SAXS of zein and FA/Z in 75% EtOH solutions were illustrated in Figure V-8 – Figure V-9. The slopes at large q range (0.04-0.15) did not change much and were all around -1.56 for zein and LA/Z solutions (Figure V-8). pH values have a great influence on the slope in this area, that pH 10.5 provided the smallest exponent (- 1.56), while pH 8.0 gave the highest one (-1.84 for zein and -1. 68 for LA/Z) (Figure V-9). The slopes at this q range were kept the same for FA/Z complexes with different chain lengths (C12-C18) (Figure V-9, C). The X-ray scattering profiles in this large q range represent the shape of the protein in solutions (*326*). A scaling exponent around -1 in this range implies a rod-like structure (*327*).

In the small q range, the slopes increased a little bit with an increase of the zein concentration. For LA/Z (0.1:1), when the concentration changed from 10 mg/mL to 20 mg/mL, the slope increased from -2.42 to -2.61. For zein, when the protein concentration changed from 5 mg/mL to 10 mg/mL, the slope increased from -1.76 to -2.61. A further increase of zein led to a slight decrease of the slope. The slight increase of slope suggested that there was a minor protein aggregation existing in the solution. pH values had a strong influence on the slope in the large q range. The exponent decreased in the following order for zein and for LA/Z complexes: pH 5.0> pH 8.0≥ pH 10.5> pH 3.5. The sharp increase of slope revealed that large aggregates were formed when pH was around 5.0 and 8.0. This result was consistent with our previous prediction that when pH was around pI of zein, proteins were more likely to form large aggregates. Since pH 3.5 was far away from pI of zein (6.2-6.8), it provides the smallest particles. Slope of -1, -2

and -3 suggested that the aggregates of zein and LA/Z complexes in 75% ethanol solutions may exist in a rod-like, a random walk, or a partial disk packing manner, respectively (*326*). At pH of 3.5, zein and LA/Z complexes extended in a rod like conformation. A random aggregation of random coils of alpha-zein resulted in a random walk aggregation (*326*). The large slope at pH 5.0 indicated a partial disk packing that proteins were in an oblate disk shape (*326*).

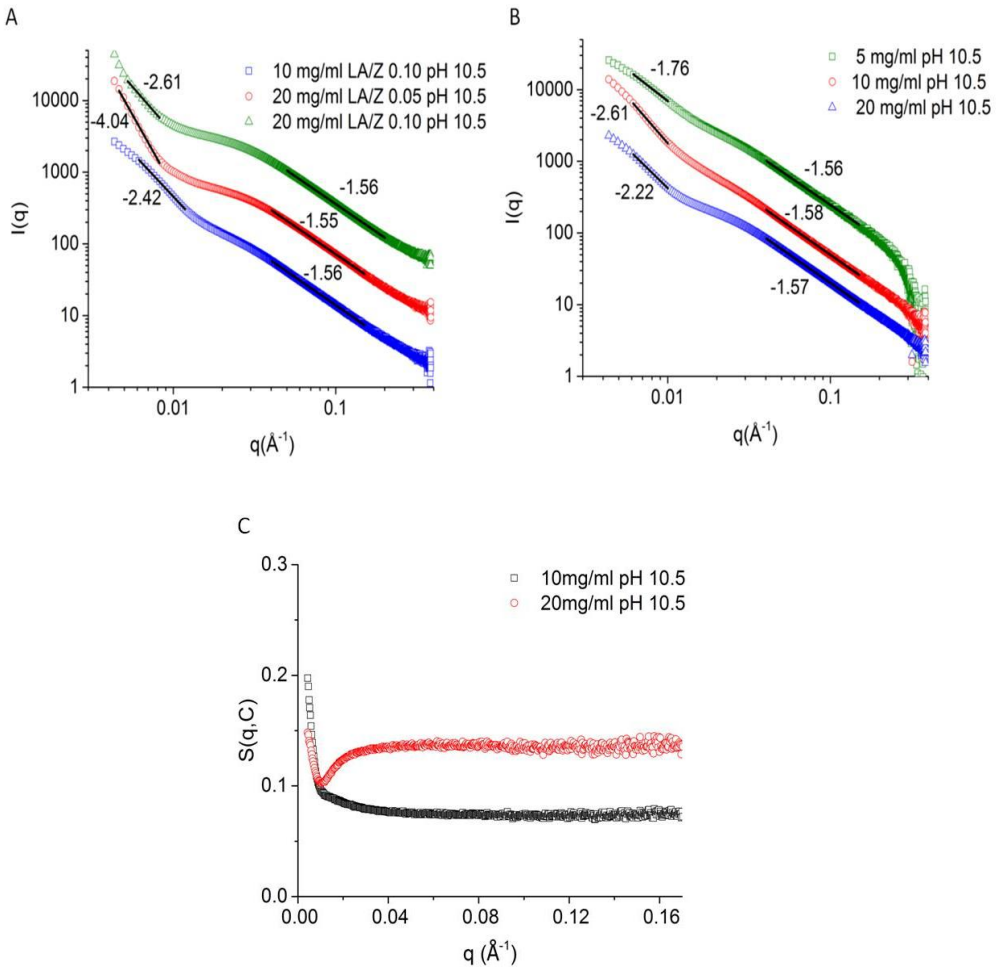

Figure V- 8. A, LA/Z complexes in different FA/Z ratios and concentrations; B, zein in 75% EtOH solution (pH 10.5) in gradient concentrations; C, Structure factor S(q) of zein in 75% EtOH solutions (pH 10.5).

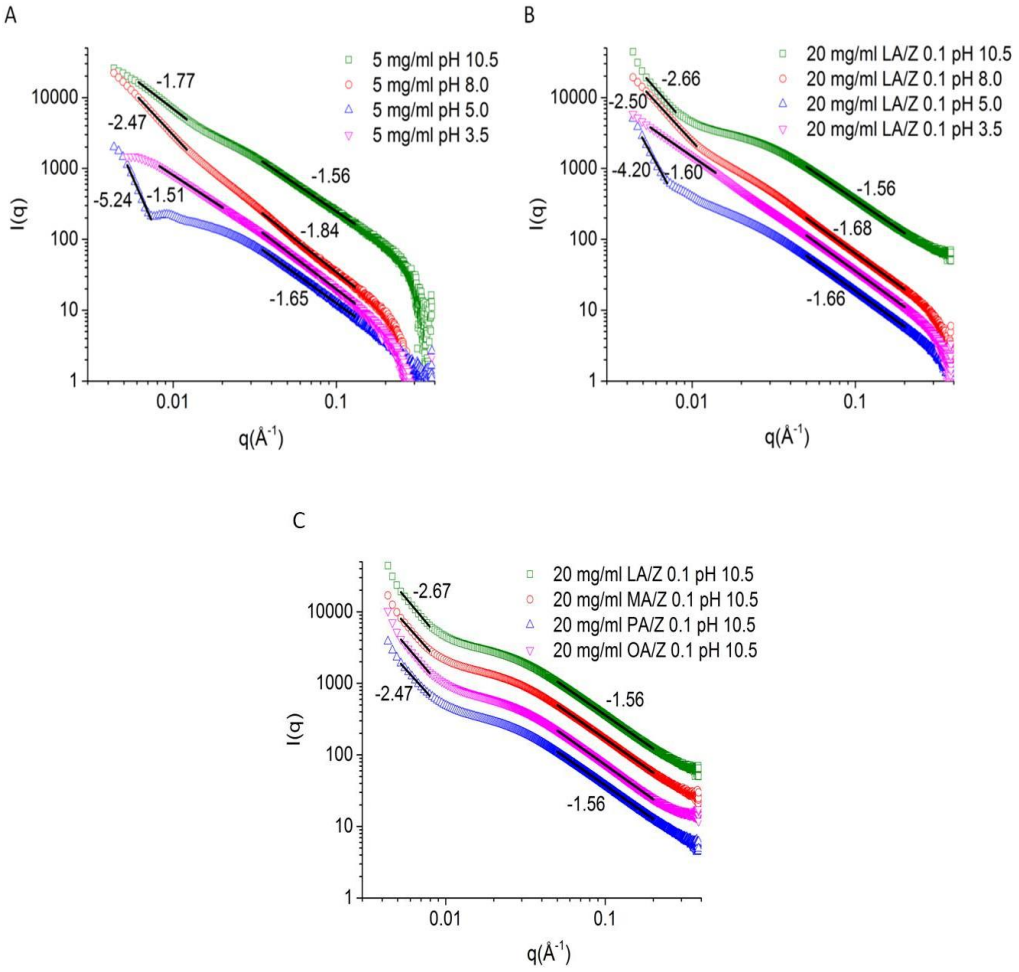

Figure V- 9. A, zein in 75% EtOH solutions with different pH; B, LA/Z complexes in 75% EtOH solutions with different pH; C, LA/Z, MA/Z, PA/Z, and OA/Z complexes in 75% EtOH solutions at pH 10.5.

P(q) is the form factor that indicates the protein shape, and S(q) is the structure factor that reflects protein structure, protein aggregation and protein−protein interaction in the solutions (*328*). The scattering intensity of monodispersed and spherically symmetric solutions can be expressed by the form factor P(q) and the structure factor S(q) (*329*)

$$I(q) = \frac{\Delta\rho^2 P(q) S(q)}{\Omega}$$

where Δρ is the electron density difference between the solute and the solvent, Ω

equals to the number of particles in unit mass of solute. The inter-particle interactions can be neglected in dilute solution (C → 0), where the form factor P(q) is the main factor that contributes to scattering intensity I(q) (*326*). Thus the structure factor can be calculated by (*330*)

$$S(q) = \frac{I(q)}{I(q)_{(C\to 0)}}$$

Practically, it is almost impossible to measure the I(q) for an infinite dilute solution due to weak scattering signals (*326*). Therefore, in order to investigate the protein at higher protein concentrations, a protein solution with a given concentration C_0 was used as a reference. In this study, 5.0 mg/mL zein 75% EtOH (pH 10.5) solution was selected as the reference for the structure factor calculation. The structure factor S(q,C) can be calculated by (*330*)

$$S(q, C) = \frac{C_0 I(q, C)}{C I(q, C_0)}$$

The effective structure factors S(q,C) of zein in 75% ethanol solution were illustrated in Figure V-8, C. The S(q,C) in the entire Q region were smaller than 0.2, which means there was few aggregation existing in the given correlation length range. An inverted peak was found at low q region (around 0.01 $Å^{-1}$). The reciprocal of this q value corresponds to the correlation length d of protein, which suggests the average separation of proteins (*328*). The correlation length d can be calculated as (*326*):

$$\mathrm{d} = \frac{2\pi}{\mathrm{q}}$$

At the low q range, the correlation length for 10 mg/mL and 20 mg/mL zein were similar to each other, both around 62.8 nm, which was larger than 40.9 nm, the correlation length of 20 mg/mL zein in glacial acetic solution.

At small Q values, the overall radius of gyration Rg can be calculated by Guinier methods (*331*):

$$\ln\big(\mathrm{I}(q)\big) = ln\big(I(q=0)\big) - \frac{1}{3}(qR_g)^2$$

where I (q=0) is the scattered intensity at zero angle. A region safe for Guinier fitting should satify the requirement that qRg < 1.57 (*326*).

If one of the particle dimensions is much larger than other two dimensions, the radius of gyration of the cross-section Rc is obtained in a larger q range through the following equation (*52*):

$$\ln(I(q)*q) = \ln\,(l(q)*q)_0 - \frac{1}{2}q^2{R_c}^2$$

Since the ratio of the longest dimension to the other two dimensions (Rg/Rc) were all above 2:1 (Figure V-10), zein and FA/Z complexes were in a rod like structure in 75% ethanol solutions. When the concentration of zein changed from 5 mg/mL to 20 mg/mL, the Rg and Rc did not change much in the range of 4.91-5.91 nm and of 1.64-2.22 nm, respectively. At pH 3.5 and 8.0, the calculated qRg $\geqslant$1.57, so there was no fitting line shown in the graph. Even though their Rg values were provided, the accuracy was not quite confirmed.

When pH increased from 5.0 to 10.5, the Rg/Rc increased gradually from 2.25 to 2.85 for zein, and from 2.34 to 3.74 for LA/Z (0.1:1) complexes, which indicated that with an increase of the pH, the protein rod became longer and longer. When the LA percentage increased from 5 wt% to 10 wt% of zein, the Rg and Rc were quite steady, maintained around 4.5 nm and 1.0 nm, respectively. The increasing of the carbon chain lengths of FAs, from 12 carbons to 18 carbons, increased the Rg a little bit from 4.39 nm

to 4.59 nm, while their Rc values were quite similar to each other, ranging from 1.25 nm to 1.33 nm.

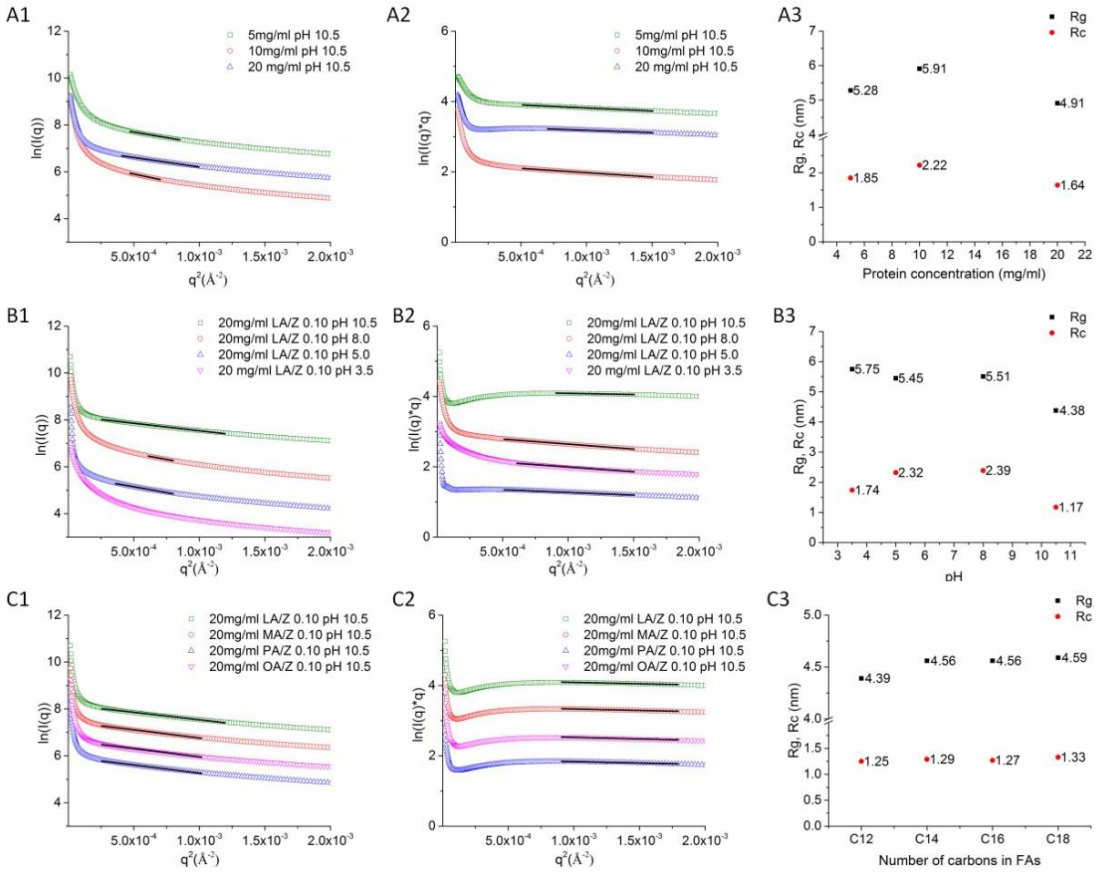

Figure V- 10. Guinier plots, cross-sectional plots and radius of gyration (Rg) and cross-section radius of gyration (Rc) plots for SAX scattering intensity profiles of zein in 75% EtOH solutions (pH 10.5) with different concentrations (A1-A3), LA/Z complexes in different pH (B1-B3), and FA/Z complexes in different chain lengths (C1-C3).

3.6. Fabrication of Double Emulsions

Up till now, the majority of reported zein stabilized Pickering emulsions were oil-in-water emulsions. In this chapter, zein was hydrophobically modified with stearic acid to see the emulsification capacity to stabilize water-in-oil emulsions. The zein and stearic acid complexes were prepared using the traditional anti-solvent method. But at this time, zein stock solution was trickled into oil phase instead of water phase. The formed

colloidal particles were left stirring at least overnight at room temperature, which allows for enough time for the growth of stearic acid crystals on the surface of zein colloidal particles. Palmitic acid was also tried in the same method, but it did not form emulsions as stable as the ones of stearic acid, which may be due to the fact that stearic acid is more hydrophobic than palmitic acid. Furthermore, stearic acid has higher melting point than palmitic acid, which facilitates the formation of fatty acids crystals at room temperature. After overnight stirring, the particle dispersion has a clear ethanol layer on the top and turbid oil layer at the bottom (Figure V-11A). Homogeneous emulsions were formed after handshaking for 1 min. After 24 hours storage, a clear serum layer on the top of the emulsions and an opaque cream layer on the bottom of the emulsions were observed (Figure V-11B). After 6 weeks storage, the creaming emulsion layer of SA/Z (0.1:1) was almost completely broken down, while the one of SA/Z (0.5:1) was still quite stable (Figure V-11C). Coalescence was very obvious after 6 weeks storage for SA/Z (0.25:1) group, where small droplets merged into large droplets at the bottom of the bottle. This phenomenon was very similar to the bridging effect of Pickering emulsions, in which adjacent droplets share the same colloidal particles, and these colloidal particles bridge several faceted droplets, as shown in Figure V-11C. After the removal of the top serum layer for the SA/Z (0.5:1) group, the bottom part was shaken again for 1 min. It gradually formed a firm gel-like structure as shown in Figure V-11D. The formation of emulsion gels may be due to two factors, including the gelling property of zein and the possible solidification effect of stearic acid.

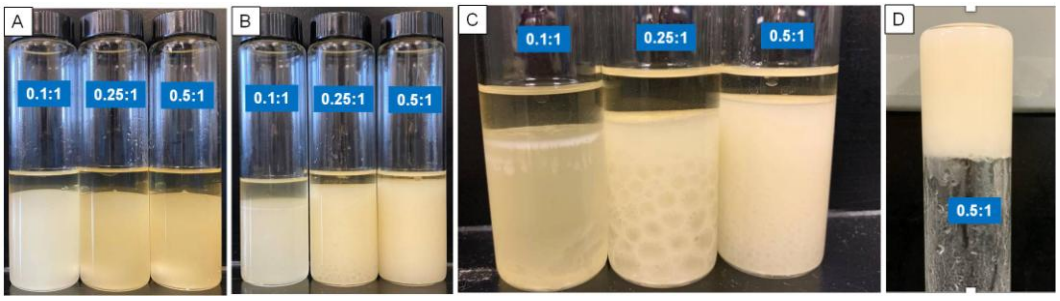

Figure V- 11. Digital images of particle dispersions before handshaking (A), emulsions formed after handshaking and storage of 24 hours (B), emulsions formed after handshaking and storage of 6 weeks (C), and emulsion gel formed after removal of top serum layer (D).

In order to determine the emulsion type, 1 mL of emulsion was added into excessive amount of deionized water or corn oil. As illustrated in Figure V-12, oil-in-water emulsions were easily dispersed in deionized water and formed an oil creaming layer on the top of water, while water droplets of water-in-oil emulsions were evenly dispersed in the corn oil. The oil-in-water emulsion in Figure V-12 was formed by handshaking a mixture of 3 mL 40 mg/mL zein in 75% EtOH solution, 3 mL corn oil, and 500 μL deionized water for 1 min. After storage for 24 hours, it was utilized to test emulsion types. The water-in-oil emulsion was achieved after the addition of stearic acid. The SA/Z ratio was 0.2:1 and zein stock solution to corn oil volume ratio was 1:3 as illustrated in the preparation method.

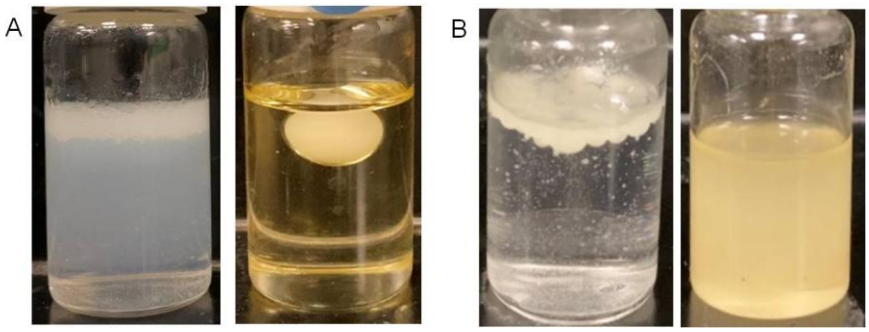

Figure V- 12. A, Digital images of oil-in-water emulsions dispersed in water (left) and oil (right) phase; B, digital images of water-in-oil emulsions dispersed in water (left) and oil (right) phase.

In order to see if stable emulsions can be formed by pure zein or pure stearic acid, emulsions were formed in the same way without the addition of stearic acid or zein. As illustrated in Figure V-13, the structure of colloidal particles was exclusively observed in zein stabilized emulsions, while droplets with smooth surface were observed in stearic acid stabilized emulsions. Once the droplets were broken down, zein stabilized emulsions released numerous colloidal particles as shown in Figure V-13A, while only a few irregular shaped stearic acid crystals were observed in Figure V-13B.

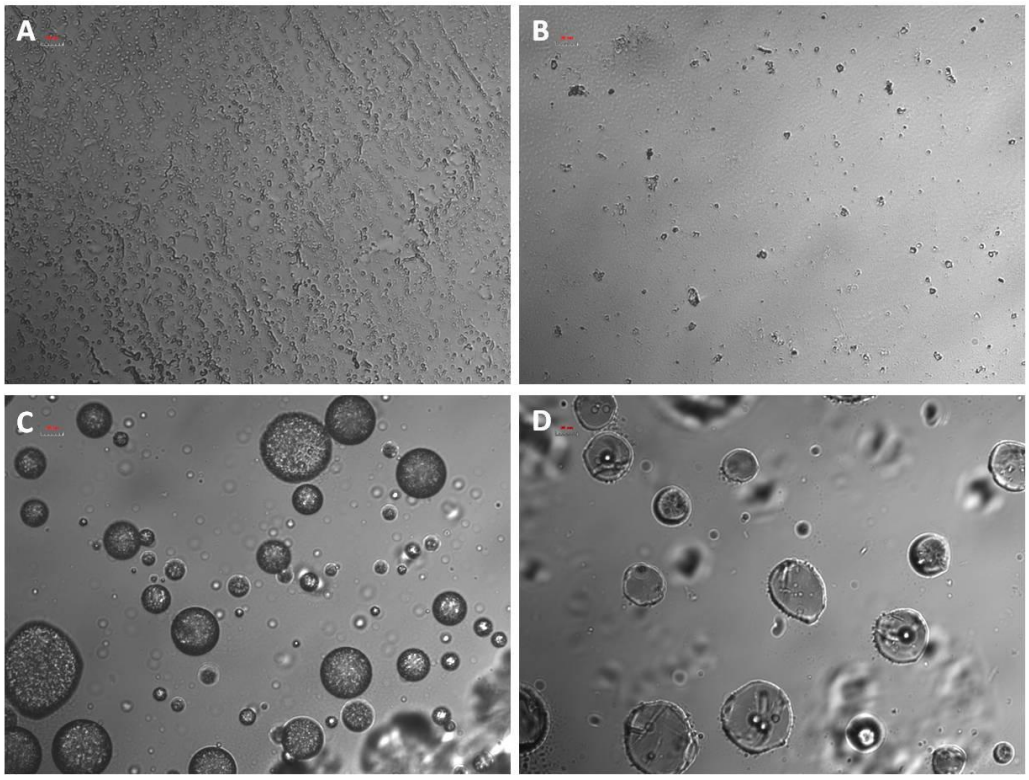

Figure V- 13. Optical microscopic images of zein particles (A), stearic acid (B), emulsion droplets formed by zein particles (C), and emulsion droplets formed by stearic acid (D); scale bars are 20 μm.

As illustrated in Figure V-14, with an increase of the SA/Z ratio, from 0.1:1 to 0.5:1, the size of colloidal particles in the oil phase increased gradually, which may be due to the growth of stearic acid crystals on the colloidal surface at high stearic acid

content. Zein was chemically labeled with FITC in an alkaline condition, and the unattached FITC was removed by dialysis. After the formation of colloidal particles with stearic acid, the green fluorescence of FITC-labeled zein was clearly observed as shown in Figure V-14C, which indicated that the colloidal particles were mainly formed by zein, and the zein protein provided a nuclear for the crystallization of stearic acid.

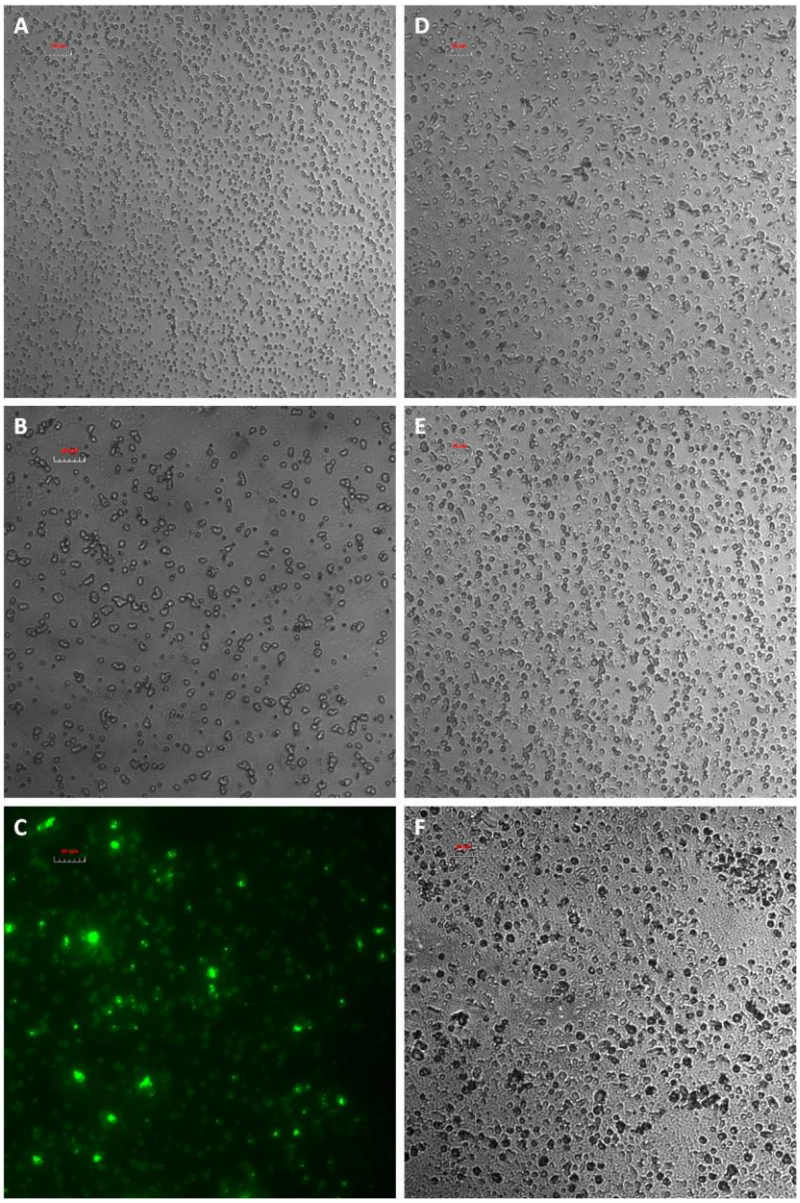

Figure V- 14. Optical and fluorescence microscopic images of SA/Z complexes formed at different ratios, i.e. 0.1:1 (A), 0.2:1 (B), 0.2:1 (C), 0.3:1 (D), 0.4:1 (E), and 0.5:1 (F); scale bars are 20 μm.

Since the emulsions were fabricated through handshaking and they were stabilized by insoluble colloidal particles, here we firstly proposed a term “self-emulsifying Pickering emulsions (SEPE)”. The phenomenon of SEPE was also reported in another study, in which they used commercially available fumed silicate particles together with chitosan to stabilize sunflower oil based emulsions either by handshaking for 30 seconds or rotor-stator mechanical shearing for 120 seconds (*332*). Without high speed homogenization, Pickering emulsions can also be achieved through vortex. It was reported that poly (methyl methacrylate-co-butyl acrylate) latex particles were able to encapsulate lactic acid bacteria in W/O sunflower oil Pickering emulsions by vortex for 1 min (*333*). But the mechanism and the specific requirements for colloidal particles for the formation of SEPE were still unknown.

Figure V-15 showed optical microscopic images of emulsions formed by SA/Z complexes at different SA/Z ratios. The structures of double emulsions were clearly observed in all different ratios. There were large numbers of smaller droplets trapped in the droplets of secondary emulsions. After the broken down of secondary emulsion droplets, droplets of primary emulsions were released to the surrounding environment. Since the emulsions can be easily dispersed in oil phase as shown in Figure V-12B, the obtained emulsions were O/W/O double emulsions.

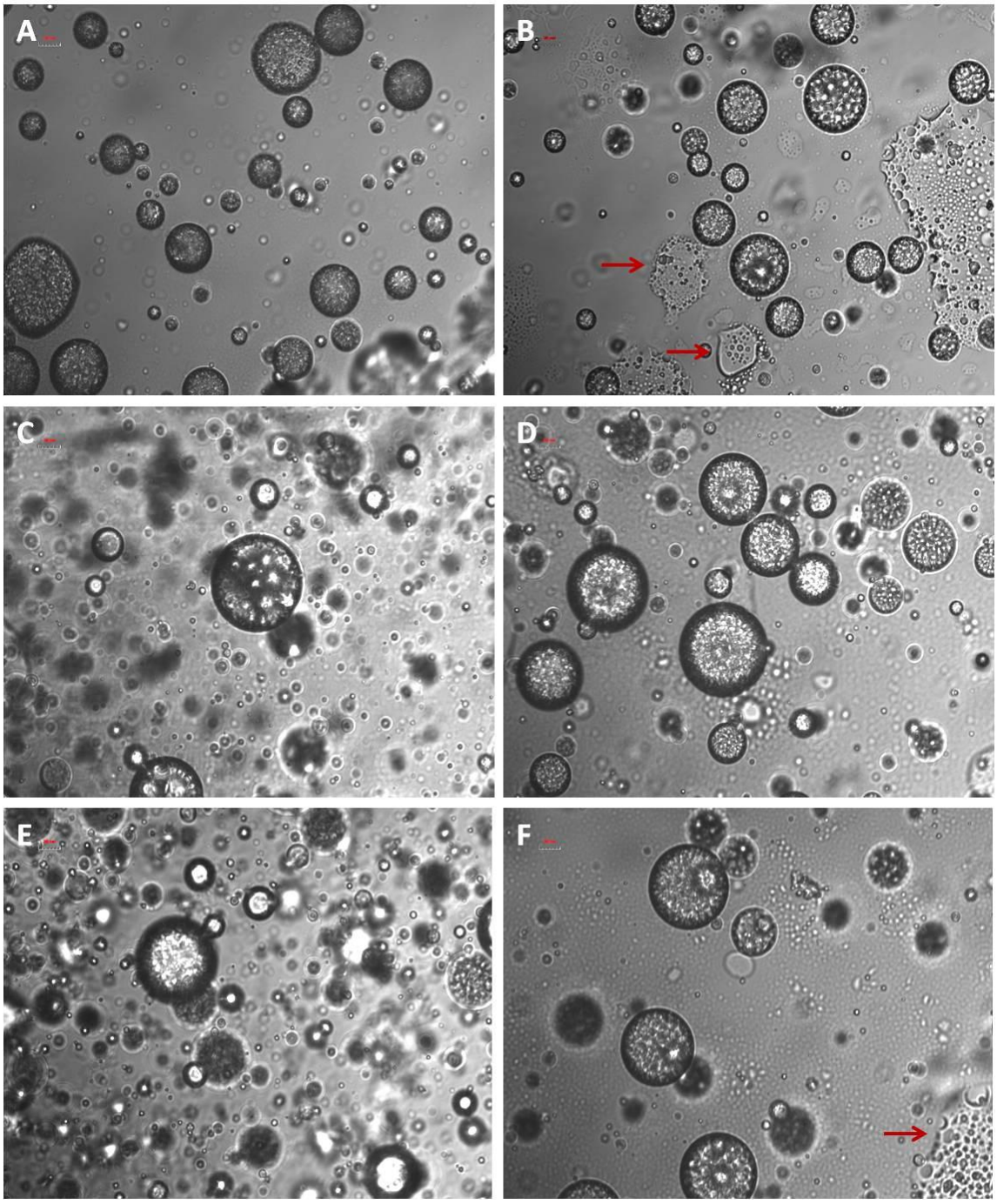

Figure V- 15. Optical microscopic images of emulsions stabilized by SA/Z complexes formed at different ratios, i.e. 0:1 (A), 0.1:1 (B), 0.2:1 (C), 0.3:1 (D), 0.4:1 (E), and 0.5:1 (F); the red arrows indicated the broken down of secondary emulsion droplets with a release of droplets of primary emulsions; scale bars are 20 μm.

4. Conclusion

Zein was able to form stable complexes with fatty acids under alkaline condition. The addition of FAs would increase the transparency of particle dispersions which may be due to the possibility that FAs increase the molecular distance between single zein molecules. SA/Z complexes have the highest hydrophobicity, with a contact angle around 90˚. The SEM image indicated that FAs could lead to the partial fusion of zein colloidal particles, so that FAs have the ability to reduce the brittleness and increase the plasticity of zein films. The SAXS profiles reflected the particle structures and aggregations in solutions. Both zein and FA/Z complexes existed in a rod-like shape with Rg/Rc values in a range from about 2.3 to 3.5. The SA/Z complexes have good emulsification capacity to stabilize O/W/O double emulsions through handshaking.

CHAPTER VI. NANOENCAPSULATION OF HESPERIDIN USING LA/ZEIN COMPLEXES

1. Introduction

With an increase of the age, the risk of heart disease and cancer has gradually increased. Based on a report from the Centers for Disease Control and Prevention (CDC), the heart disease and cancer are the 1st and 2nd leading cause of death for the population aged 65 and over, which account for 25.6 % and 21.4% of deaths, respectively (*334*). Hesperidin, also known as hesperitin-7-rhamnoglucoside, is an abundant and inexpensive flavanone glycoside found in lemons and sweet oranges as well as in some other fruits and vegetables (*335*). It can protect heart and brain against cardiovascular disease and reduce diabetes symptoms (*336-338*), and also prevent cancer risk, such as colon cancer (*339, 340*), bladder cancer (*341*), skin cancer (*342*), and oesophagus cancer (*343*), etc. The anti-cancer property of hesperidin is mainly due to its antioxidation and anti-inflammation effect (*344*).

However, the utilization of hesperidin as a nutraceutical ingredient in functional food and beverage products is currently quite limited due to its low water solubility and poor oral bioavailability (*345*). Bioavailability, defined as the fraction that eventually reaches the systemic circulation after oral adiminitration, is related to the amount of bioactive compounds released into the small intestine, the amount of bioactive compounds absorbed through the gut wall, and the amount of bioactive compound remained intact by the first pass metabolism (*272*). According to a clinical study on five healthy volunteers, after ingestion of 0.5 or 1 L of a commercial orange juice (equivalent

to 444 mg/L hesperidin), the peak plasma concentration of hesperetin was 0.46 ± 0.07 μmol/L and 1.28 ± 0.13 μmol/L after the 0.5 or 1 L intake, respectively (*346*). The hesperetin enters the systemic circulation in the forms of glucuronides (87%) and sulphoglucuronides (13%) (*346*). Nearly all hesperidin was excreted out through urine after 24 hours oral administration, and the relative urinary excretion rate ranged from around 4-8% of the intake (*346*).

There are several reasons for the poor bioavailability of hesperidin. First of all, it is the low aqueous solubility, which limited the loading capacity of hesperidin in formulations so as to reduce the amount of hesperidin arriving at the human gut system. Secondly, the high metabolism rate affected the amount of hesperidin entering the human circulating system, reducing the therapeutic dosages it can be achieved to the target organs. Thirdly, the poor bioavailability of hesperidin was also probably due to the rutinoside moiety attached to the flavonoid (*347*). The sugar moiety of flavonoids was considered as the main determining factor for the bio-absorption in human bodies, saying that compared with their aglycones (hesperitin) and glucoside (rutinose) forms, glycosides with rhamnose has poorer bio-absorption (*348*). What's more, the intestinal efflux protein, P-glycoprotein (P-pg), also limited its intestinal absorption (*349*).

In order to overcome these constraints, encapsulation technique has been used to develop noval delivery systems for nutraceuticals. A wide variety of encapsulation systems, including solid nanoparticles, classical emulsions, or double emulsions have been developed in laboratory. Pickering emulsions are one of the most promising delivery systems, since they have high loading capacity and high storage stability. Zein proteins, for instance, are a type of particles surfactants to stabilize these peculiar

emulsions. The study was aimed at fabrication of Pickering emulsions stabilized by lauric acid/zein complexes, and the usage of this new encapsulation system for the delivery of a lipophilic ingredient, hesperidin.

2. Materials and Methods

2.1. Materials

Zein was bought from Wako Pure Chemical Industries, Ltd. (Tokyo, Japan). Lauric acid (LA) was bought from ACROS (New Jersey, USA). Hesperidin (HPLC purity 98%) was purchased from Kingherbs Limited (Yongzhou, Hunan, China). Soybean oil, sunflower oil, canola oil and mint oil was purchased from the local supermarket. Medium chain triglycerides, including Captex 355, Captex 100 and Neobee 1053, were purchased from Abitec Company (Columbus, OH) and Stepan Company (Northfield, IL), respectively. Unless otherwise stated, other chemicals were purchased from Sigma-Aldrich (St. Louis, MO, USA).

2.2. Preparation of Hesperidin Pickering Emulsions

To improve the loading capacity of hesperidin in emulsions, the approximate solubility was tested using different oils, including short-chain triglycerides (triacetin, tripropionin, tributyrin), medium-chain triglycerides (Captex 355, Captex 100 and Neobee 1053) and long-chain triglycerides (soybean oil, sunflower oil, canola oil and mint oil). Eventually, 1 mg/mL hesperidin was dissolved in soybean oil to prepare Pickering emulsions. In order to reduce the intake of ethanol in the oral delivery system, zein was dissolved in propylene glycol. The synthesis of zein colloidal particles was also based on an antisolvent precipitation method with a little modification (*57*). Briefly, 0.25 g of zein was dissolved in 10 mL propylene glycol, and then the dissolved mixture was

added into 25 mL of pH 10.5 buffer solution. Different amount of fatty acids were also dissolved in propylene glycol phase to make final LA/Z ratio to be 0.1:1, 0.25:1, 0.5:1, and 1:1. The obtained zein concentration was at 7.14 mg/mL. The oil fraction was fixed at 60% (w/w) in emulsions. Different speeds of high-speed homogenization were determined, including 8 000 rpm, 10 000 rpm, 12 000 rpm and 14 000 rpm.

2.3. Optical Microscopy

Samples (100 μL) were placed on a clean glass slide, and diluted with a drop of deionized water if needed before imaging. Microscopic images were taken using the Nikon TE2000 microscope (Japan). And particle size distributions were analyzed using Image J software. Average sizes of droplets in Pickering emulsions and colloidosomes were calculated using 50-200 droplets.

2.4. TNO gastro-Intestinal Model (TIM-1)

The TNO gastro-Intestinal Model (TIM-1) was used to simulate the consecutive dynamic digestion and absorption in the stomach, duodenum, jejunum and ileum. Before starting the experiment, each reactor was pre-infused with individual start residues to mimic the real gastrointestinal digestion conditions in a fed state. pH values of each reactors were monitored and adjusted using computer programs, which also controlled the peristaltic movements of each compartment and modulated the secretion and the transit times of various digestion fluids. The temperature was maintained at 37 °C through surrounding water jackets. In TIM-1 model, bioaccessibility is determined by the accumulative amount of compound absorbed through the simulated jejunal and ileal membranes over different time periods (*266*). Therefore, the digested samples collected at the jejunum and ileum capillary membranes at specific time intervals were considered

as the bioaccessible portion available for absorption. Collected samples were immediately stored at -20 °C before HPLC analysis. The entire digestion in the TIM-1 model lasted for 360 min.

Two different samples were ingested by the system and each sample was tested twice to see the reproducibility of results. For the control group, it is a mixture of oil and water both containing hesperidin in the same concentration as the emulsion previously formulate. Control has 60 mL of oil phase with 60 mg of hesperidin to obtain the maximum concentration (1 mg/mL), and 40 mL of aqueous phase (propylene glycol+buffer) containing 142.5 mg of hesperidin. Pickering emulsions stabilized by with hesperidin encapsulated LA/zein particles provided that same total amount of hesperidin as the control group (202.5 mg). Hesperidin and zein were dissolved into propylene glycol under magnetic stirring for 2 hours at different mass ratio: 0.1:1; 0.25:1; 0.5:1; 1:1. The above mixture was added dropwise into buffer to form particles. Emulsions were prepared in the same condition as mentioned before using Ultra-Turrax homogenizer for 3 min.

2.5. Extraction and HPLC Analysis of Hesperidin

Tangeratin was used as internal standard for hesperidin. First, 0.8 mL of sample was added to 0.4 mL of hexane and 0.2 mL of internal standard into an eppendorf tube. Hexane is used to remove oil from sample which cannot be introduced into HPLC. The water phase at the bottom was collected and mixed with 0.4 mL of ethyl acetate. After that, sample was mixed by vortex for 5 minutes and then centrifuged at 3000rpm for 3 minutes. Ethyl acetate at the top was transferred into another container whereas the rest of the sample went throough another cycle of vortex/centrifugation with 0.4 mL ethyl

acetate again. All ethyl acetate collected after that was fully evaporated under hood overnight. Next day, 1ml of HPLC grade methanol was used to redissolve hesperidin still stuck on the wall of container. Samples are filtrated with a syringe filter (0.22 μm) to remove all possible particles.

The UltiMate 3000 HPLC system (Dionex, Sunnyvale, USA) combined with a Luna® 5 μm C18 100 Å Column (250×4.6mm i.d.) (Phenomenex, Macclesfield, UK) was used to analyze hesperidin. The system consisting of a C18 column connected to an ultraviolet detector set up at 280nm and 286nm for tangeratin and hesperidin respectively. 0.1% phosphoric acid-water solution (A) and acetonitrile (B) were the mobile phases for HPLC analysis. The elution condition was set as below: at 0–10 min, solvent A changed from 60% to 45%; at 10–15 min, solvent A changed from 45% to 30% A; at 15–17 min, solvent A changed from 30% to 0%; at 17–24 min, solvent A changed back from 0% to 60%. Quantification of hesperidin based on a standard curve of hesperidin and tangeratin (internal standard).

3. Results and Discussion

3.1. Preparation of LA/Z Complexes

Zein is known for its good solubility in alcohol solution but not in aqueous media. These solubility characteristics have been used by researchers to prepare zein nanoparticles in the antisolvent precipitation method using 70-85% ethanol solution. The formation of insoluble colloidal particles consists of the following three steps, i.e. super-saturation, nucleation and progression. At first when the compound dissolved in a good solvent (e.g. alcohols or propylene glycol) is rapidly mixed into a poor solvent (e.g. water), precipitation occurred immediately and the compound became supersaturated.

The lower solubility of the compound in the solvent mixture drove the formation of insoluble colloidal particles. And then particles can nucleate and growth gradually after the mixing was completed.

As mentioned before, the formation of LA and zein complexes was pH-dependant. In order to obtain spherical particles, zein has been synthesized at pH 10.5. Buffer solution was prepared by using sodium carbonate ($NaHCO_3$) and sodium bicarbonate (Na_2CO_3). pH was tuned with sodium hydroxide (NaOH) and hydrochloric acid (HCl) to obtain an accurate value of 10.5. During the dissolution step, different ratios of lauric acid were also added into solutions, i.e. 0.1:1; 0.25:1; 0.5:1; 1:1, which allowed for the formation of particles with different hydrophobicities. And our goal is to use the smallest amount of lauric acid to form LA/zein complexes as emulsifiers, and they are sufficiently enough to produce stable emulsions.

Depending on the different amount of LA introduced, the appearance of complex particles changed gradually. At lower LA/zein ratios, solutions are more opaque than the ones at higher ratios, which was consistent with our previous findings. In our previous study, LA/zein complexes were prepared by 70% ethanol solution (Chapter V). In order to broaden the application of the formulation in food industries, ethanol was replaced by propylene glycol (PG), propane-1.2-propanediol, which is found in a large amount of processed foods products as well as various cosmetics products.

3.2. Optimization of Pickering Emulsions

Due to the amphiphilic properties, LA/zein complexes tend to adsorb at the oil-water interface to decrease the surface tension. Emulsification is a complex process, strongly influenced by emulsion composition as well as preparation procedure, such as

particles size of stabilizers, concentration of stabilizers, oil type, water/oil ratio, homogenization speed, and mechanical mixing conditions.

Variation of homogenization speed

The input energy has a great influence on the droplets size of emulsions. In order to determine the optimum homogenization speed, different speeds were tried, including 8 000 rpm, 10 000 rpm, 12 000 rpm and 14 000 rpm. Zein concentration was fixed at 7.14 mg/mL in the particle suspension (the aqueous phase), with a LA/zein ratio of 0.1:1 and an oil fraction of 50% (w/w). Under low speed homogenization, emulsions immediately began to have a phase separation. Droplets floated to the top of the container, forming a creaming layer. And then coalescence occurred, in which droplets merged together forming larger droplets, and eventually breaking down and leaving a thin oil layer. As illustrated in Figure VI-1, the most stable emulsion with the smallest droplet size was obtained by the highest speed 14 000 rpm. The size of the emulsion droplets can be reduced by increasing the homogenization intensity or duration time of energy input. Under most circumstances, droplet size decreases as the energy input increases.

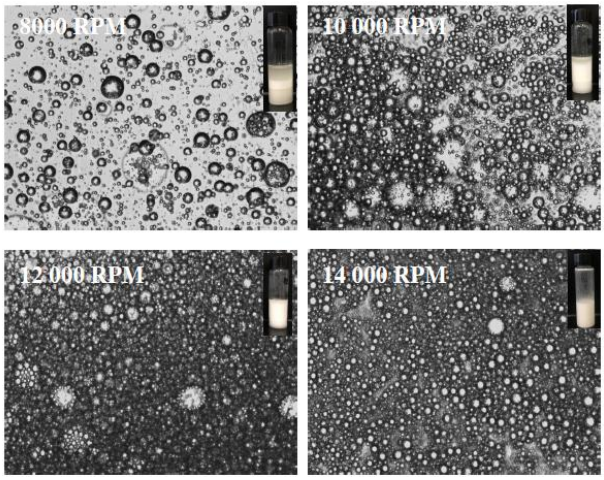

Figure VI- 1. Optical microcopy of emulsions at different homogenization speeds; zein concentration was fixed at 7.14 mg/mL, with a LA/zein ratio of 0.1:1 and an oil fraction of 50% (w/w).

Variation of Lauric acid/Zein ratio

Lauric acid (or dodecanoic acid) is a saturated medium-chain fatty acid, with 12 carbon atoms. Fatty acid itself has certain emulsification capacities due to its hydrophobic tail (carbon chain) and polar head (carboxyl group). However, lauric acid alone was not able to form emulsions as stable as the one stabilized by the LA/zein complexes under the same emulsification condition. As mention before, different ratio of lauric acid has been introduced into zein solutions to study the influence on wetting properties. As shown in Figure VI-2, the addition of lauric acid dramatically decreased size of droplets. Zein concentration was fixed at 7.14 mg/mL, with homogenization speed of 14 000 rpm and an oil fraction of 50% (w/w). At higher LA/zein ratios, emulsions were stable for a longer time, which indicated that lauric acid not only decreased droplet diameters, but also enhanced the stability of emulsions.

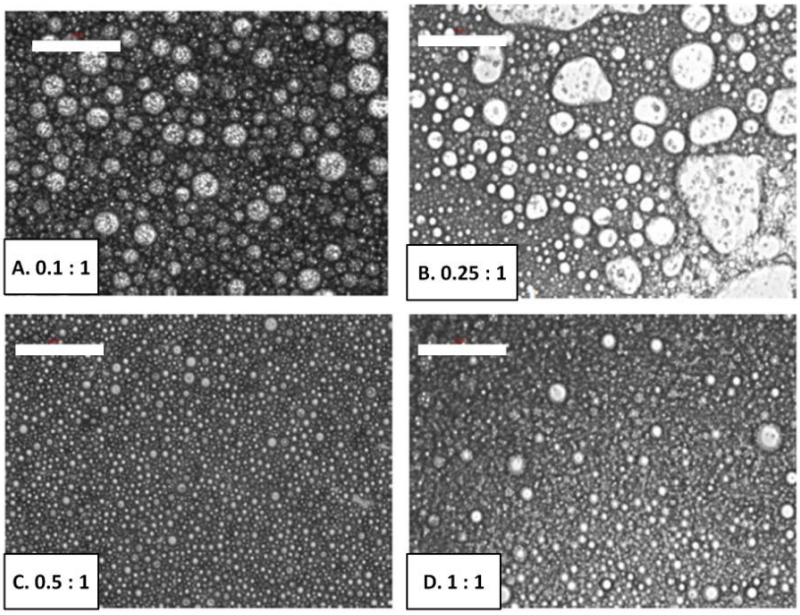

Figure VI- 2. Optical microcopy of emulsions with different LA/zein ratios; zein concentration was fixed at 7.14 mg/mL, with homogenization speed of 14 000 rpm and an oil fraction of 50% (w/w).

Variation of oil fraction

Oil fractions play an important role in the determination of emulsion appearance, viscosity, stability, and drug loading capacity. Oil-in-water emulsion was prepared using commercially available soybean oil with different oil fractions, i.e. 40%, 50%, 60%, 70% and 80%. The emulsions were prepared at zein concentration of 7.14 mg/mL, with homogenization speed of 14 000 rpm and a LA/zein ratio of 0.25:1. According to their macroscopic appearance (Figure VI-3), low amount of oil makes emulsions less viscous and less stables. The increase of oil phase fraction caused significant increase of viscosity of all emulsions. The higher the oil fraction is, the higher the emulsification layer was obtained. Therefore, higher droplets concentration was obtained in the emulsions, where droplets were densely packed together without movement. At certain critical point, the emulsions viscosity further increased and eventually formed a gel structure. And this fraction is called the critical disperse phase volume fraction. In our study, when the oil fraction increased to 70%, emulsion gel was formed.

Figure VI- 3. Oil-in water emulsions with different oil fractions, i.e. 40%, 50%, 60%, 70% and 80% (from left to right); zein concentration was fixed at 7.14 mg/mL, with homogenization speed of 14 000 rpm and a LA/zein ratio of 0.25:1.

3.3. Determination of the Oil Phase

The poor aqueous solubility of hesperidin results in its poor bioavailability, which finally limited its various applications. In order to encapsulate it into formulations, hesperidin has to be soluble in the lipid phase, since the dissolved one is more amorphous and more absorbable as compared with crystalline form. The challenge in this study is to find the suitable oil as a carrier vehicle to dissolve this compound. It was reported that 1mg/mL of hesperidin has been dissolved in soybean oil to form lecithin-enhanced Pickering emulsions stabilized by chitosan nanoparticles (*350*). In order to further increase the oil solubility of hesperidin, oils with different polarities were tested in the study, including short-chain triglycerides (SCT) (e.g. triacetin, tripropionin, tributyrin), medium-chain triglycerides (MCT) (e.g. Captex 355, Captex 100 and Neobee 1053) and long-chain triglycerides (LCT) from natural plant source (e.g. soybean oil, sunflower oil, canola oil and mint oil).

Only 4 of 10 oils have a high solubility of hesperidin, i.e. mint oil, triacetin, tributyrin and tripropionin. Mint oil is one of the most widely used oils in food flavors, cosmetics, fragrances and pharmaceutics. Mint oil has high content of alcohols (43.47-50.10%) and terpenes (18.55-21.07%), in which menthol is the major detected compound, accounting for 28.19-30.35% (*351*). Therefore, mint oil has higher polarity as compared with common cooking oils (e.g. vegetable oils). Triglyceride is an ester consisting of glycerol and three fatty acids. Short chain triglycerides refer to the triglycerides formed between fatty acids of 2-5 carbons and glycerol, while medium chain triglycerides contain fatty acid with 6 to 12 carbons. The shorter the carbon chain

length is, the less the hydrophobicity of the oil is. So it was very obvious that hesperidin has higher solubility in oils with high polarities, as compared with MCT and LCT.

After finding suitable carrier oils, emulsions were prepared using these four oils. Aqueous phase was the same as the optimized emulsion previously described. However, none of the oils with high hesperidin solubility was suitable for formulating emulsions. Ostwald ripening and coalescence occurred immediately after the emulsions were formed. Oil droplets merged together and small droplets grew into bigger one. As a result, MCT with low polarity was added into mint oil in diverse ratios to see if the emulsion stability could be improved. However, the enhancement of emulsion stability was not sufficient. It indicated that HLB values of LA/zein complexes were not high enough to stabilize these oils with high polarities. Ideally, stable emulsions are best formulated by emulsifiers with desired HLB (hydrophile-lipophile balance) values that are close to the one required by oil phase. For instance, soybean oil requires surfactant with HLB value around 7 to stabilize it, whereas mint oil or SCT requires higher HLB value, around 12. In addition, zein colloidal particles have previously demonstrated their ability to stabilize soybean oil emulsion. Thus the HLB value of zein colloidal particles was approximately around 7. That’s the reason why it cannot stabilize emulsions containing mint oil or SCT or even the mixture of MCT and mint oil. So eventually soybean oil was used as the oil phase to make Pickering emulsions.

3.4. Encapsulation of Hesperidin

Right now, the maximum concentration dissolved into soybean oil is 1mg/ml. The feeding volume of Pickering emulsions on TIM-1 was 100 mL. So the maximum loading into formulation was 60 mg with the oil fraction of 60%. In order to further increase the

loading capacity of hesperidin in formulations, it was not only dissolved in the oil phase, but also encapsulated in zein particles. It was found that desperidin was also soluble in propylene glycol like zein. Thus hesperidin-zein nanoparticles were prepared using the same antisolvent precipitation method. Hesperidin and zein were dissolved into propylene glycol under magnetic stirring for 2 hours at different mass ratio: 0.1:1; 0.25:1; 0.5:1; 1:1. The above mixture was added dropwise into buffer to form particles. Emulsions were prepared in the same condition as mentioned before using Ultra-Turrax homogenizer for 3 min.

As illustrated in Figure VI-4, translucent solutions were observed for the three first ratios, while the last ratio (1:1) gave more opaque appearance, which was due to the formation of larger particle suspensions. Without the addition of Lauric acid, the corresponding Pickering emulsions creamed soon after emulsion was prepared. Creaming is a characteristic phenomenon that has been commonly observed in Pickering emulsions, which is due to floating effect of large droplet size as compared with the small droplet size of nanoemulsions. In order to prepare a more homogeneous emulsion, lauric acid was added to see if it could improve the emulsification capacity of zein. Thus, zein to hesperidin ratio was set as1:1, and lauric acid with different ratio was added into the propylene solution, and then trickled into the aqueous phase. For example, 0.25:1:1 ratio indicated the mass ratio of lauric acid, zein, and hesperidin was 0.25: 1:1. The obtained particle suspensions were then utilized to stabilized Pickering emulsions with 60% oil fraction. It was found that 1:1:1 ratio gave the highest stability as compared with other ratios. In the end, the Pickering emulsion was stabilized by hesperidin encapsulated LA/zein complexes in a mass ratio of 1:1:1, and the zein concentration in particle

suspension was 3.57 mg/mL, the emulsions were homogenized at14 000rpm with oil fraction of 60%. Loading capacity of hesperidin in the final emulsion was increased from 0.06% to 2%.

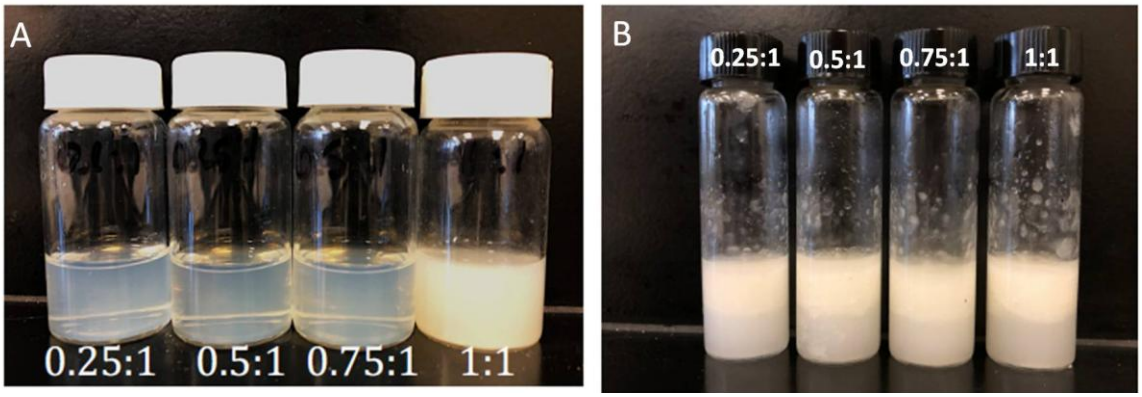

Figure VI- 4. Appearance of hesperidin encapsulated LA/zein complexes at different hesperidin to zein mass ratios (A) and the Pickering emulsions stabilized by the hesperidin encapsulated LA/zein complexes (B).

3.5. TNO Gastro Intestinal Model

The TNO Gastro-Intestinal Model (TIM) has an advantageous characteristic that it does not have any regulatory and ethical concerns related to animal studies or human clinical trials. And it's also very convenient to do the sampling in different digestion organs at different time points during digestion, which is quite difficult to achieve in animal or human studies. TIM-1 system is an *in vitro* model that has multiple compartments and closely simulates the digestion and absorption of the human gastrointestinal tract. It is precisely controlled or programmed by computer system. Furthermore, TIM-1 model could mimic different parameters during digestion, such as peristaltic movement, body temperature, pH, food transit, secretion of gastric, biliary, pancreatic juice, and absorption through small intestine.

In the stomach compartment the ingested foods were mixed with secreted gastric acid, gastric enzymes (lipase, pepsin) and electrolytes. Beforehand, all stock solutions

and secretions were freshly prepared in the morning. Stomach compartment was connected to the duodenum compartment by a valve that gradually transfers food from one to the other compartments. In the duodenum compartment, the pH was increased to 6.4 by the secretion of sodium bicarbonate, and the digestion process occurred continuously by secretion of bile and pancreatic juice under simulated peristaltic mixing. After a short residence time, food is transported to jejunum (pH 6.9) where it was exposed to a higher pH and then ileum (pH 7.2) until all foods was digested.

Samples went through a standard 6-hour experiment, simulating a fed-state digestion in an adult after the intake of formulations. The control was a mixture of 60 mL 1 mg/mL hesperidin in oil solution and 40 mL of aqueous phase (propylene glycol + buffer) containing 142.5mg of hesperidin. The total intake amount of hesperidin for both control and Pickering emulsions was 202.5 mg. During the experiment, jejunum and ileum and efflux secretions were taken directly from the filtrates every 30 minutes for the first two hours, and then every one hour until the end of the experiment. Unabsorbed hesperidin was delivered to the colon, which corresponded to the efflux secretion.

As shown in Figure VI-5, with an increase of the digestion time, the LA/zein stabilized Pickering emulsion had slight higher bio-absorption as compared with the control. Control had a final bioavailability around 53% whereas formulation arrived at 68%. Small droplet size at high LA/zein ratio (1:1) increased the surfaces contact areas of emulsions, which facilitated its digestion and absorption in the small intestine. However, the difference between Pickering emulsions and the control was not significant. The results indicated that Pickering emulsions stabilized by hesperidin encapsulated LA/zein

complexes slightly increased the bioavailability of hesperidin, but the effectiveness needs to be further improved.

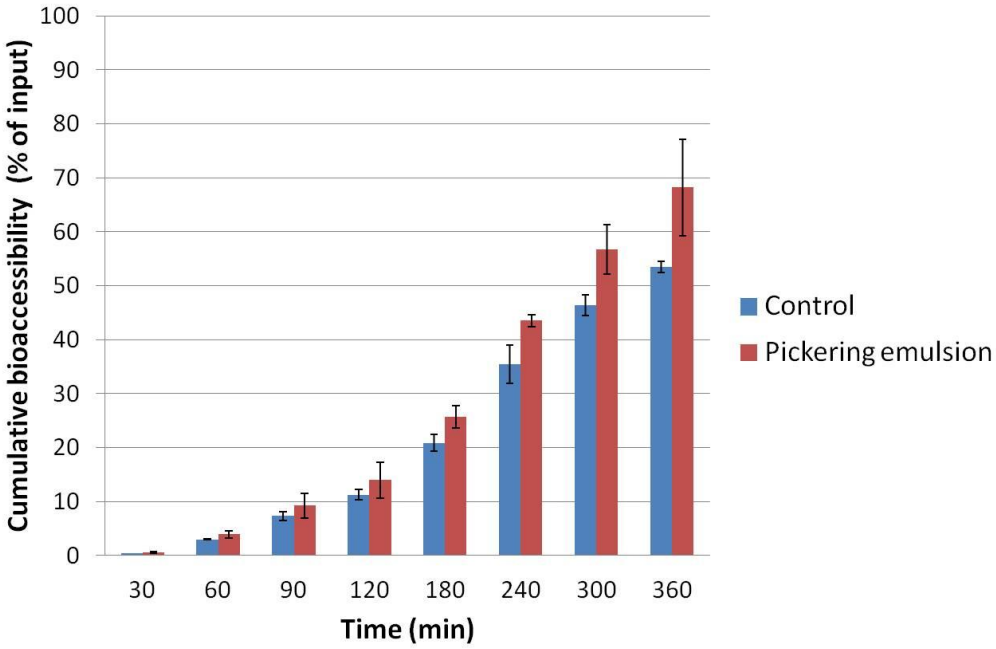

Figure VI- 5. Cummulative bioaccessibility of hesperidin during the digestion in TIM-1 model.

4. Conclusion

LA/zein complexes have demonstrated great capacity to stabilize emulsions. It was shown that factors like homogenization speed, LA/zein ratio, and oil fraction have pronounced effect on the emulsion stability. The optimized formulation was obtained at a 1:1 mass ratio of zein to lauric acid at zein concentration of 3.54mg/mL in the aqueous phase, and homogenized at 14 000rpm for 3 min with an oil fraction of 60%. Due to the limited solubility of hesperidin into soybean oil, hesperidin was encapsulated into LA/zein complexes in order to increase its loading capacity in emulsions. *In vitro* TNO Gastro intestinal model (TIM-1) was applied to evaluate the bioavailability of hesperidin. Results indicated that the bioavailability of hesperidin was enhanced from 53% to 68%.

This study may trigger deeper research into other water insoluble proteins acting as particles emulsifier, as a kind of promising environmental friendly biomaterials. Moreover, more studies need to be conducted to investigate in details about the control release kinetics of the formulation.

CHAPTER VII. SUMMARY AND FUTURE WORK

In this study, the surface activity of zein was adjusted through hydrophilic modification with a water-soluble protein, sodium caseinate (SC), and hydrophobic modification with saturated fatty acids with different chain lengths, including lauric acid (LA), myristic acid (MA), palmitic acid (PA) and stearic acid (SA). As an amphiphilic prolamin, the zein-based insoluble colloidal particles were formed through traditional anti-solvent precipitation method. The obtained zein/SC complexes had good emulsification ability to stabilize toluene, hexane, and common cooking oils extracted from plants, such as soybean oil, corn oil, sunflower oil, etc. But they had limited emulsification capacity to stabilize oils with high polarities such as octanol, triacetin and tributyrin. The obtained Pickering emulsions were then utilized to encapsulate resveratrol (RES) for a controlled release purpose. The loading capacity of RES in Pickering emulsions was as high as 10 mg/mL, which was around 20-500 times higher than the loading capacities in the recent reported emulsion-based formulations. Based on the TNO gastro-Intestinal Model (TIM-1) results, conventional emulsions had the highest bioaccessibility compared with Pickering emulsions and bulk oil solutions. In SHIME experiment, the structure of Pickering emulsions was observed during the digestion in the stomach. Both TIM-1 and Franz Cell experiments showed that Pickering emulsion effectively slowed down the bio-absorption in small intestine as compared with nanoemulsion and bulk oil solutions. In addition, lecithin stabilized nanomemusions retarded the growth of probiotics, while Pickering emulsions even promoted its growth. Therefore, Pickering emulsions are more suitable for delivery of resveratrol into colon, while nanoemulsions are more suitable for improvement of bioavailability of RES. With

the presence of PGPR, zein/SC complexes were able to stabilize W/O/W double emulsions either through magnetic stirring method or high speed homogenization method. The Pickering emulsions stabilized by zein/SC complexes were further utilized as a template to fabricate colloidosomes. The colloidosomes had a characteristic hollow shell structures, which was successfully stabilized either through layer-by-layer deposition of polysaccharides or covalent cross-linking with genipin.

In the hydrophobic modification of zein, it formed stable complexes with fatty acids under alkaline condition. The addition of FAs increased the transparency of particle dispersions. SA/Z complexes have the highest hydrophobicity, with a contact angle around 90˚. The SAXS profiles indicated that zein and FA/Z complexes existed in a rod-like shape in ethanol solutions. The SA/Z complexes displayed good emulsification capacity to stabilize O/W/O double emulsions through handshaking. And the LA/Z complexes stabilized emulsions were able to improve the bioavailability of hesperidin. This study indicated the potentials of zein to develop promising delivery systems for both oil soluble and water soluble drugs or nutraceuticals.

In the future, further studies could be conducted in the following directions:

1. *In vivo* animal studies need to be conducted to investigate in details about the control release kinetics of the formulations.
2. The emulsification capacity of zein-based complexes can be further improved so that they are able to stabilize oils with high polarities.
3. Simplification of the synthesis procedure of colloidosomes is also quite necessary, which could facilitate the further applicability of this encapsulation technology.

REFERENCE

1. Zhu, J.; Huang, Q., Nanoencapsulation of functional food ingredients. In *Advances in food and nutrition research*, Elsevier: 2019; Vol. 88, pp 129-165.
2. Hu, B.; Pan, C.; Sun, Y.; Hou, Z.; Ye, H.; Zeng, X., Optimization of fabrication parameters to produce chitosan− tripolyphosphate nanoparticles for delivery of tea catechins. *Journal of agricultural and food chemistry* **2008,** *56*, 7451-7458.
3. Hu, B.; Ting, Y.; Zeng, X.; Huang, Q., Bioactive peptides/chitosan nanoparticles enhance cellular antioxidant activity of (−)-epigallocatechin-3-gallate. *Journal of agricultural and food chemistry* **2013,** *61*, 875-881.
4. Wan, Z.-L.; Wang, J.-M.; Wang, L.-Y.; Yang, X.-Q.; Yuan, Y., Enhanced physical and oxidative stabilities of soy protein-based emulsions by incorporation of a water-soluble stevioside–resveratrol complex. *Journal of agricultural and food chemistry* **2013,** *61*, 4433-4440.
5. Sessa, M.; Balestrieri, M. L.; Ferrari, G.; Servillo, L.; Castaldo, D.; D'Onofrio, N.; Donsì, F.; Tsao, R., Bioavailability of encapsulated resveratrol into nanoemulsion-based delivery systems. *Food chemistry* **2014,** *147*, 42-50.
6. Spigno, G.; Donsì, F.; Amendola, D.; Sessa, M.; Ferrari, G.; De Faveri, D. M., Nanoencapsulation systems to improve solubility and antioxidant efficiency of a grape marc extract into hazelnut paste. *Journal of Food Engineering* **2013,** *114*, 207-214.
7. Hemar, Y.; Cheng, L. J.; Oliver, C. M.; Sanguansri, L.; Augustin, M., Encapsulation of Resveratrol Using Water-in-Oil-in-Water Double Emulsions. *Food Biophysics* **2010,** *5*, 120-127.
8. Matos, M.; Gutiérrez, G.; Coca, J.; Pazos, C., Preparation of water-in-oil-in-water (W1/O/W2) double emulsions containing trans-resveratrol. *Colloids and Surfaces A: Physicochemical and Engineering Aspects* **2014,** *442*, 69-79.
9. Matos, M.; Gutiérrez, G.; Iglesias, O.; Coca, J.; Pazos, C., Enhancing encapsulation efficiency of food-grade double emulsions containing resveratrol or vitamin B12 by membrane emulsification. *Journal of Food Engineering* **2015,** *166*, 212-220.
10. Teskač, K.; Kristl, J., The evidence for solid lipid nanoparticles mediated cell uptake of resveratrol. *International Journal of Pharmaceutics* **2010,** *390*, 61-69.
11. Caddeo, C.; Teskač, K.; Sinico, C.; Kristl, J., Effect of resveratrol incorporated in liposomes on proliferation and UV-B protection of cells. *International Journal of Pharmaceutics* **2008,** *363*, 183-191.
12. Das, S.; Lin, H.-S.; Ho, P. C.; Ng, K.-Y., The impact of aqueous solubility and dose on the pharmacokinetic profiles of resveratrol. *Pharmaceutical research* **2008,** *25*, 2593-2600.
13. Das, S.; Ng, K.-Y., Resveratrol-loaded calcium-pectinate beads: effects of formulation parameters on drug release and bead characteristics. *Journal of pharmaceutical sciences* **2010,** *99*, 840-860.
14. Das, S.; Ng, K.-Y., Colon-specific delivery of resveratrol: Optimization of multi-particulate calcium-pectinate carrier. *International Journal of Pharmaceutics* **2010,** *385*, 20-28.
15. Ting, Y.; Jiang, Y.; Lan, Y.; Xia, C.; Lin, Z.; Rogers, M. A.; Huang, Q., Viscoelastic emulsion improved the bioaccessibility and oral bioavailability of crystalline compound: A mechanistic study using in vitro and in vivo models. *Molecular pharmaceutics* **2015,** *12*, 2229-2236.
16. Ting, Y.; Xia, Q.; Li, S.; Ho, C.-T.; Huang, Q., Design of high-loading and high-stability viscoelastic emulsions for polymethoxyflavones. *Food Research International* **2013,** *54*, 633-640.

17. Yu, H.; Li, J.; Shi, K.; Huang, Q., Structure of modified ε-polylysine micelles and their application in improving cellular antioxidant activity of curcuminoids. *Food & function* **2011,** *2*, 373-380.
18. Wang, X.; Jiang, Y.; Wang, Y.-W.; Huang, M.-T.; Ho, C.-T.; Huang, Q., Enhancing anti-inflammation activity of curcumin through O/W nanoemulsions. *Food Chemistry* **2008,** *108*, 419-424.
19. Xiao, J.; Li, C.; Huang, Q., Kafirin nanoparticle-stabilized Pickering emulsions as oral delivery vehicles: Physicochemical stability and in vitro digestion profile. *Journal of agricultural and food chemistry* **2015,** *63*, 10263-10270.
20. Cui, J.; Yu, B.; Zhao, Y.; Zhu, W.; Li, H.; Lou, H.; Zhai, G., Enhancement of oral absorption of curcumin by self-microemulsifying drug delivery systems. *International Journal of Pharmaceutics* **2009,** *371*, 148-155.
21. Yallapu, M. M.; Gupta, B. K.; Jaggi, M.; Chauhan, S. C., Fabrication of curcumin encapsulated PLGA nanoparticles for improved therapeutic effects in metastatic cancer cells. *Journal of Colloid and Interface Science* **2010,** *351*, 19-29.
22. Yu, H.; Shi, K.; Liu, D.; Huang, Q., Development of a food-grade organogel with high bioaccessibility and loading of curcuminoids. *Food Chemistry* **2012,** *131*, 48-54.
23. Yu, H.; Huang, Q., Improving the oral bioavailability of curcumin using novel organogel-based nanoemulsions. *Journal of agricultural and food chemistry* **2012,** *60*, 5373-5379.
24. Yang, X.; Tian, H.; Ho, C.-T.; Huang, Q., Inhibition of citral degradation by oil-in-water nanoemulsions combined with antioxidants. *Journal of agricultural and food chemistry* **2011,** *59*, 6113-6119.
25. Zhao, Q.; Ho, C.-T.; Huang, Q., Effect of ubiquinol-10 on citral stability and off-flavor formation in oil-in-water (O/W) nanoemulsions. *Journal of agricultural and food chemistry* **2013,** *61*, 7462-7469.
26. Yang, X.; Tian, H.; Ho, C.-T.; Huang, Q., Stability of citral in emulsions coated with cationic biopolymer layers. *Journal of agricultural and food chemistry* **2011,** *60*, 402-409.
27. Ghosh, V.; Mukherjee, A.; Chandrasekaran, N., Eugenol-loaded antimicrobial nanoemulsion preserves fruit juice against, microbial spoilage. *Colloids and Surfaces B: Biointerfaces* **2014,** *114*, 392-397.
28. Salvia-Trujillo, L.; Rojas-Graü, A.; Soliva-Fortuny, R.; Martín-Belloso, O., Physicochemical characterization and antimicrobial activity of food-grade emulsions and nanoemulsions incorporating essential oils. *Food Hydrocolloids* **2015,** *43*, 547-556.
29. Donsì, F.; Annunziata, M.; Vincensi, M.; Ferrari, G., Design of nanoemulsion-based delivery systems of natural antimicrobials: effect of the emulsifier. *Journal of biotechnology* **2012,** *159*, 342-350.
30. Topuz, O. K.; Özvural, E. B.; Zhao, Q.; Huang, Q.; Chikindas, M.; Gölükçü, M., Physical and antimicrobial properties of anise oil loaded nanoemulsions on the survival of foodborne pathogens. *Food Chemistry* **2016,** *203*, 117-123.
31. Zahi, M. R.; Liang, H.; Yuan, Q., Improving the antimicrobial activity of d-limonene using a novel organogel-based nanoemulsion. *Food control* **2015,** *50*, 554-559.
32. Ma, Q.; Zhong, Q., Incorporation of soybean oil improves the dilutability of essential oil microemulsions. *Food Research International* **2015,** *71*, 118-125.
33. Zhang, L.; Critzer, F.; Davidson, P. M.; Zhong, Q., Formulating essential oil microemulsions as washing solutions for organic fresh produce production. *Food Chemistry* **2014,** *165*, 113-118.
34. Ma, Q.; Zhang, Y.; Critzer, F.; Davidson, P. M.; Zivanovic, S.; Zhong, Q., Physical, mechanical, and antimicrobial properties of chitosan films with microemulsions of cinnamon bark oil and soybean oil. *Food Hydrocolloids* **2016,** *52*, 533-542.

35. Were, L. M.; Bruce, B.; Davidson, P. M.; Weiss, J., Encapsulation of nisin and lysozyme in liposomes enhances efficacy against Listeria monocytogenes. *Journal of Food Protection* **2004,** *67*, 922-927.
36. Chopra, M.; Kaur, P.; Bernela, M.; Thakur, R., Surfactant assisted nisin loaded chitosan-carageenan nanocapsule synthesis for controlling food pathogens. *Food control* **2014,** *37*, 158-164.
37. Kopermsub, P.; Mayen, V.; Warin, C., Potential use of niosomes for encapsulation of nisin and EDTA and their antibacterial activity enhancement. *Food Research International* **2011,** *44*, 605-612.
38. Chung, C.; Rojanasasithara, T.; Mutilangi, W.; McClements, D. J., Enhanced stability of anthocyanin-based color in model beverage systems through whey protein isolate complexation. *Food Research International* **2015,** *76*, 761-768.
39. Ersus Bilek, S.; Yılmaz, F. M.; Özkan, G., The effects of industrial production on black carrot concentrate quality and encapsulation of anthocyanins in whey protein hydrogels. *Food and Bioproducts Processing* **2017,** *102*, 72-80.
40. Robert, P.; Gorena, T.; Romero, N.; Sepulveda, E.; Chavez, J.; Saenz, C., Encapsulation of polyphenols and anthocyanins from pomegranate (Punica granatum) by spray drying. *International journal of food science & technology* **2010,** *45*, 1386-1394.
41. Liang, R.; Shoemaker, C. F.; Yang, X.; Zhong, F.; Huang, Q., Stability and bioaccessibility of β-carotene in nanoemulsions stabilized by modified starches. *Journal of agricultural and food chemistry* **2013,** *61*, 1249-1257.
42. Liang, R.; Huang, Q.; Ma, J.; Shoemaker, C. F.; Zhong, F., Effect of relative humidity on the store stability of spray-dried beta-carotene nanoemulsions. *Food Hydrocolloids* **2013,** *33*, 225-233.
43. Yanagi, K.; Miyata, Y.; Kataura, H., Highly Stabilized β-Carotene in Carbon Nanotubes. *Advanced Materials* **2006,** *18*, 437-441.
44. Helgason, T.; Awad, T. S.; Kristbergsson, K.; Decker, E. A.; McClements, D. J.; Weiss, J., Impact of surfactant properties on oxidative stability of β-carotene encapsulated within solid lipid nanoparticles. *Journal of agricultural and food chemistry* **2009,** *57*, 8033-8040.
45. Fernandez, A.; Torres-Giner, S.; Lagaron, J. M., Novel route to stabilization of bioactive antioxidants by encapsulation in electrospun fibers of zein prolamine. *Food Hydrocolloids* **2009,** *23*, 1427-1432.
46. Shukla, R.; Cheryan, M., Zein: the industrial protein from corn. *Industrial crops and products* **2001,** *13*, 171-192.
47. Swarup, S.; Timmermans, M. C.; Chaudhuri, S.; Messing, J., Determinants of the high-methionine trait in wild and exotic germplasm may have escaped selection during early cultivation of maize. *The Plant Journal* **1995,** *8*, 359-368.
48. Esen, A., Separation of alcohol-soluble proteins (zeins) from maize into three fractions by differential solubility. *Plant Physiology* **1986,** *80*, 623-627.
49. Esen, A., A proposed nomenclature for the alcohol-soluble proteins (zeins) of maize (Zea mays L.). *Journal of Cereal Science* **1987,** *5*, 117-128.
50. Li, Y.; Li, J.; Xia, Q.; Zhang, B.; Wang, Q.; Huang, Q., Understanding the dissolution of α-zein in aqueous ethanol and acetic acid solutions. *The Journal of Physical Chemistry B* **2012,** *116*, 12057-12064.
51. Tatham, A.; Field, J.; Morris, V.; I'Anson, K.; Cardle, L.; Dufton, M.; Shewry, P., Solution conformational analysis of the alpha-zein proteins of maize. *Journal of Biological Chemistry* **1993,** *268*, 26253-26259.
52. Matsushima, N.; Danno, G.-i.; Takezawa, H.; Izumi, Y., Three-dimensional structure of maize α-zein proteins studied by small-angle X-ray scattering. *Biochimica et Biophysica Acta (BBA)-Protein Structure and Molecular Enzymology* **1997,** *1339*, 14-22.

53. Argos, P.; Pedersen, K.; Marks, M.; Larkins, B., A structural model for maize zein proteins. *Journal of Biological Chemistry* **1982,** *257*, 9984-9990.
54. Garratt, R.; Oliva, G.; Caracelli, I.; Leite, A.; Arruda, P., Studies of the zein-like α-prolamins based on an analysis of amino acid sequences: Implications for their evolution and three-dimensional structure. *Proteins: Structure, Function, and Bioinformatics* **1993,** *15*, 88-99.
55. Wang, Q.; Geil, P.; Padua, G., Role of hydrophilic and hydrophobic interactions in structure development of zein films. *Journal of Polymers and the Environment* **2004,** *12*, 197-202.
56. Feng, Y.; Lee, Y., Surface modification of zein colloidal particles with sodium caseinate to stabilize oil-in-water pickering emulsion. *Food Hydrocolloids* **2016,** *56*, 292-302.
57. Patel, A. R.; Bouwens, E. C.; Velikov, K. P., Sodium caseinate stabilized zein colloidal particles. *Journal of agricultural and food chemistry* **2010,** *58*, 12497-12503.
58. Luo, Y.; Teng, Z.; Wang, T. T.; Wang, Q., Cellular uptake and transport of zein nanoparticles: effects of sodium caseinate. *Journal of agricultural and food chemistry* **2013,** *61*, 7621-7629.
59. Gao, Z.-M.; Yang, X.-Q.; Wu, N.-N.; Wang, L.-J.; Wang, J.-M.; Guo, J.; Yin, S.-W., Protein-based pickering emulsion and oil gel prepared by complexes of zein colloidal particles and stearate. *Journal of agricultural and food chemistry* **2014,** *62*, 2672-2678.
60. Dai, L.; Sun, C.; Wei, Y.; Mao, L.; Gao, Y., Characterization of Pickering emulsion gels stabilized by zein/gum arabic complex colloidal nanoparticles. *Food Hydrocolloids* **2018,** *74*, 239-248.
61. Piriyaprasarth, S.; Juttulapa, M.; Sriamornsak, P., Stability of rice bran oil-in-water emulsions stabilized by pectin–zein complexes: Effect of composition and order of mixing. *Food Hydrocolloids* **2016,** *61*, 589-598.
62. Juttulapa, M.; Piriyaprasarth, S.; Sriamornsak, P. In *Effect of pH on stability of oil-in-water emulsions stabilized by pectin-zein complexes*, Advanced Materials Research, 2013; Trans Tech Publ: 2013; pp 127-130.
63. Wang, L.-J.; Hu, Y.-Q.; Yin, S.-W.; Yang, X.-Q.; Lai, F.-R.; Wang, S.-Q., Fabrication and characterization of antioxidant pickering emulsions stabilized by zein/chitosan complex particles (ZCPs). *Journal of agricultural and food chemistry* **2015,** *63*, 2514-2524.
64. Zou, Y.; Guo, J.; Yin, S.-W.; Wang, J.-M.; Yang, X.-Q., Pickering emulsion gels prepared by hydrogen-bonded zein/tannic acid complex colloidal particles. *Journal of agricultural and food chemistry* **2015,** *63*, 7405-7414.
65. Zhu, Q.; Lu, H.; Zhu, J.; Zhang, M.; Yin, L., Development and characterization of pickering emulsion stabilized by zein/corn fiber gum (CFG) complex colloidal particles. *Food Hydrocolloids* **2019,** *91*, 204-213.
66. Padgett, T.; Han, Y.; Dawson, P., Effect of lauric acid addition on the antimicrobial efficacy and water permeability of corn zein films containing nisin. *Journal of Food Processing and Preservation* **2000,** *24*, 423-432.
67. Lai, H.-M.; Padua, G. W.; Wei, L. S., Properties and microstructure of zein sheets plasticized with palmitic and stearic acids. *Cereal Chemistry* **1997,** *74*, 83-90.
68. Lai, H.-M.; Padua, G. W., Water vapor barrier properties of zein films plasticized with oleic acid. *Cereal Chemistry* **1998,** *75*, 194-199.
69. Tan, Y.; Xu, K.; Liu, C.; Li, Y.; Lu, C.; Wang, P., Fabrication of starch-based nanospheres to stabilize pickering emulsion. *Carbohydrate Polymers* **2012,** *88*, 1358-1363.
70. Kalashnikova, I.; Bizot, H.; Cathala, B.; Capron, I., New Pickering Emulsions Stabilized by Bacterial Cellulose Nanocrystals. *Langmuir* **2011,** *27*, 7471-7479.
71. de Folter, J. W. J.; van Ruijven, M. W. M.; Velikov, K. P., Oil-in-water Pickering

emulsions stabilized by colloidal particles from the water-insoluble protein zein. *Soft Matter* **2012,** *8*, 6807-6815.
72. Xiao, J.; Wang, X. a.; Perez Gonzalez, A. J.; Huang, Q., Kafirin nanoparticles-stabilized Pickering emulsions: Microstructure and rheological behavior. *Food Hydrocolloids* **2016,** *54*, 30-39.
73. Xiao, J.; Li, Y.; Huang, Q., Recent advances on food-grade particles stabilized Pickering emulsions: Fabrication, characterization and research trends. *Trends in Food Science & Technology* **2016,** *55*, 48-60.
74. Joye, I. J.; McClements, D. J., Production of nanoparticles by anti-solvent precipitation for use in food systems. *Trends in Food Science & Technology* **2013,** *34*, 109-123.
75. de Folter, J. W.; van Ruijven, M. W.; Velikov, K. P., Oil-in-water Pickering emulsions stabilized by colloidal particles from the water-insoluble protein zein. *Soft Matter* **2012,** *8*, 6807-6815.
76. Hu, B.; Huang, Q.-r., Biopolymer based nano-delivery systems for enhancing bioavailability of nutraceuticals. *Chinese Journal of Polymer Science* **2013,** *31*, 1190-1203.
77. Xiao, J.; Nian, S.; Huang, Q., Assembly of kafirin/carboxymethyl chitosan nanoparticles to enhance the cellular uptake of curcumin. *Food Hydrocolloids* **2015,** *51*, 166-175.
78. Shah, R. K.; Kim, J.-W.; Weitz, D. A., Monodisperse Stimuli-Responsive Colloidosomes by Self-Assembly of Microgels in Droplets. *Langmuir* **2010,** *26*, 1561-1565.
79. Utada, A.; Lorenceau, E.; Link, D.; Kaplan, P.; Stone, H.; Weitz, D., Monodisperse double emulsions generated from a microcapillary device. *Science* **2005,** *308*, 537-541.
80. Kargar, M.; Spyropoulos, F.; Norton, I. T., The effect of interfacial microstructure on the lipid oxidation stability of oil-in-water emulsions. *Journal of Colloid and Interface Science* **2011,** *357*, 527-533.
81. Kargar, M.; Fayazmanesh, K.; Alavi, M.; Spyropoulos, F.; Norton, I. T., Investigation into the potential ability of Pickering emulsions (food-grade particles) to enhance the oxidative stability of oil-in-water emulsions. *Journal of Colloid and Interface Science* **2012,** *366*, 209-215.
82. Velev, O. D.; Furusawa, K.; Nagayama, K., Assembly of Latex Particles by Using Emulsion Droplets as Templates. 1. Microstructured Hollow Spheres. *Langmuir* **1996,** *12*, 2374-2384.
83. Dinsmore, A. D.; Hsu, M. F.; Nikolaides, M. G.; Marquez, M.; Bausch, A. R.; Weitz, D. A., Colloidosomes: Selectively Permeable Capsules Composed of Colloidal Particles. *Science* **2002,** *298*, 1006-1009.
84. Velev, O. D.; Furusawa, K.; Nagayama, K., Assembly of Latex Particles by Using Emulsion Droplets as Templates. 2. Ball-like and Composite Aggregates. *Langmuir* **1996,** *12*, 2385-2391.
85. Zhou, Z.; Chu, B., Fractal study of polystyrene latex and silica particle aggregates. *Physica A: Statistical Mechanics and its Applications* **1991,** *177*, 93-100.
86. Yow, H. N.; Routh, A. F., Formation of liquid core-polymer shell microcapsules. *Soft Matter* **2006,** *2*, 940-949.
87. Zhao, Y.; Pan, Y.; Nitin, N.; Tikekar, R. V., Enhanced stability of curcumin in colloidosomes stabilized by silica aggregates. *LWT - Food Science and Technology* **2014,** *58*, 667-671.
88. Caruso, F.; Caruso, R. A.; Möhwald, H., Production of Hollow Microspheres from Nanostructured Composite Particles. *Chemistry of Materials* **1999,** *11*, 3309-3314.
89. Rayner, M.; Marku, D.; Eriksson, M.; Sjöö, M.; Dejmek, P.; Wahlgren, M., Biomass-based particles for the formulation of Pickering type emulsions in food and topical applications. *Colloids and Surfaces A: Physicochemical and Engineering Aspects* **2014,**

458, 48-62.
90. Velev, O. D.; Nagayama, K., Assembly of Latex Particles by Using Emulsion Droplets. 3. Reverse (Water in Oil) System. *Langmuir* **1997,** *13*, 1856-1859.
91. Yow, H. N.; Routh, A. F., Release Profiles of Encapsulated Actives from Colloidosomes Sintered for Various Durations. *Langmuir* **2009,** *25*, 159-166.
92. Binks, B. P., Particles as surfactants—similarities and differences. *Current Opinion in Colloid & Interface Science* **2002,** *7*, 21-41.
93. Dickinson, E., *Interfacial particles in food emulsions and foams*. Cambridge University Press: 2006; p 298-327.
94. Morse, A. J.; Tan, S.-Y.; Giakoumatos, E. C.; Webber, G. B.; Armes, S. P.; Ata, S.; Wanless, E. J., Arrested coalescence behaviour of giant Pickering droplets and colloidosomes stabilised by poly(tert-butylaminoethyl methacrylate) latexes. *Soft Matter* **2014,** *10*, 5669-5681.
95. Thompson, K. L.; Chambon, P.; Verber, R.; Armes, S. P., Can Polymersomes Form Colloidosomes? *Journal of the American Chemical Society* **2012,** *134*, 12450-12453.
96. Velev, O.; Furusawa, K.; Nagayama, K., Assembly of latex particles by using emulsion droplets as templates. 1. Microstructured hollow spheres. *Langmuir* **1996,** *12*, 2374-2384.
97. Caruso, F.; Spasova, M.; Susha, A.; Giersig, M.; Caruso, R. A., Magnetic Nanocomposite Particles and Hollow Spheres Constructed by a Sequential Layering Approach. *Chemistry of Materials* **2001,** *13*, 109-116.
98. Frank Caruso, X. S., Rachel A. Caruso, andAndrei Susha, Hollow Titania Spheres from Layered Precursor Deposition on Sacrificial Colloidal Core Particles. *Advanced Materials* **2001,** *13*, 740–744.
99. Caruso, R. A.; Susha, A.; Caruso, F., Multilayered Titania, Silica, and Laponite Nanoparticle Coatings on Polystyrene Colloidal Templates and Resulting Inorganic Hollow Spheres. *Chemistry of Materials* **2001,** *13*, 400-409.
100. Williams, M.; Armes, S. P.; Verstraete, P.; Smets, J., Double Emulsions and Colloidosomes-in-Colloidosomes Using Silica-Based Pickering Emulsifiers. *Langmuir* **2014,** *30*, 2703-2711.
101. Li, J.; Stöver, H. D. H., Pickering Emulsion Templated Layer-by-Layer Assembly for Making Microcapsules. *Langmuir* **2010,** *26*, 15554-15560.
102. Dezhong Yin, a. Q. Z., Changjie Yin, Xingbo Zhao, Hepeng Zhang, Hollow microspheres with covalent-bonded colloidal and polymeric shell by Pickering emulsion polymerization. *Polymers for Advanced Technologies* **2012,** *23*, 273–277.
103. Rossier-Miranda, F. J.; Schroën, K.; Boom, R., Microcapsule production by an hybrid colloidosome-layer-by-layer technique. *Food Hydrocolloids* **2012,** *27*, 119-125.
104. Cayre, O. J.; Noble, P. F.; Paunov, V. N., Fabrication of novel colloidosome microcapsules with gelled aqueous cores. *Journal of Materials Chemistry* **2004,** *14*, 3351-3355.
105. Williams, M.; Armes, S. P.; York, D. W., Clay-based colloidosomes. *Langmuir* **2011,** *28*, 1142-1148.
106. San Miguel, A.; Behrens, S. H., Permeability control in stimulus-responsive colloidosomes. *Soft Matter* **2011,** *7*, 1948-1956.
107. Walsh, A.; Thompson, K.; Armes, S.; York, D., Polyamine-functional sterically stabilized latexes for covalently cross-linkable colloidosomes. *Langmuir* **2010,** *26*, 18039-18048.
108. Liu, H.; Gu, X.; Hu, M.; Hu, Y.; Wang, C., Facile fabrication of nanocomposite microcapsules by combining layer-by-layer self-assembly and Pickering emulsion templating. *Rsc Advances* **2014,** *4*, 16751-16758.
109. Chen, Y.; Wang, C.; Chen, J.; Liu, X.; Tong, Z., Growth of lightly crosslinked

PHEMA brushes and capsule formation using pickering emulsion interface-initiated ATRP. *Journal of Polymer Science Part A: Polymer Chemistry* **2009,** *47*, 1354-1367.
110. Cayre, O. J.; Biggs, S., Hollow microspheres with binary porous membranes from solid-stabilised emulsion templates. *Journal of Materials Chemistry* **2009,** *19*, 2724-2728.
111. Loxley, A.; Vincent, B., Preparation of Poly(methylmethacrylate) Microcapsules with Liquid Cores. *Journal of Colloid and Interface Science* **1998,** *208*, 49-62.
112. Shahidan, N. N.; Liu, R.; Thaiboonrod, S.; Alexander, C.; Shakesheff, K. M.; Saunders, B. R., Hollow Colloidosomes Prepared Using Accelerated Solvent Evaporation. *Langmuir* **2013,** *29*, 13676-13685.
113. McClements, D. J., Theoretical Analysis of Factors Affecting the Formation and Stability of Multilayered Colloidal Dispersions. *Langmuir* **2005,** *21*, 9777-9785.
114. Gough, J. E.; Scotchford, C. A.; Downes, S., Cytotoxicity of glutaraldehyde crosslinked collagen/poly (vinyl alcohol) films is by the mechanism of apoptosis. *Journal of biomedical materials research* **2002,** *61*, 121-130.
115. Berg, H. C., *Random walks in biology*. Princeton University Press: 1993.
116. Horecha, M.; Senkovskyy, V.; Stamm, M.; Kiriy, A., One-Pot Synthesis of Thermoresponsive PNIPAM Hydrogel Microcapsules Designed to Function in Apolar Media. *Macromolecules* **2009,** *42*, 5811-5817.
117. Croll, L. M.; Stöver, H. D. H., Mechanism of Self-Assembly and Rupture of Cross-Linked Microspheres and Microgels at the Oil−Water Interface. *Langmuir* **2003,** *19*, 10077-10080.
118. Kim, J.-W.; Fernández-Nieves, A.; Dan, N.; Utada, A. S.; Marquez, M.; Weitz, D. A., Colloidal assembly route for responsive colloidosomes with tunable permeability. *Nano letters* **2007,** *7*, 2876-2880.
119. Rodriguez, B. E.; Wolfe, M. S.; Fryd, M., Nonuniform Swelling of Alkali Swellable Microgels. *Macromolecules* **1994,** *27*, 6642-6647.
120. San Miguel, A.; Scrimgeour, J.; Curtis, J. E.; Behrens, S. H., Smart colloidosomes with a dissolution trigger. *Soft Matter* **2010,** *6*, 3163-3166.
121. Thompson, K. L.; Williams, M.; Armes, S. P., Colloidosomes: Synthesis, properties and applications. *Journal of Colloid and Interface Science* **2015,** *447*, 217-228.
122. Duan, H.; Wang, D.; Sobal, N. S.; Giersig, M.; Kurth, D. G.; Möhwald, H., Magnetic Colloidosomes Derived from Nanoparticle Interfacial Self-Assembly. *Nano letters* **2005,** *5*, 949-952.
123. Lee, D.; Weitz, D. A., Double emulsion-templated nanoparticle colloidosomes with selective permeability. *Advanced Materials* **2008,** *20*, 3498-3503.
124. Lee, D.; Weitz, D. A., Nonspherical colloidosomes with multiple compartments from double emulsions. *Small* **2009,** *5*, 1932-1935.
125. Rossier-Miranda, F. J.; Schroën, C. G. P. H.; Boom, R. M., Colloidosomes: Versatile microcapsules in perspective. *Colloids and Surfaces A: Physicochemical and Engineering Aspects* **2009,** *343*, 43-49.
126. Shilpi, S.; Jain, A.; Gupta, Y.; Jain, S. K., Colloidosomes: an emerging vesicular system in drug delivery. *Critical Reviews™ in Therapeutic Drug Carrier Systems* **2007,** *24*.
127. Chaikof, E. L., Engineering and material considerations in islet cell transplantation. *Annual review of biomedical engineering* **1999,** *1*, 103-127.
128. Park, J. K.; Chang, H. N., Microencapsulation of microbial cells. *Biotechnology Advances* **2000,** *18*, 303-319.
129. Keen, P. H.; Slater, N. K.; Routh, A. F., Encapsulation of yeast cells in colloidosomes. *Langmuir* **2011,** *28*, 1169-1174.
130. Wang, Z.; van Oers, M.; Rutjes, F. P.; van Hest, J., Polymersome colloidosomes for enzyme catalysis in a biphasic system. *Angewandte Chemie* **2012,** *124*, 10904-10908.
131. Wu, C.; Bai, S.; Ansorge-Schumacher, M. B.; Wang, D., Nanoparticle cages for

enzyme catalysis in organic media. *Advanced Materials* **2011,** *23*, 5694-5699.
132. Giovinazzo, G.; Ingrosso, I.; Paradiso, A.; De Gara, L.; Santino, A., Resveratrol biosynthesis: plant metabolic engineering for nutritional improvement of food. *Plant foods for human nutrition* **2012,** *67*, 191-199.
133. Soleas, G. J.; Diamandis, E. P.; Goldberg, D. M., Resveratrol: a molecule whose time has come? And gone? *Clinical biochemistry* **1997,** *30*, 91-113.
134. Langcake, P.; Pryce, R., The production of resveratrol by Vitis vinifera and other members of the Vitaceae as a response to infection or injury. *Physiological Plant Pathology* **1976,** *9*, 77-86.
135. Gülçin, İ., Antioxidant properties of resveratrol: a structure–activity insight. *Innovative Food Science & Emerging Technologies* **2010,** *11*, 210-218.
136. Alarcon De La Lastra, C.; Villegas, I., Resveratrol as an anti-inflammatory and anti-aging agent: Mechanisms and clinical implications. *Molecular nutrition & food research* **2005,** *49*, 405-430.
137. Das, S.; Das, D. K., Anti-inflammatory responses of resveratrol. *Inflammation & Allergy-Drug Targets (Formerly Current Drug Targets-Inflammation & Allergy)* **2007,** *6*, 168-173.
138. Docherty, J. J.; Fu, M. M. H.; Stiffler, B. S.; Limperos, R. J.; Pokabla, C. M.; DeLucia, A. L., Resveratrol inhibition of herpes simplex virus replication. *Antiviral research* **1999,** *43*, 145-155.
139. Heredia, A.; Davis, C.; Redfield, R., Synergistic inhibition of HIV-1 in activated and resting peripheral blood mononuclear cells, monocyte-derived macrophages, and selected drug-resistant isolates with nucleoside analogues combined with a natural product, resveratrol. *Journal of acquired immune deficiency syndromes (1999)* **2000,** *25*, 246-255.
140. Wang, L.-X.; Heredia, A.; Song, H.; Zhang, Z.; Yu, B.; Davis, C.; Redfield, R., Resveratrol glucuronides as the metabolites of resveratrol in humans: characterization, synthesis, and anti-HIV activity. *Journal of pharmaceutical sciences* **2004,** *93*, 2448-2457.
141. Bastianetto, S.; Ménard, C.; Quirion, R., Neuroprotective action of resveratrol. *Biochimica et Biophysica Acta (BBA)-Molecular Basis of Disease* **2015,** *1852*, 1195-1201.
142. Lopez, M. S.; Dempsey, R. J.; Vemuganti, R., Resveratrol neuroprotection in stroke and traumatic CNS injury. *Neurochemistry international* **2015,** *89*, 75-82.
143. Fonseca-Kelly, Z.; Nassrallah, M.; Uribe, J.; Khan, R. S.; Dine, K.; Dutt, M.; Shindler, K. S., Resveratrol neuroprotection in a chronic mouse model of multiple sclerosis. *Frontiers in neurology* **2012,** *3*, 84.
144. Kopp, P., Resveratrol, a phytoestrogen found in red wine. A possible explanation for the conundrum of the'French paradox'? *European Journal of Endocrinology* **1998,** *138*, 619-620.
145. Frémont, L., Biological effects of resveratrol. *Life sciences* **2000,** *66*, 663-673.
146. Athar, M.; Back, J. H.; Kopelovich, L.; Bickers, D. R.; Kim, A. L., Multiple molecular targets of resveratrol: Anti-carcinogenic mechanisms. *Archives of biochemistry and biophysics* **2009,** *486*, 95-102.
147. Jang, M.; Cai, L.; Udeani, G. O.; Slowing, K. V.; Thomas, C. F.; Beecher, C. W.; Fong, H. H.; Farnsworth, N. R.; Kinghorn, A. D.; Mehta, R. G., Cancer chemopreventive activity of resveratrol, a natural product derived from grapes. *Science* **1997,** *275*, 218-220.
148. Athar, M.; Back, J. H.; Tang, X.; Kim, K. H.; Kopelovich, L.; Bickers, D. R.; Kim, A. L., Resveratrol: a review of preclinical studies for human cancer prevention. *Toxicology and applied pharmacology* **2007,** *224*, 274-283.
149. Schneider, Y.; Vincent, F.; Duranton, B. t.; Badolo, L.; Gossé, F.; Bergmann, C.; Seiler, N.; Raul, F., Anti-proliferative effect of resveratrol, a natural component of grapes and wine, on human colonic cancer cells. *Cancer Letters* **2000,** *158*, 85-91.
150. Vanamala, J.; Reddivari, L.; Radhakrishnan, S.; Tarver, C., Resveratrol suppresses

IGF-1 induced human colon cancer cell proliferation and elevates apoptosis via suppression of IGF-1R/Wnt and activation of p53 signaling pathways. *BMC cancer* **2010,** *10*, 238.
151. Cui, X.; Jin, Y.; Hofseth, A. B.; Pena, E.; Habiger, J.; Chumanevich, A.; Poudyal, D.; Nagarkatti, M.; Nagarkatti, P. S.; Singh, U. P., Resveratrol suppresses colitis and colon cancer associated with colitis. *Cancer prevention research* **2010**, 1940-6207. CAPR-09-0117.
152. Walle, T.; Hsieh, F.; DeLegge, M. H.; Oatis, J. E.; Walle, U. K., High absorption but very low bioavailability of oral resveratrol in humans. *Drug metabolism and disposition* **2004,** *32*, 1377-1382.
153. Amri, A.; Chaumeil, J.; Sfar, S.; Charrueau, C., Administration of resveratrol: what formulation solutions to bioavailability limitations? *Journal of Controlled Release* **2012,** *158*, 182-193.
154. Andlauer, W.; Kolb, J.; Siebert, K.; Fürst, P., Assessment of resveratrol bioavailability in the perfused small intestine of the rat. *Drugs under experimental and clinical research* **2000,** *26*, 47-55.
155. De Santi, C.; Pietrabissa, A.; Spisni, R.; Mosca, F.; Pacifici, G., Sulphation of resveratrol, a natural product present in grapes and wine, in the human liver and duodenum. *Xenobiotica* **2000,** *30*, 609-617.
156. De Santi, C.; Pietrabissa, A.; Mosca, F.; Pacifici, G., Glucuronidation of resveratrol, a natural product present in grape and wine, in the human liver. *Xenobiotica* **2000,** *30*, 1047-1054.
157. Wolter, F.; Akoglu, B.; Clausnitzer, A.; Stein, J. r., Downregulation of the cyclin D1/Cdk4 complex occurs during resveratrol-induced cell cycle arrest in colon cancer cell lines. *The Journal of nutrition* **2001,** *131*, 2197-2203.
158. Wolter, F.; Stein, J. r., Resveratrol enhances the differentiation induced by butyrate in caco-2 colon cancer cells. *The Journal of nutrition* **2002,** *132*, 2082-2086.
159. Ferrandina, G.; Stoler, A.; Fagotti, A.; Fanfani, F.; Sacco, R.; De Pasqua, A.; Mancuso, S.; Scambia, G., p21WAF1/CIP1 protein expression in primary ovarian cancer. *International journal of oncology* **2000,** *17*, 1231-1236.
160. Tessitore, L.; Davit, A.; Sarotto, I.; Caderni, G., Resveratrol depresses the growth of colorectal aberrant crypt foci by affecting bax and p21 CIP expression. *Carcinogenesis* **2000,** *21*, 1619-1622.
161. Firestein, R.; Blander, G.; Michan, S.; Oberdoerffer, P.; Ogino, S.; Campbell, J.; Bhimavarapu, A.; Luikenhuis, S.; de Cabo, R.; Fuchs, C., The SIRT1 deacetylase suppresses intestinal tumorigenesis and colon cancer growth. *PloS one* **2008,** *3*, e2020.
162. Park, S.-J.; Ahmad, F.; Philp, A.; Baar, K.; Williams, T.; Luo, H.; Ke, H.; Rehmann, H.; Taussig, R.; Brown, A. L., Resveratrol ameliorates aging-related metabolic phenotypes by inhibiting cAMP phosphodiesterases. *Cell* **2012,** *148*, 421-433.
163. Juan, M. E.; Alfaras, I.; Planas, J. M., Colorectal cancer chemoprevention by trans-resveratrol. *Pharmacological Research* **2012,** *65*, 584-591.
164. Hague, A.; Manning, A.; Hanlon, K.; Hart, D.; Paraskeva, C.; Huschtscha, L., Sodium butyrate induces apoptosis in human colonic tumour cell lines in a p53-independent pathway: implications for the possible role of dietary fibre in the prevention of large-bowel cancer. *International journal of cancer* **1993,** *55*, 498-505.
165. Orchel, A.; Dzierżewicz, Z.; Parfiniewicz, B.; Wilczok, T., Butyrate-induced differentiation of colon cancer cells is PKC and JNK dependent. *Digestive diseases and sciences* **2005,** *50*, 490-498.
166. Lupton, J. R., Microbial degradation products influence colon cancer risk: the butyrate controversy. *The Journal of nutrition* **2004,** *134*, 479-482.
167. Letai, A. G., Diagnosing and exploiting cancer's addiction to blocks in apoptosis. *Nature Reviews Cancer* **2008,** *8*, 121.

168. Kroemer, G.; Galluzzi, L.; Brenner, C., Mitochondrial membrane permeabilization in cell death. *Physiological reviews* **2007,** *87*, 99-163.
169. Degterev, A.; Yuan, J., Expansion and evolution of cell death programmes. *Nature reviews Molecular cell biology* **2008,** *9*, 378.
170. Tinhofer, I.; Bernhard, D.; Senfter, M.; Anether, G.; Loeffler, M.; Kroemer, G.; Kofler, R.; Csordas, A.; Greil, R., Resveratrol, a tumor-suppressive compound from grapes, induces apoptosis via a novel mitochondrial pathway controlled by Bcl-2. *The FASEB Journal* **2001,** *15*, 1613-1615.
171. Park, J.-W.; Choi, Y.-J.; Suh, S.-I.; Baek, W.-K.; Suh, M.-H.; Jin, I.-N.; Min, D. S.; Woo, J.-H.; Chang, J.-S.; Passaniti, A., Bcl-2 overexpression attenuates resveratrol-induced apoptosis in U937 cells by inhibition of caspase-3 activity. *Carcinogenesis* **2001,** *22*, 1633-1639.
172. Opipari, A. W.; Tan, L.; Boitano, A. E.; Sorenson, D. R.; Aurora, A.; Liu, J. R., Resveratrol-induced autophagocytosis in ovarian cancer cells. *Cancer research* **2004,** *64*, 696-703.
173. Kroemer, G.; Jäättelä, M., Lysosomes and autophagy in cell death control. *Nature Reviews Cancer* **2005,** *5*, 886.
174. Danial, N. N.; Korsmeyer, S. J., Cell death: critical control points. *Cell* **2004,** *116*, 205-219.
175. Yang, J.; Liu, X.; Bhalla, K.; Kim, C. N.; Ibrado, A. M.; Cai, J.; Peng, T.-I.; Jones, D. P.; Wang, X., Prevention of apoptosis by Bcl-2: release of cytochrome c from mitochondria blocked. *Science* **1997,** *275*, 1129-1132.
176. Woo, K. J.; Lee, T. J.; Lee, S. H.; Lee, J.-M.; Seo, J.-H.; Jeong, Y.-J.; Park, J.-W.; Kwon, T. K., Elevated gadd153/chop expression during resveratrol-induced apoptosis in human colon cancer cells. *Biochemical pharmacology* **2007,** *73*, 68-76.
177. Um, H. J.; Bae, J. H.; Park, J.-W.; Suh, H.; Jeong, N. Y.; Yoo, Y. H.; Kwon, T. K., Differential effects of resveratrol and novel resveratrol derivative, HS-1793, on endoplasmic reticulum stress-mediated apoptosis and Akt inactivation. *International journal of oncology* **2010,** *36*, 1007-1013.
178. Park, J.-W.; Woo, K. J.; Lee, J.-T.; Lim, J. H.; Lee, T.-J.; Kim, S. H.; Choi, Y. H.; Kwon, T. K., Resveratrol induces pro-apoptotic endoplasmic reticulum stress in human colon cancer cells. *Oncology reports* **2007,** *18*, 1269-1273.
179. Oyadomari, S.; Mori, M., Roles of CHOP/GADD153 in endoplasmic reticulum stress. *Cell death and differentiation* **2004,** *11*, 381.
180. Trincheri, N. F.; Nicotra, G.; Follo, C.; Castino, R.; Isidoro, C., Resveratrol induces cell death in colorectal cancer cells by a novel pathway involving lysosomal cathepsin D. *Carcinogenesis* **2006,** *28*, 922-931.
181. Mahyar-Roemer, M.; Köhler, H.; Roemer, K., Role of Bax in resveratrol-induced apoptosis of colorectal carcinoma cells. *BMC cancer* **2002,** *2*, 27.
182. Miki, H.; Uehara, N.; Kimura, A.; Sasaki, T.; Yuri, T.; Yoshizawa, K.; Tsubura, A., Resveratrol induces apoptosis via ROS-triggered autophagy in human colon cancer cells. *International journal of oncology* **2012,** *40*, 1020-1028.
183. Juan, M. E.; Wenzel, U.; Daniel, H.; Planas, J. M., Resveratrol Induces Apoptosis through ROS-Dependent Mitochondria Pathway in HT-29 Human Colorectal Carcinoma Cells. *Journal of agricultural and food chemistry* **2008,** *56*, 4813-4818.
184. Siddiqui, I. A.; Sanna, V.; Ahmad, N.; Sechi, M.; Mukhtar, H., Resveratrol nanoformulation for cancer prevention and therapy. *Ann. NY Acad. Sci* **2015,** *1348*, 20-31.
185. Gosslau, A.; Chen, M.; Ho, C.-T.; Chen, K., A methoxy derivative of resveratrol analogue selectively induced activation of the mitochondrial apoptotic pathway in transformed fibroblasts. *British journal of cancer* **2005,** *92*, 513.
186. Jung, C. M.; Heinze, T. M.; Schnackenberg, L. K.; Mullis, L. B.; Elkins, S. A.;

Elkins, C. A.; Steele, R. S.; Sutherland, J. B., Interaction of dietary resveratrol with animal-associated bacteria. *FEMS microbiology letters* **2009,** *297*, 266-273.
187. Taguri, T.; Tanaka, T.; Kouno, I., Antibacterial spectrum of plant polyphenols and extracts depending upon hydroxyphenyl structure. *Biological and Pharmaceutical Bulletin* **2006,** *29*, 2226-2235.
188. Wang, W.-B.; Lai, H.-C.; Hsueh, P.-R.; Chiou, R. Y.-Y.; Lin, S.-B.; Liaw, S.-J., Inhibition of swarming and virulence factor expression in Proteus mirabilis by resveratrol. *Journal of medical microbiology* **2006,** *55*, 1313-1321.
189. Qiao, Y.; Sun, J.; Xia, S.; Tang, X.; Shi, Y.; Le, G., Effects of resveratrol on gut microbiota and fat storage in a mouse model with high-fat-induced obesity. *Food & function* **2014,** *5*, 1241-1249.
190. Turnbaugh, P. J.; Ley, R. E.; Mahowald, M. A.; Magrini, V.; Mardis, E. R.; Gordon, J. I., An obesity-associated gut microbiome with increased capacity for energy harvest. *Nature* **2006,** *444*, 1027.
191. Sung, M. M.; Kim, T. T.; Denou, E.; Soltys, C.-L. M.; Hamza, S. M.; Byrne, N. J.; Masson, G.; Park, H.; Wishart, D. S.; Madsen, K. L., Improved glucose homeostasis in obese mice treated with resveratrol is associated with alterations in the gut microbiome. *Diabetes* **2017,** *66*, 418-425.
192. Etxeberria, U.; Arias, N.; Boqué, N.; Macarulla, M.; Portillo, M.; Martínez, J.; Milagro, F., Reshaping faecal gut microbiota composition by the intake of trans-resveratrol and quercetin in high-fat sucrose diet-fed rats. *The Journal of nutritional biochemistry* **2015,** *26*, 651-660.
193. Neyrinck, A. M.; Possemiers, S.; Verstraete, W.; De Backer, F.; Cani, P. D.; Delzenne, N. M., Dietary modulation of clostridial cluster XIVa gut bacteria (Roseburia spp.) by chitin–glucan fiber improves host metabolic alterations induced by high-fat diet in mice. *The Journal of nutritional biochemistry* **2012,** *23*, 51-59.
194. Gao, Z.; Yin, J.; Zhang, J.; Ward, R. E.; Martin, R. J.; Lefevre, M.; Cefalu, W. T.; Ye, J., Butyrate improves insulin sensitivity and increases energy expenditure in mice. *Diabetes* **2009,** *58*, 1509-1517.
195. Larrosa, M.; Yañéz-Gascón, M. a. J.; Selma, M. a. V.; Gonzalez-Sarrias, A.; Toti, S.; Cerón, J. J. n.; Tomas-Barberan, F.; Dolara, P.; Espín, J. C., Effect of a low dose of dietary resveratrol on colon microbiota, inflammation and tissue damage in a DSS-induced colitis rat model. *Journal of agricultural and food chemistry* **2009,** *57*, 2211-2220.
196. Chassaing, B.; Aitken, J. D.; Malleshappa, M.; Vijay-Kumar, M., Dextran sulfate sodium (DSS)-induced colitis in mice. *Current protocols in immunology* **2014,** *104*, 15.25. 1-15.25. 14.
197. Taurog, J. D.; Richardson, J. A.; Croft, J.; Simmons, W. A.; Zhou, M.; Fernández-Sueiro, J. L.; Balish, E.; Hammer, R. E., The germfree state prevents development of gut and joint inflammatory disease in HLA-B27 transgenic rats. *Journal of Experimental Medicine* **1994,** *180*, 2359-2364.
198. Rath, H. C.; Herfarth, H. H.; Ikeda, J. S.; Grenther, W. B.; Hamm, T. E.; Balish, E.; Taurog, J. D.; Hammer, R. E.; Wilson, K. H.; Sartor, R. B., Normal luminal bacteria, especially Bacteroides species, mediate chronic colitis, gastritis, and arthritis in HLA-B27/human beta2 microglobulin transgenic rats. *The Journal of clinical investigation* **1996,** *98*, 945-953.
199. Borody, T. J.; Warren, E. F.; Leis, S.; Surace, R.; Ashman, O., Treatment of ulcerative colitis using fecal bacteriotherapy. *Journal of clinical gastroenterology* **2003,** *37*, 42-47.
200. Noor, S. O.; Ridgway, K.; Scovell, L.; Kemsley, E. K.; Lund, E. K.; Jamieson, C.; Johnson, I. T.; Narbad, A., Ulcerative colitis and irritable bowel patients exhibit distinct abnormalities of the gut microbiota. *BMC gastroenterology* **2010,** *10*, 134.

201. Jadamus, A.; Vahjen, W.; Schäfer, K.; Simon, O., Influence of the probiotic strain Bacillus cereus var. toyoi on the development of enterobacterial growth and on selected parameters of bacterial metabolism in digesta samples of piglets. *Journal of Animal Physiology and Animal Nutrition* **2002,** *86*, 42-54.
202. Chen, M.-l.; Yi, L.; Zhang, Y.; Zhou, X.; Ran, L.; Yang, J.; Zhu, J.-d.; Zhang, Q.-y.; Mi, M.-t., Resveratrol attenuates trimethylamine-N-oxide (TMAO)-induced atherosclerosis by regulating TMAO synthesis and bile acid metabolism via remodeling of the gut microbiota. *MBio* **2016,** *7*, e02210-15.
203. Jones, M. L.; Tomaro-Duchesneau, C.; Prakash, S., The gut microbiome, probiotics, bile acids axis, and human health. *Trends in microbiology* **2014,** *22*, 306-308.
204. Degirolamo, C.; Rainaldi, S.; Bovenga, F.; Murzilli, S.; Moschetta, A., Microbiota modification with probiotics induces hepatic bile acid synthesis via downregulation of the Fxr-Fgf15 axis in mice. *Cell reports* **2014,** *7*, 12-18.
205. Queipo-Ortuño, M. I.; Boto-Ordóñez, M.; Murri, M.; Gomez-Zumaquero, J. M.; Clemente-Postigo, M.; Estruch, R.; Cardona Diaz, F.; Andres-Lacueva, C.; Tinahones, F. J., Influence of red wine polyphenols and ethanol on the gut microbiota ecology and biochemical biomarkers. *The American journal of clinical nutrition* **2012,** *95*, 1323-1334.
206. Walle, T., Bioavailability of resveratrol. *Annals of the new York Academy of Sciences* **2011,** *1215*, 9-15.
207. Ruotolo, R.; Calani, L.; Fietta, E.; Brighenti, F.; Crozier, A.; Meda, C.; Maggi, A.; Ottonello, S.; Del Rio, D., Anti-estrogenic activity of a human resveratrol metabolite. *Nutrition, Metabolism and Cardiovascular Diseases* **2013,** *23*, 1086-1092.
208. Boocock, D. J.; Faust, G. E.; Patel, K. R.; Schinas, A. M.; Brown, V. A.; Ducharme, M. P.; Booth, T. D.; Crowell, J. A.; Perloff, M.; Gescher, A. J., Phase I dose escalation pharmacokinetic study in healthy volunteers of resveratrol, a potential cancer chemopreventive agent. *Cancer Epidemiology and Prevention Biomarkers* **2007,** *16*, 1246-1252.
209. Boocock, D. J.; Patel, K. R.; Faust, G. E.; Normolle, D. P.; Marczylo, T. H.; Crowell, J. A.; Brenner, D. E.; Booth, T. D.; Gescher, A.; Steward, W. P., Quantitation of trans-resveratrol and detection of its metabolites in human plasma and urine by high performance liquid chromatography. *Journal of Chromatography B* **2007,** *848*, 182-187.
210. Burkon, A.; Somoza, V., Quantification of free and protein-bound trans-resveratrol metabolites and identification of trans-resveratrol-C/O-conjugated diglucuronides–Two novel resveratrol metabolites in human plasma. *Molecular nutrition & food research* **2008,** *52*, 549-557.
211. Meng, X.; Maliakal, P.; Lu, H.; Lee, M.-J.; Yang, C. S., Urinary and plasma levels of resveratrol and quercetin in humans, mice, and rats after ingestion of pure compounds and grape juice. *Journal of agricultural and food chemistry* **2004,** *52*, 935-942.
212. Van Duynhoven, J.; Vaughan, E. E.; Jacobs, D. M.; Kemperman, R. A.; Van Velzen, E. J.; Gross, G.; Roger, L. C.; Possemiers, S.; Smilde, A. K.; Doré, J., Metabolic fate of polyphenols in the human superorganism. *Proceedings of the National Academy of Sciences* **2011,** *108*, 4531-4538.
213. Velderrain-Rodríguez, G.; Palafox-Carlos, H.; Wall-Medrano, A.; Ayala-Zavala, J.; Chen, C. O.; Robles-Sánchez, M.; Astiazaran-García, H.; Alvarez-Parrilla, E.; González-Aguilar, G., Phenolic compounds: their journey after intake. *Food & function* **2014,** *5*, 189-197.
214. Rechner, A. R.; Smith, M. A.; Kuhnle, G.; Gibson, G. R.; Debnam, E. S.; Srai, S. K. S.; Moore, K. P.; Rice-Evans, C. A., Colonic metabolism of dietary polyphenols: influence of structure on microbial fermentation products. *Free Radical Biology and Medicine* **2004,** *36*, 212-225.
215. Bode, L. M.; Bunzel, D.; Huch, M.; Cho, G.-S.; Ruhland, D.; Bunzel, M.; Bub, A.;

Franz, C. M.; Kulling, S. E., In vivo and in vitro metabolism of trans-resveratrol by human gut microbiota. *The American journal of clinical nutrition* **2013,** *97*, 295-309.
216. Gakh, A. A.; Anisimova, N. Y.; Kiselevsky, M. V.; Sadovnikov, S. V.; Stankov, I. N.; Yudin, M. V.; Rufanov, K. A.; Krasavin, M. Y.; Sosnov, A. V., Dihydro-resveratrol—a potent dietary polyphenol. *Bioorganic & medicinal chemistry letters* **2010,** *20*, 6149-6151.
217. Cichewicz, R. H.; Kouzi, S. A., Biotransformation of resveratrol to piceid by Bacillus cereus. *Journal of natural products* **1998,** *61*, 1313-1314.
218. Barroso, E.; Sánchez-Patán, F.; Martín-Alvarez, P. J.; Bartolomé, B. a.; Moreno-Arribas, M. V.; Peláez, C.; Requena, T.; Van de Wiele, T.; Martínez-Cuesta, M. C., Lactobacillus plantarum IFPL935 favors the initial metabolism of red wine polyphenols when added to a colonic microbiota. *Journal of agricultural and food chemistry* **2013,** *61*, 10163-10172.
219. Gianazza, E.; Viglienghi, V.; Righetti, P. G.; Salamini, F.; Soave, C., Amino acid composition of zein molecular components. *Phytochemistry* **1977,** *16*, 315-317.
220. Podaralla, S.; Perumal, O., Influence of Formulation Factors on the Preparation of Zein Nanoparticles. *AAPS PharmSciTech* **2012,** *13*, 919-927.
221. Davidov-Pardo, G.; McClements, D. J., Resveratrol encapsulation: designing delivery systems to overcome solubility, stability and bioavailability issues. *Trends in food science & technology* **2014,** *38*, 88-103.
222. Szkudelska, K.; Szkudelski, T., Resveratrol, obesity and diabetes. *European journal of pharmacology* **2010,** *635*, 1-8.
223. Liazid, A.; Palma, M.; Brigui, J.; Barroso, C. G., Investigation on phenolic compounds stability during microwave-assisted extraction. *Journal of Chromatography A* **2007,** *1140*, 29-34.
224. Zupančič, Š.; Lavrič, Z.; Kristl, J., Stability and solubility of trans-resveratrol are strongly influenced by pH and temperature. *European Journal of Pharmaceutics and Biopharmaceutics* **2015,** *93*, 196-204.
225. Trela, B. C.; Waterhouse, A. L., Resveratrol: isomeric molar absorptivities and stability. *Journal of agricultural and food chemistry* **1996,** *44*, 1253-1257.
226. Pinto, M. d. C.; García-Barrado, J. A.; Macías, P., Oxidation of resveratrol catalyzed by soybean lipoxygenase. *Journal of agricultural and food chemistry* **2003,** *51*, 1653-1657.
227. Hung, C.-F.; Chen, J.-K.; Liao, M.-H.; Lo, H.-M.; Fang, J.-Y., Development and evaluation of emulsion-liposome blends for resveratrol delivery. *Journal of nanoscience and nanotechnology* **2006,** *6*, 2950-2958.
228. NCBI, PubChem Substance Database; SID 6374. In 2014.
229. Sessa, M.; Tsao, R.; Liu, R.; Ferrari, G.; Donsì, F., Evaluation of the Stability and Antioxidant Activity of Nanoencapsulated Resveratrol during in Vitro Digestion. *Journal of agricultural and food chemistry* **2011,** *59*, 12352-12360.
230. Xu, H.; Jiang, Q.; Reddy, N.; Yang, Y., Hollow nanoparticles from zein for potential medical applications. *Journal of Materials Chemistry* **2011,** *21*, 18227-18235.
231. Radford, S. J.; Dickinson, E., Depletion flocculation of caseinate-stabilised emulsions: what is the optimum size of the non-adsorbed protein nano-particles? *Colloids and Surfaces A: Physicochemical and Engineering Aspects* **2004,** *238*, 71-81.
232. Boda, A.; Joshi, J. M.; Ali, S. M.; Shenoy, K. T.; Ghosh, S. K., Density functional theoretical study on the preferential selectivity of macrocyclic dicyclohexano-18-crown-6 for Sr^{+2} ion over Th^{+4} ion during extraction from an aqueous phase to organic phases with different dielectric constants. *Journal of Molecular Modeling* **2013,** *19*, 5277-5291.
233. Harraz, F. A.; Ismail, A. A.; Bouzid, H.; Al-Sayari, S. A.; Al-Hajry, A.; Al-Assiri, M. S., A capacitive chemical sensor based on porous silicon for detection of polar and non-polar organic solvents. *Applied Surface Science* **2014,** *307*, 704-711.

234. Brazier, D. W.; Freeman, G. R., The effects of pressure on the density, dielectric constant, and viscosity of several hydrocarbons and other organic liquids. *Canadian Journal of Chemistry* **1969,** *47*, 893-899.
235. Tatikolov, A. S.; Costa, S. M. B., Photophysical and aggregation properties of a long-chain squarylium indocyanine dye. *Journal of Photochemistry and Photobiology A: Chemistry* **2001,** *140*, 147-156.
236. Lide, D. R., *CRC Handbook of Chemistry and Physics*. 85 th ed.; CRC Press, Boca Raton, FL: 2004.
237. Sekirov, I.; Russell, S. L.; Antunes, L. C. M.; Finlay, B. B., Gut microbiota in health and disease. *Physiological reviews* **2010,** *90*, 859-904.
238. Ley, R. E.; Peterson, D. A.; Gordon, J. I., Ecological and evolutionary forces shaping microbial diversity in the human intestine. *Cell* **2006,** *124*, 837-848.
239. Whitman, W. B.; Coleman, D. C.; Wiebe, W. J., Prokaryotes: the unseen majority. *Proceedings of the National Academy of Sciences* **1998,** *95*, 6578-6583.
240. Mason K.L., H. G. B., Noverr M.C., Kao J.Y. , Overview of gut immunology. In *GI Microbiota and Regulation of the Immune System* Huffnagle G.B., N. M. C., Ed. Springer, New York: Advances in Experimental Medicine and Biology, 2008; Vol. 635.
241. Sommer, F.; Bäckhed, F., The gut microbiota—masters of host development and physiology. *Nature Reviews Microbiology* **2013,** *11*, 227.
242. Rhee, S. H.; Pothoulakis, C.; Mayer, E. A., Principles and clinical implications of the brain–gut–enteric microbiota axis. *Nature reviews Gastroenterology & hepatology* **2009,** *6*, 306.
243. Lutgendorff, F.; Akkermans, L.; Soderholm, J. D., The role of microbiota and probiotics in stress-induced gastrointestinal damage. *Current molecular medicine* **2008,** *8*, 282-298.
244. Stappenbeck, T. S.; Hooper, L. V.; Gordon, J. I., Developmental regulation of intestinal angiogenesis by indigenous microbes via Paneth cells. *Proceedings of the National Academy of Sciences* **2002,** *99*, 15451-15455.
245. Lan, Y.; Verstegen, M.; Tamminga, S.; Williams, B., The role of the commensal gut microbial community in broiler chickens. *World's Poultry Science Journal* **2005,** *61*, 95-104.
246. Genovese, K.; Anderson, R.; Harvey, R.; Callaway, T.; Poole, T.; Edrington, T.; Fedorka-Cray, P.; Nisbet, D., Competitive exclusion of Salmonella from the gut of neonatal and weaned pigs. *Journal of food protection* **2003,** *66*, 1353-1359.
247. Wagner, C. L.; Taylor, S. N.; Johnson, D., Host factors in amniotic fluid and breast milk that contribute to gut maturation. *Clinical reviews in allergy & immunology* **2008,** *34*, 191-204.
248. Ley, R. E.; Turnbaugh, P. J.; Klein, S.; Gordon, J. I., Microbial ecology: human gut microbes associated with obesity. *Nature* **2006,** *444*, 1022.
249. Qin, J.; Li, Y.; Cai, Z.; Li, S.; Zhu, J.; Zhang, F.; Liang, S.; Zhang, W.; Guan, Y.; Shen, D., A metagenome-wide association study of gut microbiota in type 2 diabetes. *Nature* **2012,** *490*, 55.
250. Mueller, N. T.; Bakacs, E.; Combellick, J.; Grigoryan, Z.; Dominguez-Bello, M. G., The infant microbiome development: mom matters. *Trends in molecular medicine* **2015,** *21*, 109-117.
251. Benjamin, J. L.; Hedin, C. R.; Koutsoumpas, A.; Ng, S. C.; McCarthy, N. E.; Prescott, N. J.; Pessoa-Lopes, P.; Mathew, C. G.; Sanderson, J.; Hart, A. L., Smokers with active Crohn's disease have a clinically relevant dysbiosis of the gastrointestinal microbiota. *Inflammatory bowel diseases* **2011,** *18*, 1092-1100.
252. Beamish, L. A.; Osornio-Vargas, A. R.; Wine, E., Air pollution: An environmental factor contributing to intestinal disease. *Journal of Crohn's and Colitis* **2011,** *5*, 279-286.

253. Voigt, R. M.; Forsyth, C. B.; Green, S. J.; Mutlu, E.; Engen, P.; Vitaterna, M. H.; Turek, F. W.; Keshavarzian, A., Circadian disorganization alters intestinal microbiota. *PloS one* **2014,** *9*, e97500.
254. De Filippo, C.; Cavalieri, D.; Di Paola, M.; Ramazzotti, M.; Poullet, J. B.; Massart, S.; Collini, S.; Pieraccini, G.; Lionetti, P., Impact of diet in shaping gut microbiota revealed by a comparative study in children from Europe and rural Africa. *Proceedings of the National Academy of Sciences* **2010,** *107*, 14691-14696.
255. McAllan, L.; Skuse, P.; Cotter, P. D.; O'Connor, P.; Cryan, J. F.; Ross, R. P.; Fitzgerald, G.; Roche, H. M.; Nilaweera, K. N., Protein quality and the protein to carbohydrate ratio within a high fat diet influences energy balance and the gut microbiota in C57BL/6J mice. *PloS one* **2014,** *9*, e88904.
256. Beaumont, M.; Portune, K. J.; Steuer, N.; Lan, A.; Cerrudo, V.; Audebert, M.; Dumont, F.; Mancano, G.; Khodorova, N.; Andriamihaja, M., Quantity and source of dietary protein influence metabolite production by gut microbiota and rectal mucosa gene expression: a randomized, parallel, double-blind trial in overweight humans. *The American journal of clinical nutrition* **2017,** *106*, 1005-1019.
257. Cani, P. D.; Neyrinck, A. M.; Fava, F.; Knauf, C.; Burcelin, R. G.; Tuohy, K. M.; Gibson, G.; Delzenne, N. M., Selective increases of bifidobacteria in gut microflora improve high-fat-diet-induced diabetes in mice through a mechanism associated with endotoxaemia. *Diabetologia* **2007,** *50*, 2374-2383.
258. Cardona, F.; Andrés-Lacueva, C.; Tulipani, S.; Tinahones, F. J.; Queipo-Ortuño, M. I., Benefits of polyphenols on gut microbiota and implications in human health. *The Journal of nutritional biochemistry* **2013,** *24*, 1415-1422.
259. Stoupi, S.; Williamson, G.; Drynan, J. W.; Barron, D.; Clifford, M. N., A comparison of the in vitro biotransformation of (–)-epicatechin and procyanidin B2 by human faecal microbiota. *Molecular nutrition & food research* **2010,** *54*, 747-759.
260. Lee, H. C.; Jenner, A. M.; Low, C. S.; Lee, Y. K., Effect of tea phenolics and their aromatic fecal bacterial metabolites on intestinal microbiota. *Research in microbiology* **2006,** *157*, 876-884.
261. Hervert-Hernández, D.; Pintado, C.; Rotger, R.; Goñi, I., Stimulatory role of grape pomace polyphenols on Lactobacillus acidophilus growth. *International journal of food microbiology* **2009,** *136*, 119-122.
262. Molly, K.; Woestyne, M. V.; Smet, I. D.; Verstraete, W., Validation of the simulator of the human intestinal microbial ecosystem (SHIME) reactor using microorganism-associated activities. *Microbial Ecology in Health and Disease* **1994,** *7*, 191-200.
263. De Boever, P.; Deplancke, B.; Verstraete, W., Fermentation by gut microbiota cultured in a simulator of the human intestinal microbial ecosystem is improved by supplementing a soygerm powder. *The Journal of nutrition* **2000,** *130*, 2599-2606.
264. Grootaert, C.; Van den Abbeele, P.; Marzorati, M.; Broekaert, W. F.; Courtin, C. M.; Delcour, J. A.; Verstraete, W.; Van de Wiele, T., Comparison of prebiotic effects of arabinoxylan oligosaccharides and inulin in a simulator of the human intestinal microbial ecosystem. *FEMS microbiology ecology* **2009,** *69*, 231-242.
265. Naylor, T.; Connolly, P.; Martini, L.; Elder, D.; Minekus, M.; Havenaar, R.; Zeijdner, E., Use of a gastro-intestinal model and Gastroplus™ for the prediction of in vivo performance. *Journal of Applied Therapeutic Research* **2006,** *6*, 15.
266. Ribnicky, D. M.; Roopchand, D. E.; Oren, A.; Grace, M.; Poulev, A.; Lila, M. A.; Havenaar, R.; Raskin, I., Effects of a high fat meal matrix and protein complexation on the bioaccessibility of blueberry anthocyanins using the TNO gastrointestinal model (TIM-1). *Food chemistry* **2014,** *142*, 349-357.
267. Verwei, M.; Minekus, M.; Zeijdner, E.; Schilderink, R.; Havenaar, R., Evaluation

of two dynamic in vitro models simulating fasted and fed state conditions in the upper gastrointestinal tract (TIM-1 and tiny-TIM) for investigating the bioaccessibility of pharmaceutical compounds from oral dosage forms. *International journal of pharmaceutics* **2016,** *498*, 178-186.
268. Lu, M.; Ho, C.-T.; Huang, Q., Improving quercetin dissolution and bioaccessibility with reduced crystallite sizes through media milling technique. *Journal of Functional Foods* **2017,** *37*, 138-146.
269. Minekus, M., The TNO gastro-intestinal model (TIM). In *The impact of food bioactives on health*, Springer: 2015; pp 37-46.
270. Fang, J.-Y.; Yu, S.-Y.; Wu, P.-C.; Huang, Y.-B.; Tsai, Y.-H., In vitro skin permeation of estradiol from various proniosome formulations. *International Journal of Pharmaceutics* **2001,** *215*, 91-99.
271. Liebenberg, W.; Engelbrecht, E.; Wessels, A.; Devarakonda, B.; Yang, W.; De Villiers, M. M., A comparative study of the release of active ingredients from semisolid cosmeceuticals measured with Franz, enhancer or flow-through cell diffusion apparatus. *Journal of Food and Drug Analysis* **2004,** *12*, 19-28.
272. Ting, Y.; Jiang, Y.; Ho, C.-T.; Huang, Q., Common delivery systems for enhancing in vivo bioavailability and biological efficacy of nutraceuticals. *Journal of Functional Foods* **2014,** *7*, 112-128.
273. Liu, L.; Fishman, M. L.; Kost, J.; Hicks, K. B., Pectin-based systems for colon-specific drug delivery via oral route. *biomaterials* **2003,** *24*, 3333-3343.
274. Lu, X.; Zhu, J.; Pan, Y.; Huang, Q., Assessment of dynamic bioaccessibility of curcumin encapsulated in milled starch particle stabilized Pickering emulsions using TNO's gastrointestinal model. *Food & function* **2019,** *10*, 2583-2594.
275. Wei, Z.; Zhu, J.; Cheng, Y.; Huang, Q., Ovotransferrin fibril–stabilized Pickering emulsions improve protection and bioaccessibility of curcumin. *Food Research International* **2019,** *125*, 108602.
276. Baert, B.; Boonen, J.; Burvenich, C.; Roche, N.; Stillaert, F.; Blondeel, P.; Van Bocxlaer, J.; De Spiegeleer, B., A new discriminative criterion for the development of Franz diffusion tests for transdermal pharmaceuticals. *Journal of Pharmacy and Pharmaceutical Sciences* **2010,** *13*, 218-230.
277. Pineau, A.; Guillard, O.; Fauconneau, B.; Favreau, F.; Marty, M.-H.; Gaudin, A.; Vincent, C. M.; Marrauld, A.; Marty, J.-P., In vitro study of percutaneous absorption of aluminum from antiperspirants through human skin in the Franz™ diffusion cell. *Journal of inorganic biochemistry* **2012,** *110*, 21-26.
278. Leveque, N.; Makki, S.; Hadgraft, J.; Humbert, P., Comparison of Franz cells and microdialysis for assessing salicylic acid penetration through human skin. *International Journal of Pharmaceutics* **2004,** *269*, 323-328.
279. Kaddar, N.; Harthé, C.; Déchaud, H.; Mappus, E.; Pugeat, M., Cutaneous penetration of bisphenol A in pig skin. *Journal of Toxicology and Environmental Health, Part A* **2008,** *71*, 471-473.
280. Sonavane, G.; Tomoda, K.; Sano, A.; Ohshima, H.; Terada, H.; Makino, K., In vitro permeation of gold nanoparticles through rat skin and rat intestine: effect of particle size. *Colloids and Surfaces B: Biointerfaces* **2008,** *65*, 1-10.
281. Martin, B.; Watts, O.; Shroot, B.; Jamoulle, J., A new diffusion cell—an automated method for measuring the pharmaceutical availability of topical dosage forms. *International Journal of Pharmaceutics* **1989,** *49*, 63-68.
282. Ng, S.-F.; Rouse, J. J.; Sanderson, F. D.; Meidan, V.; Eccleston, G. M., Validation of a static Franz diffusion cell system for in vitro permeation studies. *Aaps Pharmscitech* **2010,** *11*, 1432-1441.
283. Helander, H. F.; Fändriks, L., Surface area of the digestive tract–revisited.

Scandinavian journal of gastroenterology **2014,** *49*, 681-689.
284. Caruso, F.; Shi, X.; Caruso, R. A.; Susha, A., Hollow titania spheres from layered precursor deposition on sacrificial colloidal core particles. *Advanced Materials* **2001,** *13*, 740-744.
285. Yin, D.; Zhang, Q.; Yin, C.; Zhao, X.; Zhang, H., Hollow microspheres with covalent-bonded colloidal and polymeric shell by Pickering emulsion polymerization. *Polymers for Advanced Technologies* **2012,** *23*, 273-277.
286. Xiao, J.; Wang, X.; Perez Gonzalez, A. J.; Huang, Q., Kafirin nanoparticles-stabilized Pickering emulsions: Microstructure and rheological behavior. *Food Hydrocolloids* **2016,** *54, Part A*, 30-39.
287. Tsm, T.-H.; Westly, J.; Lee, T.-F.; Chen, C.-F., Identification and determination of geniposide, genipin, gardenoside, and geniposidic acid from herbs by HPLC/photodiode-array detection. *Journal of Liquid Chromatography & Related Technologies* **1994,** *17*, 2199-2205.
288. Tseng, T.-H.; Chu, C.-Y.; Huang, J.-M.; Shiow, S.-J.; Wang, C.-J., Crocetin protects against oxidative damage in rat primary hepatocytes. *Cancer Letters* **1995,** *97*, 61-67.
289. Koo, H.-J.; Song, Y. S.; Kim, H.-J.; Lee, Y.-H.; Hong, S.-M.; Kim, S.-J.; Kim, B.-C.; Jin, C.; Lim, C.-J.; Park, E.-H., Antiinflammatory effects of genipin, an active principle of gardenia. *European Journal of Pharmacology* **2004,** *495*, 201-208.
290. Sung, H. W.; Huang, R. N.; Huang, L. L.; Tsai, C. C.; Chiu, C. T., Feasibility study of a natural crosslinking reagent for biological tissue fixation. *Journal of biomedical materials research* **1998,** *42*, 560-567.
291. Sung, H.-W.; Huang, R.-N.; Huang, L. L.; Tsai, C.-C., In vitro evaluation of cytotoxicity of a naturally occurring cross-linking reagent for biological tissue fixation. *Journal of Biomaterials Science, Polymer Edition* **1999,** *10*, 63-78.
292. Karnchanajindanun, J.; Srisa-ard, M.; Baimark, Y., Genipin-cross-linked chitosan microspheres prepared by a water-in-oil emulsion solvent diffusion method for protein delivery. *Carbohydrate Polymers* **2011,** *85*, 674-680.
293. Pujana, M. A.; Pérez-Álvarez, L.; Iturbe, L. C. C.; Katime, I., Biodegradable chitosan nanogels crosslinked with genipin. *Carbohydrate Polymers* **2013,** *94*, 836-842.
294. Muzzarelli, R. A., Genipin-crosslinked chitosan hydrogels as biomedical and pharmaceutical aids. *Carbohydrate Polymers* **2009,** *77*, 1-9.
295. Pujana, M. A.; Pérez-Álvarez, L.; Iturbe, L. C. C.; Katime, I., Water soluble folate-chitosan nanogels crosslinked by genipin. *Carbohydrate Polymers* **2014,** *101*, 113-120.
296. Mi, F. L.; Sung, H. W.; Shyu, S. S., Release of indomethacin from a novel chitosan microsphere prepared by a naturally occurring crosslinker: examination of crosslinking and polycation–anionic drug interaction. *Journal of applied polymer science* **2001,** *81*, 1700-1711.
297. Mi, F.-L.; Sung, H.-W.; Shyu, S.-S.; Su, C.-C.; Peng, C.-K., Synthesis and characterization of biodegradable TPP/genipin co-crosslinked chitosan gel beads. *Polymer* **2003,** *44*, 6521-6530.
298. Butler, M. F.; Ng, Y. F.; Pudney, P. D., Mechanism and kinetics of the crosslinking reaction between biopolymers containing primary amine groups and genipin. *Journal of Polymer Science Part A: Polymer Chemistry* **2003,** *41*, 3941-3953.
299. Muzzarelli, R. A. A., Genipin-crosslinked chitosan hydrogels as biomedical and pharmaceutical aids. *Carbohydrate Polymers* **2009,** *77*, 1-9.
300. Bigi, A.; Cojazzi, G.; Panzavolta, S.; Roveri, N.; Rubini, K., Stabilization of gelatin films by crosslinking with genipin. *Biomaterials* **2002,** *23*, 4827-4832.
301. Chitpan, M.; Wang, X.; Ho, C.-T.; Huang, Q., Monitoring the Binding Processes of Black Tea Thearubigin to the Bovine Serum Albumin Surface Using Quartz Crystal

Microbalance with Dissipation Monitoring. *Journal of agricultural and food chemistry* **2007,** *55*, 10110-10116.
302. Patel, A.; Hu, Y.; Tiwari, J. K.; Velikov, K. P., Synthesis and characterisation of zein-curcumin colloidal particles. *Soft Matter* **2010,** *6*, 6192-6199.
303. Luo, Y.; Zhang, B.; Cheng, W.-H.; Wang, Q., Preparation, characterization and evaluation of selenite-loaded chitosan/TPP nanoparticles with or without zein coating. *Carbohydrate Polymers* **2010,** *82*, 942-951.
304. Sauerbrey, G., Verwendung von schwingquarzen zur wägung dünner schichten und zur mikrowägung (The use of quartz oscillators for weighing thin layers and for microweighing). *ZPhyse. A: Hadrons Nucl.* **1959,** *155*, 206–222.
305. Voinova, M. V.; Rodahl, M.; Jonson, M.; Kasemo, B., Viscoelastic Acoustic Response of Layered Polymer Films at Fluid-Solid Interfaces: Continuum Mechanics Approach. *Physica Scripta* **1999,** *59*, 391-396.
306. Xiao, J.; Shi, C.; Li, Y.; Pan, Y.; Huang, Q., Pickering emulsions immobilized within hydrogel matrix with enhanced resistance against harsh processing conditions and sequential digestion. *Food Hydrocolloids* **2017,** *62*, 35-42.
307. Chen, H.; Ouyang, W.; Lawuyi, B.; Prakash, S., Genipin Cross-Linked Alginate-Chitosan Microcapsules: Membrane Characterization and Optimization of Cross-Linking Reaction. *Biomacromolecules* **2006,** *7*, 2091-2098.
308. Lasztity, R., *The chemistry of cereal proteins*. Routledge: 2017.
309. Lai, H. M.; Geil, P.; Padua, G., X-ray diffraction characterization of the structure of zein–Oleic acid films. *Journal of applied polymer science* **1999,** *71*, 1267-1281.
310. Izzo, M. T.; Ho, C., Protein-lipid interaction during single-screw extrusion of zein and corn oil. *Cereal Chem* **1989,** *66*, 47-51.
311. Wang, L. J.; Hu, Y. Q.; Yin, S. W.; Yang, X. Q.; Lai, F. R.; Wang, S. Q., Fabrication and characterization of antioxidant pickering emulsions stabilized by zein/chitosan complex particles (ZCPs). *J Agric Food Chem* **2015,** *63*, 2514-24.
312. Zou, Y.; Guo, J.; Yin, S. W.; Wang, J. M.; Yang, X. Q., Pickering Emulsion Gels Prepared by Hydrogen-Bonded Zein/Tannic Acid Complex Colloidal Particles. *J Agric Food Chem* **2015,** *63*, 7405-14.
313. Gezer, P. G.; Brodsky, S.; Hsiao, A.; Liu, G. L.; Kokini, J. L., Modification of the hydrophilic/hydrophobic characteristic of zein film surfaces by contact with oxygen plasma treated PDMS and oleic acid content. *Colloids Surf B Biointerfaces* **2015,** *135*, 433-40.
314. Shi, K.; Kokini, J. L.; Huang, Q., Engineering zein films with controlled surface morphology and hydrophilicity. *Journal of agricultural and food chemistry* **2009,** *57*, 2186-2192.
315. Barratt, M. D., Quantitative structure-activity relationships (QSARs) for skin corrosivity of organic acids, bases and phenols: Principal components and neural network analysis of extended datasets. *Toxicology in Vitro* **1996,** *10*, 85-94.
316. Liptak, M. D.; Shields, G. C., Experimentation with different thermodynamic cycles used for pKa calculations on carboxylic acids using complete basis set and Gaussian-n models combined with CPCM continuum solvation methods. *International Journal of Quantum Chemistry* **2001,** *85*, 727-741.
317. Nyrén, V.; Back, E., The ionization constant, solubility product and solubility of abietic and dehydroabietic acid. *Acta chem. scand* **1958,** *12*, 1516-1520.
318. Kanicky, J. R.; Shah, D. O., Effect of Premicellar Aggregation on the pKa of Fatty Acid Soap Solutions. *Langmuir* **2003,** *19*, 2034-2038.
319. Kanicky, J. R.; Poniatowski, A. F.; Mehta, N. R.; Shah, D. O., Cooperativity among Molecules at Interfaces in Relation to Various Technological Processes: Effect of Chain Length on the pKa of Fatty Acid Salt Solutions†. *Langmuir* **2000,** *16*, 172-177.
320. Heikkila, R. E.; Deamer, D. W.; Cornwell, D. G., Solution of fatty acids from

monolayers spread at the air-water interface: identification of phase transformations and the estimation of surface charge. *Journal of lipid research* **1970,** *11*, 195-200.
321. Christodoulou, A. P.; Rosano, H. L., Effect of pH and nature of monovalent cations on surface isotherms of saturated C16 to C22 soap monolayers. *Adv. Chem. Ser* **1968,** *84*, 210-234.
322. Kanicky, J. R.; Shah, D. O., Effect of Degree, Type, and Position of Unsaturation on the pKa of Long-Chain Fatty Acids. *Journal of Colloid and Interface Science* **2002,** *256*, 201-207.
323. Wang, Q.; Yin, L.; Padua, G. W., Effect of hydrophilic and lipophilic compounds on zein microstructures. *Food Biophysics* **2008,** *3*, 174-181.
324. Lai, H.-M.; Padua, G. W., Properties and microstructure of plasticized zein films. *Cereal Chemistry* **1997,** *74*, 771-775.
325. Shi, K.; Huang, Y.; Yu, H.; Lee, T.-C.; Huang, Q., Reducing the brittleness of zein films through chemical modification. *Journal of agricultural and food chemistry* **2010,** *59*, 56-61.
326. Li, Y.; Xia, Q.; Shi, K.; Huang, Q., Scaling behaviors of α-zein in acetic acid solutions. *The Journal of Physical Chemistry B* **2011,** *115*, 9695-9702.
327. Zeghal, M.; Auvray, L., Structure of polymer complexes in water. *EPL (Europhysics Letters)* **1999,** *45*, 482.
328. Xiao, J.; Li, Y.; Li, J.; Gonzalez, A. P.; Xia, Q.; Huang, Q., Structure, Morphology, and Assembly Behavior of Kafirin. *Journal of agricultural and food chemistry* **2015,** *63*, 216-224.
329. Pedersen, J. S., Analysis of small-angle scattering data from colloids and polymer solutions: modeling and least-squares fitting. *Advances in colloid and interface science* **1997,** *70*, 171-210.
330. Svergun, D. I.; Koch, M. H., Small-angle scattering studies of biological macromolecules in solution. *Reports on Progress in Physics* **2003,** *66*, 1735.
331. Guimer, A.; Fournet, G., Small angle scattering of X-rays. *J. Wiley & Sons, New York* **1955**.
332. Skelhon, T. S.; Grossiord, N.; Morgan, A. R.; Bon, S. A., Quiescent water-in-oil Pickering emulsions as a route toward healthier fruit juice infused chocolate confectionary. *Journal of Materials Chemistry* **2012,** *22*, 19289-19295.
333. Keen, P. H.; Slater, N. K.; Routh, A. F., Encapsulation of lactic acid bacteria in colloidosomes. *Langmuir* **2012,** *28*, 16007-16014.
334. Heron, M. P., Deaths: leading causes for 2013. **2016**.
335. Garg, A.; Garg, S.; Zaneveld, L.; Singla, A., Chemistry and pharmacology of the citrus bioflavonoid hesperidin. *Phytotherapy research* **2001,** *15*, 655-669.
336. Morand, C.; Dubray, C.; Milenkovic, D.; Lioger, D.; Martin, J. F.; Scalbert, A.; Mazur, A., Hesperidin contributes to the vascular protective effects of orange juice: a randomized crossover study in healthy volunteers. *The American journal of clinical nutrition* **2010,** *93*, 73-80.
337. Mahmoud, A. M.; Ashour, M. B.; Abdel-Moneim, A.; Ahmed, O. M., Hesperidin and naringin attenuate hyperglycemia-mediated oxidative stress and proinflammatory cytokine production in high fat fed/streptozotocin-induced type 2 diabetic rats. *Journal of Diabetes and its Complications* **2012,** *26*, 483-490.
338. Ibrahim, S. S., Protective effect of hesperidin, a citrus bioflavonoid, on diabetes-induced brain damage in rats. *J Appl Sci Res* **2008,** *4*, 84.
339. Park, H.; Kim, M.-J.; Ha, E.; Chung, J.-H., Apoptotic effect of hesperidin through caspase3 activation in human colon cancer cells, SNU-C4. *Phytomedicine* **2008,** *15*, 147-151.
340. Miyagi, Y.; Om, A.; Chee, K.; Bennink, M., Inhibition of azoxymethane-induced

colon cancer by orange juice. *Nutrition and cancer* **2000,** *36*, 224-229.
341. Yang, M.; Tanaka, T.; Hirose, Y.; Deguchi, T.; Mori, H.; Kawada, Y., Chemopreventive effects of diosmin and hesperidin on N-butyl-N-(4-hydroxybutyl) nitrosamine-induced urinary-bladder carcinogenesis in male ICR mice. *International Journal of Cancer* **1997,** *73*, 719-724.
342. Koyuncu, H.; Berkarda, B.; Baykut, F.; Soybir, G.; Alatli, C.; Gül, H.; Altun, M., Preventive effect of hesperidin against inflammation in CD-1 mouse skin caused by tumor promoter. *Anticancer research* **1999,** *19*, 3237-3241.
343. Tanaka, T.; Makita, H.; Kawabata, K.; Mori, H.; Kakumoto, M.; Satoh, K.; Hara, A.; Sumida, T.; Fukutani, K.; Tanaka, T., Modulation of N-methyl-N-amylnitrosamine-induced rat oesophageal tumourigenesis by dietary feeding of diosmin and hesperidin, both alone and in combination. *Carcinogenesis* **1997,** *18*, 761-769.
344. Roohbakhsh, A.; Parhiz, H.; Soltani, F.; Rezaee, R.; Iranshahi, M., Molecular mechanisms behind the biological effects of hesperidin and hesperetin for the prevention of cancer and cardiovascular diseases. *Life Sciences* **2015,** *124*, 64-74.
345. Ameer, B.; Weintraub, R. A.; Johnson, J. V.; Yost, R. A.; Rouseff, R. L., Flavanone absorption after naringin, hesperidin, and citrus administration. *Clinical Pharmacology & Therapeutics* **1996,** *60*, 34-40.
346. Manach, C.; Morand, C.; Gil-Izquierdo, A.; Bouteloup-Demange, C.; Remesy, C., Bioavailability in humans of the flavanones hesperidin and narirutin after the ingestion of two doses of orange juice. *European journal of clinical nutrition* **2003,** *57*, 235-242.
347. Nielsen, I. L. F.; Chee, W. S.; Poulsen, L.; Offord-Cavin, E.; Rasmussen, S. E.; Frederiksen, H.; Enslen, M.; Barron, D.; Horcajada, M.-N.; Williamson, G., Bioavailability is improved by enzymatic modification of the citrus flavonoid hesperidin in humans: a randomized, double-blind, crossover trial. *The Journal of nutrition* **2006,** *136*, 404-408.
348. Hollman, P. C.; Bijsman, M. N.; van Gameren, Y.; Cnossen, E. P.; de Vries, J. H.; Katan, M. B., The sugar moiety is a major determinant of the absorption of dietary flavonoid glycosides in man. *Free radical research* **1999,** *31*, 569-573.
349. Tsai, T.-H.; Liu, M.-C., Determination of extracellular hesperidin in blood and bile of anaesthetized rats by microdialysis with high-performance liquid chromatography: a pharmacokinetic application. *Journal of Chromatography B* **2004,** *806*, 161-166.
350. Dammak, I.; do Amaral Sobral, P. J., Formulation optimization of lecithin-enhanced pickering emulsions stabilized by chitosan nanoparticles for hesperidin encapsulation. *Journal of Food Engineering* **2018,** *229*, 2-11.
351. Tsai, M.-L.; Wu, C.-T.; Lin, T.-F.; Lin, W.-C.; Huang, Y.-C.; Yang, C.-H., Chemical composition and biological properties of essential oils of two mint species. *Tropical Journal of Pharmaceutical Research* **2013,** *12*, 577-582.